**Carla Maria Moreira Machado**

Mestre em Engenharia Mecânica

# Empirical Models for Quantification of Machining Damage in Composite Materials

Dissertação para obtenção do Grau de Doutor em
Engenharia Mecânica

Orientador: Professor Doutor Jorge Joaquim Pamies Teixeira,
Professor Catedrático, Universidade Nova de Lisboa

Júri:

Presidente: Prof. Doutor António Manuel Flores Romão de Azevedo Gonçalves Coelho

Arguentes: Prof. Doutor António Torres Marques
Prof. Doutor Luís Miguel Pereira Durão

Vogais: Prof. Doutora Maria Teresa Freire Vieira
Prof. Doutor António Paulo Monteiro Baptista
Prof. Doutora Rosa Maria Mendes Miranda
Prof. Doutor Telmo Jorge Gomes dos Santos

FACULDADE DE CIÊNCIAS E TECNOLOGIA
UNIVERSIDADE NOVA DE LISBOA

**Outubro 2012**

**Empirical Models for Quantification of Machining Damage in Composite Materials**

*In memory of my father*

# Acknowledgments

It's almost impossible to mention all the people who have been important during the preparation of this work. My acknowledgments are addressed to all those who directly or indirectly contributed to the completion of this work.

First I would like to thank my supervisor, Professor Pamies Teixeira, who has been instrumental in guiding me towards the successful completion of this thesis. I also thank for the patience shown and for teaching me throughout these years the importance of values such as honesty and scientific rigor. I doubt that I will ever be able to convey my appreciation fully, so I express him my gratitude and deepest admiration.

My thanks are also address to Eng. Mário Almeida Santos and Eng. José Levezinho from OGMA for the willingness shown and the composite material provided.

For the readiness in carrying out SEM observations, my sincere thanks to Dr. Nuno Leal from the Department of Earth Sciences (DCT) FCT-UNL.

A special reference should be made to Professor Luis Durão from ISEP for the information provided regarding the radiography equipment and X-ray technique.

I extend my gratitude to my colleagues in the Section of Industrial Technology, Professor Rosa Miranda, Professor Telmo Santos and Professor Caiado Ferreira, for their constant encouragement and support, especially in the difficult moment I had to go through in elapsing of this work.

My sincere thanks also go to António Campos, Paulo Magalhães and Maria da Conceição Pereira for always being present and available to help.

To my friends and colleagues Alberto Martinho, Ana Sofia Matos, Daniel Vaz and Raquel Almeida, I don’t have words to express my gratefulness. They demonstrate, throughout these years, what is the true value of friendship and were always there, helping and incentivizing. I cannot forget Helena Navas that always shown her readiness to assist, and always had a word of encouragement.

Finally, I wish to thank my friends and family, especially my mother, for instilling in me confidence and a drive for pursuing my goals. They understood my absences being always available and motivators, and even in the most difficult moments they managed to convey comfort and always believed, making me believe.

To all my deepest gratitude.

# Abstract

The tremendous growth which occurs at a global level of demand and use of composite materials brings with the need to develop new manufacturing tools and methodologies. One of the major uses of such materials, in particular plastics reinforced with carbon fibres, is their application in structural components for the aircraft industry with low weight and high stiffness. These components are produced in near-final form but the so-called secondary processes such as machining are often unavoidable. In this type of industry, drilling is the most frequent operation due to the need to obtain holes for riveting and fastening bolt assembly of structures. However, the problems arising from drilling, particularly the damage caused during the operation, may lead to rejection of components because it is an origin of lack of resistance. The delamination is the most important damage, as it causes a decrease of the mechanical properties of the components of an assembly and, irrefutably, a reduction of its reliability in use. It can also raise problems with regard to the tolerances of the assemblies. Moreover, the high speed machining is increasingly recognized to be a manufacturing technology that promotes productivity by reducing production times. However, the investigation whose focus is in high speed drilling is quite limited, and few studies on this subject have been found in the literature review. Thus, this thesis aims to investigate the effects of process variables in high speed drilling on the damage produced. The empirical models that relate the delamination damage, the thrust force and the torque with the process parameters were established using Response Surface Methodology. The process parameters considered as input factors were the spindle speed, the feed per tooth, the tool diameter and the workpiece thickness. A new method for fixing the workpiece was developed and tested. The results proved to be very promising since in the same cutting conditions and with this new methodology, it was observed a significant reduction of the delamination damage. Finally, it has been found that is possible to use high speed drilling, using conventional twist drills, to produce holes with good quality, minimizing the damage.

***Keywords:*** High Speed Drilling; Carbon Fibre Reinforced Plastics; Composite Laminate; Delamination; Response Surface Methodology

# Resumo

O enorme crescimento, a nível global, da procura e utilização de materiais compósitos traz consigo a necessidade de desenvolvimento de novas ferramentas e metodologias para os processar. Uma das principais utilizações deste tipo de materiais e em particular dos plásticos reforçados com fibra de carbono, é a construção de componentes estruturais para a indústria aeronáutica, de baixo peso e grande rigidez. Estes componentes são produzidos em formas quase-finais mas os processos secundários, como a maquinagem, podem ser inevitáveis. Neste tipo de indústria, a operação mais utilizada é a furação, devido à necessidade de obtenção de furos para a rebitagem e fixação aparafusada das montagens de estruturas. No entanto, os problemas decorrentes da furação, nomeadamente o dano causado durante a operação, podem levar à rejeição de componentes, por ser uma origem de falta de resistência. A delaminação é o dano com maior importância, dado causar uma diminuição das propriedades mecânicas dos componentes e, concludentemente, uma redução da sua fiabilidade quando em utilização. Por outro lado, a maquinagem de alta velocidade é cada vez mais reconhecida como tecnologia de fabrico que promove a produtividade, reduzindo os tempos de produção. No entanto, a investigação realizada cujo enfoque é a furação com alta velocidade é bastante limitada, tendo sido encontrados na literatura poucos trabalhos acerca deste tema. Assim, nesta dissertação pretende-se investigar os efeitos das variáveis do processo de furação a alta velocidade sobre o dano produzido. Utilizando a Metodologia de Resposta em Superfície, foram estabelecidos modelos empíricos que relacionam o dano de delaminação, a força axial e o torque com os parâmetros do processo, designadamente a velocidade de rotação, o avanço por dente, o diâmetro da ferramenta e a espessura da peça. Foi ainda desenvolvido um novo sistema de fixação da peça e os resultados mostraram-se promissores, uma vez que, nas mesmas condições de corte, se conseguiu reduzir significativamente o dano. Em termos globais, verificou-se ser possível utilizar a furação de alta velocidade para produzir furos com minimização do dano, com a utilização de brocas helicoidais convencionais.

***Termos Chave:*** Furação a Alta Velocidade; Plásticos Reforçados com Fibra de Carbono; Compósitos Laminados; Delaminação; Metodologia de Resposta em Superfície.

# Table of Contents

# List of Figures

# List of Tables

# List of Symbols and Abbreviations

| | |
|---|---|
| $\nu$ | Poisson ratio |
| $A_0$ | Nominal area |
| $A_d$ | Damage area |
| $A_{max}$ | $D_{max}$ corresponding area |
| ANOVA | Analysis of variance |
| CFRP | Carbon fibre reinforced plastic |
| CTBN | Acrylonitrile-butadiene liquid rubber |
| $d$ | Tool diameter |
| $D_0$ | Hole nominal diameter |
| $D_{max}$ | Maximum diameter in the damage zone |
| DOE | Design of experiments |
| $E$ | Elastic modulus |
| $F$ | Thrust force |
| $f$ | Feed rate |
| $F_C$ | Critical thrust force |
| $F_d$ | Delamination factor |
| $F_{da}$ | Adjusted delamination factor |
| $f_z$ | Feed per tooth |
| GFRP | Glass fibre reinforced plastic |
| $G_{IC}$ | Critical strain energy release rate (in mode I fracture) |
| HSS | High speed steel |
| KFRP | Kevlar fibre reinforced plastic |
| NDT | Non-destructive testing |
| PAN | Polyacrylonitrile |
| PCD | Polycrystalline diamond |
| RSM | Response Surface Methodology |
| $S$ | Spindle speed |
| $t$ | Workpiece thickness |
| $T$ | Torque |
| $T_g$ | Glass transition temperature |
| $V$ | Cutting speed |

# 1

# Objectives, Structure of the Thesis and Literature Review

## 1.1 Motivation and Objectives

The main motivation that led to the development of the work presented in this thesis deals with the real difficulties experienced by the aeronautic industry whenever it becomes necessary to minimize the resultant damage when drilling composite materials. These questions include not only the influence of process variables and their correlation with the damage obtained but also factors such as production time and resource allocation.

Furthermore, the scientific research conducted on this area shows that there are still some difficulties in quantifying this type of damage. Situations exist where the experiments take in consideration only some of the variables that influence the process and have significance on the resultant damage. By choosing these conditions, some of the process variables are fixed which determines a rather limited field of experimental results. In addition, most studies relate to conventional processes, whereupon the parameters used have relatively low values. While high-productivity process, the use of high speed drilling is not yet fully clarified.

This work was initially supported by *OGMA – Indústria Aeronáutica de Portugal S.A.*, which provided the material used. Hence, this study was constrained by the quantity and configuration availability of the composite material. Nevertheless, the experiments were conducted with composite materials which are actually used at industrial level and this fact allowed providing an effective response to the actual concerns. This composite, a carbon fibre reinforced plastic, is the material used in the production of the NH-90 helicopter airframe.

Thus, one of the scopes of this work is to develop strategies in order to minimize the machining damage, namely the delamination, when drilling carbon fibre reinforced plastics.

Therefore, the main objective of this thesis is to characterize the delamination damage in high-speed drilling composite materials by developing empirical models that correlate the output responses with the process variables and establish methodologies to minimize the occurrence of this type of defect.

## 1.2 Structure of the Thesis

The thesis is divided into four parts: **Introduction**, **Methodology**, **Experimental Work**, and finally the **Conclusions**. Figure 1.1 illustrates this structure.

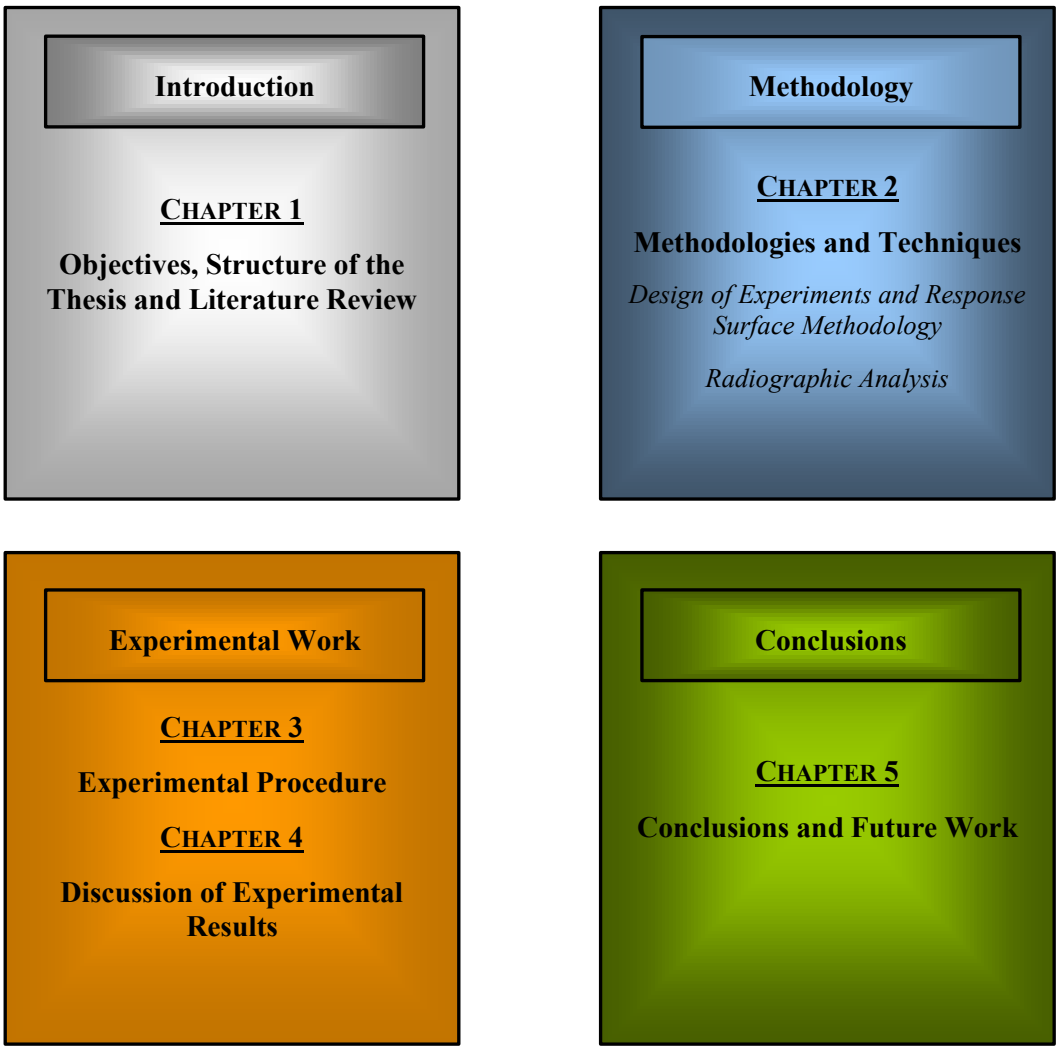


**Figure 1.1** Structure of the Thesis by Chapters

**Introduction –** In the first part of this thesis, consisting of the Chapter 1, are presented the main motivations and objectives that consist on the basis of the study. It is presented the literature review, comprising the fundamental concepts concerning the work in question, namely, materials, cutting tools, input (variables) and output (responses) parameters for the drilling process, damage description and analysis techniques and tool wear. Furthermore, the review of the literature also includes the state of the art with regard to this investigation. The synthesis of the knowledge here presented focuses on the essential aspects related to the process.

**Methodology –** This part of the work, Chapter 2, is dedicated to the study of the methodologies and techniques to be used in this work. The Design of Experiments and Response Surface Methodology are analysed to provide the understanding of the theory and practice of this methodology. The reasons for choosing a specific design and the specifications for the type of model are presented, allowing the awareness of the choices made.

Before conducting the tests, all samples are radiographed to estimate the damage that already existed prior to the completion of the holes. In this section we intend to explain the methodology developed for the quantification of damage, describing step by step all the procedures, techniques and resources for measuring the resulting damage, which is intended to be as accurate as possible.

**Experimental Work –** Chapters 3 and 4 represent the actual application, where the experimental work is described. In Chapter 3 all the experimental procedure is defined, including the selection of tools and materials that are also characterized. The resources used are described, with particular emphasis on those that have been designed especially for this work.

In Chapter 4 the experimental results are presented and discussed. An empirical model is developed for each case, by statistical analysis, using the Response Surface Methodology. Each empirical model is then validated by experimental tests. Based on the analysis, there is a discussion on the importance of operating parameters and their variation on the desired responses.

A new method that consists of a different fastening device is developed and validated through a set of experiments planned according to the empirical knowledge resulting from the previous analysis.

**Conclusions -** Finally, Chapter 5 presents the conclusions, innovative contributions proposed in this work and further suggestions for future developments.

## 1.3 Literature Review

Composite materials have currently a widespread use, especially in the automotive and aeronautics, but the trend points to increasing and broadening its scope to other areas. The performance of such materials has been confirmed not only with specific studies, but also the experience of use in industry, whose standards are established. Consequently, research in this field has been developing as one of its aspects is the question of machining operations. In fact, the composite components are produced in near-final form with the use of primary manufacturing processes such as autoclave polymerization, compression moulding, vacuum bagging and pultrusion, but the so-called secondary processes such as machining, are often unavoidable [1]. With the expansion of the scope of this type of material, the use of machining processes like turning, drilling and milling tends to increase [2], and their wide use is due to the availability of equipment and consolidated experience in conventional machining [3]. In the aircraft, drilling is the most frequent operation due to the need to obtain holes for riveting and fastening bolt assembly of structures [4, 5]. However, the problems arising from drilling lead to rejection of a considerable branch of constituent parts of an aircraft, mainly due to the fact that this type of setting can be a critical part of the structure, as it is a source of lack of resistance. On the other hand, such connections helps to increase the weight of the assembly [6, 7].

Once one of the axes of this type of technology industry is the set of manufacturing technologies, it makes sense to try to develop new processes, tools and manufacturing aids. In this case, and because it is applied research to industry is crucial to analyse the balance between the economic and technological benefits to the operations. The tools scientifically proven as the most effective are often not used, only because they demonstrate to be not viable economically.

The high performance and low weight structures considered are assemblies of components that must have a high level of integration. Because they are designed to operate in extreme conditions, is required of them a high standard with regard to safety and reliability.

### 1.3.1 Materials

Composite materials are macroscopic combinations of two or more distinct materials that have a recognizable interface and can be independently identified. In practical terms, composite materials are those that contain reinforcement and a bind matrix. The reinforcement is the strongest and stiffer constituent [8].

Composites are multitudinous and complex. Depending on the characteristics of the matrix and reinforcements, can be grouped into two main groups:

- Composites for broad general dissemination, which represent 95% of the composites used and are generally short fibre reinforced plastics, low mechanical strength and reinforcement rate approaching 30%;

- The high performance composites which have mechanical properties (strength and rigidity) superior than those of metals, and the reinforcement rate greater than 50%. High performance composites, quite expensive, are reserved for high value-added sectors: aerospace, medical, sporting goods and, more recently, wind energy and automobile.

The earliest reference to composite materials is to be found in Exodus, the second book of the Old Testament, and points to their use in 1500 B.C. The first use of composites was in form of bricks made of clay and straw kneaded together, and then dried in the sun.

In the early 1900s, with the development of plastics started the modern era of composites, since the new synthetic materials outperformed resins derived from nature. In addition, in 1938, *Owens Corning* presented the first glass fibre, Fiberglas®. A suitable resin for combining the Fiberglas® with a plastic was developed in 1936 by *DuPont*. The beginning of modern composites is referenced to be the moulding of small boats using these two new products combined, as part of a manufacturing experiment [9].

Historically, the development of composites was driven by war, and was World War II that led to the great development of fibre reinforced plastics, which ceased to be mere laboratory studies and started to be produced industrially, mainly for applications in military aircraft. With the end of World War II, and consequently with decreasing demand in terms of products of military application, the need arose to expand the composite materials to other markets. At this time Brandt Goldsworthy developed new manufacturing processes and products, one of them the pultrusion process, widely used at present. In terms of commercial application, the first boat hull was introduced in 1946. The composite materials industry outgrowth significantly in the 70's with the development of improved resins and reinforcing fibres, namely the aramid fibre (Kevlar) and the carbon fibre. Since then the use of composite materials reinforced with carbon fibre has increased significantly, mainly due to the substitution of metals in applications which require higher strength, higher stiffness, less weight and better durability [10].

Nowadays, the development of lower cost carbon fibres and the improvements in production processes making them more cost effective have widespread the use of this type of material. Despite being more expensive than traditional materials, the present requirements in terms of performance benefits are making their use increasingly broad. There are several examples of

applications where the carbon fibre composites industry is still evolving with continuous research of improved materials and processes, such as nano-materials, and a growing concern with environmental issues, for example with the use of resins incorporating recycled plastics and bio-based polymers.

Composite materials commonly used in the aerospace industry are the fibre reinforced plastics (FRP), which use polymer matrix (thermosetting or thermoplastic matrix) and fibre reinforcement material of glass, carbon or aramid (Kevlar) [11]. The fibre reinforced plastics are composite materials for structural components with excellent properties that make them crucial for the development of new products. These properties include factors such as high specific strength and stiffness, corrosion resistance and wear performance and fatigue [4]. In the case of the aircraft industry, their use meets the fundamental issues that relate to performance and economy of resources. Considering their characteristics, the use of composite materials allows, for example, the increase in payload or range and fuel economy, from reducing the weight of structures, increasing component life and reducing costs maintenance [12].

According to the *Visiongain* author of *The Composites Market 2012-2022: Glass Fibre, Carbon Fibre & Aramid Fibre report*, 'The global composites market will experience robust and accelerating growth, as the economic conditions in Europe improve and as the emerging markets increase their usage of composites. The demand for renewable energy in the form of wind turbines and the demand for light-weight fuel efficient aircraft and cars are major drivers increasing composites markets' [13].

However, applications of carbon fibre reinforced plastics (CFRP) are not restricted to those indicated. Indeed, their use is becoming increasingly common and evolving substantially in other areas.

For example, in the marine industries CFRP are used not only in the construction of hull, but also to make key fixtures and fittings of a boat, steering wheels and wind transducers. The civil engineering applications should also be mentioned and can be either reinforcing concrete structures or retrofitting to strengthen an existing structure. In the sporting goods industry its use is becoming commonplace and there are numerous examples of equipment manufactured with this material, such as bicycles, fishing rods, golf club shafts, rackets, paddles or longboards. Even the consumer goods are following this tendency and the application of CFRP is so vast that covers furniture products, watches, high end audio components, laptop covers and even shoes. Of course in some of these cases their use is merely due to a matter of luxury and not only because of their characteristics. Figure 1.2 shows some of the application of carbon fibre reinforced plastics.

**a)** Each Boeing 787 contains approximately 32 tons of carbon fibre (Source: *Boeing*)

**b)** NH-90 (Source: *NH industries*)

**c)** Visby Class Corvette. The vessel is built of sandwich-construction carbon fibre reinforced plastic. (Source: *Kockums*)

**d)** BMW i8 showing the CFRP life module (Source: *BMWi*)

**e)** Carbon composite pedestrian bridge in Madrid

(Source: Reinforced Plastics)

**f)** V164 7.0MW wind turbine, with 80m blades, uses carbon fibre to enhance stiffness and as a mass optimising feature in the central blade spar. (Source: *Vestas*)

**g)** Sporting goods - Kayak paddle, golf shafts and bicycle made of CFRP (Sources: Reinforced Plastics and *AUDI*)

**h)** Consumer goods (Sources: *Hublot* and Carbon Fiber Gear)

**Figure 1.2** Applications of carbon fibre reinforced plastics

The producers of carbon fibre are spread worldwide and since 2010 several new companies are emerging. The comparison between the global market shares of carbon fibre production in 2010 and 2011 is shown in Figure 1.3.

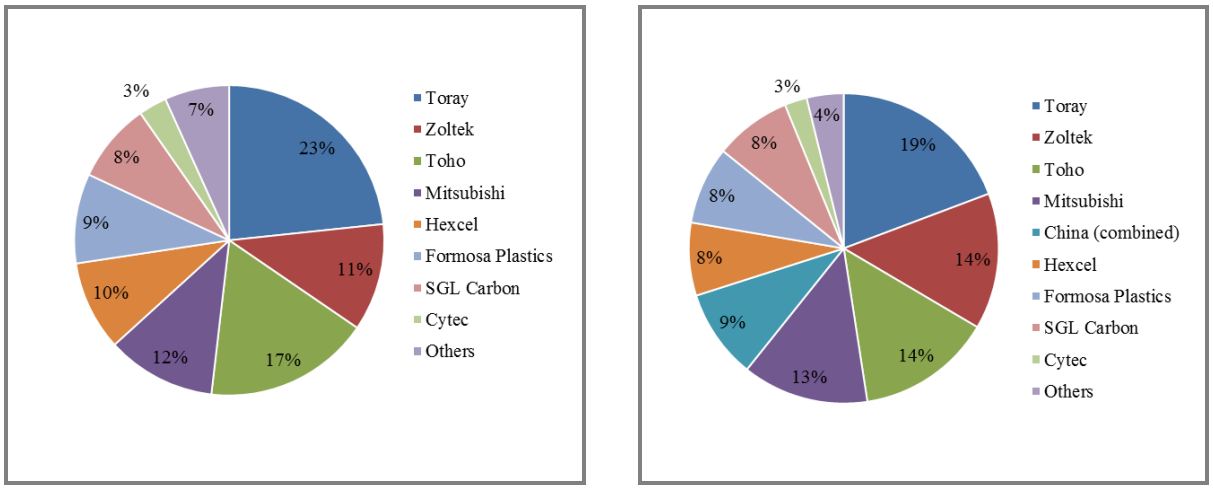


**a)** **b)**

**Figure 1.3** Global Market Share – Carbon fibre production:
**a)** Estimated annual capacity in 2010 [14]; **b)** Actual 2011 market share [15]

*Lucintel*, a global market research and management consulting firm whose clients include the main composite, aircraft and automobile producers, forecasts that the value of the global composite materials market until 2017 will have a compound annual growth rate of 7% (Figure 1.4a). *Toray*, the main supplier of carbon fibres for aircraft applications, estimates a "dramatic expansion" of this material mainly due to the full-scale increase in aircraft and automobile (Figure 1.4b).

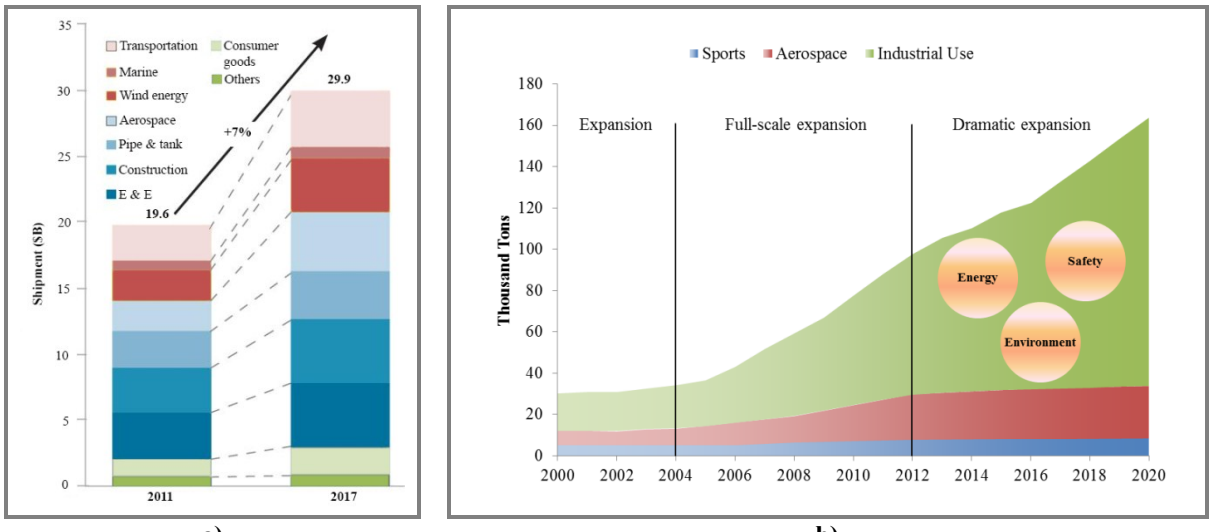


**a)** **b)**

**Figure 1.4** Carbon fibre market evolution by application: **a)** *Lucintel* forecast [16]; **b)** *Toray* forecast [17]

The aerospace industry will continue to be the main user of advanced composites and is expected to growth significantly, due to continued use in military aircraft and helicopters, the increasing penetration of advanced composites into commercial aircraft, such as the Boeing 787, the Airbus A350 XWB and the market's increasing demand for weight reduction. In the wind energy market, ever-larger turbine capacities and increases in average blade length that require lighter and stiffer materials are driving the growth of advanced composites, creating a burgeoning market for carbon fibre. The automotive industry holds perhaps the greatest potential for high performance composites. Despite the global trend of automobile manufacturers of using carbon fibre to reduce the weight of the structures, the opinions are divided. According to *Freedonia* consultants, this market will see only moderate gains in demand, as their use continues to be restrained by high cost and slow production speeds. In turn, the carbon fibre manufacturers are very optimistic about the increase in demand. [16, 18].

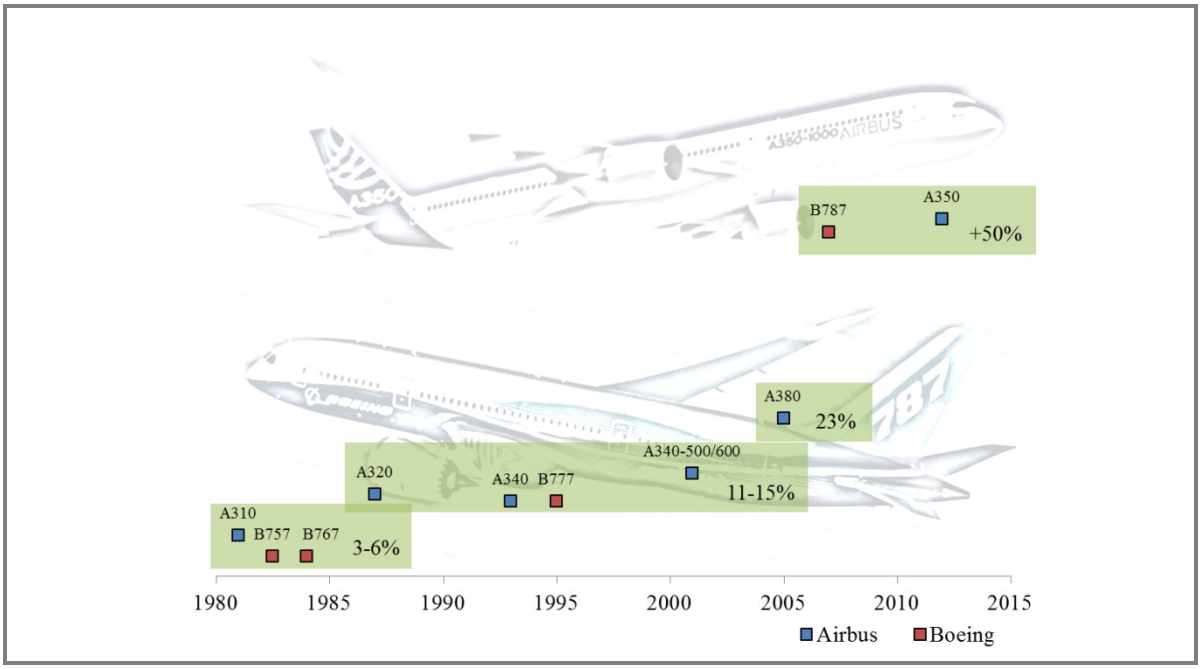


**Figure 1.5** Evolution of composite content by weight in commercial aircraft (Airbus and Boeing) (Adapted from *Hexcel Corporation*)

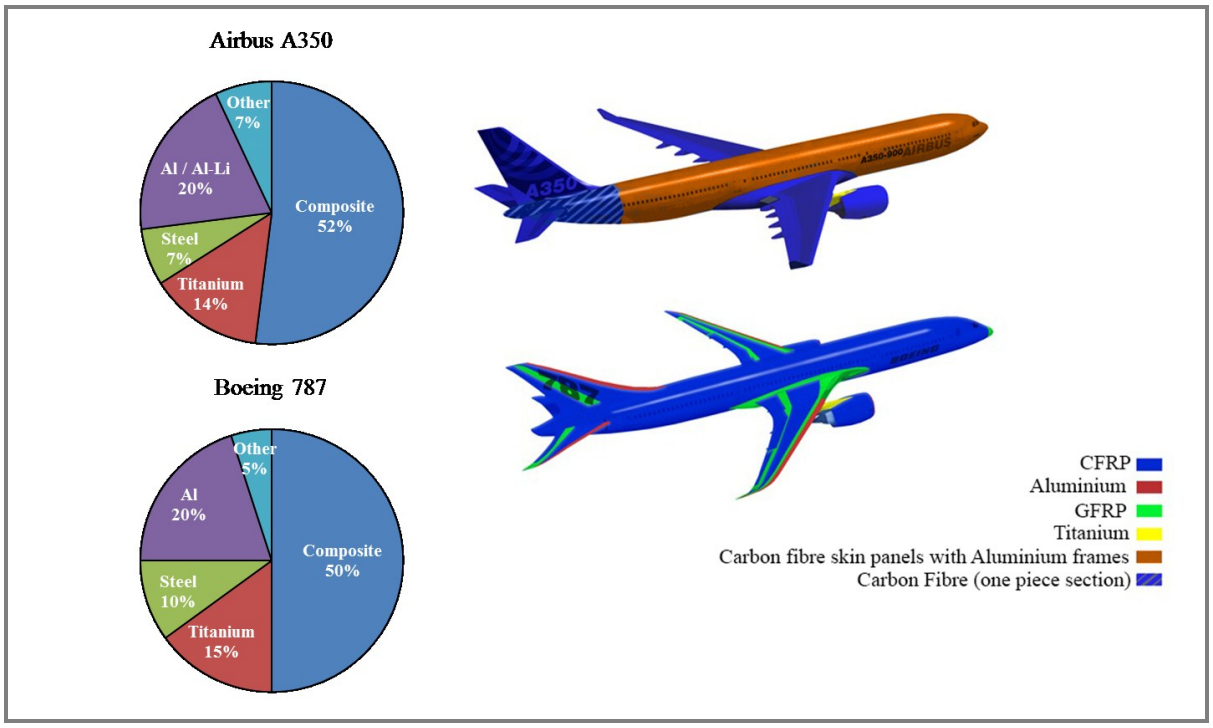


**Figure 1.6** Composite use on Airbus A350 vs. Boeing 787 (Adapted from *Boeing* and *Airbus*)

From all these considerations, and taking into account their characteristics, carbon fibre reinforced plastic is estimated to remain the composite material with greater demand, totalling 84% of the high performance market in 2016 [18]. CFRP is extremely versatile and despite being an expensive material, as compared to other high performance composites presents a moderate cost.

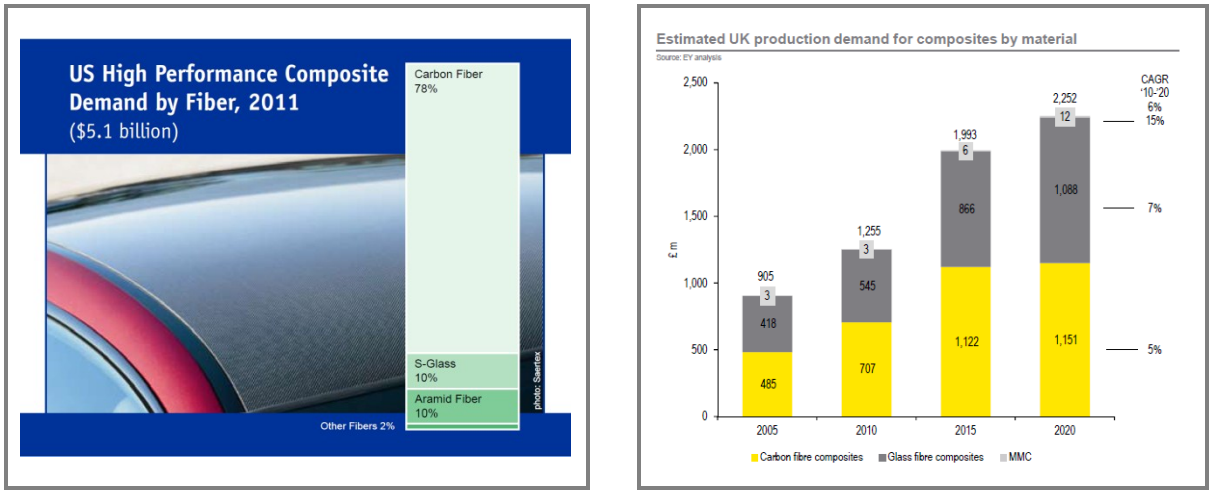


**a)** **b)**

**Figure 1.7 a)** United States composite demand by fibre, 2011 [18]; **b)** United Kingdom composite production demand, 2005-2020 [19]

#### 1.3.1.1 Reinforcement fibres

The most commonly used reinforcement materials are the fibres of glass, carbon, aramid and various high temperature ceramics, referred to as high performance fibres [8]. A variety of materials in the form of fibres can also be used as reinforcement, including asbestos, sisal, polyamides and polyesters but its application is normally associated with structures having lower performance requirement [11].

With regard to the performance of the composite, fibre properties are the most important as regards the mechanical properties, namely stiffness and strength, thermal, electric and chemical properties, and weight saving. Other aspects, such as the maximum service temperature and interlaminar shear strongly depend on the matrix. On the other hand, when discussing properties such as composite dielectric constant and moisture absorption, the volume fraction of the fibres and the matrix is the most important contribution. Thus, it can be seen that to make the selection of materials it is necessary to clearly understand the origins of these properties to properly define a composite structure.

Carbon fibre is produced by the controlled oxidation, carbonisation and graphitisation of carbon-rich organic precursors which are already in fibre form, made by extrusion. These organic precursors are mainly rayon, pitch and polyacrylonitrile (PAN). The most common is PAN as it is less expensive and gives the best carbon fibre properties. Variation of the graphitisation process produces either high strength fibres or high modulus fibres. Thus, the carbon fibres are classified according to the correspondent stiffness and their designations are high strength (HS), intermediate modulus (IM), high modulus (HM) and ultra-high modulus (UHM).

The primary factors governing the physical properties are the degree of carbonisation (or the carbon content, usually greater than 92 per cent by weight), the orientation of the layered carbon planes, and the degree of crystallization [20]. Table 1.1 compares the properties of high strength and ultra-high modulus carbon fibres with those of E-glass, R-Glass, Kevlar 29 and Kevlar 49 fibres. When comparing carbon fibres with other high performance fibres, it is evident their better stiffness.

**Table 1.1** Properties of carbon fibres compared to other high performance fibres [21]

| Material | Density [g/cm$^3$] | Tensile strength [MPa] | Tensile modulus [GPa] |
|---|---|---|---|
| HS carbon | 1.75 | 3 000 – 4 000 | 230 |
| UHM carbon | 1.95 | 2 000 | 600 |
| E-glass | 2.60 | 3 400 | 73 |
| R-glass | 2.55 | 4 400 | 86 |
| Kevlar 29 | 1.44 | 3 000 | 60 |
| Kevlar 49 | 1.45 | 3 000 | 120 |

These are, as well as the cost, the main criteria for fibre selection based on these properties and the comparison between materials is shown in Figure 1.8.

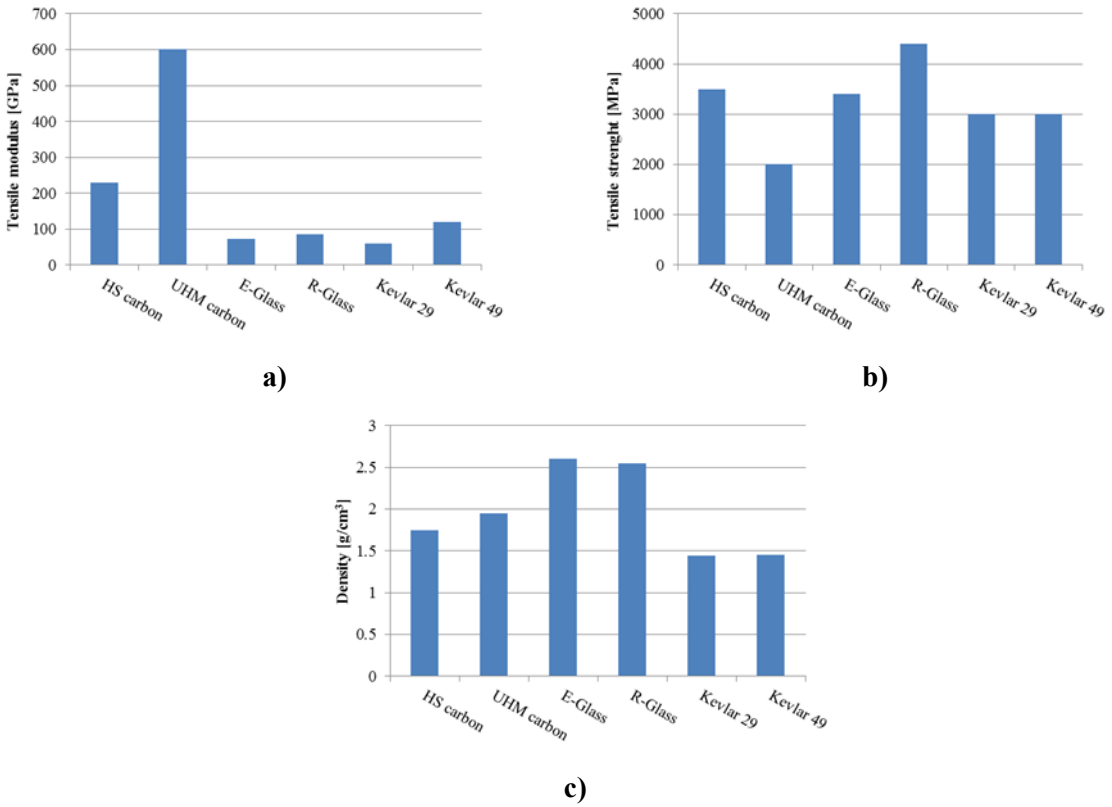


**Figure 1.8** Criteria for fibre selection [22]

The carbon fibre filaments are bundled together to create a tow. There are several variations of tow sizes, the most common 3k, 6k, and 12k. Therefore, a 3k tow will have 3,000 individual filaments. The fibres can be shaped in several forms which are disposed within the material according to the desired properties and there are particulate reinforcements, whisker reinforcements, continuous fibre laminated composites, and woven composites [8]. By varying fibre orientation, composites can be tailored to suit the required specifications. There are several reinforcement fibre architectures namely, roving (the carbon fibre tow wound into a coil), mat (randomly distributed fibres - chopped or continuous - aggregate with a binding material), 2D fabrics (unidirectional, woven or knitted) and 3D fabrics (braids).

Woven fabric is the most common and versatile carbon fibre architecture. The bidirectional fabrics are composed by two sets of yarns. One set of yarns, the warp, runs along the length of the fabric. The other set of yarns, the fill or weft, is perpendicular to the warp. Woven fabrics are held together by weaving the warp and the fill yarns over and under each other. Woven fabrics can present several patterns, being the most common the plain weave, twill weave and satin weave (Figure 1.9). Plain weave is the simplest form, in which one warp yarn interlaces over and under one fill yarn, having low drapeability and high crimp. Twill weave has one or more warp yarns passing over at least two fill yarns, featuring average drapeability and crimp. Satin weave consists of one warp yarn interfacing over three and under one fill yarn to give an irregular pattern in the fabric and given the good drapeability, but low crimp. Low crimp provides better mechanical performance because straighter fibres carry greater loads. The drapeability increases the ability for the fabric to lay up over complex forms.

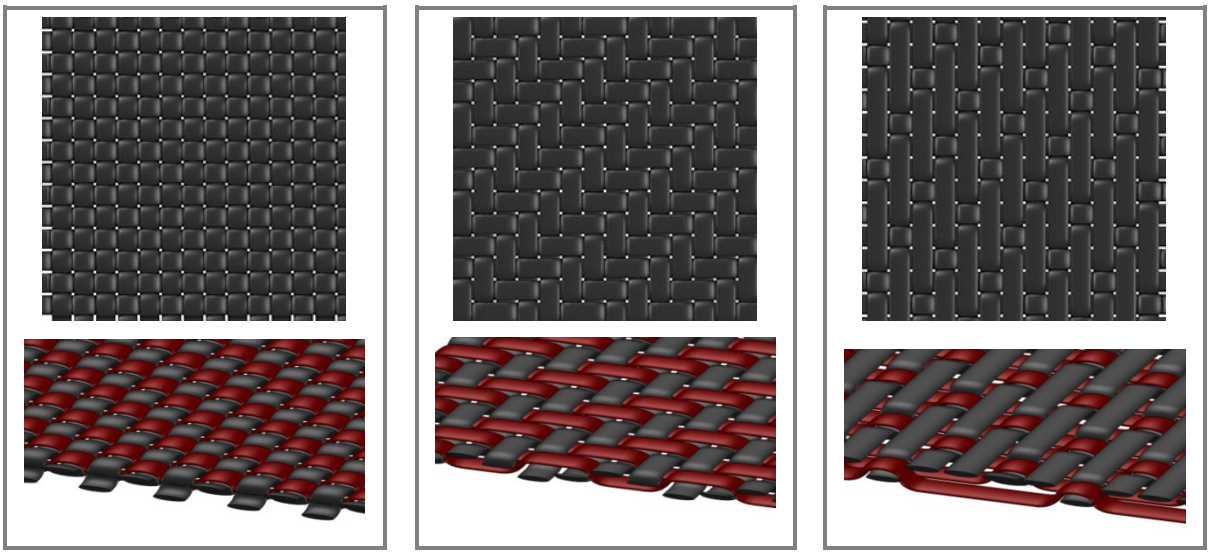

**a)** **b)** **c)**

**Figure 1.9** Different styles of fabrics: **a)** Plain weave; **b)** Twill weave; **c)** Satin weave

#### 1.3.1.2 Matrix

Matrix materials are usually organic (polymer), metal or ceramic. The matrices of polymeric nature are the most common, and although there are a large number of polymers used as organic matrix composites, they are divided into two categories:

- Crystalline polymers or semi-crystalline (thermoplastic resins);

- Amorphous polymers (thermoplastics, thermosets and elastomers).

The most commonly used polymers are thermosetting and thermoplastic resins.

The main function of the matrix is to hold the reinforcements and bond them in an orderly pattern. The matrix also transfers the applied loads among the reinforcements, since they are discontinuous.

Thermoplastic resins are developing strongly but are not yet widely used as structural matrix composite. They are processed by heating up the amorphous thermoplastics to the glass transition temperature or up to the melting temperature for semi-crystalline thermoplastics, and consolidated during cooling. The transformation is reversible. The thermoplastic resins used in composite aircraft include polyamides (PA), polyetherimide (PEI), polypropylene (PP), polyphenylene sulfides (PPS), polyetheretherketone (PEEK), polyetherketoneketone (PEKK).

Thermosetting resins are the products most used as structural matrix composites. They account for more than 80% of all matrices in reinforced plastics and essentially all matrices used in advanced composites [8]. The most widely used thermosetting resins are the unsaturated polyesters, vinylester and phenolic resins. For high performance composites, the most common are the epoxy, bismaleimide and polyimide resin [11]. They are liquid or viscous liquids with viscosities below those of thermoplastics, which is advantageous because there is a greater ease of impregnation of the reinforcing, and harden after a cure cycle. The transformation is irreversible.

When selecting a thermoset resin, consideration is usually given to tensile strength, modulus and strain, compression strength and modulus, notch sensitivity, impact resistance, heat deflection temperature or glass transition temperature ($T_g$), flammability, durability in service, material availability, ease of processing, and price [8].

Although the amount of epoxies used in reinforced plastics is small in comparison to the volume of polyester used, for more demanding structural uses, epoxy resins are the most adequate. Even though their cost is about four times higher than that of polyester resins, epoxy resins provide a unique combination of properties that are unattainable with other thermoset resins combined with extreme processing versatility. Epoxy resins have excellent mechanical performance, such as good environmental resistance and high toughness and are easily processed. Other advantages of epoxy

resins are abrasion and chemical resistance, good adhesion properties, great dimensional stability, low water absorption and a good range of operating temperatures.

These resins have good mechanical properties but are sensitive to shocks. To improve the toughness and impact resistance of thermosetting resins, a certain percentage of thermoplastic resin can be incorporated, such as CTBN rubber.

#### 1.3.1.3 Prepreg and laminates

A prepreg consists of a reinforcement material pre-impregnated with a resin matrix in controlled quantities. Using prepregs during the final composite fabrication process can offer significant advantages. Prepregs usually have very precisely controlled fibre-resin ratios, highly controlled handling, self-adhesion layers when piling up, controlled resin flow during the cure process, and, in some processes, better control of fibre angle and placement.

Woven fabric prepregs are one of the most widely used fibre-reinforced resin forms. The prepreg can be processed through various processes, depending on its final application. The following figure (Figure 1.10) shows some of the most common manufacturing processes using prepreg.

Vacuum bag and autoclave processing are the two main methods for the manufacture, from prepreg, of components of large and complex geometries. The processing method is determined by the quality, cost and type of component being manufactured. The autoclave process, adequate for the manufacturing of components subject to the most stringent requirements of mechanical performance and quality, as is the case of aerospace industry, should be highlighted because it was the process used to manufacture the material used in this work.

**Table 1.2** Comparison between vacuum bag and autoclave processing [22]

| | Component | | Processing Costs | |
|---|---|---|---|---|
| **Process** | **Quality** | **Section thickness** | **Equipment cost** | **Cure cycling time** |
| **Vacuum Bag** | Good | Thin | Moderate | Short |
| **Autoclave** | Excellent | Thick | High | Long |

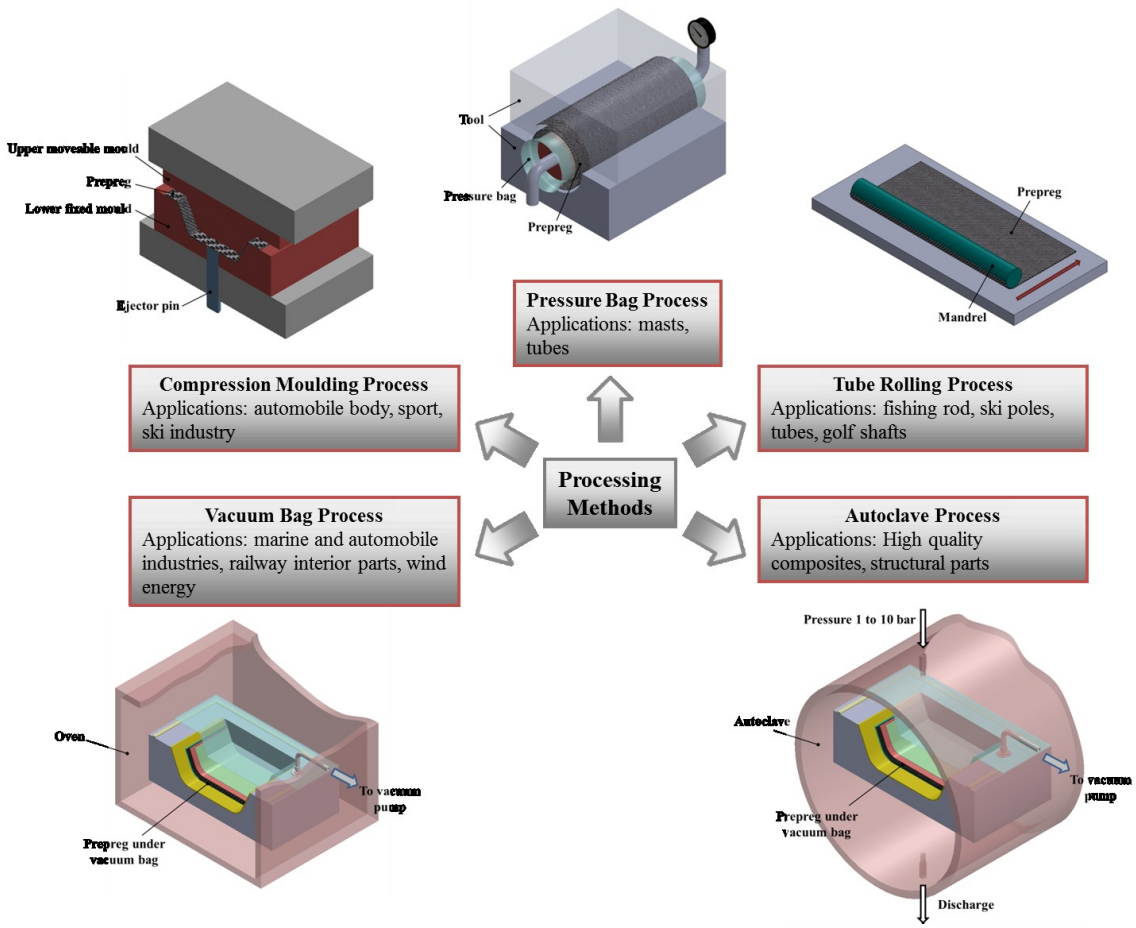


**Figure 1.10** Prepreg processing methods [22]

The laminates obtained consist of a stack of single plies each having a specific orientation with respect to a common reference to the layers and designated as the reference of the laminate. The choice of the stacking sequence and especially the orientation will provide specific mechanical properties. Stacking sequence of laminates can be:

- Balanced: A laminate in which the individual plies occur in +/- pairs at various angles except for 0° and 90°. The pairs must be the same thickness but they are not required to be in any particular order.

- Symmetrical: A laminate in which the layers below the midplane form a mirror image of the stacking sequence of the layers above the midplane. Symmetrical laminates may have an odd number of layers or an even number of layers.

- Crossply: A laminate in which the ply orientations are oriented at right angles to each other, with ply orientations limited to 0° and 90° only. It is usually best to arrange stacking sequences with fibres oriented in different directions.

The angle value represents the direction of the warp fibres.

The composite materials used, in the form of laminates, in the various surveys are essentially epoxy matrix reinforced with glass, carbon or Kevlar fibres.

**Table 1.3** Composite laminates used in literature

| Material | Refs. |
|---|---|
| CFRP/epoxy | Jain and Yang [23]; Stone and Krishnamurthy [24]; Lin and Chen [25]; Chen [26]; Persson et al. [27]; Piquet et al. [28]; Zhang et al. [29, 30]; Lachaud et al. [31]; Enemuoh et al. [32, 33]; Murphy et al. [34]; Won and Dharan [35]; Tsao and Hocheng [36–42]; Davim and Reis [43, 44]; Wang et al. [45]; Durão et al. [46–54]; Hocheng and Tsao [55]; Hamdoun et al. [56]; Sardinas et al. [57]; Fernandes and Cook [58, 59]; Davim et al. [60]; Tsao [61–68]; Zitoune and Collombet [69]; Campos Rubio et al. [70, 71]; Karnik et al. [72]; Gaitonde et al. [73]; Faraz et al. [74]; Marques et al. [75]; Rawat and Attia [76, 77]; Shyha et al. [78, 79]; Iliescu et al. [80]; Curnik [81]; Krishnamoorthy et al. [82]; Rahmé et al. [83]; Tsao and Chiu [84]; Lazar and Xirouchakis [85]; Sedlacek and Slany [86]; Krishnaraj et al. [87] |
| GFRP/epoxy | Inoue et al. [88]; Mathew et al. [89]; Lin and Shen [90]; Wang et al. [45]; Zhang et al. [29]; Singh et al. [1, 91]; Ramkumar et al. [92–94]; Khashaba [95]; Capello [96]; El-Sonbaty et al. [97]; Bhatnagar et al. [98]; Langella et al. [99]; Krishnaraj et al. [100]; Singh and Bhatnagar [101]; Durão [48],[49]; Arul et al. [4, 102–104]; Campos Rubio et al. [70]; Palanikumar and Davim [105]; Abrão et al. [5]; Faria et al. [106]; Palanikumar et al. [107]; Srinivasa Rao et al. [108]; Ariffin et al. [109]; Latha and Senthilkumar [110]; Khashaba et al. [111, 112]; Kilickap [113, 114]; Mishra et al. [115, 116]; Baskaran et al. [117]; Palanikumar [118, 119]; Curnik [81]; Latha et al. [120]; Sudha et al. [121] |
| GFRP/polyester | Caprino and Tagliaferri [122]; Dini [123]; Khashaba [95, 124]; Davim et al. [125, 126]; Mohan [2, 127]; Varatharajan et al. [128]; Davim and Mata [129]; Sedláček and Humár [130]; Işik and Ekici [131]; Jayabal and Natarajan [132, 133]; Schulze et al. [134] |
| GFRP/phenolic | Velayudham et al. [135, 136] |
| KFRP/epoxy | Bhattacharyya and Horrigan [137]; Shuaib et al. [138] |

Some authors compared different matrices in order to assess their influence on the output factors of the drilling experiments.

Davim et al. [125] evaluated the influence of the matrix on the specific cutting force, the delamination factor and surface roughness, as they compared two materials reinforced with 65% of glass fibre namely, a matrix of unsaturated polyester (Viapal VUP 9731), and a propoxylated bisphenol A-fumarate polyester (ATLAC 382-05). They observed that the three parameters have lower values when processing the matrix of unsaturated polyester.

Khashaba [95] found that using polyester matrix composite the delamination at hole entrance increases with increasing cutting speed and peel off decreases. When using the epoxy matrix materials, the delamination decreases with increasing cutting speed. For the same form of fibre, epoxy matrix materials have less delamination than the polyester matrix. However, both have nearly equal thrust forces.

Varatharajan et al. [128] compared a thermoset and a thermoplastic matrix to study their influence on material response, comparing the tensile, flexural and interlaminar properties of woven roving fibre reinforced composites. They found that thermoset composites presented higher order thrust force which promotes more machining induced damage such as debonding and delamination. Thermoplastics experienced lower thrust force, thus less damage is expected. Moreover, the increased temperature in the cutting zone leads to minimizing tool wear.

### 1.3.2 Drilling of Composite Materials

In machining of composites, the behaviour of the material is non-homogeneous, anisotropic, depends on the different properties of reinforcement materials and matrix and the corresponding volume fractions [136]. Thus, the efficient choice of cutting conditions is difficult due to the coexistence of two phase materials with different mechanical properties (hard abrasive fibres and soft matrix). The difficulty is enhanced by the relative complexity of variable fibre orientation and stacking sequence of layers [91]. The mechanism of material removal is different when compared with metals [3, 129, 139, 140]. The machining of composite materials requires that the conventional machining processes (commonly used in metalworking) are properly adapted, with regard to the selection of the tool and cutting parameters for which they can ensure the accuracy and efficiency of the process and its final result.

When using the same tool to perform a large number of holes, the wear can also be a problem since the cutting force increases with increasing wear, increasing the possibility of occurring delamination [25].

There are countless research on the drilling of composites, focusing on the effect of material and geometry of tools and cutting parameters on cutting force and torque, on the damage, on the quality of the hole obtained and the tool wear in conventional drilling process. These research studies will be further described later in this chapter.

In the field of printed circuit boards (epoxy matrix composites reinforced with glass fibre) there are several studies. In these cases it is essentially a micro-drilling process, in which the increase in cutting speed and the reduced diameter of the tool led to the need for more research into the process with regard, for example, the relationship between cutting force and surface roughness, tool wear or quality of the hole obtained [141]. Inoue et al. [88] had already investigated the relationship between the internal damage around the hole and the number of holes produced [Spindle speed: 20 000 - 80 000 rpm; $d$ = 1 mm]. Kao [141] evaluated the effect of coating (MoS2-Cr) on the tools wear in drilling of high-speed [Spindle speed: 99 700 rpm; $d$ = 0.3 mm]. Wang et al. [45] also used micro-drilling process to carry out a study on vibration drilling [Spindle speed: 22 000 rpm; $d$ = 0.5 mm].

However, there are few studies whose attention is high speed drilling. Durão [49] focused mainly on the tool geometry ($d$ = 6 mm) in is research about the conventional process of drilling three types of fibre reinforced plastics (glass, carbon and hybrid glass and carbon) in epoxy matrix. Despite the visible limitations, he has acknowledged the need to recommend, as future work, the study of the effects of high-speed drilling of composite materials.

#### 1.3.2.1 High Speed Drilling

With regard to high speed drilling, the following studies were found in literature review:

- Lin and Chen [25] studied the effect of increased speed (9 550 - 38 650 rpm) in epoxy matrix composites reinforced with carbon fibre on the cutting force, the torque, the tool wear and quality of the holes obtained. Two different tool geometries ($d$ = 7 mm) were used, namely multifaceted drill and twist drill. They concluded that the effect of increasing cutting speed is different for both geometries. The average thrust force increases for both drills but the torque slightly increases for a multifaceted drill, while it decreases for the twist drill. Tool wear increases significantly as cutting speed increases. However, an acceptable hole quality was obtained because relatively small feed rates were used (0.03 - 0.07 mm/rev). Finally, they found no differences in performance of both geometries drills.

- Lin and Shen [90] made a similar study in drilling glass fibre reinforced composite (epoxy matrix), using the same tool geometries and tool diameter. The cutting parameters had also the same values. The main conclusions drawn were that delamination was slightly improved by using multifaceted drills, but this geometry worn out much faster than twist drills as cutting speed increases. Thrust force is affected by all input parameters: cutting speed, feed rate, number of holes drilled and tool geometry, and increases as tool wear increases at high speed. The damage at entrance increases seriously with cutting speed increase for both tool geometries.

- Krishnaraj et al. [100] investigate the cutting characteristics of different tool geometries, and established relations between spindle speed (14 000 - 19 000 rpm) and feed rate (0.02 - 0.08 mm/rev) on thrust force and surface roughness. They found that the use of special geometries can improve the hole quality. The main conclusions about cutting parameters were that the feed rate is strongly influent on thrust force and surface roughness, and spindle speed increasing reduces the surface roughness.

- Gaitonde et al. [73] performed the study of the effects of process parameters (cutting speed, feed rate and point angle) on delamination using epoxy reinforced with carbon fibre [Spindle speed: 4 011, 763, 38 197 rpm; Feed rate: 0.03 - 1.5 mm/rev; $d$ = 5 mm; Point angle: 85º, 115º, 130º]. The observations shown that high speed cutting plays a major role in reducing damage at the entrance of the hole. The delamination factor is lower with lower feed rate and point angle.

- Campos Rubio et al. [70] investigated the effect of cutting parameters (cutting speed and feed rate) and tool geometry on the delamination of epoxy reinforced with glass fibre, using high performance drilling [Spindle speed: 4 000 - 40 000 rpm; Feed rate: 0.25 - 2.25 mm/rev; cemented carbide tool, $d$ = 5 mm]. The drill geometries used were two twist drills with different point angle and “Brad & Spur” drill. They found that delamination decreases with spindle speed increasing and increases with feed speed for spindle speed values up to 8 000 rpm. For the highest spindle speed (40 000 rpm) feed does not seem to have appreciable influence on delamination. The geometry that led to less delamination was the “Brad & Spur”. The main conclusion was that higher spindle speed should be used when seeking to higher material removal rate, because delamination is minimal, irrespectively of the feed speed employed.

- Another study conducted by Campos Rubio et al. [71], this time using carbon/epoxy composite as workpiece material with similar parameters and tool geometries as the previously referred [Spindle speed: 4 000 - 40 000 rpm; Feed rate: 0.25 - 2.25 mm/rev; cemented carbide tool, $d$ = 5 mm], resulted in similar conclusions. Therefore, the same behaviour was found for CFRP as for GFRP.

- Karnik et al. [72] carried out the investigations on delamination analysis in high speed drilling developing an artificial neural network model considering spindle speed (4 000 - 40 000 rpm), feed rate (0.025 - 2.25 mm/rev) and point angle (85º - 130º) as input factors. The workpiece material was carbon/epoxy composite and the tools were cemented carbide twist drills ($d$ = 5 mm). The main effects of the variables were analysed independently, i.e., keeping the other variables constant. It was found that all parameters have influence on the delamination, being the best selection to minimize damage a combination of high spindle speed and low feed rate and point angle. They also observed that employing a 40 000 rpm is advantageous since there is a reduction of the delamination at entrance of the holes.

- Rawat and Attia [76, 77] investigated the wear mechanisms of tungsten carbide twist drills during high speed drilling of CFRP epoxy composites. Using the concept of machinability maps, established the effect of speed (1 500 - 15 000 rpm) and feed rate (0.02 - 0.2 mm/rev) on the damage mechanisms. The tool diameter was $d$ = 5 mm and the point angle 118º. The observations showed that the effect of thrust force is significant on tool wear and quality of the final hole, and the delamination increases with increased tool wear. From the machinability maps, they concluded that the optimal cutting conditions for minimum damage and maximum productivity are $S$ = 8 500 rpm and $f$ = 0.1 mm/rev.

- Iliescu et al. [80] evaluated the thrust force in high speed drilling of carbon/epoxy composite material and developed a model correlating the thrust force, the drilling parameters and the tool wear. The high speed drilling conditions were obtained using $S$ = 12 000 rpm and $f$ = 0.05 mm/rev, and the tools employed were uncoated and diamond-coated carbide twist drills ($d$ = 6 mm). They observed that the thrust force increases with the tool wear; the spindle speed does not have much influence on thrust force. The conclusions drawn indicate that to achieve a greater number of holes without the occurrence of the delamination process parameters should be $S$ = 9 000 rpm and $f$ = 0.05 mm/rev and the tool should be diamond-coated. However the authors do not emphasize significant differences in the performance of both coated and uncoated drills.

- Krishnaraj et al. [87] investigated the high speed drilling of thin CFRP laminates ($t$ = 2 mm) by varying the drilling parameters, namely spindle speed (12 000, 16 000 and 20 000 rpm) and feed rate (0.01, 0.05, 0.1 and 0.3 mm/rev) to determine optimum cutting conditions. The tool diameter was $d$ = 5 mm and the point angle 118º. The observations led to the conclusion that the optimal parameters were $S$ = 12 000 rpm and $f$ = 0.137 mm/rev. Besides, feed rate has high influence on thrust force, push-out delamination and hole diameter. Using higher feed rates results in holes closer to the nominal diameter. Neither spindle speed nor feed rate showed influence on the peel-up delamination and no significant delamination could be observed till 30 holes.

It must be pointed that in all of these research works the workpiece thickness was kept constant in all trials, and have never been considered as a process variable.

#### 1.3.2.2 Cutting Tools

Since the focus of the current work is the carbon fibre reinforced composite, from this point the literature survey will be exposed based on studies conducted with the use of this material. This is due to the fact that, from the analysis of all the literature consulted, no significant differences were found about the behaviour and influence of the process parameters on the thrust force, torque and quality of the holes produced, specially the delamination damage.

The twist drills are the most commonly used as a cutting tool. The tool geometry influences the quality of the hole, in particular by the degree of delamination. The material of the tool equally affects the process of drilling of composite materials to the extent that the larger the tool wear, the greater the thrust force, and consequently there is greater likelihood of damage. The drilling of composite materials requires the use of cutting tools with high resistance to wear and abrasion resistance in particular. This is due to the nature of the reinforcements which are highly abrasive. Several authors confirm this and showed that the wear of high speed steel tools is greater than that of carbide tools [25, 90]. Likewise, the wear of carbide tools is greater than that of polycrystalline diamond (PCD) coated tools and better quality holes are produced [24, 80]. The main disadvantage of using PCD tools is its high cost which compromises their use in industrial terms. In fact, the cost / tool wear / hole quality obtained relation does not justify their use when compared with the cemented carbide tools.

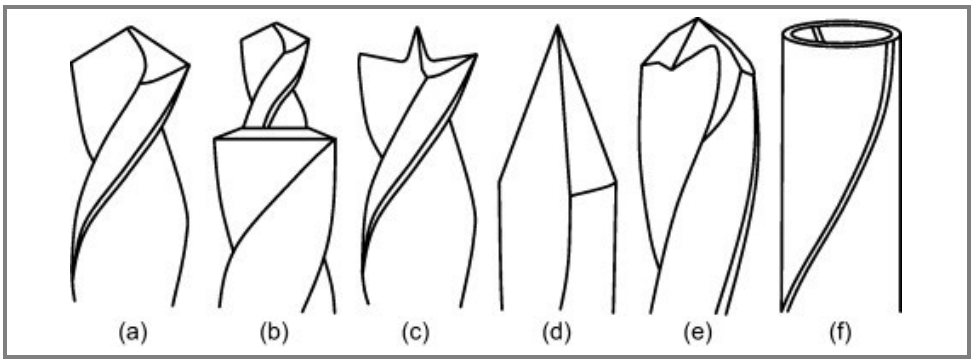


**Figure 1.11** Tools used on CFRP drilling: **a)** standard twist drill; **b)** step drill; **c)** W-shape drill; **d)** straight flute drill; **e)** multifaceted drill; **f)** core drill [134]

**Table 1.4** Twist drill materials found in literature for drilling of carbon composite laminates

| Geometry | Drill material | Refs. |
|---|---|---|
| Twist drill | HSS | Chen [26]; Enemuoh et al. [32]; Zhang et al. [30]; Tsao and Hocheng [36, 37, 39, 42, 142]; Davim and Reis [43]; Wang et al. [45]; Hocheng and Tsao [55]; Curnick [81]; Sedlacek and Slany [86] |
| | Uncoated carbide | Chen [26]; Piquet et al. [28]; Lin and Chen [25]; Dharan and Won [143]; Won and Dharan [35]; Davim and Reis [43, 44]; Wang et al. [45]; Durão et al. [46, 47, 50–53]; Hamdoun et al. [56]; Sardinas et al. [57]; Davim et al. [60]; Campos Rubio et al. [71]; Gaitonde et al. [73]; Karnik et al. [72]; Rawat and Attia [76, 77]; Faraz et al. [74]; Marques et al. [75]; Shyha et al. [78]; Rahmé et al. [83]; Lazar and Xirouchakis [85]; Iliescu et al. [80]; Krishnaraj et al. [87] |
| | Coated carbide | Shyha et al. [78]; Iliescu et al. [80] |

**Table 1.5** Other drill geometries (and materials) for drilling of carbon composite laminates used in literature

| Geometry | Drill material | Refs. |
|---|---|---|
| Multifaceted drill | HSS | Curnick [81] |
| | Carbide | Lin and Chen [25]; Lazar and Xirouchakis [85] |
| Step drill | HSS | Hocheng and Tsao [55]; Tsao [66] |
| | Carbide | Durão et al. [46, 53]; Marques et al. [75]; Shyha et al. [78, 79]; Durão et al. [53] |
| | Coated carbide | Shyha et al. [78] |
| W-shape drill | HSS | Tsao and Hocheng [37, 41, 42]; Hocheng and Tsao [55]; |
| | Carbide | Davim and Reis [44]; Durão et al. [46, 50, 53]; Campos Rubio et al. [71]; Marques et al. [75]; Krishnamoorthy et al. [82] |
| Straight-flute drill | Carbide | Murphy et al. [34]; Davim and Reis [43]; Durão et al. [46, 53]; Fernandes and Cook [58, 59]; Faraz et al. [74]; Marques et al. [75]; Lazar and Xirouchakis [85] |
| | Coated carbide | Murphy et al. [34] |
| Core drill | Polycrystalline diamond (PCD) | Tsao and Hocheng [38, 40, 42]; Hocheng and Tsao [55]; Tsao [61] |
| Step core drill | Carbide/ Polycrystalline diamond (PCD) | Tsao [64, 65, 67, 68]; Tsao and Chiu [84] |
| Saw drill | HSS | Tsao and Hocheng [37, 38, 42]; Hocheng and Tsao [55]; Tsao [62, 63] |

Lin and Chen [25] found that the multifaceted drill is no superior in performance to twist drill. However, the multifaceted drills are worn out much faster than twist drills as spindle speed increases.

Piquet et al. [28] compared the performance of twist drills with a specific tool whose reference dimensions are given by ISO 3002-2: E66-504. The tool used, recommended over the diamond drills because of its cost, is made of tungsten carbide (micro grain) K20 class and has shown satisfactory results, better than the twist drill.

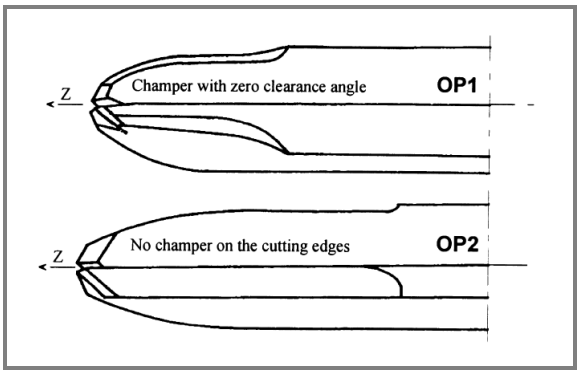


**Figure 1.12** Specific cutting tool geometry defined by Piquet et al. [28]

Murphy et al. [34] studied the effect of coatings on the performance of tungsten carbide drills when drilling carbon fibre reinforced composites. The comparison was made between two coated drills, namely titanium nitride (TiN)-coated and diamond-like carbon (DLC)-coated, and an uncoated drill. The coatings were not found to reduce either tool wear or workpiece damage.

Tsao and Hocheng [36] studied an analytical approach to identifying the optimal range of chisel edge length with respect to drill diameter, and verified that controlling the ratio of chisel edge length, medium to large holes could be drilled at higher feed rate without delamination damage.

Davim and Reis [43] employed analysis of variance (ANOVA) to investigate the cutting characteristics of CFRP using helical flute high speed steel (HSS) and cemented carbide (K10) drills and a four-flute cemented carbide (K10) drill, and concluded that the helical flute K10 is the one that presents better performance with less damage on the composite laminate. The carbide drills showed almost null wear, but not the HSS drill. The same authors [44] investigated the cutting characteristics of CFRP comparing the helical flute cemented carbide (K10) with a "Brad & Spur" (W-shape) K10 drill, verifying that the "Brad & Spur" drill produces less delamination than the helical flute.

Wang et al. [45] found that the thrust force increases with the increasing of axial displacement when a HSS drill is employed and the thrust force is lower when using a carbide drill than a HSS drill. The conclusion is that the carbide drill is more appropriate for drilling fibre reinforced plastics.

Tsao and Hocheng [37] observed that the quality of the hole and delamination are reduced using W drill and saw drill geometries when compared to twist drill geometry.

Hocheng and Tsao [55] compared the effects of five different HSS drill bits, namely twist drill, saw drill, W-shape (candlestick) drill, core drill and step drill, on the onset of delamination. They found that the special geometries can be operated at larger feed rate without delamination damage when compared to the twist drill.

Campos Rubio et al. [71, 144] compared the effects of three different tools, namely two cemented carbide twist drills with different point angle (118º and 85º) and a "Brad & Spur" (W-shape) drill, on the induced damage and concluded that the "Brad & Spur" geometry and the twist drill with lower point angle produced less delamination than the twist drill with higher point angle.

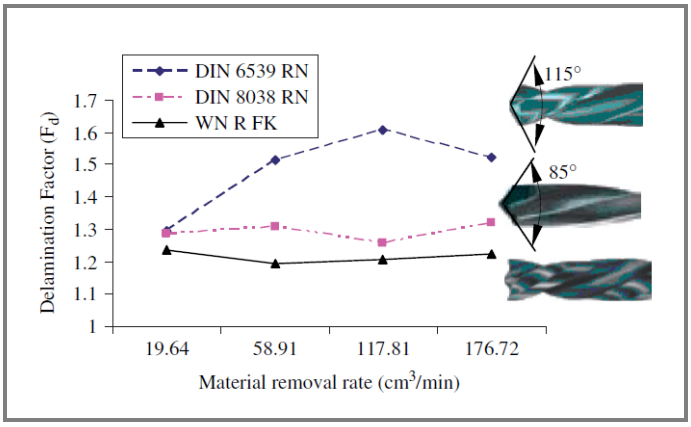


**Figure 1.13** Comparison of the effect of material removal rate on $F_d$ measured at the drill entrance ($S$ = 40 000 rpm) [71, 144]

Marques et al. [75] verified that the choice of a dedicated tool for drilling carbon fibre reinforced laminates, namely a special step drill bit, can be useful to reduce delamination. However, the special step tool tested does not yet show a significant advantage when compared to the commercial tools available. Thus, further developments are needed.

Shyha et al. [78] compared the performance of uncoated and TiN-coated step drill and twist drill and observed that the drill geometry was, along with feed rate, the main contributing factor for tool wear and thrust force. In terms of tool life, the best results were obtained for the uncoated step drill, while the worst results were found for the TiN-coated conventional twist drill. The type of damage was very similar for all tool geometries.

Tsao and Chiu [84] found that using compound core-special drills is more advantageous when drilling CFRP, since a reduction of thrust force, delamination, chip clogging occurs with higher chip removal.

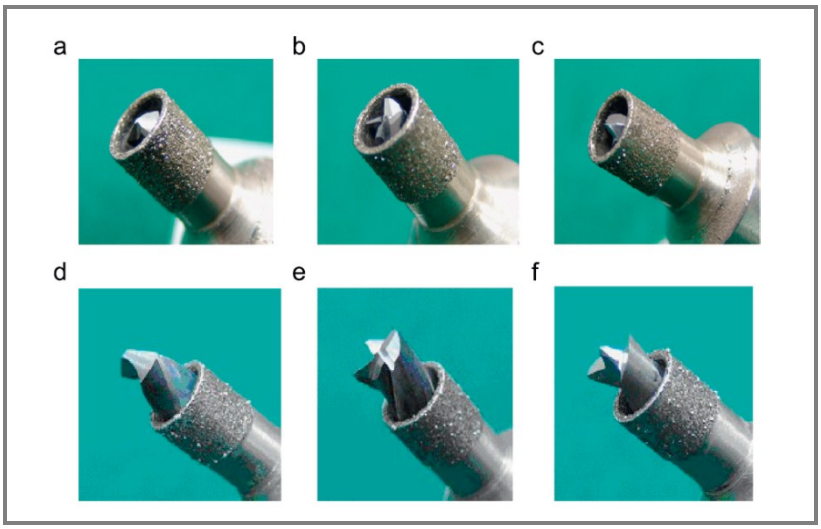


**Figure 1.14** Photographs of various types of the compound core-special drills: **a)** Core-twist drill, **b)** core-saw drill, **c)** core-candlestick drill, **d)** step-core-twist drill, **e)** step-core-saw drill, **f)** step-core-candlestick drill. [84]

Curnick [81] related the multifaceted drill geometry with the twist drill geometry and observed that, using the same cutting parameters, the multifaceted drill presents less damage on the hole produced than the HSS drill when drilling carbon fibre reinforced composite material.

Lazar and Xirouchakis [85] compared three different drills, namely a straight flute drill, a multifaceted drill and a twist drill, and concluded that the tool geometry is one of the most important parameters in order to reduce thrust force and point to multifaceted drill as being the tool that offers better performance. They also emphasize the need to extent the investigation to the high-speed domain.

Durão et al. [46, 53] studied the differences of various tool geometries (twist drill, straight flute drill, "Brad" (W-shape) drill and step drill) and concluded that all tool geometries are appropriate for drilling CFRP, but they all need further developments in order to achieve free delamination drilling. They observed that higher feed has a considerable impact on "Brad" and straight flute drills, while twist and step drills did not return significant changes. For minimal delamination, the use of twist drill was recommended.

#### 1.3.2.3 Cutting Parameters

The research for the optimal parameters for drilling carbon reinforced composite materials aims at minimizing the surface roughness and the thrust force while maintaining tool life economically viable. Several studies fit this assumption.

The most influential cutting parameters in the drilling process are the spindle speed (*S*) and the feed rate (*f*). The quality of the hole depends on these parameters and is the main factor to take into account when drilling of composites. An inappropriate choice of these parameters can lead to unacceptable degradation of the material [122]. In all the literature survey about conventional drilling, the authors found that the damage is heavily dependent on feed rate, that using small feed values produce less damage, and therefore better quality holes. The spindle speed was considered of minor influence.

Enemuoh et al. [32], presented an approach, based on a combination of Taguchi techniques and multi-objective optimization criterion, to select cutting parameters for damage free drilling. Two case studies were made to demonstrate the effectiveness of the approach. It was concluded that, in general, high speed and low feed rate is the recommended combination.

Davim and Reis [43] studied another approach to select cutting parameters, based on a combination of Taguchi techniques and on the analysis of variance. The conclusions found were that the delamination factor increases with both spindle speed and feed rate, and the spindle speed is the most significant factor. Using the same approach, in another study [44], the authors found that the feed rate was the most significant factor on power and specific cutting force and cutting speed is the most significant factor on delamination. In both studies it was concluded that damage is bigger for higher cutting speed and feed.

Another approach based on Taguchi techniques and on the analysis of variance was carried out by Tsao and Hocheng [37], considering as input factors the feed rate, the spindle speed and the tool diameter. It was observed that the largest contribution to the overall performance was made by feed rate and tool diameter, and the spindle speed showed low significance.

Sardinas et al. [57] discussed the selection of cutting parameters for drilling composite carbon fibre, using multi-objective optimization approach, in order to improve two objectives: material removal rate and delamination. The models developed show that both feed rate and speed have influence on the damage. Analysing the outcomes of the optimisation process, they concluded that higher material removal rate implies higher delamination.

Tsao [61] investigated the interactions between the input factors (spindle speed, feed rate, tool thickness and grit size of diamond) in drilling carbon fibre reinforced plastic with a core drill, using Taguchi methodology. The conclusions were that thickness and feed rate were the most

significant factors for the overall process and, in general, high speed and low feed were recommended for delamination-free. Similar study was made by this author [64, 65] using step-core drills, and the significant factors found were the diameter ratio, feed rate and spindle speed. Delamination increases with decreasing diameter ratio and spindle speed, and increasing feed rate.

Shyha et al. [78] conducted a study to ascertain the influence of drilling process variables (cutting speed and feed rate) and drill geometry ($d$ = 1.5 mm) on tool life and hole quality, using Taguchi methodology with analysis of variance (ANOVA). Drill geometry and feed rate was found to be the most significant parameters on measured outputs. Cutting speed and feed rate had the most significant effect on torque.

Sedlacek and Slany [86] investigated the effect of drilling parameters on delamination using design of experiments (DOE) with input variables being fed rate, tool geometry, cutting speed and tool wear. The sequence of significant factors obtained was: feed rate, tool wear, tool geometry and cutting speed.

Curnick [81] carried out an experimental investigation in drilling carbon fibre reinforced polymer using a series of controlled parameters, namely spindle speed and feed rate. They found that with increasing feed rate, delamination increases and with increasing spindle speed, delamination reduces. To further improve performance, their advice is to applying a variable feed reducing it prior to drill exit.

With regard to high-speed machining, in general, the results obtained to date do not differ much from those obtained for conventional drilling. This is due to the fact that productivity is always increased only by increasing the spindle speed while maintaining relatively low values of feed rate. It will be interesting to know the effect not only of increasing spindle speed for values considered high speed (typically with $V \geq 200$ m/min) but also of the increase in the feed rate and consequent reduction of machining time. Only then can it be effectively be defined as a process of high productivity / high profitability. Nonetheless, the authors that used higher values for feed rate observed some changes in the drilling mechanisms since for high spindle speed, namely $S$ = 40 000 rpm, the increase in feed rate did not result in significant increase of delamination and verified a reduction in the delamination at entrance [70–73]. When high speed drilling carbon composites, one of the most important factors that influence the thrust force is the tool wear. The dimensional accuracy of the drilled hole is better when using high feed rate.

#### 1.3.2.4 Damage

The mechanical and thermal demands experienced by the composite material during the drilling operation usually generate damage. There are several problems associated with drilling of composite materials, namely, the existence of intralaminar cracking, tearing of fibres, damage from overheating and delamination, which significantly reduce the materials resistance to either static loading or fatigue. The strength of riveted or bolted joints can be influenced by the quality and accuracy of the holes [27, 58]. The most important damage is the delamination as it causes a decrease of the mechanical properties of the components of an assembly and, consequently, a reduction in their reliability when in use. It can also create problems with regard to the tolerances of the assembly. The most common defects that appear in literature are:

***Fibre breakage*** – individual fibres broken, either due to cutting or can be caused by excessive fibre curvature at sharp radii corners.

***V*oids** – are due to inclusion of air, solvents or other contamination during mixing of resin. Can act as stress concentrations and will have an effect on some of the mechanical properties, i.e., lower transverse and through-thickness tensile, flexural, shear and compression strengths.

***Porosity*** - similar to voids, except being very small in size and often more dispersed. Void content considered negligible if less than 1 - 2%.

**Delamination** – separation of the individual plies within the laminate. This type of defect typically occurs when drilling and/or in-service due to impacts, and can have a severe detrimental effect on mechanical properties, particularly in compression.

Delamination mechanism is characterized by the separation of adjacent composite plies. It is distinguished by the formation of interlaminar cracks in the material. This damage occurs when drilling particularly at hole entrance (peel-up delamination at entrance) and hole exit (push-out delamination at exit). At the entrance of the drill in the composite spindle movement combined with the inclination of the helix tends to move the material upwardly. The material spirals up before it is machined completely. The parameter defining the initial delamination at the exit of the drill is the intensity of the thrust force. Thus, all parameters that influence the thrust force will implicitly influence the delamination. The spindle speed is null at the tool centre (tip) and not very high at the web. The material located at the core of the drill bit undergoes an axial force, which is pushed by deformation before being sheared by the main cutting edges. Particularly found in drilling on the outskirts of free surfaces of composite, delamination accompanied by complete tear of fibres of plies is called spalling.

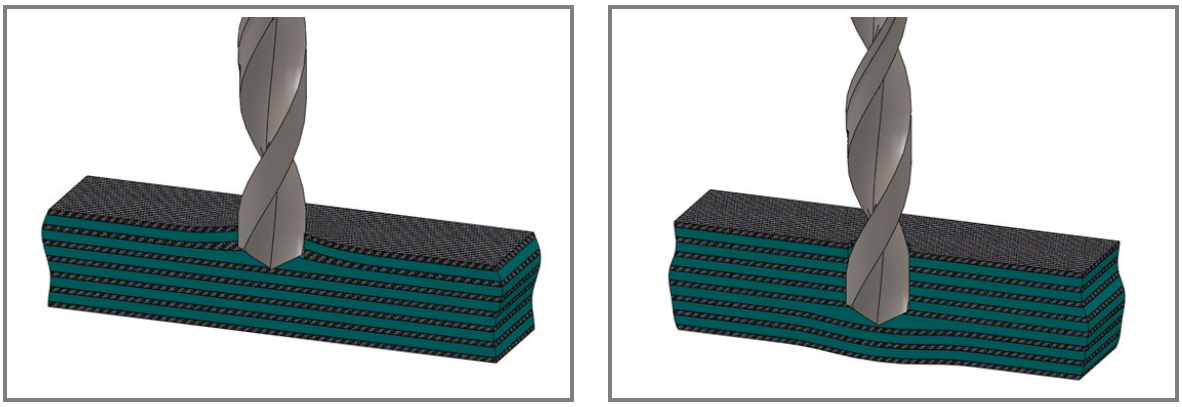

**a)** **d)**

**Figure 1.15** Mechanism of: **a)** peel-up delamination at entrance; **b)** push-out delamination at exit [145]

There are several methods for monitoring and analysis (quantitative and qualitative) of the damage. The different methods can be destructive or non-destructive and allow visualization or measurement of defects and damage of composite materials. Most methods of non-destructive testing (NDT) detect surface defects (for instance, visual examination). The NDT methods to detect defects in volume (e.g., porosity, voids or inclusions, delamination) are less numerous: radiography, ultrasonic scan, computerized tomography. These techniques allow obtaining the needed information for measuring the delamination factor.

Durão et al. [47] studied the use of different NDT methods, namely radiography and ultrasonic C-Scan, and observed that the delamination measured presented unlike values, denoting the dissimilar analysis.

Tsao and Hocheng [142] compared the computerized tomography and ultrasonic C-Scan, and verified that the drilling induced delamination of CFRP can be visualised and measured. The obtained results indicate that both NDT methods perform similarly.

Gao and Kim [146] presented a comparison between major inspection techniques on impact damage in CFRP. This can also be useful when considering delamination damage:

**Table 1.6** Comparisons of sensitivity to impact damage in CFRPs [146]

| Damage | De-ply | Fractography | Visual inspection | Ultrasonic | Radiography |
|---|---|---|---|---|---|
| *Damage type:* | | | | | |
| Delamination | Good | Very good | Good | Good | Fair |
| Fibre breakage | Fair | Good | Fair | Very poor | Good |
| Matrix cracks | Fair | Fair | Fair | Very poor | Good |
| Surface defects | Good | Good | Very good | Poor | None |
| *Damage size:* | Good | Good | Fair | Good | Good |
| *Damage location:* | | | | | |
| Distance from surface | Good | Very good | Fair | Good | Good |
| **Damage** | **Thermal imaging** | **Acoustic emission** | **Laser-based optical im.** | **Microwave** | **Eddy-current testing** |
| *Damage type:* | | | | | |
| Delamination | Fair | Poor | Fair | Very Poor | Very Poor |
| Fibre breakage | Poor | Poor | Poor | Poor | Good |
| Matrix cracks | Poor | Poor | Poor | Poor | Poor |
| Surface defects | Poor | Very Poor | Poor | None | Poor |
| *Damage size:* | Fair | Very Poor | Poor | Fair | Fair |
| *Damage location:* | | | | | |
| Distance from surface | Poor | Very Poor | Very Poor | Very Poor | Poor |

In this thesis, several NDT methods for the analysis of defects and damage were used such as optical observation, X-ray radiography, and scanning electron microscopy (SEM).

The NDT tests allow having an image of the hole and associated damage. However, the extent of this damage must be measured and evaluated quantitatively, in order to assess the effect of the input parameters on the delamination.

The delamination factor ($F_d$), proposed by Chen [26], is the most widely used to characterize the damage on the workpiece material caused by peel-up delamination at entrance and push-out delamination at exit of the drill. The delamination factor is calculated from the ratio of the maximum diameter $D_{max}$ in the damage zone to the hole nominal diameter $D_0$, as shown in figure:

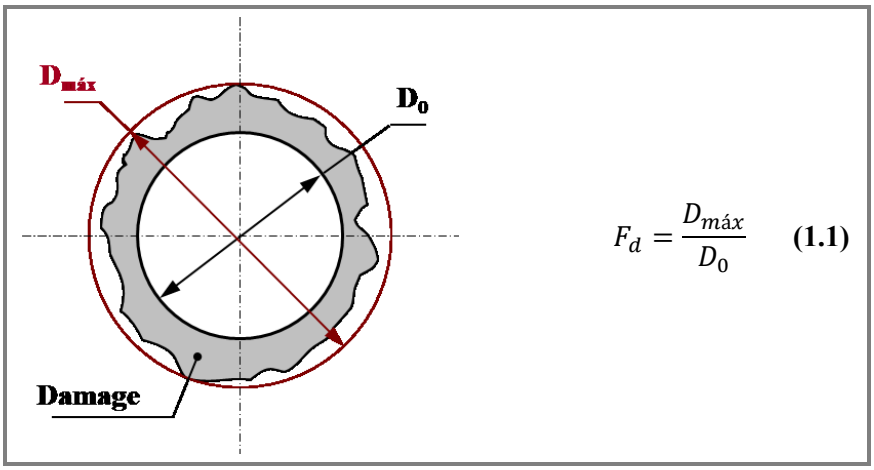


**Figure 1.16** Schematic and equation for the delamination factor

Davim et al. [60], proposed a new adjusted delamination factor ($F_{da}$), to be used mainly in CFRP when delamination does not possess a regular pattern. The brittle nature of carbon fibres causes delamination to present an irregular shape, containing breaks and cracks. Therefore, this new model measures not only the size of the crack contribution (conventional delamination factor) as it adds the damage area contribution. The adjusted delamination damage is given by equation:

$$F_{da} = F_d + \frac{A_d}{(A_{max} - A_0)}\left({F_d}^2 - F_d\right) \quad \textbf{(1.2)}$$

where $A_d$ is the damage area, $A_{max}$ the area corresponding to $D_{max}$ and $A_0$ is the nominal area.

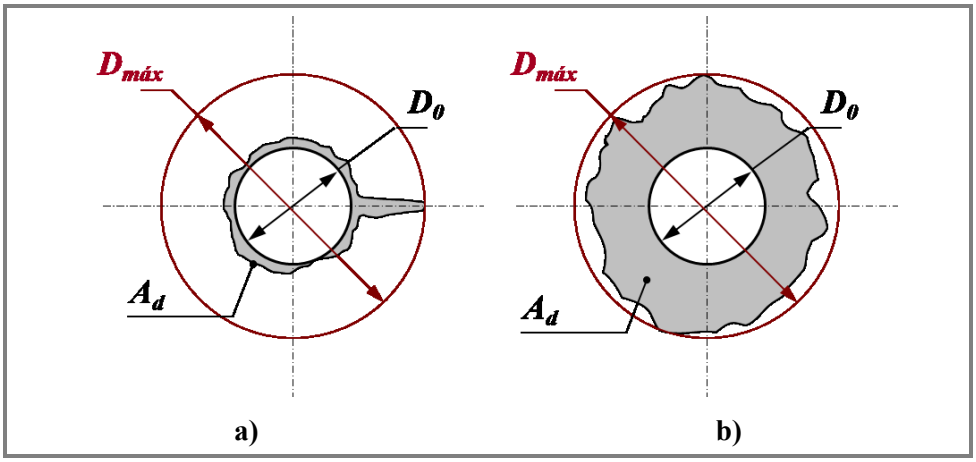


**Figure 1.17** Delamination patterns when drilling FRP laminate: **a)** fine cracks, **b)** uniform damage area [60, 79]

#### 1.3.2.5 Thrust Force, Torque and Tool Wear

It is important to know the amount of force applied by the tool on the material during the drilling process since it is strongly connected to the probability delamination of damage during the process. According to several authors it is possible to correlate analytically the thrust force with the onset of delamination. Thus, various analytical approaches were conducted and the respective models were presented [55, 145, 147, 148]. These models are based on the value of the thrust force needed to penetrate a composite laminate from the material characteristics, namely tensile modulus, interlaminar fracture toughness in mode I and Poisson ratio, the application of the load on the tool and tool dimensions.

**Table 1.7** Models of critical thrust force $F_C$ at onset of drilling induced delamination found in literature survey [55, 145, 147–149]

| Drill type | Model of critical thrust force | | Fig. |
|---|---|---|---|
| Twist drill (T) | $F_{CT} = \pi \left[\frac{8 G_{IC} E h^3}{3(1-\nu^2)}\right]^{1/2}$ | | Fig.1.18 |
| Saw drill (S) | $F_{CS} = \frac{1}{\sqrt{(1-2s^2+s^4)}} F_{CT}$ | $S = R_t / R_{dl}$ | Fig.1.19 |
| W-shape drill (W) | $F_{CW} = \frac{1+\alpha}{\sqrt{1+\alpha^2(1-2s^2+s^4)}} F_{CT}$ | $S = R_t / R_{dl}$ | Fig.1.19 |
| Core drill (C) | $F_{CC} = \frac{\beta(2-\beta)}{\sqrt{\{[1-(1-\beta)^4]-(1/2)s^2[1-(1-\beta)^6]\}}} F_{CT}$ | $S = R_{oc} / R_{dl}$ | Fig.1.19 |
| Step drill (ST) | $F_{CST} = \frac{\sqrt{2}}{1-\nu} \left[\frac{\{(1-\nu)+2(1+\nu)\xi^2\}^2}{(1+\nu)\{2(1-\nu)(1+2\nu^2)-(12-4\nu+3\nu^2+3\nu^3)\xi^2-8(1+3\nu)\xi^2 \ln \xi\}}\right]^{1/2} F_{CT}$ | | Fig.1.19 |

Where:

| | |
|---|---|
| $E$ | Elastic modulus |
| $\nu$ | Poisson ratio |
| $G_{IC}$ | Critical strain energy release rate (in mode I fracture) |
| $h$ | Uncut-plies thickness under drill bit |
| $R_t$ | Radius of drill bit |
| $R_{dl}$ | Radius of delamination |
| $\alpha$ | Ratio between concentrated load ($P_1$) and peripheral circular load ($P_2$) |
| $\beta$ | $= t/R_{oc}$ |
| $t$ | Thickness of core drill bit |
| $R_{oc}$ | Outer radius of core drill bit |

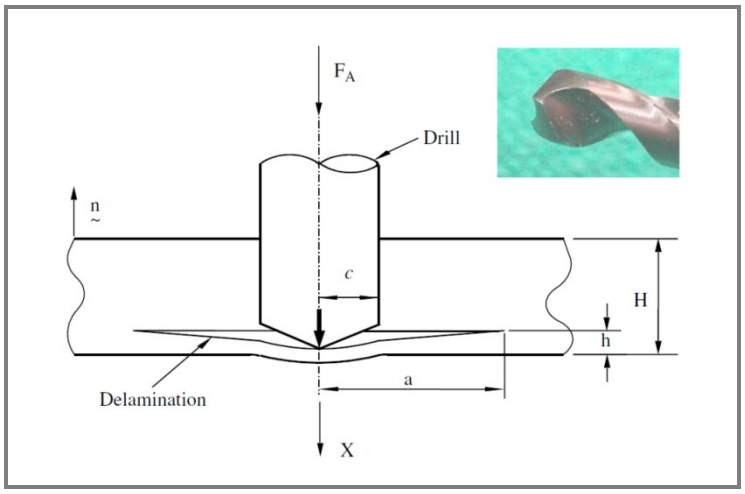


**Figure 1.18** Circular plate model for delamination analysis for twist drill [55]

The spread of delamination in a composite material is associated with the movement of the tool ($dx$) with the force applied ($F_A$), and is given by the equation of energy balance of the material, from linear elastic fracture mechanics:

$$G_{IC}(D + 2a)da = F_A dx - dU \tag{1.3}$$

where $G_{IC}$ is the energy release rate per unit area, $dU$ is infinitesimal stored strain energy and $da$ is the increase of the delamination area.

The model is based on an isotropic behaviour and pure decohesion fibre/matrix composite by a concentrated load on a circular area. The strain energy U is given by:

$$U = \frac{8\pi M x^2}{\left(a + \frac{D}{2}\right)^2} \tag{1.4}$$

Where,

$$M = \frac{Eh^3}{12(1 - \nu^2)} \tag{1.5}$$

The displacement is expressed by:

$$x = \frac{F_a \left(a + \frac{D}{2}\right)^2}{16\pi M} \tag{1.6}$$

The thrust force at the onset of crack propagation is given by:

$$F_{CT} = \pi\sqrt{32G_{IC}M} = \pi\left[\frac{8G_{IC}Eh^3}{3(1-\nu^2)}\right]^{1/2} \quad \textbf{(1.7)}$$

The models for the different geometries derive from the model presented:

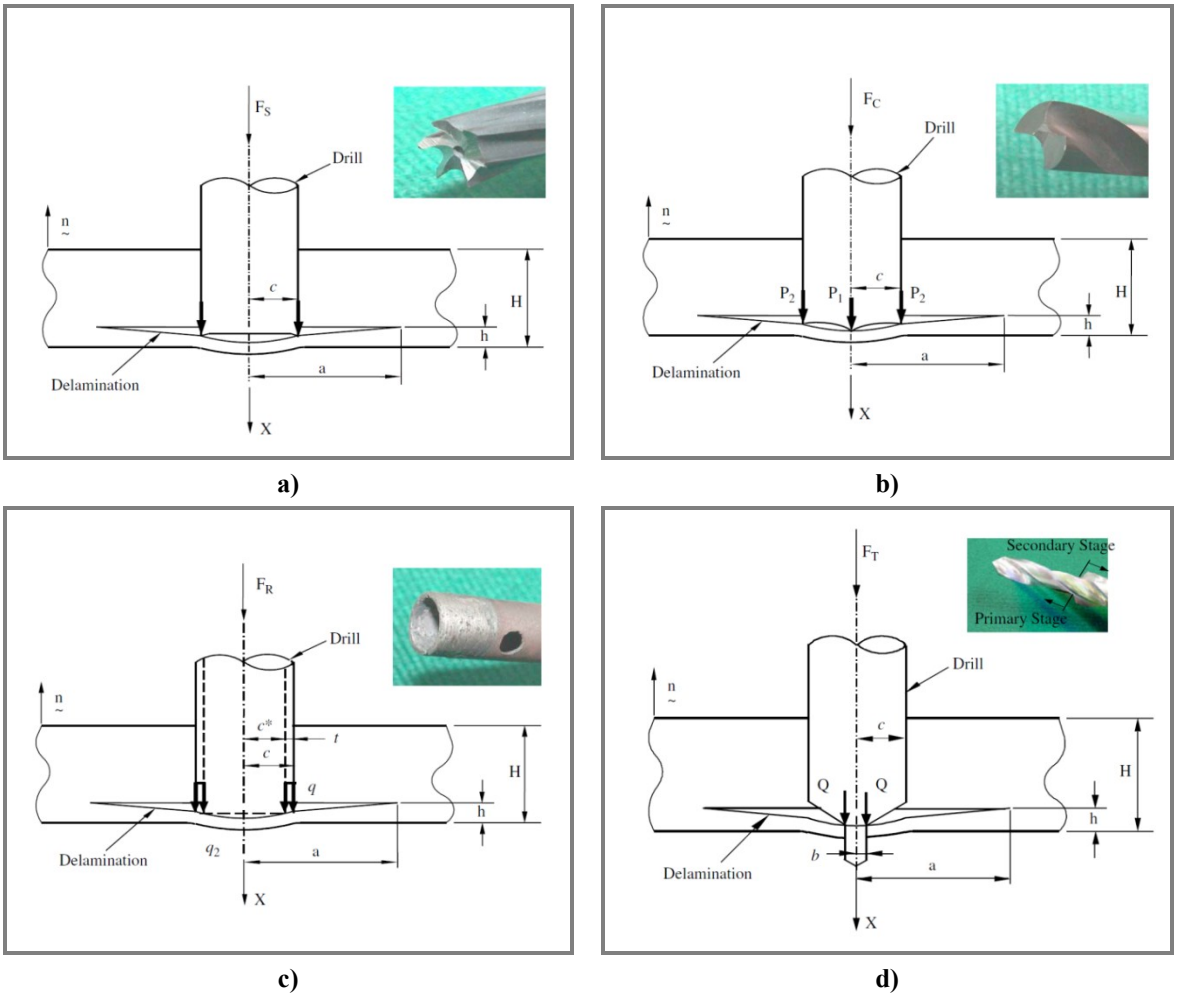


**Figure 1.19** Circular plate model for delamination analysis for: **a)** saw drill; **b)** W-shape drill; **c)** core drill; **d)** step drill [55]

Tsao and Hocheng [36] observed that the thrust force is greatly reduced by eliminating the effect of transverse edge, i.e., controlling the ratio between length of the transverse edge of the tool and its diameter. The thrust force increases with increasing the length of the transverse edge and feed speed.

Fernandes and Cook [58] modelled the drilling process with a straight flute drill as a five step process, depending on the position of drill bit in relation to workpiece. Thrust force and torque are influenced by feed rate, tool geometry, workpiece thickness and tool wear. Thrust force increases with the number of holes produced with the same tool, while torque is not particularly affected. The effect of the tool wear varies for the different stages. The thrust force is higher at the bottom of the workpiece, when breaking through. The workpiece thickness as effect on the thrust force since lower thickness implies more wear, thus higher thrust force. The thrust force and wear both increase with increased feed rate.

Tsao and Hocheng [40, 61, 68] investigated the thrust force of a special drill (core drill) variation with the cutting condition when drilling CFRP. The conclusions from this study present the thickness of the tool and the feed rate as having the higher influence on thrust force, with the recommendation for using high speed and low feed rate.

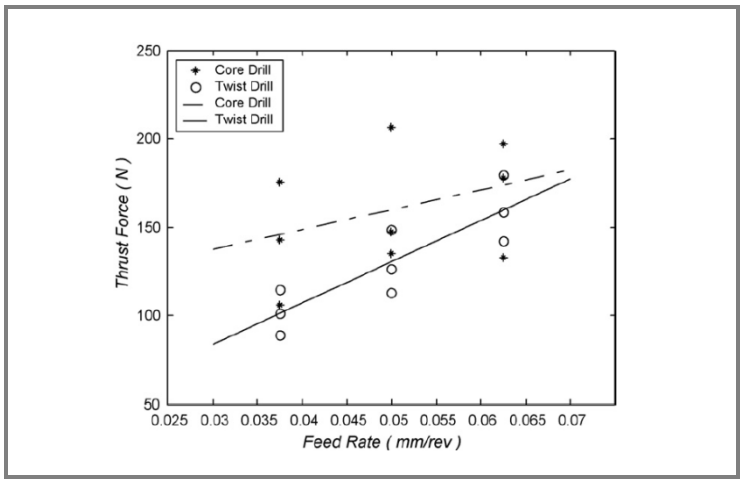


**Figure 1.20** Correlation between thrust force and feed rate for core drill and twist drill [40]

Tsao [66] investigated the thrust force of step drill with the drilling parameters, namely step angle, stage ratio, feed rate and spindle speed). The results indicate that the parameters concerning the tool and feed rate were the most significant.

Lazar and Xirouchakis [85] analysed the cutting loads distribution (axial and tangential) by analysing the thrust and torque curves when drilling CFRP. The observations indicate that maximum loads (and the overall cutting forces distribution) are directly proportional to the feed rate. The spindle speed has showed limited influence. They recommend increasing spindle speed to increase productivity without increasing the chances of delamination.

Behavioural studies in tool wear when cutting polymer matrix composites were mainly conducted for drilling operations. Due to the diversity and complexity of tool geometries used, the usual parameters for quantifying tool wear (flank wear, crater wear), may not be the best way to determine the wear rate.

Lin and Chen [25] verified the sharply increase of the thrust force with the increase of cutting speed and consider that this is due to tool wear. They found that the wear of tungsten carbide drills becomes very important when the cutting speed increases. There are changes in the tool geometry since wear starts at the outer corner of the tool and increases as drilled length increases. Thus, the geometry of the cutting edge is changed, causing possible changes in the drilling mechanisms.

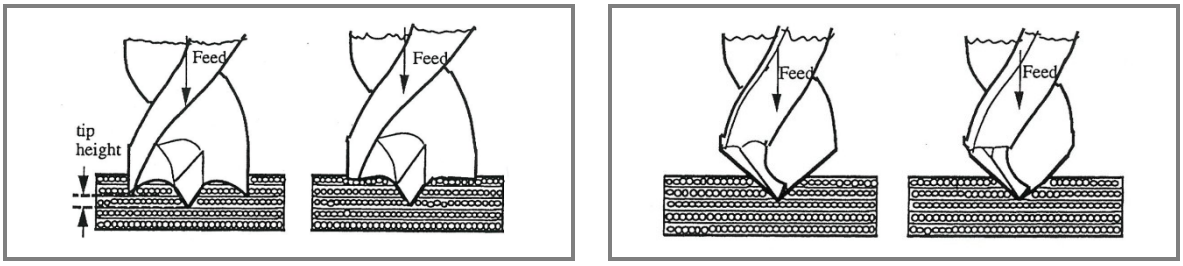


**a)** **b)**

**Figure 1.21** Effects of tool wear on tool geometry: **a)** multifaceted drill; **b)** twist drill [25, 90]

This finding was also confirmed by Lin and Shen [90], whose observations showed that, after 30 holes drilled with the same twist drill, thrust force was higher for 24 100 rpm than for 38 650 rpm when feed was higher, although the wear was smaller for 24 100 rpm.

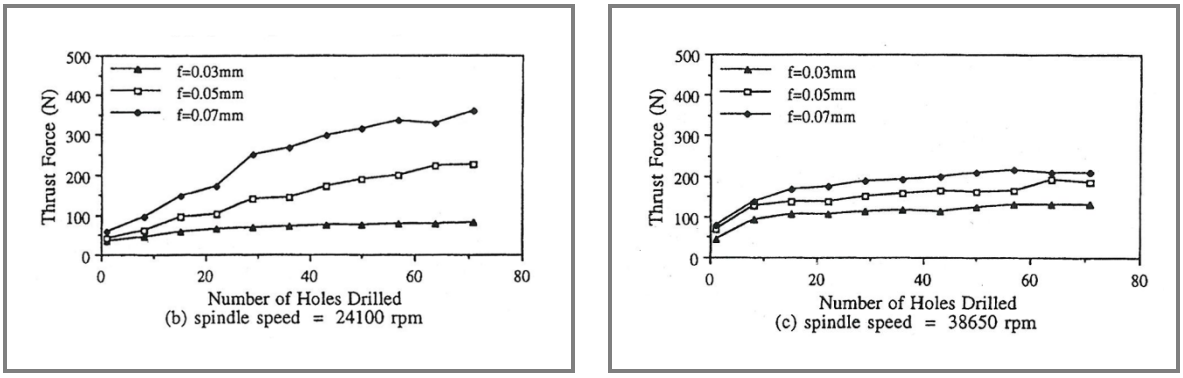


**a)** **b)**

**Figure 1.22** Correlation between thrust force and number of drilled holes (twist drill): **a)** $S$ = 24 100 rpm; **b)** $S$ = 38 650 rpm [90]

Chen [26] studied the effect of tool wear on the delamination factor and verified that the delamination had a serious increase as the wear rate increases and shows the relation between the delamination factor and the flank wear with the number of drilled holes, when drilling CFRP with twist drills. He also observed that the thrust factor increases with increasing flank wear of the drill

and consequently, the delamination factor increases. The effect of the tool wear also increases as the spindle speed increases as the flank surface temperature increases with increasing spindle speed and decreasing feed rate. A step-linear relation between the delamination factor and the thrust force was found.

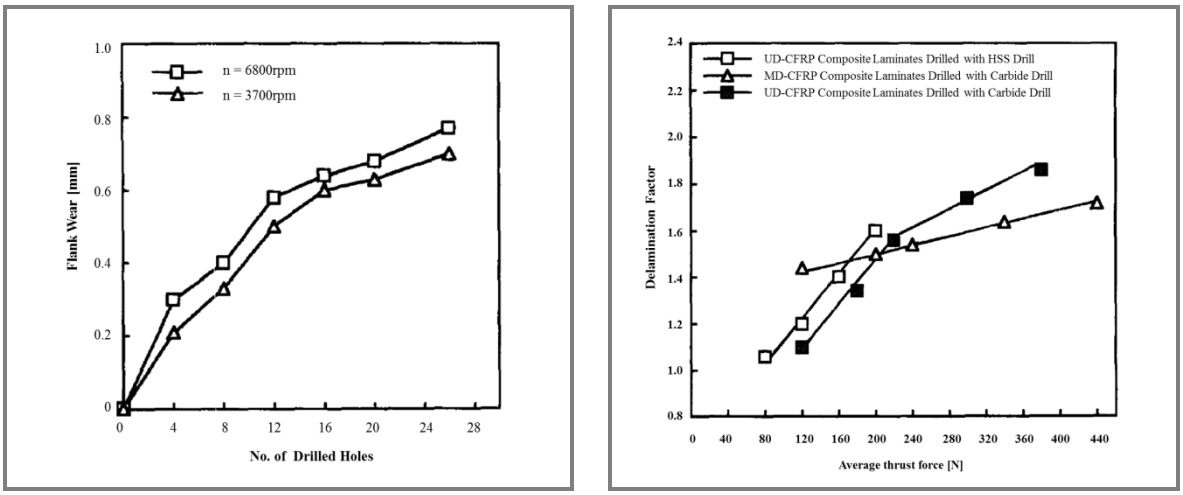


**a)** **b)**

**Figure 1.23 a)** Correlation between flank wear and number of drilled holes; **b)** Correlation between delamination factor and average thrust force [26]

Rawat and Attia [77] present an experimental investigation of the wear mechanisms when high speed drilling CFRP with tungsten carbide drills. The main wear mechanisms observed were fracture (chipping) at the start of the drilling process and abrasion mainly on the rake and flank face of the cutting edge. Tool wear by abrasion occurs as a result of hard abrasion by fracture of the WC grains and soft abrasion mode. They also divide the non-uniform progression in the flank wear into three regions, namely, initial (or primary) wear region, steady wear (secondary) region and severe (tertiary) wear region. The effect of flank wear on the thrust force, cutting force and delamination, as studied by these authors, is shown below:

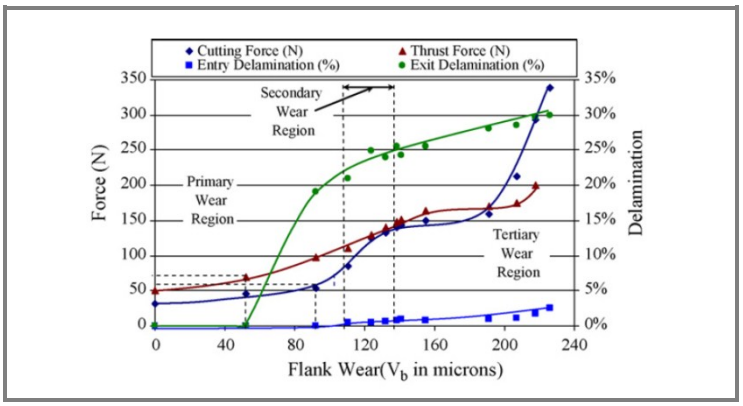


**Figure 1.24** Effect of flank wear on thrust force, cutting force, entry delamination and exit delamination ($S$ = 15 000 rpm; $f$ = 0.1 mm/rev) [77]

### 1.3.3 Concluding Remarks

The literature review about the knowledge and phenomena related to drilling composite materials presented in this chapter shows that the machining parameters, mainly tool geometry, tool mechanical characteristics and cutting conditions and the material parameters, mostly the mechanical characteristics, are the main agents of cutting mechanisms and damage induced in the workpiece.

The high temperatures generated during the machining of fibre reinforced plastics greatly limit the increase of the cutting speed when using high speed steel (HSS) tools. The use of other tool material, such as cemented carbide (coated or uncoated) or polycrystalline diamond (PCD), does not contribute significantly to eliminate problems such as delamination, debonding of the fibre-matrix interface and the cracking of the matrix. These local and microscopic phenomena contribute to the degradation of performance of the composite at the macroscopic scale. The coatings were not found to reduce either tool wear or workpiece damage.

In terms of tool geometry, the use of special tools can bring advantages in terms of minimizing the damage. However, the benefits are not as obvious to justify, in an industrial environment, the choice of tools much more expensive. The twist drill is a tool that typically shows worse results compared to the other under the same conditions. With this geometry, the best results are obtained for the smaller point angles.

After the analysis of various studies made on the influence of process parameters on the hole quality, it is evident that the feed rate is preponderant, regardless of spindle speed employed.

The thrust force is influenced by all process parameters and the spindle speed is always the less significant factor.

Delamination is lower when the feed rate is low, then when it is intended to use higher material removal rates the spindle speed is pointed as the parameter to increase. However, from the few studies performed at high speed drilling it is shown that on these conditions the feed rate has less influence on the damage obtained. This can point out to the feasibility of minimizing delamination when using high productivity drilling (high spindle speed, high feed rate).

# 2

# Methodologies and Techniques

## 2.1 Design of Experiments and Response Surface Methodology

### 2.1.1 Introduction

The statistical design of experiments (DOE) is an efficient procedure to analyse the data obtained from experiments in order to obtain valid and objective conclusions about the process characterization. The aim is to identify the key inputs and outputs of the process, estimate the operating conditions for the desired response variables and build mathematical models describing the process with the purpose of monitoring and improving.

This procedure begins with the selection of factors that physically influence the desired response and seeks to maximize the amount of information obtained from a reduced number of experiments, through structured data tables. This structure will then be used as a basis for multivariate modelling, which will guarantee stable and robust models. The level of influence on the response of each of the factors can be statistically evaluated, but the knowledge of either the process fundamentals or the empirical relationships between variables cannot be neglected.

Montgomery [150], shows an outline of the recommended procedure (Table 2.1):

**Table 2.1** Guidelines for Designing an Experiment [150]

| | |
|---|---|
| 1. Recognition of and statement of the problem.<br>2. Choice of factors, levels and ranges. [a]<br>3. Selection of the response variable. [a] | Pre-experimental planning. |
| 4. Choice of experimental design. | |
| 5. Performing the experiment. | |
| 6. Statistical analysis of the data. | |
| 7. Conclusions and recommendations. | |

[a] In practice, steps 2 and 3 are often done simultaneously or in reverse order.

The response surface methodology (RSM) can be defined as a set of techniques used in the empirical study of the relationship between one or more responses and the set of input variables. These techniques consist of the experimental design and the subsequent analysis of experimental results.

Box and Draper [151] identified the desirable properties for a response surface design, whose importance depends on the experimental circumstances. These requirements must be considered when selecting the most suitable design, but according to the situation, the best compromise must be achieved.

- Generate a satisfactory distribution of information throughout the experimental region (rotatability);
- Ensure that the fitted value is as close as possible to the true value;
- Effective detectability of lack of fit;
- Provide an internal estimation of the error;
- Verification of "constancy of variance";
- Possibility to estimate transformations;
- Blocking suitability;
- Allow sequential construction of higher-order from simple designs;
- Require of a minimum number of tests;
- Good graphical analysis through data of the model;
- Good behaviour when errors occur in the definition of input variables.

In this context, this methodology is applicable hence the aim is to achieve an understanding of the overall system response, in order to quantify the relationship between the values of the variables of response (measurable) and the values relative to the set of experimental factors assumed to affect the response. This relationship is typically unknown therefore the first approach is to find a suitable approximation, usually using low order polynomials. The natural variables, who correspond to the real set of values for each factor, are transformed into coded or "standardized" variables, dimensionless, with zero mean and the same spread of standard deviation [152].

When the resulting set of variables is established is desirable, as a first approximation, to verify the possibility to reduce it. Such reduction occurs by identifying the factors that may be critical and those who have little or no effect on the response. This will be made so that attention

can be focused on controlling the factors that show significance, thus reducing the number of tests needed. This procedure is called *Screening Experiments*.

When all the input factors (predictors) are known as well as the range and it is clear that the first-order polynomial cannot suit the process characterization, a second-order polynomial should be used. Generally a second-order model is sufficient to adequately fit a process response.

The experimental design in which all input factors are established on two levels is particularly advantageous in the early phase of experimental work, when there are several factors to be investigated. In this case the coded variables take the notation +1 and -1 for, respectively, the highest and lowest values in the range of experimentation desired. Such planning, on two levels, provides the least number of experiments on which the factors *k* can be studied [150], as it provides the necessary information to effectively accomplish the planning experiments using the response surface methodology.

### 2.1.2 Response Functions for RSM

The general model for the process can be expressed as [152]:

$$\eta = f(x_1, x_2, \dots, x_k) \quad \textbf{(2.1)}$$

$\eta$ is assumed to be a continuous function of the $x_i$, whose value corresponds to each combination of the variables levels. Because there is always an experimental error, the value of the truly observed response for a given combination of factor levels is different and is denoted by *Y*, being $Y = (\eta + \varepsilon)$. $\varepsilon$ is the term that represents other sources of variability not accounted for in the initial function, treated as a statistical error, assuming it to have a normal distribution with mean zero and variance

As stated above, since the structural form of equation (2.1) is usually unknown, a low order polynomial approximation (first or second order) may be used to represent the functional relationship between the expected value (mean response) and the levels of the *k* inputs.

The first-order or linear model is appropriate for a first phase of experiments, when it is not known nor is it intended to define the shape of the surface or location of the best response values [153]. Because there are only two levels for each variable, the response is considered to be approximately linear in the range of levels chosen for each factor [150].

It is assumed that the data is obtained in $2^k$ points of a two levels factorial design, with *k* predictor variables.

The polynomial representation of the surface response is a multiple linear regression model with interaction terms [154]:

$$Y = \beta_0 + \sum_{i=1}^{k} \beta_i x_i + \sum_{i}^{k} \sum_{j>i}^{k} \beta_{ij} x_i x_j + \varepsilon \quad \textbf{(2.2)}$$

Wherein $Y$ is the process response, $x_i$ and $x_j$ the regressor or predictor variables, $\beta_0$, $\beta_i$ and $\beta_{ij}$ are the polynomial coefficients obtained by regression estimated by the method of least squares and ε the error. The term $x_i x_j$, the interaction term, is added to consider the possible cross-effects between variables. To ease the estimation of the model coefficients, the variables are transformed into coded variables, with no physical meaning, which are designated by level.

The number of coefficients, $n\beta$, of the polynomial obtained is:

$$n\beta = (k+1) + \frac{k(k+1)}{2} \quad \textbf{(2.3)}$$

### 2.1.3 Experimental Design for Fitting Second-order Models

To adjust the second degree polynomial model, the most used class of experimental design is called central composite design (CCD). This is the most common class of second-order designs and was introduced by Box and Wilson in 1951 [152].

The use of CCD in sequential experimentation contributes to define accurately the region of interest in terms of the range of the operational parameters. In general, this type of planning consists in a $2^k$ full factorial design with $n_F$ runs, $2k$ axial or "star" points and $n_C$ centre runs, with $k$ the number of factors to consider. The total number of experiments is given by:

$$N = n_F + 2k + n_C \quad \textbf{(2.4)}$$

The three components of the central composite design are important and their function is distinct:

- $n_F = 2^k$ experimental points (a full factorial design) corresponding to the vertices of a k-dimensional polyhedron, contribute to the estimation of linear terms and two-factor interactions and are the only points that contribute to the estimation of the interaction terms.

- *2k* experimental points corresponding to vertices of a k-dimensional star, designated star points. These points contribute to estimation of quadratic terms, and without them only the sum of the quadratic terms can be estimated. The star points represent new extreme values (low and high) for each factor in the design.
- $n_C \geq 1$ central runs which provide an internal estimate of error (pure error). They also contribute to the estimation of quadratic terms.

A measure of precision associated with the predicted value $\hat{Y}_u$, is the variance. The variance of the predicted response at a point *x* is:

$$V\left[\hat{Y}(x)\right] = \sigma^2 x'(X'X)^{-1}x \quad \textbf{(2.5)}$$

An experimental design is said to be rotatable if by rotating the design points about the centre, the moments of the distribution of the design points remains unchanged in all situations, i.e., if the variance of the estimated response is constant at all points equidistant from the design centre [153].

The rotatability is an adequate criterion to evaluate designs which assume a spherical region of interest. Box and Hunter suggested choosing $\alpha$* to induce rotatability and choose $n_C$ to try to get uniform precision. A central composite design is made rotatable by the choice of $\alpha$*. For there to be this property, the value of $\alpha$* depends on the number of points in the factorial component of design:

$$\alpha^* = (n_F)^{1/4} \quad \textbf{(2.6)}$$

This property is a support for the selection a response surface design, since for this type of experimental work it makes sense to use a design that provides equal precision of estimation in all directions [150].

**Table 2.2** Values of $\alpha^*$ for the CCD to be rotatable

| $k =$ | 2 | 3 | 4 | 5 | 6 | 7 |
|---|---|---|---|---|---|---|
| $n\beta = \frac{(k+1)(k+2)}{2}$ | 6 | 10 | 15 | 21 | 28 | 36 |
| $n_F + 2k$ | 8 | 14 | 24 | 42 | 76 | 142 |
| $\alpha^*(rot)$ | 1.414 | 1.682 | 2.000 | 2.378 | 2.828 | 3.364 |

There are three types of central composite designs: circumscribed (CCC), face-centered (CCF) and inscribed (CCI), which differ by the arrangement of star points, as shown in Figure 2.1 and Figure 2.2, and whose a comparison is made in Table 2.3 [155].

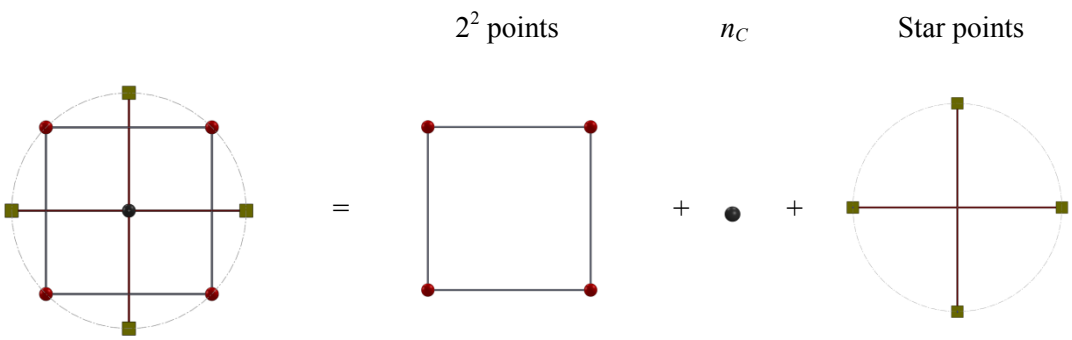


**Figure 2.1** Central composite design for $k = 2$ variables

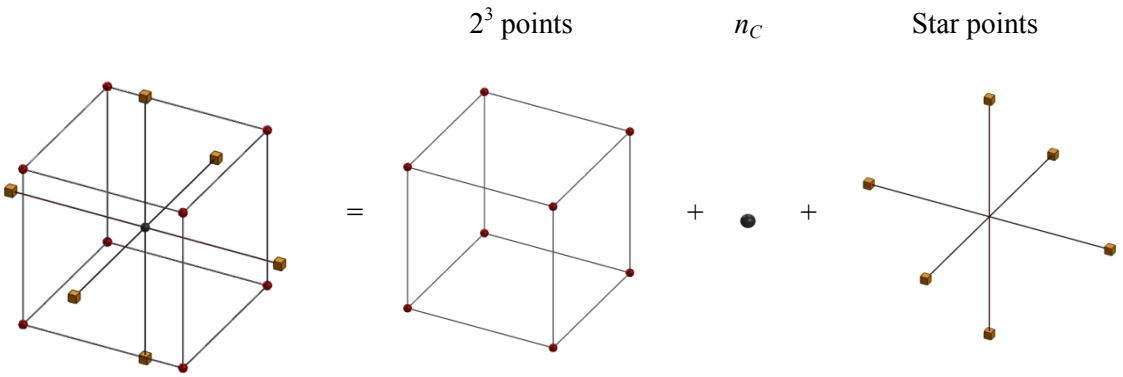


**Figure 2.2** Central composite design for $k = 3$ variables

**Table 2.3** Central composite designs [155]

| | | |
|---|---|---|
| 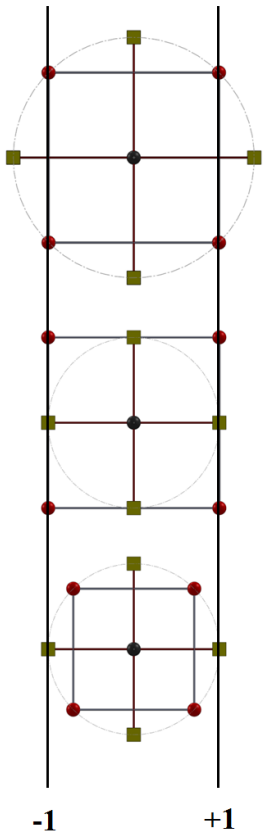 | CCC | This is the original form of the CCD. The star points are at some distance from the centre based on the properties desired and the number of factors in the design. The new low and high extremes for all factors are established the star points. These designs have circular, spherical, or hyper spherical symmetry and require 5 levels for each factor. |
| | CCF | In this design the star points are at the centre of each face of the factorial space, so $\alpha^* = \pm 1$. This variety requires 3 levels of each factor. |
| | CCI | The CCI design uses the factor settings as the star points and creates a factorial or fractional factorial design within truly limits. This design also requires 5 levels of each factor. |

It should be noted that the CCC design explores a wider domain of space, while CCI explores the smallest. These two kinds of design are called spherical, and are rotatable designs, while the CCF is not.

From the considerations described above, the model to be used in this work will be a central composite circumscribed (CCC) design which requires at least 5 levels for each factor, which will be - $\alpha^*$, *-1, 0, +1,* + $\alpha^*$.

#### 2.1.3.1 Second-order Model

The second-order model is extensively used in surface response methodology because is very flexible, often being adequate as an approximation to the true surface response. Also, there is sufficient practical experience attesting that these models have a good performance solving real problems. On the other hand, it is easy to estimate the coefficients using, for example, the method of least squares.

Using Central Composite Design, the second-degree polynomial to represent mathematically the response function is:

$$Y = \beta_0 + \sum_{i=1}^{k} \beta_i x_i + \sum_{i=1}^{k} \beta_{ii} {x_i}^2 + \sum_{i}^{k} \sum_{j>i}^{k} \beta_{ij} x_i \, x_j + \varepsilon \qquad \textbf{(2.7)}$$

Where the polynomial coefficients obtained by regression are $\beta_0$, $\beta_i$, $\beta_{ii}$ e $\beta_{ij}$. The first step to obtain the fitted model consists of estimating the $n\beta$ coefficients:

$$n\beta = \frac{(k+1)(k+2)}{2} \qquad \textbf{(2.8)}$$

Considering the sets of points of the central composite design, the following sets of combinations are defined:

$Y_1, Y_2, \ldots, Y_{n_F}$ collected at the factorial portion ($x_i = \pm 1$)

$Y_{n_F+2i-1}, Y_{n_F+2i}$ collected at the axial settings $x_i = \pm\alpha$, $x_i = 0$, $j \neq i$

$Y_{n_F+2k+1}, \ldots, Y_N$ collected at the centre point $x_i = 0$, all $i$

The estimates $b_0$, $b_i$, $b_{ii}$ and $b_{ij}$ of the respective coefficients $\beta_0$, $\beta_i$, $\beta_{ii}$ e $\beta_{ij}$ in the model, are calculated using [153]:

$$b_0 = \frac{2\left(\frac{1-k}{\sqrt{n_F}}\right)}{D} \sum_{u=1}^{n_F} Y_u + \frac{(k-\sqrt{n_F})}{D} \sum_{u=n_F+1}^{n_F+2k} Y_u + \frac{(k+2)}{D} \sum_{u=n_F+2k+1}^{N} Y_u \qquad \textbf{(2.9)}$$

$$b_i = \frac{1}{H} \sum_{u=1}^{n_F} x_{ui} Y_u + \frac{\sqrt[4]{n_F}}{H} \left(Y_{n_F+2i} - Y_{n_F+2i-1}\right) \qquad 1 \leq i \leq k \qquad \textbf{(2.10)}$$

$$b_{ii} = \frac{(N - n_F - 2\sqrt{n_F})}{n_F \cdot D} \sum_{u=1}^{n_F} Y_u + \frac{(n_F + 2\sqrt{n_F} - N)}{2\sqrt{n_F} \cdot D} \sum_{u=n_F+1}^{n_F+2k} Y_u - \frac{\left(1 + \frac{2}{\sqrt{n_F}}\right)}{D} \sum_{u=n_F+2k+1}^{N} Y_u + \frac{1}{2\sqrt{n_F}} \left(Y_{n_F+2i} - Y_{n_F+2i-1}\right) \qquad \textbf{(2.11)}$$

$$b_{ij} = \frac{1}{n_F} \sum_{u=1}^{n_F} x_{ui} x_{uj} Y_u \qquad 1 \leq i < j \leq k \qquad \textbf{(2.12)}$$

Where $N$ is the total number of runs and $D$ and $H$ given by:

$$D = N(k+2) - \left(2 + \sqrt{n_F}\right)^2 \cdot k \quad \textbf{(2.13)}$$

$$H = n_F + 2\sqrt{n_F} \quad \textbf{(2.14)}$$

Once the estimates are obtained they are substituted in equation 2.7 to produce the fitted model.

$$\hat{Y} = b_0 + \sum_{i=1}^{k} b_i x_i + \sum_{i=1}^{k} b_{ii} {x_i}^2 + \sum_{i}^{k} \sum_{j>i}^{k} b_{ij} x_i \, x_j \quad \textbf{(2.15)}$$

The model is then referred to as prediction equation. The predicted values of the response are obtained using this equation by selecting values for the variables, calculating their coded values, and substituting the calculated values of the coded variables.

### 2.1.3.2 Analysis of Variance, Hypothesis Testing and Confidence Intervals

Analysis of variance is a statistical hypothesis testing whose purpose is to test for significant differences between means. Therefore, the analysis of variance model applies when comparing the effects of various levels of a variable, with several observations at each level. This variable can be either discrete or continuous.

The results of the analysis of data from the set of experiments are presented in an analysis of variance table (ANOVA table). Therein are represented the sources that contribute to the total variation in the data values.

**Table 2.4** The Analysis of Variance Table

| Source | SS | df | MS | F | p |
|---|---|---|---|---|---|
| | Sum of Squares | Degrees of freedom | Mean Square | F-Statistics | P-value |
| Due to Regression (fitted model) | SSR | $n\beta$-1 | MSR | MSR/MSE | |
| Residual | SSE | $N$-$n\beta$ | MSE | | |
| Total | SST | $N$-1 | | | |

The total variation in the data values is called the Total Sum of Squares, *SST*, and it's the sum of two quantities: the Sum of Squares due to the Regression (*SSR*), or accounted by the fitted model, plus the Sum of Squares of the Residuals (*SSE*), not accounted for by the fitted model.

$$SST = \sum_{u=1}^{N} (Y_u - \bar{Y})^2 \quad \textbf{(2.16)}$$

$$SSR = \sum_{u=1}^{N} \left(\hat{Y}_u - \bar{Y}\right)^2 \quad \textbf{(2.17)}$$

$$SSE = \sum_{u=1}^{N} (Y_u - \bar{Y}_u)^2 \quad \textbf{(2.18)}$$

Where $Y_u$ is the observed response value in each of the experiments, $\overline{Y}$ is the overall average of the observed response values and $\hat{Y}_u$ is the value predicted by the fitted model for each observed value.

Performing hypotheses testing in multiple linear regression problems helps measuring the utility of the model. The F statistic, used by the test for significance of regression, is expressed by the ratio between the mean squares determined:

$$MSR = \frac{SSR}{(n\beta - 1)} \quad \textbf{(2.19)}$$

$$MSE = \frac{SSE}{(N - n\beta)} \quad \textbf{(2.20)}$$

$$F = \frac{MSR}{MSE} = \frac{\frac{SSR}{(n\beta - 1)}}{\frac{SSE}{(N - n\beta)}} \quad \textbf{(2.21)}$$

The usual test of significance, assuming normality of the errors, is a test of the null hypothesis $H_0$ against the alternative hypothesis $H_A$. These assumptions are as follows:

$H_0$ – All of the $\beta$s (excluding $\beta_0$) are zero;

$H_A$ – At least one of the $\beta$s (excluding $\beta_0$) is not zero.

The F ratio mentioned above follows an F distribution with $n\beta$-*1* degrees of freedom in the numerator and *N*-$n\beta$ degrees of freedom in the denominator, if the null hypothesis, $H_0$, is true.

In this case, the mean square estimate the same amount (variance), and should have approximately equal magnitude, namely, their ratio should be close to 1.

The significance level $\alpha$ for a given hypothesis test is a value for which a P-value less than or equal to $\alpha$ is considered statistically significant. Typical values for $\alpha$ are 0.1, 0.05, and 0.01. These values correspond to the probability of observing such an extreme value by chance. For example, if the level of confidence $\alpha$ is 0.05, it is considered a confidence interval (1-$\alpha$) of 95%.

Thus, the value of F is compared with the table value of $F_{(n\beta-1,\ N-n\beta,\ \alpha)}$. If the value of F exceeds the table value, the null hypothesis is rejected for this level of significance, and this indicates that the coefficient estimates are not all equal to zero, therefore *MSR* should have a higher value than *MSE*. Thus, the regression model is adopted.

The statistical analysis of the model is often complemented by the value of $R^2$, which is a measure of the proportion of the total variation of the process responses, $Y_u$, about the mean $\overline{Y}$. When $R^2 = 1$ the model faithfully represents the response of the process, and is often expressed as a percentage.

$$R^2 = \frac{SSR}{SST} \tag{2.22}$$

$R^2$ is used as a criterion of suitability but has the drawback that when the number of estimated parameters in the model approaches the number of experiments takes a value close to 1 even if the model is not the appropriate. Thus we use the value adjusted, designated $\overline{R}^2$:

$$\bar{R}^2 = 1 - \frac{\frac{SSE}{(N-n\beta)}}{\frac{SST}{(N-1)}} = 1 - (1-R^2)\frac{(N-1)}{(N-n\beta)} \tag{2.23}$$

It must be pointed out that a fitted model may exhibit “lack of fit” (LOF) even if it is significant according to the significance of regression test and has a high $R^2$ statistic. The reasons for lack of fit are mainly two [154]:

1. Factors were omitted but affect the response;

2. Higher order terms of factors already in the model were omitted but affect the response.

The terms in the regression model adopted (significant terms) are determined using the t test. The value of t is calculated for each term by the quotient of the regression coefficient and its associated error. The term is considered significant if the calculated value exceeds the value of table t, or $t > t_{(N-n\beta,\ \alpha)}$.

## 2.2 Radiographic Analysis

Radiography is an effective method of non-destructively detecting internal flaws in materials and structures. Despite being a process of great performance in the characterization of volume defects, this method presents the limitation of having reduced sensitivity to detect flat defects such as cracks located in geometric planes not coincident with the direction of the radiation beam.

The radiation source emits energy that travels in straight lines and penetrates the test piece. As the radiation energy passes through the test piece, an image is received on the recording medium opposite the x-ray source. In this work a digitized system coupled with video monitors was used. These new digital techniques, when compared with the potential of conventional radiographic film have the problem that their spatial resolution is considerably lower. Therefore, it is necessary to have a better measure for spatial resolution and to measure it separately of contrast resolution.

Defects in composite materials are very small and the material contains only elements with low X-ray absorption. Hence, the energy of radiation must be reduced for these materials in order to maintain object contrast.

X-ray radiography has been used successfully by several researchers [7–9] to measure the extension of the delamination damage caused by the drilling operation. However, the images obtained require analysis processing in order to the quantitative assessment of the damage can be accomplished. The image processing methodology implemented in this work is carried out in five distinct stages:

1. The area of interest is selected in the radiographic image obtained;
2. The image is then handled in *Photoshop* software to be held its binarization with a set out threshold;
3. Using the software *Matrox*, the boundaries of the hole and the delaminated area are determined. The edges are rendered parametrically by this software;
4. The edges are imported into *Solidworks* software and a two-dimensional representation of the area of the damage is made so that it can be quantified. The delaminated area is then calculated;
5. Using the same software (*Solidworks*) the measurement of the maximum diameter and the nominal diameter is performed.

The methodology employed in this study is shown schematically in Figure 2.3.

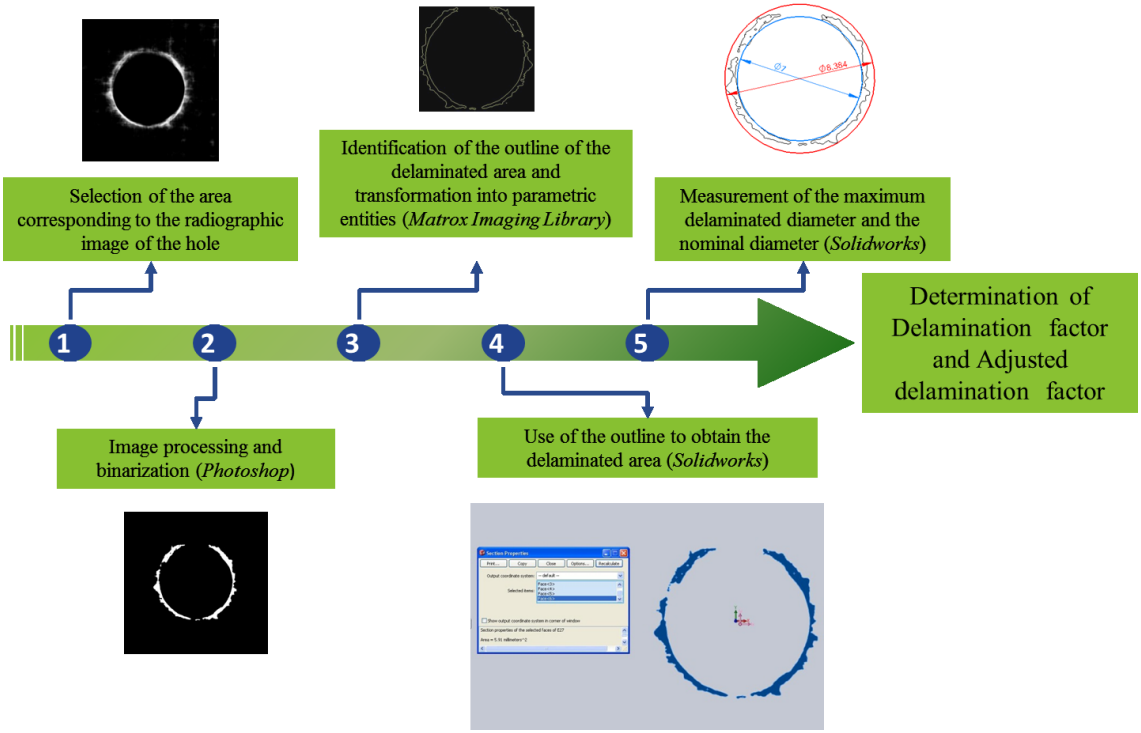


**Figure 2.3** Schematic representation of the image processing methodology used.

# 3

# Experimental Procedure

## 3.1 Introduction

This chapter will define the complete experimental setup and procedure for collecting the data needed for this study.

Firstly we describe the equipment used for drilling and the systems for monitoring and collect the experimental values of the thrust force and torque.

Following are defined the specimens used for making the holes, with regard to its configuration and materials. The characterization of the material is carried out based on the material procurement specification provided together with the composite, which the manufacturer follows for its production. The material had already been tested, so there is a guarantee that meets the requirements presented.

Next, the selection of tools is presented and the choices on materials of which they consist, their geometry and dimensions will be justified.

Later, the ranges of values of the cutting parameters used are shown. These ranges were chosen to cover values considered to be conventional drilling, already used in previous studies, and extend the study domain to values that determine high performance drilling, with high material removal rates. Thereby, it is intended to ensure continuity in the study that shall permit to observe the differences between the conventional and high speed drilling in order to demonstrate if they are significant or even if the process mechanism differs.

Finally, the radiography equipment is described, as well as the process for acquiring the images relative to damage, whose methodology of analysis has been explained in Chapter 2.

## 3.2 Equipment

All drilling tests were performed in a LEADWELL VMC-15 vertical machining centre with the use of a spindle speeder Nikken BT30-NX5-153, which allows a maximum rotation of 20 000 rpm.

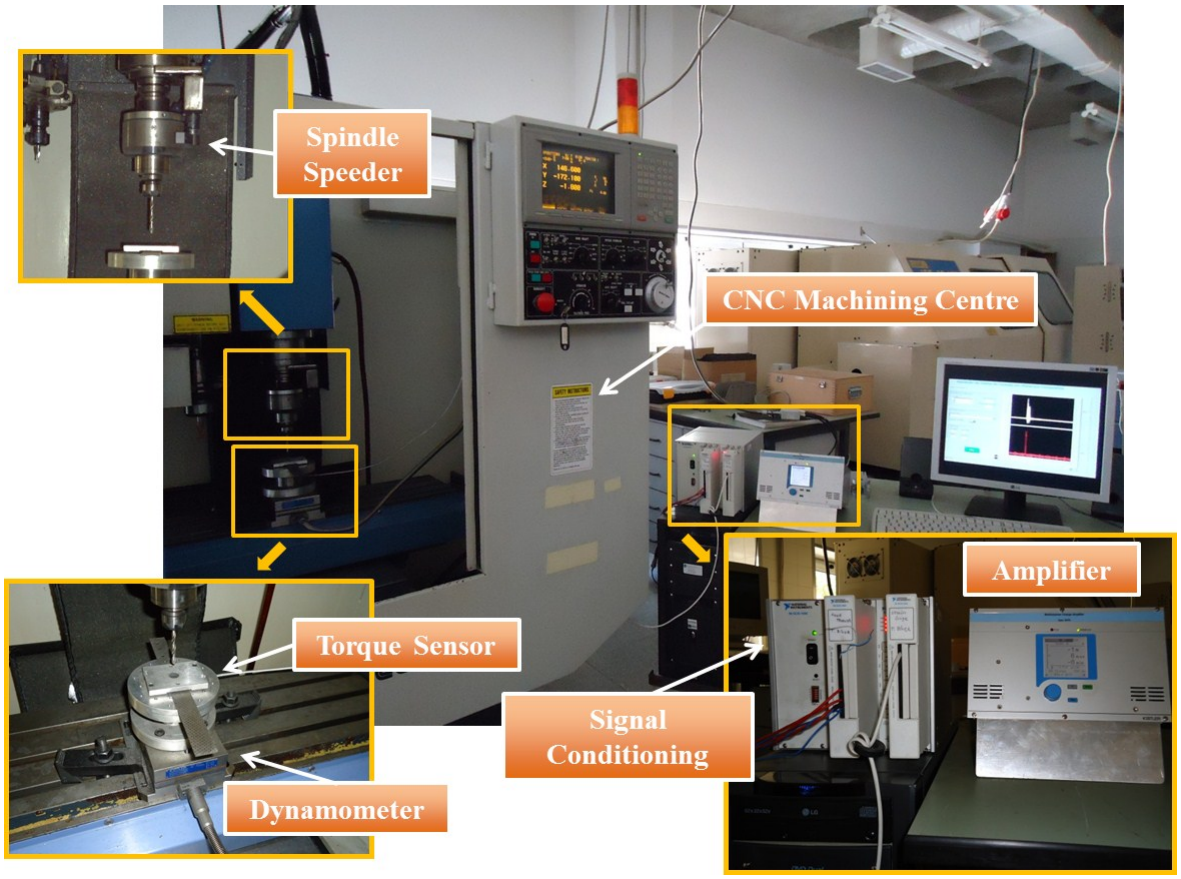


**Figure 3.1** Experimental setup

The measurement of thrust force and torque during drilling consists in an acquisition pathway composed of a torque sensor, a multicomponent dynamometer Kistler 9257B, a Kistler 5070 multichannel charge amplifier and a DAQ (data acquisition) system comprising signal conditioning, analog-to-digital converter (ADC) in a computer bus and a computer with *LabVIEW* software. The experimental setup scheme is presented in Figure 3.2.

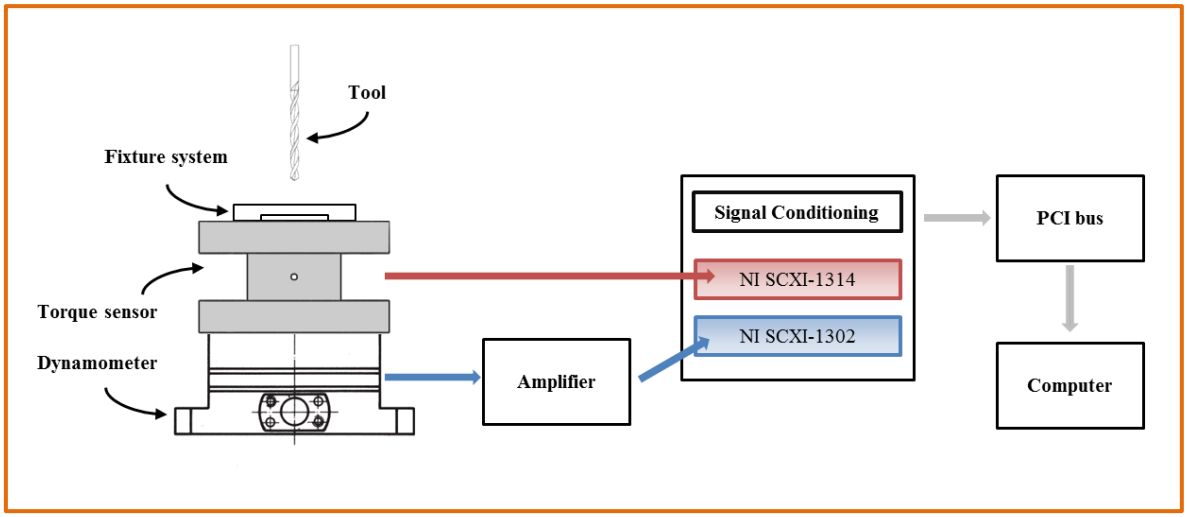


**Figure 3.2** Schematic representation of the experimental setup

The multicomponent dynamometer consists of four piezoelectric sensors. Each sensor contains three pairs of quartz plates, one sensitive to pressure in the z direction and the other two responding to shear in the x and y directions respectively. The main characteristics of the dynamometer Kistler 9257B are shown in Table 3.1.

**Table 3.1** Characteristics of the multicomponent dynamometer Kistler 9257B

| | | |
|---|---|---|
| Range [kN] | $F_x$, $F_y$ | -5 – 5 |
| | $F_z$ | -5 – 10 |
| Sensitivity [pC/N] | $F_x$, $F_y$ | ≈ -7.5 |
| | $F_z$ | ≈ -3.7 |
| Threshold [N] | | < 0.01 |
| Natural frequency [kHz] | $f_n(x,y,z)$ | ≈ 3.5 |
| Clamping area [mm] | | |

The amplifier converts the charge output into a proportional voltage, which is used as an input variable for analysis systems.

There was the need to build a sensor for measuring torque, since the available multicomponent dynamometer can only measure the three orthogonal components of a force. The torque sensor development was held based on the typical values of the torque expected to obtain. Performed the modelling of its components using *SolidWorks* software, design validation was executed to predict the behaviour and assess the dimensions. The components were then machined and a strain gage full-bridge system was applied. This development will be enclosed in Appendix A.

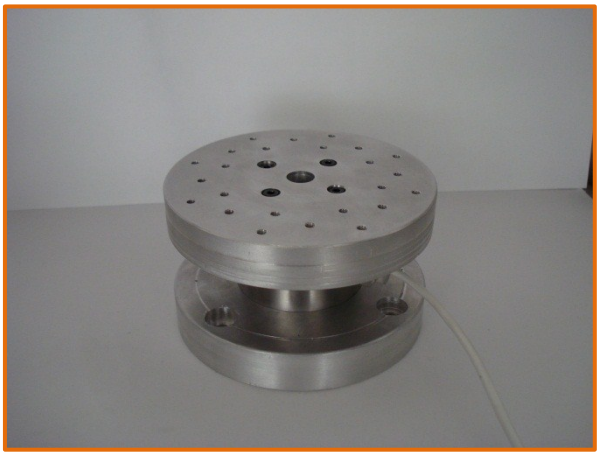

**Figure 3.3** Torque sensor

Signal conditioning circuitry manipulates a signal into a form that is suitable for input into an ADC, so the signal can be effectively and accurately measured. The signal conditioning apparatus employed is a SCXI-1000 chassis that houses two shielded modules, namely a SCXI-1180 feed through panel and a SCXI-1520 universal strain gage input. In those modules are respectively connected a SCXI-1302 50-screw terminal block and a SCXI-1314 front-mounting terminal block. National Instruments SCXI modules provide signal conditioning and isolation separate from the data acquisition hardware.

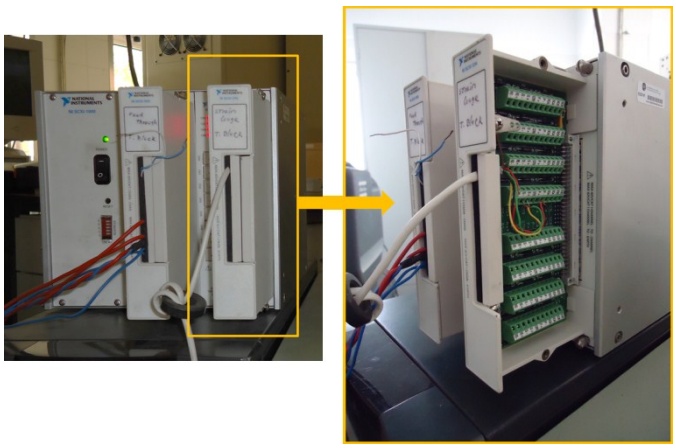

**Figure 3.4** Signal conditioning device showing the SCXI-1314 connections

Finally, the device connected to a slot in the computer motherboard is an M Series multifunction DAQ device PCI-6259 from National Instruments. PCI is one of the most widely adopted internal buses for desktop and this one shows improved measurement accuracy, resolution, and sensitivity. It includes a system controller application specific integrated circuit (ASIC) NI-STC-2) that provides a number of benefits including an integrated PCI bus interface. Also, a separate ADC per channel enables all inputs to be simultaneously sampled at full speed.

In brief, the important points of the analog input-related aspects of multifunction modules are: separate per-channel ADC, simultaneous sampling, integrated signal conditioning, input characteristics to match signal type and isolation.

The graphical programming environment software *LabVIEW* is used to process the obtained signal and report the results, namely to manipulate and store the experimental data. The two different windows serve diverse purposes. The front panel is where the input data can be changed and the results can be viewed, it is the user interface. The block diagram window is the place to generate the underlying code of the program that is graphically created using the inputs and outputs placed in the Front Panel and objects from the Functions window.

In this case, the sampling rate and acquisition time define the number of samples whose data must be stored. The name and location of the stored data file is also chosen in the front panel, allowing organizing the information for subsequent analysis. This data is stored as an ASCII text file and later processed and analysed using *MATLAB* software. Figure 3.5 represents an example of the front panel interface after performing an experiment. The correspondent block diagram is shown in Appendix B.

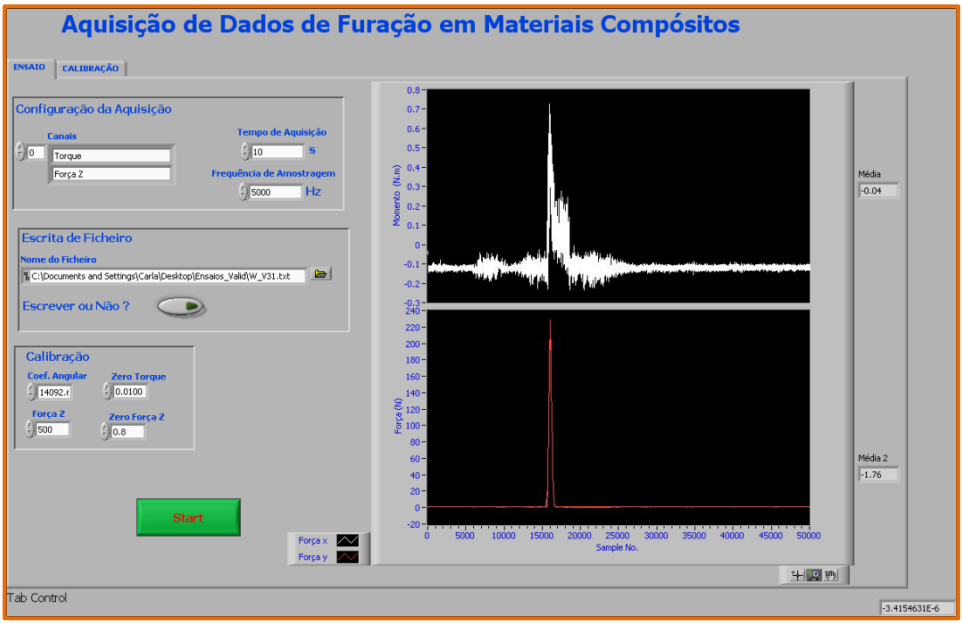


**Figure 3.5** Front panel designed for this work

## 3.3 Material and specimen details

The composite used to perform the experiments is a material according to AGUSTA procurement specification for epoxy impregnated graphite fabrics for high temperature application. This material is a Polyacrilonitrile (PAN) precursor graphite fibre following the AMS 3892/9 (Aerospace Material Specifications) requirements with curing epoxy resin systems used for fire resistance requirements for critical applications. The curing conditions to obtain a laminate are defined as follows:

**Table 3.2** Curing conditions to obtain the laminate used on the experiments (Source: AGUSTA)

| | |
|---|---|
| Heat up rate | 2 – 5 ºC/min |
| Temperature | 175 ± 5 ºC |
| Pressure | 7 atm (100 psi) maximum, 2.7 – 3.5 atm (40 - 50 psi) is preferred |
| Time | 110 to 180 min |
| Cooling | To 60 ºC under pressure |
| The material shall be capable of a minimum of 3 cycles at the cure temperature without degradation of its properties | |

**Table 3.3** Requirements for physical properties (prepreg individual requirements) (Source: AGUSTA)

| | |
|---|---|
| Volatile max. content [%] | 2 |
| Resin content by weight [%w/w] | 42 ± 2 |
| Fibre weight [g/m$^2$] | 193 ± 8 |
| Prepreg weight [g/m$^2$] | 331 ± 10 |
| Gel time [min] (175 ± 2 ºC) | 9 - 18 |

**Table 3.4** Requirements for physical properties (laminate average requirements) (Source: AGUSTA)

| | |
|---|---|
| Maximum void content [%] | 2 |
| Fibre content by volume [%v/v] | 50 ± 3 |
| Comp. density [g/cm$^3$] | 1.46 – 1.51 |
| Ply thickness [mm] | 0.20 – 0.24 |

**Table 3.5** Specification of service temperature (according STA 110-K-0026) (Source: AGUSTA)

| | |
|---|---|
| *Tg* dry (dry material) | At least 175ºC |
| *Tg* wet (material hot-wet conditioned)[1] | At least 130ºC |
| [1] tested on specimens cured as follows: | |
| Vacuum: during all cycle | |
| Heating rate: 2 – 3 ºC min | |
| Pressure: 2.7 atm (40 psi) | |
| Time: 120 ± 10 min | |
| Temperature: 175 ± 3 ºC | |

The polymeric materials, such as composite matrix, are capable of absorbing relatively small but potentially significant amounts of moisture from the surrounding environment. Although the moisture flow occurs relatively slow, after a period of exposure to a humid environment, a significant amount of water will eventually be absorbed by the material. This absorbed water may produce dimensional changes (as swelling), lower the glass transition temperature of the polymer, and reduce the matrix and matrix/fibre interface dependent mechanical properties of the composite (Figure 3.6).

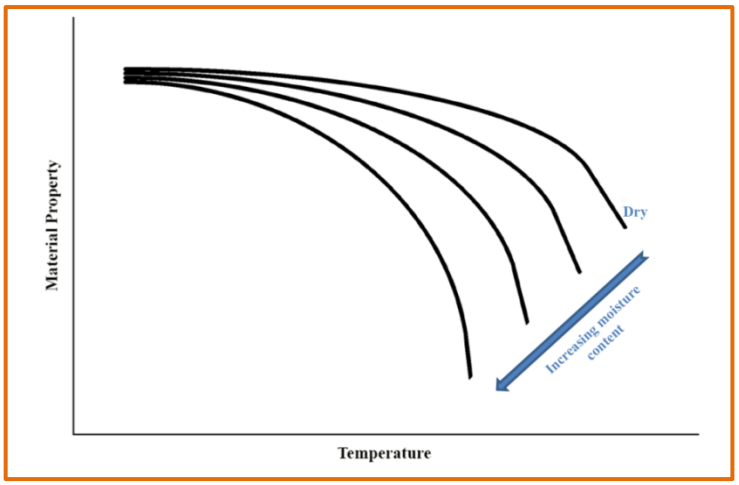


**Figure 3.6** Influence of temperature and moisture on matrix-dependent failure strength [156]

The glass transition temperature (*Tg*) is the temperature that when reached causes the transition of the polymer to a rubbery state, making the material less stiff. As the application of this material requires elevated temperatures, it is important to make sure the FRP composite's *Tg* will be higher than temperature it might ever be exposed to. Therefore, the mechanical properties must be determined for dry and after hot-wet conditioning. [156]

**Table 3.6** Minimum requirements for mechanical properties (Source: AGUSTA and OGMA)

| Mechanical property | T [ºC] | Direction | Dry | T [ºC] | Hot-wet |
|---|---|---|---|---|---|
| Tensile strength [MPa]/modulus[GPa] | -55 ºC | warp | 490/48 | --- | --- |
| | 23 ºC | warp | 490/48 | 23 ºC | 490/48 |
| | | fill | 460/48 | | 460/48 |
| | 132 ºC | warp | 460/43 | 110 ºC | 380/47 |
| | | fill | 430/43 | | 360/46 |
| Flexural strength [MPa]/modulus[GPa] | 23 ºC | warp | 652/42 | --- | --- |
| | | fill | 595/41 | --- | --- |
| | 132 ºC | warp | 510/39 | --- | --- |
| | | fill | 495/38 | --- | --- |
| Compressive strength [MPa]/modulus[GPa] | -55 ºC | warp | 590/49 | --- | --- |
| | 23 ºC | warp | 590/49 | 23 ºC | 500/--- |
| | | fill | 525/47 | | 450/--- |
| | 132 ºC | warp | 490/49 | 110 ºC | 290/--- |
| | | fill | 360/47 | | 265/--- |
| Interlaminar shear strength (ILSS) [MPa] | 23 ºC | warp | 69 | 23 ºC | 65 |
| | 132 ºC | warp | 41 | 110 ºC | 31 |

The specimens, prepared by OGMA, were manufactured using autoclave process. These specimens consist of 10 prepreg plies of plain weave 3K yarn, each ply having a thickness of 0.2 mm. The laminate stacking sequence is $[0_{10}]$, resulting in final thickness of approximately 2 mm. Figure 3.7 shows the arrangement of the layers along the longitudinal section of the test pieces. Figure 3.8 presents a detail of plain weave configuration used.

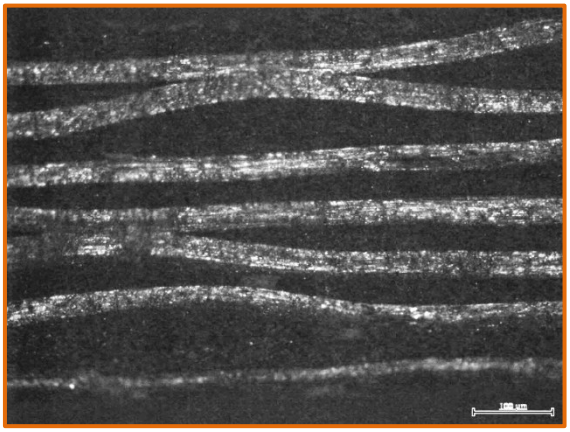

**Figure 3.7** Microscopic image of the longitudinal section of the specimens

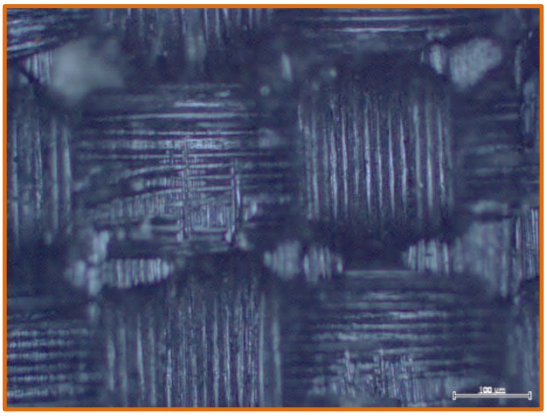

**Figure 3.8** Microscopic image detailing the plain weave configuration of the specimens

Since the conditions have not permitted the material to be purposely manufactured according to the specifications required for this work, the material used is from the leftovers of test specimens of the laminates from the NH Industries NH-90 program. Thus, and having the necessity to produce test pieces with different thicknesses, the solution found was to join several specimens. Apparently, this procedure is usual in industry when it is needed a higher material thickness, in specific and isolated cases, and does not cause significant differences in the results obtained. Consequently, several test pieces were joined, applying the same technique used in manufacture, in order to obtain different specimens thicknesses. Therefore, is expected that the results obtained can effectively contribute to the practical application of this work in the aircraft industry.

The specimens were produced in order to fulfil the requirements of planning experience, namely, five different values of thickness (Figure 3.9). The high and low values in the range of experimentation desired, +1 and -1, were assigned for the factor *Thickness* and from these were calculated the remaining levels (Table 3.7).

**Table 3.7** Values to be used for the factor *Thickness* in each of the five levels

| Factor | Levels | | | | |
|---|---|---|---|---|---|
| | -2 | -1 | 0 | 1 | 2 |
| Thickness [mm] | 2 | 4 | 6 | 8 | 10 |

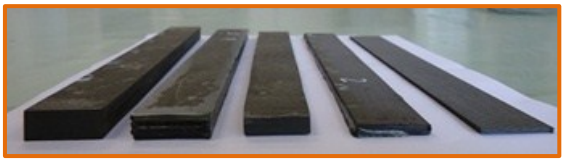

**Figure 3.9** Different thickness specimens used on experimental work

## 3.4 Tool selection

Since the aim of this work is the systematization of knowledge in order to be able to minimize the occurrence of delamination damage in practical industrial situations, it is of paramount importance the choice of tools to use. In fact, among the numerous choices available, the focus was to choose the solutions applied in industry. Several contacts have been established, including OGMA and several suppliers to understand what tools for drilling carbon composites are currently being used. The choice of tools to use in this work came upon three types of geometry: the conventional twist drill, the drill commonly used by OGMA and the aircraft industry in general - straight flute (also called spade drill) - and the drill geometry designed specifically by *DORMER* for drilling composite materials.

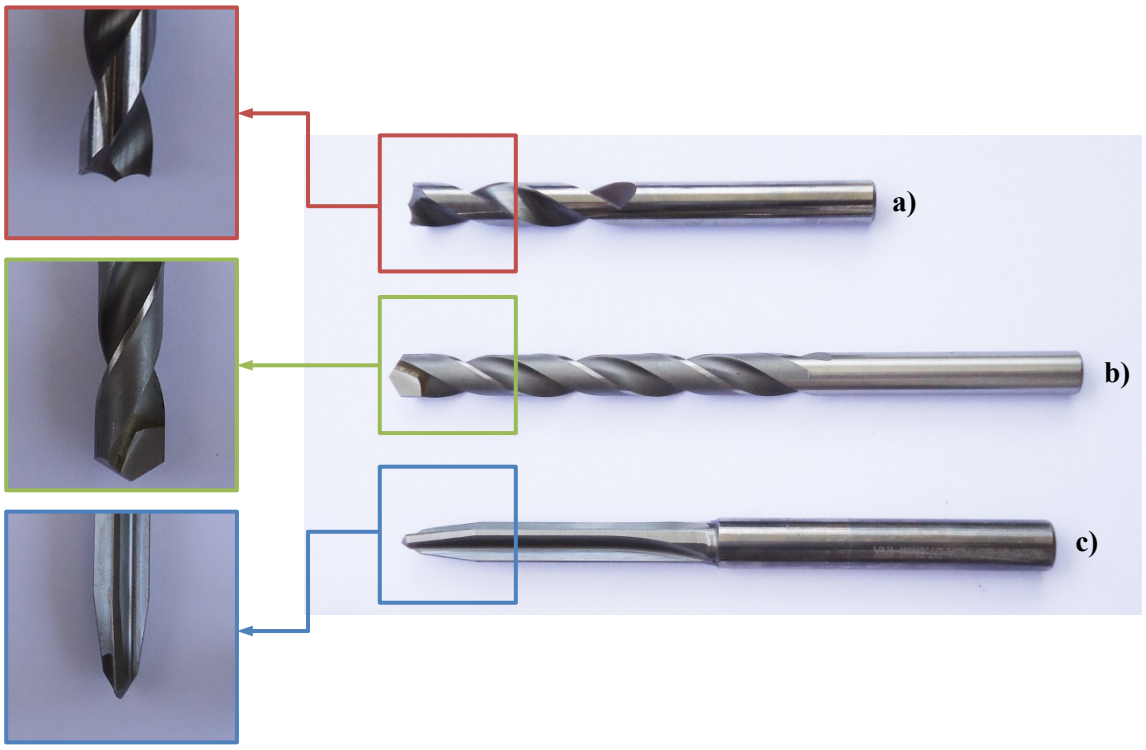


**Figure 3.10** Tool geometries used on experimental work: **a)** W-shape drill; **b)** Twist drill; **c)** Straight flute drill

The starting point of this study was to compare the three different types of tool geometries testing their influence on the obtained damage. As the experimental procedure involves response surface methodology, the method for this analysis is to divide the tests into three different designs, corresponding to the tool geometries.

The three types of drilling tools are made of tungsten carbide micrograin, grade K20. This material was chosen because it has the qualities required for drilling composites of carbon fibres: wear resistance and toughness.

The tools were chosen in order to fulfil the requirements of planning experience, namely, five different values of tool diameter. The extreme high and low values in the range of experimentation desired, +2 and -2, were taken into consideration in the selection of the tool diameter, in order to ensure that realistic values were chosen. The remaining levels for the factor *Tool diameter* were calculated from these (Table 3.8).

The straight flute geometry drill was available in all the diameters proposed. However, the smallest diameter, corresponding to level -2, has only two flutes, being different from the other diameters that have 4 flutes. Figure 3.11 illustrates the difference.

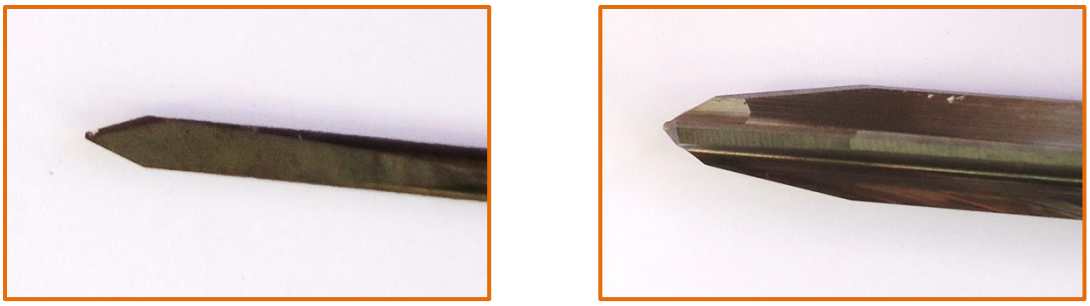

**a)** **b)**

**Figure 3.11** Different bit geometry for different diameters of the Straight flute drill:
**a)** $d$ = 3 mm; **b)** $d$ = 7 mm

**Table 3.8** Values to be used for the factor *Tool Diameter* in each of the five levels

| Factor | Levels | | | | |
|---|---|---|---|---|---|
| | -2 | -1 | 0 | 1 | 2 |
| Tool diameter [mm] | 3 | 5 | 7 | 9 | 11 |

## 3.5 Drilling Parameters

Since the drill geometries presented different number of cutting lips, the feed per tooth was the chosen factor to verify the effects of the feed rate on the responses. The preliminary tests performed permitted to ascertain the range of values to use in this phase of the experiments. Table 3.9 shows the values associated with the coded parameters.

**Table 3.9** Values to be used for the factor *Feed per tooth* in each of the five levels

| Factor | Levels | | | | |
|---|---|---|---|---|---|
| | -2 | -1 | 0 | 1 | 2 |
| Feed per tooth [mm/tooth] | 0.01 | 0.0325 | 0.055 | 0.0775 | 0.1 |

In order to study the effects of the spindle speed on the responses, similar procedure was made. The values were obtained from the results of preliminary tests, but also for the limitation of the spindle speeder (max. 20 000 rpm). The values for each level of encoding are shown in Table 3.10.

**Table 3.10** Values to be used for the factor *Spindle speed* in each of the five levels

| Factor | Levels | | | | |
|---|---|---|---|---|---|
| | -2 | -1 | 0 | 1 | 2 |
| Spindle speed [rpm] | 4 000 | 8 000 | 12 000 | 16 000 | 20 000 |

## 3.6 Radiographic Analysis

The non-destructive testing (NDT) used for evaluation of the delamination damage of the holes produced in the experiments was the radiography (X-ray). The radiography equipment used for analyzing the extent of delaminated area was a Kodak digital radiography system RVG 5100 associated with a Kodak Rx unit 2100, with the following characteristics (Table 3.11).

**Table 3.11** X-ray equipment characteristics

| **Kodak RVG 5100** | | **Kodak 2100** | |
|---|---|---|---|
| Active area: | 22x30 mm | V: | 60 kv |
| Resolution: | 30 µm | I: | 7 mA |
| Greyscale: | 32 bit | t: | 0.620 s |
| | | N: | 490 W |

To make the defects visible in the radiography and evaluate their extension, an application of X-ray opaque penetrant was needed. This penetrant fills pores, matrix cracks, delaminations and fibre-matrix debonds and forms a contrast between damage and undamaged area. This contrast is made since the penetrant absorbs X-rays more readily than the surrounding material.

All the specimens were immersed in diiodomethane before the radiographic analysis for a period of time never less than one hour. This penetrant was chosen because of the good characteristics, adequate to this type of investigation. Diiodomethane offers high-radio opacity and good penetration capabilities, and it is volatile. Since it evaporates readily the composite is quickly cleaned.

The parameters used in all tests performed were an exposure time of 0.25 s and a focal length of 50 mm.

**Figure 3.12** Radiographic analysis equipment

# 4

# Discussion of Experimental Results

## 4.1 Introduction

In a first stage of this work preliminary experiments were conducted in order to attest the methodology, ascertain the values of variables and establish the region of interest, and investigate the adequacy of the new approach proposed in order to minimize the damage. These tests were performed using input parameters considered in the domain of conventional drilling, using high speed steel twist drills, with a view to try to reproduce some of the literature results.

From these tests, it was shown that the material provided had some voids. Hence, the preliminary tests produced x-ray images that suggest the composite structure to be dissimilar which lead to the investigation of a new image analysis methodology (a study currently being conducted as part of an MSc work). It was also confirmed that the HSS tool material was not suitable for the drilling process of the carbon fibre composite material, since the drills presented unacceptable abrasive wear, after drilling a limited number of holes (approximately four). This conducted to the selection of a harder material for the tools.

Afterwards, a series of experiments was performed to evaluate the effects of spindle speed and feed per tooth for the different tool geometries, with constant workpiece thickness and tool diameter.

Once the methods, tools and equipment were established and verified, the DOE experiments were lead for the three tool geometries, to obtain the empirical models that describe the process. Response surface methodology was the approach to achieve these models, and its systematic development is presented in Appendix C.

The models were then verified by means of a series of experiments whose purpose was to validate the empirical results. The input factors chosen for the validation tests were selected randomly within the domain considered for this study. Thus it was possible to verify the

consistency of the empirical models, comparing the calculated values with the results obtained in the validation tests.

Finally, another series of experiments were conducted to investigate the feasibility of the new workpiece clamping method proposed. Three different cases were studied: a) when the part is "loose", b) with the usual tightness and c) compressed with a specific axial force, between two metal parts acting as a bushing for the drill. From these preliminary tests performed using a 4 mm diameter high speed steel (HSS) twist drill and equal process parameters ($S$ = 2 000 rpm; $f_z$ = 0.02 mm/tooth) for drilling a 2 mm thickness specimen, the effect of workpiece clamping on the damage obtained was appraised and the results looked satisfactory, leading to this new set of experiments.

## 4.2 Experimental Results for Thrust Force

According to the literature, thrust force is considered to be the major contributor of delamination during drilling. Hence, several researches have been conducted in order to prove that keeping the thrust force below a critical value, delamination during drilling would be constrained or eliminated. These analytical models have been presented earlier (1.3.2.5).

In this work, the thrust force was monitored in each experiment, and the data collected was processed using *MATLAB* software. A signal processing 5th order Butterworth low pass filter was used in order to suppress interfering signals and reduce background noise (Figure 4.1). The low pass Butterworth filter design it is the most commonly used function. Butterworth filters are characterized by a magnitude response that is maximally flat in the pass band and monotonic overall.

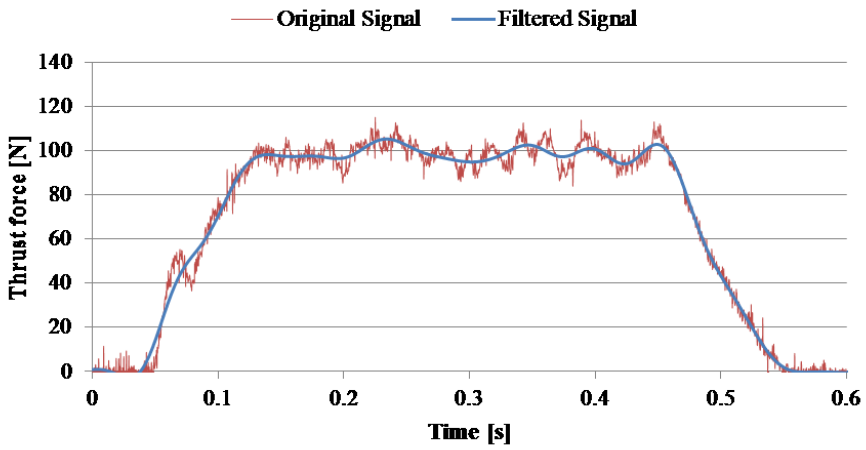


**Figure 4.1** Original and filtered signal for measured thrust force during drilling using a twist drill

The filtered signal was employed to represent the typical curves obtained with the different tool geometries. Figure 4.2 shows examples of the measured thrust force for the three geometries under analysis when drilling a composite specimen (Input parameters: $S$ = 16 000 rpm; $f_z$ = 0.0325 mm/tooth; $d$ = 5 mm; $t$ = 8 mm).

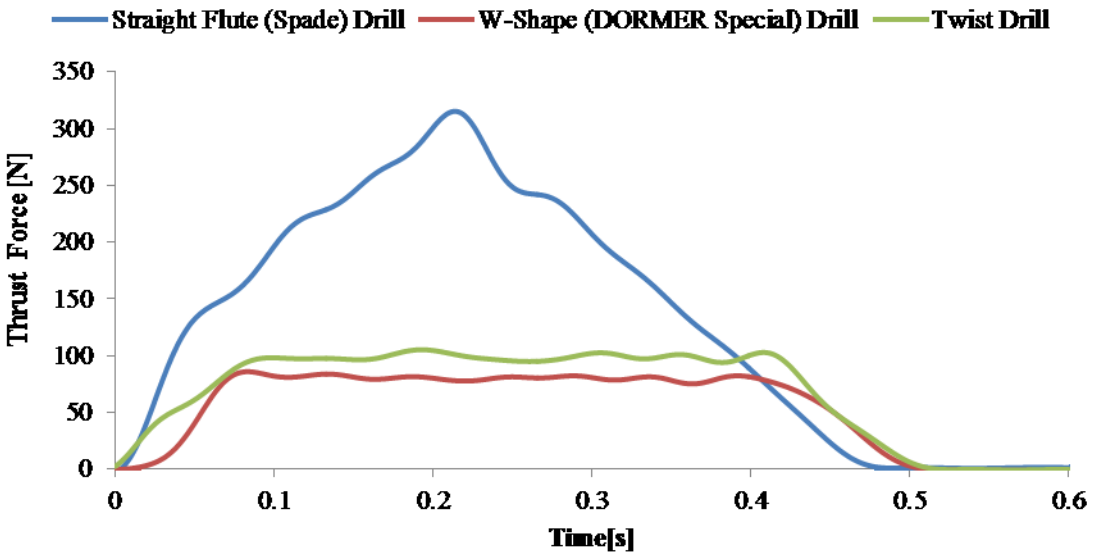


**Figure 4.2** Measured thrust force during drilling for the three different geometries

Dharan and Won [143], indicated that the relevant stages and events when drilling composite laminates using carbide-tipped twist drills are:

**Table 4.1** Evolution of a drilling operation [143]

| | | |
|---|---|---|
| 1 | Approach: | The drill approaches the workpiece. |
| 2 | Contact: | The drill tip makes contact. |
| 3 | Normal drilling: | Drilling without delamination. |
| 4 | Initiation of delamination: | When the critical thrust force is exceeded, delamination starts. |
| 5 | Drill breakthrough: | The drill tip exits the workpiece. |
| 6 | Completion: | A hole is completed. |
| 7 | Withdrawing drill: | The drill must be moved backward and withdrawn from the workpiece. |

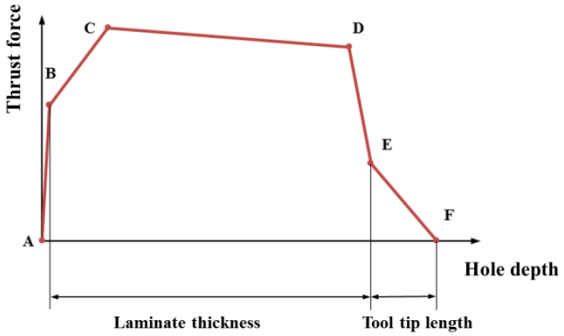


**Figure 4.3** Idealized thrust force response during drilling using carbide tipped twist drill [143]

Fernandes and Cook [58] investigated the thrust force produced during drilling using carbide straight flute drills, and divide the drilling process into five drilling stages, as follows:

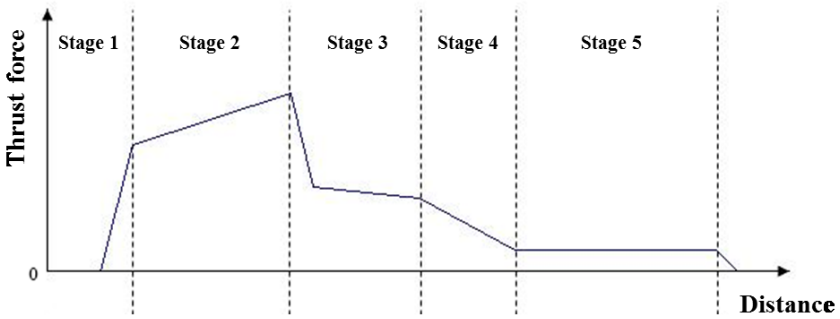


**Figure 4.4** Drilling stages for a straight flute drill when measuring thrust force [58]

**Table 4.2** Evolution of a drilling operation for a straight flute drill [58]

| | | |
|---|---|---|
| 1 | Entrance: | The drill approaches the workpiece and the drill tip makes contact. |
| 2 | Drilling: | The material removal starts as the cutting lips engage the workpiece. Delamination is associated to this stage due to the high values of thrust force. |
| 3 | Drilling and reaming: | The chisel edge reaches the bottom surface of the workpiece. |
| 4 | Reaming: | Represents the reaming process. |
| 5 | Backing out: | The drill backs out of workpiece. Reaming continues while there is contact between the workpiece and the drill. |

Lazar and Xirouchakis [85] indicate the drilling stages using carbide straight flute drill in the following manner:

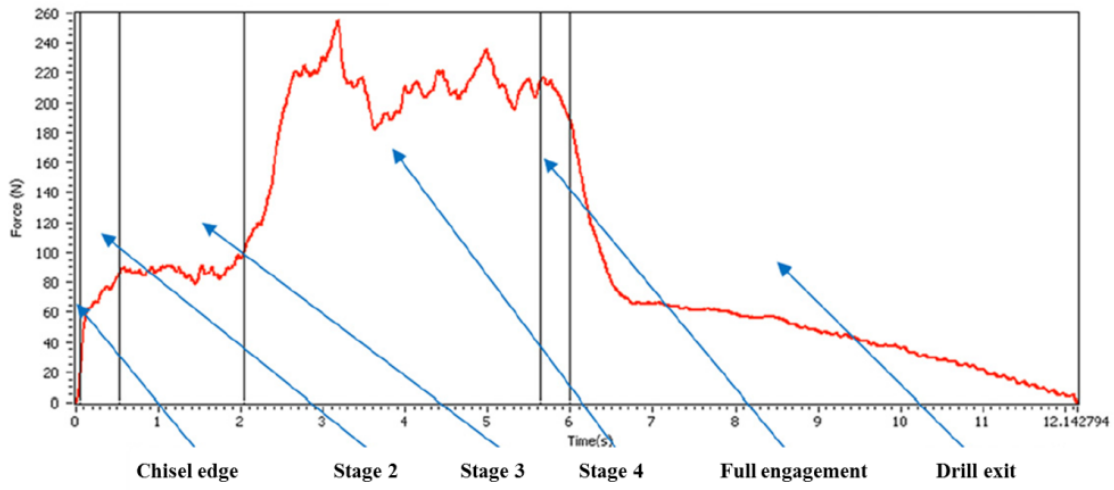


**Figure 4.5** Drilling stages for a straight flute drill [85]

**Table 4.3** Evolution of a drilling operation for a straight flute drill [85]

| | | |
|---|---|---|
| 1 | Chisel edge: | Engagement of the small chisel edge |
| 2 | Stage 2: | The main cutting lips become fully engaged. |
| 3 | Stage 3: | The long cutting lips become engaged as well (2 flutes in action). |
| 4 | Stage 4: | The secondary flutes begin to cut as well (4 flutes). At the end of this stage the maximum thrust is obtained. |
| 5 | Full engagement: | Before the chisel edge pierces through the workpiece (short period). |
| 6 | Drill exit: | The drill backs out of workpiece. |

Not all these stages are clearly visible in the graphs obtained. This would be expected since the spindle speeds and feed rates used by these authors are clearly lower than those used in this work and some of these stages occur so fast that cannot be identified. However, the evolution trend for both geometries is consistent with the literature [4, 53, 59, 143]. In the case of the W-shape drill, this information is not reported. Nevertheless, and due to the characteristics of the tool geometry, one would expect behaviour more like that of the twist drill, as is the case.

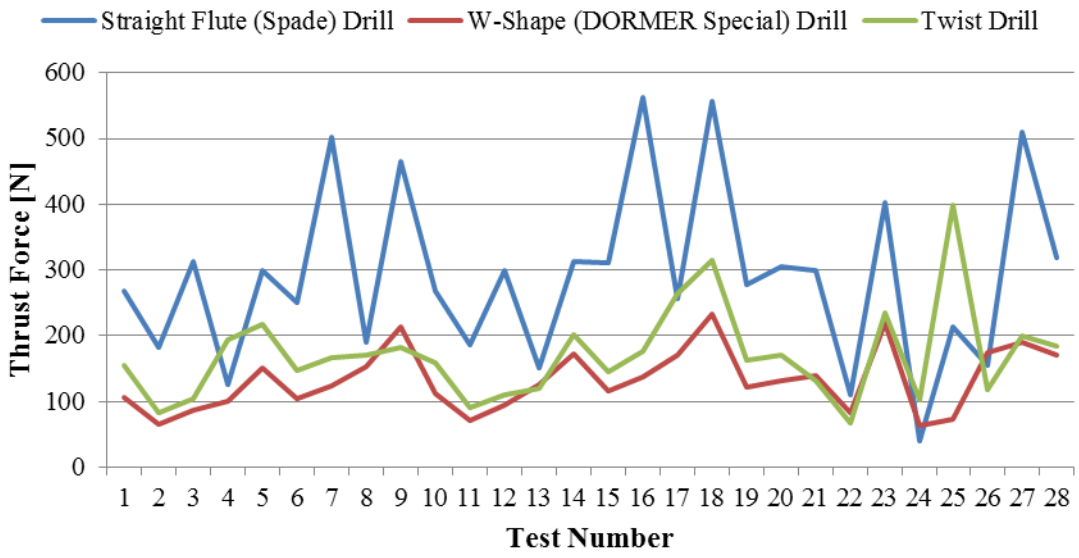


**Figure 4.6** Comparison of the thrust force depending on the type of tool geometry

Comparing the thrust force results obtained for the three different geometries (Figure 4.6), it is clear that higher values were measured for the straight flute drill. However it should be taken into account that these values were obtained on experimental design whose variable with respect to the tool progress is the feed per tooth and apart from 3 mm diameter all other tools have four flutes. Consequently, in those circumstances, the feed rate is twice the feed rate of the other tool types. The test performed with the 3mm diameter straight flute drill (Test S24) is the one that presents the lower thrust force value which can denote that for a most appropriate comparison of values the variable chosen for the planning of experiments should have been the feed rate.

In order to create the empirical model that describes this process, the Response Surface Methodology was used after the design of experiments defined previously in Chapter 2. The adequacy of the model response was checked using the F-Test with a confidence interval of 95%. The histogram of residuals and scatter plots of residual values vs. predicted and observed values were done to verify the existence of other factors which influence the responses and the consistency of the model. The application and results of this methodology are presented in Appendix C.

Figure 4.7 represents the correspondent fitted response surfaces showing the interaction effect due to feed per tooth and spindle speed for a drill diameter of 7 mm and a workpiece thickness of 6 mm (left) and to the most significant factors on thrust force (right).

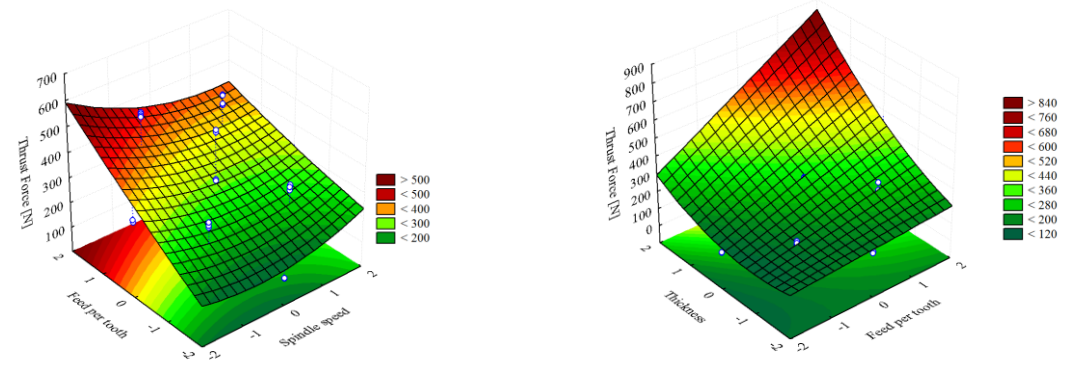


**a)**

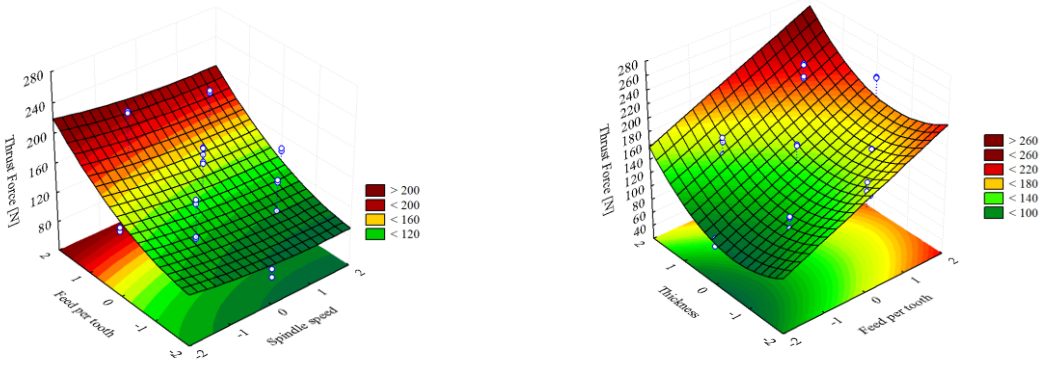


**b)**

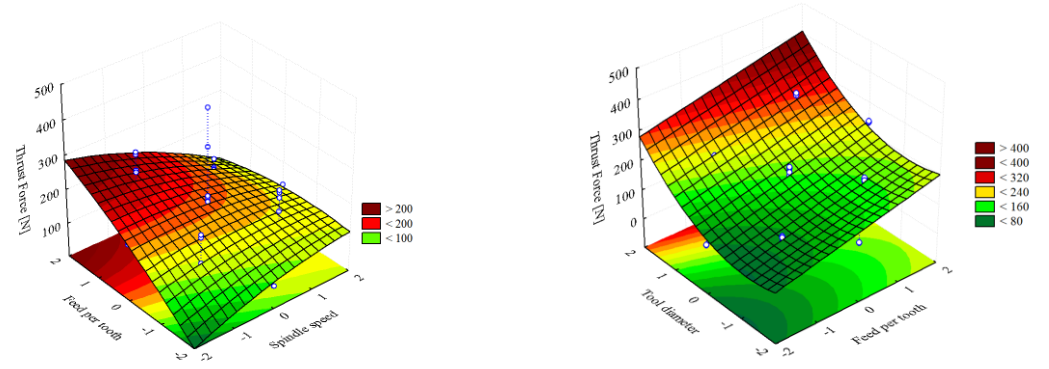


**c)**

**Figure 4.7** Fitted surface response. **Left:** $F = f(f, S)$, $d = 7$ mm; $t = 6$ mm; **Right: a)** Straight flute drill: $F = f(f_z, t)$, $S = 12\,000$ rpm; $d = 7$ mm; **b)** W-shape drill: $F = f(f_z, t)$, $S = 12\,000$ rpm; $d = 7$ mm; **c)** Twist drill: $F = f(f_z, d)$, $S = 12\,000$ rpm; $t = 6$ mm

The resulting empirical models, second-degree polynomials, to estimate each of the responses are presented below (Table 4.4).

**Table 4.4** Mathematical models to predict thrust force

| | |
|---|---|
| Straight Flute Drill ($\bar{R}^2 = 0.8872$) | $F = 286.883 - 13.236S + 13.495S^2 + 75.733f_z - 30.571d^2 + 98.606t + 20.926t^2 + 31.080f_z \cdot t$ |
| W-Shape Drill ($\bar{R}^2 = 0.7869$) | $F = 127.703 + 27.371f_z + 22.676d - 15.260d^2 + 14.048t + 13.418t^2 + 8.411d \cdot t$ |
| Twist Drill ($\bar{R}^2 = 0.8151$) | $F = 164.888 - 9.468S + 32.437f_z + 51.524d + 19.862d^2 + 17.764t - 19.415S \cdot f_z$ |

The significant terms of the regression analysis do not correspond to the same input variables for the three models. This fact indicates that the effect of the input variables is not similar for the diverse tool geometries, thus requiring an individual exploration. Nevertheless is possible to observe that feed per tooth is, in all cases, an important variable. From Figure 4.7 it can be observed that, when using twist drills, high spindle speed together with high feed rate can produce lower thrust force, which is a good indicator that using high productivity drilling allows obtaining acceptable delamination damage. The other geometries present better behaviour using lower feed rate, even for higher spindle speed, and that agrees to the suppliers' recommendations.

Figure 4.8 shows the different Pareto charts of standardized effects for the thrust force models resulting from *Statistica* software analysis of a central composite (response surface) design.

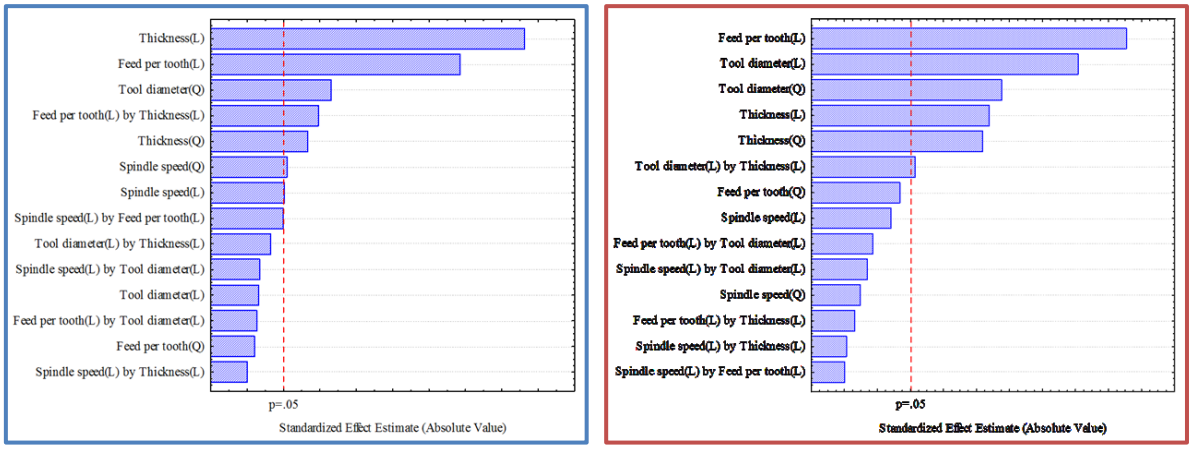


**a)** **b)**

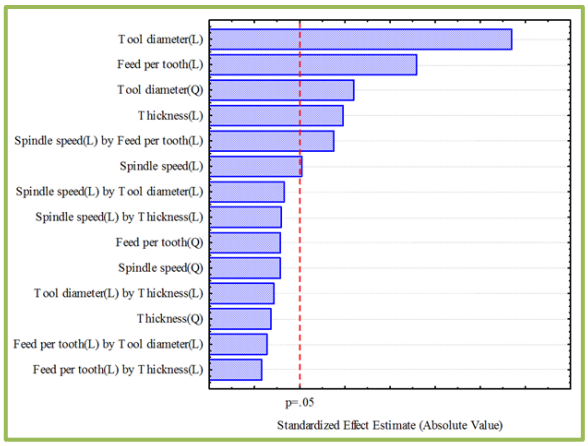


**c)**

**Figure 4.8** Pareto chart of standardized effects for the response Thrust Force: **a)** Straight flute drill; **b)** W-shape drill; **c)** Twist drill

It can be shown that the input variables *Thickness*, *Feed per tooth* and *Tool diameter* are the most significant factors in all cases, but with different weights. Spindle speed seems to be the variable that has less effect over the thrust force response which is in agreement with the consulted literature.

The results of the validation tests are presented in Appendix D (Table D.1). Due to the different characteristics of the models, for better understanding, the variation between the empirical and experimental results will be described for each model individually.

Based on the complete results set, a study was carried out to analyse the trends of variation of the response with the input factors. As it was necessary to keep all other variables constant, there are four results available for each pair of factors consisting in tool diameter and material thickness.

Figure 4.9 and Figure 4.10 show the thrust force in function of the spindle speed for the three tool geometries, namely, straight flute drill, W-shape drill and twist drill.

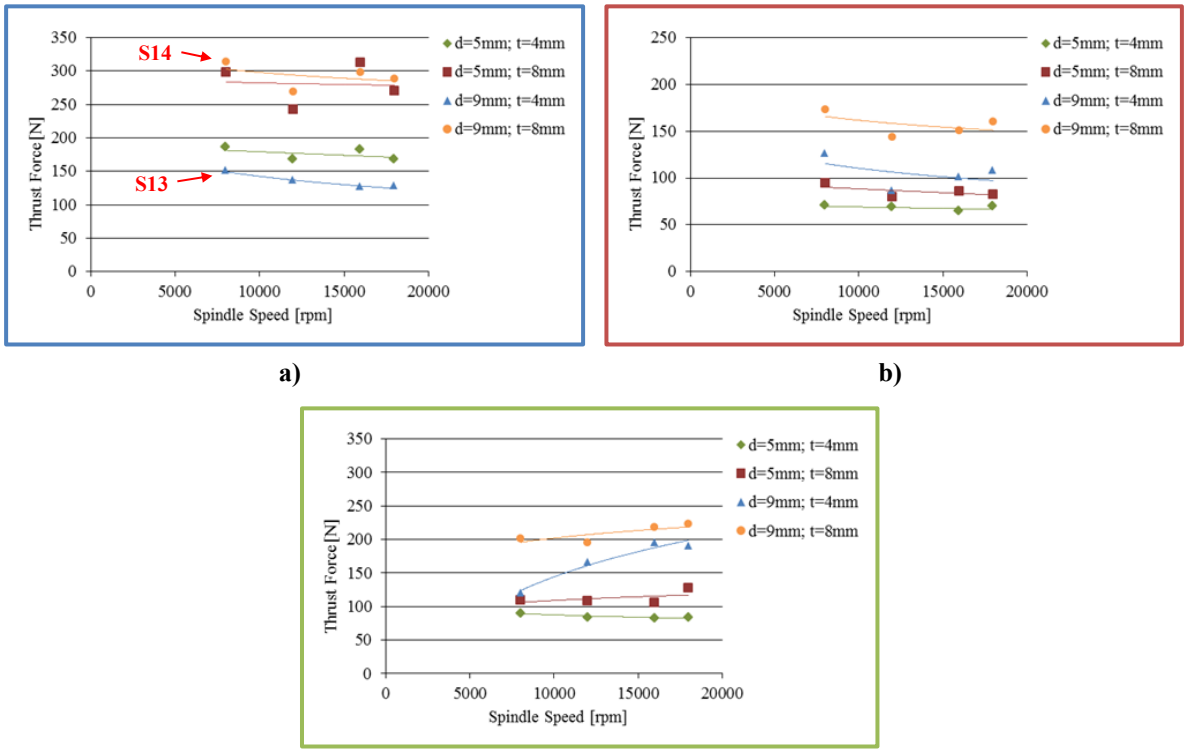


**Figure 4.9** Variation trend of thrust force with spindle speed ($f_z$ = 0.0325 mm/tooth): **a)** Straight flute drill; **b)** W-shape drill; **c)** Twist drill

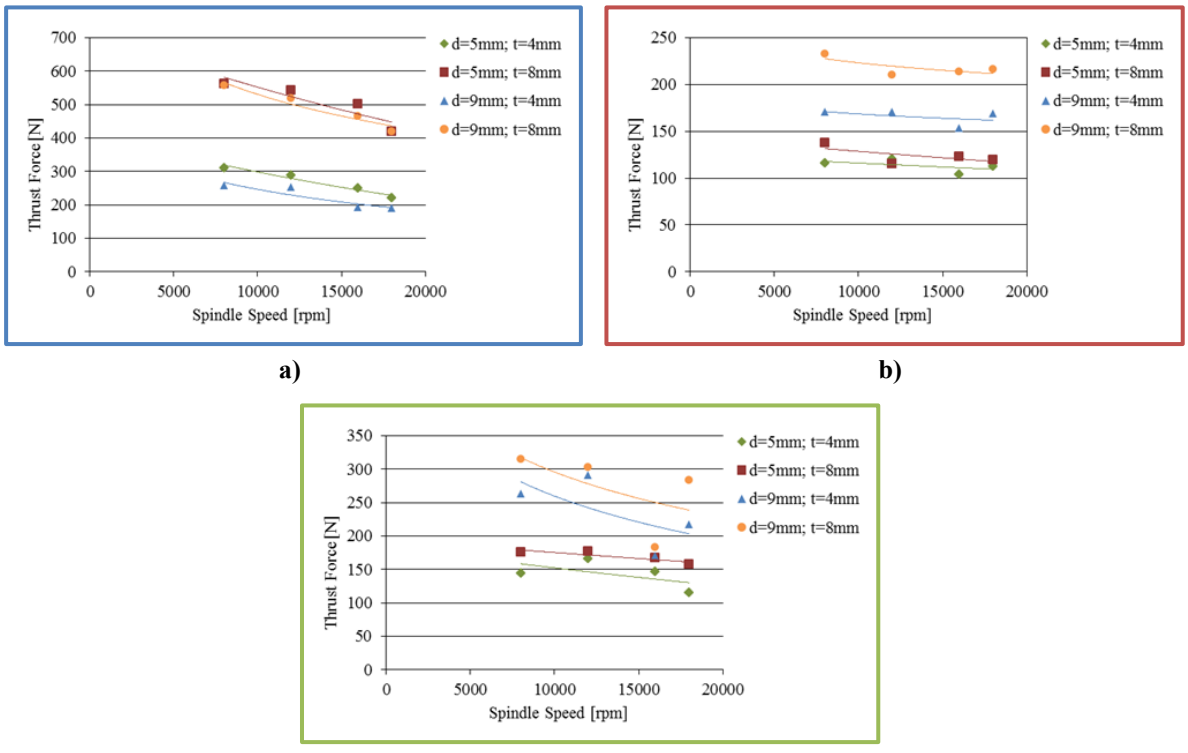


**Figure 4.10** Variation trend of thrust force with spindle speed ($f_z$ = 0.0775 mm/tooth): **a)** Straight flute drill; **b)** W-shape drill; **c)** Twist drill

As can be observed, in general, the thrust force tends to decrease with increased spindle speed, and increases with increased tool diameter and workpiece thickness, which is a likely behaviour when using conventional drilling [1, 5, 26, 34, 57, 74, 95, 97, 104, 111, 135].

When comparing the trends of the experimental values with those of the empirical models developed and presented earlier, all the results were found to be very similar. Figure 4.11 shows an example, when drilling using twist drill, of the comparison between the values from Figure 4.10 c) and the calculated values from the empirical model for the same cutting conditions.

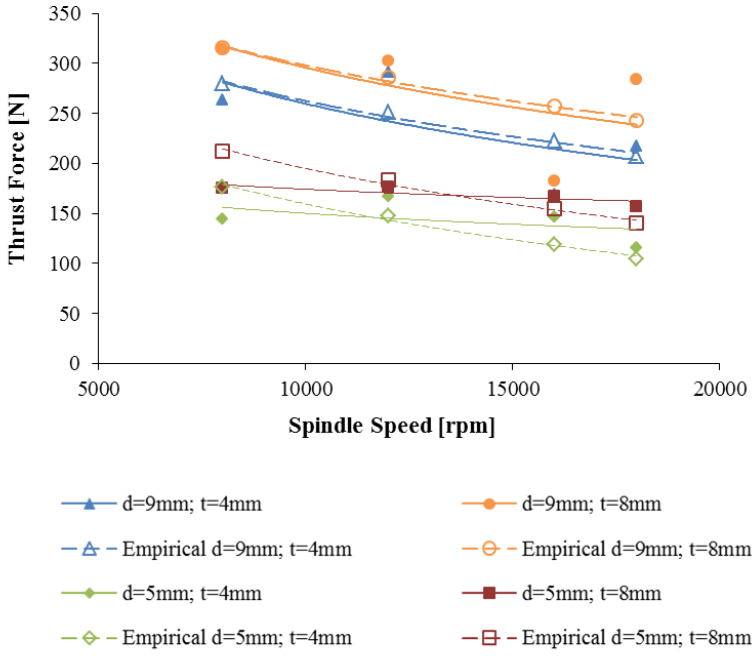


**Figure 4.11** Comparison of the trend of thrust force between experimental and empirical values (Twist drill; $f_z$ = 0.0775 mm/tooth)

The first exception of this trend consists in the results for the tests carried using a 9mm twist drill. In this case, the tendency is that the thrust force increases with increased spindle speed. This tendency was already reported in the literature. Lin and Chen [25] observed this effect of increasing force with increasing spindle speed in their study using high speed drilling, and explained it as could being due to tool wear. However, in the present work the tools were all observed after drilling, and the tool wear was found not to be significant.

This unexpected tendency may be due to the circumstances that occurred conducting the tests in question, mainly when drilling the 4mm specimen. In fact, with the exception of test T13 (first point of the curve corresponding $d$ = 9 mm and $t$ = 4 mm), problems occurred during drilling, as the specimen skip of fixing (Test V3), the drill loosen up (Test V7) and the existence of much disruption during the process (Test T4), yielding a hole with a larger diameter than expected. From the analysis made comparing the theoretical drilled area and the actual drilled area, the values obtained differ between 19.38% (Test V3) and 33.04% (Test V7) while all the other values vary between 0.8 and 3%.

Regarding to straight flute drill geometry, thrust force tends to increase with increased tool diameter and workpiece thickness, but the lowest values are obtained for the 9 mm diameter, when drilling a 4 mm specimen. This can be explained by the tool geometry since the chisel edge pierces through the workpiece before full engagement occurs. Indeed, the long cutting lips in a 9 mm straight flute drill have a length of 5 mm which is greater than the thickness of the workpiece (Figure 4.12). When the secondary flutes begin to cut as well, the reaming forces add to the measurements and, as typically happens, the maximum thrust force occurs when the drill exits the back of the specimen. In this case, the maximum value for thrust force is observed just before the drill point exits the workpiece and the reaming yet to take place, producing lower values for thrust force.

Figure 4.13 represents the measured thrust force during tests S13 and S14 using the same spindle speed, feed per tooth and tool diameter ($S$ = 8 000 rpm; $f_z$ = 0.0325 mm/tooth; $d$ = 9 mm) and thickness of, respectively, $t_{S13}$ = 4 mm and $t_{S14}$ = 8 mm. In this figure it can be seen that the maximum feed force takes place when the drill exits the test piece that is the depth corresponding to its thickness. Afterwards the curves represent the reaming and drill exit stages.

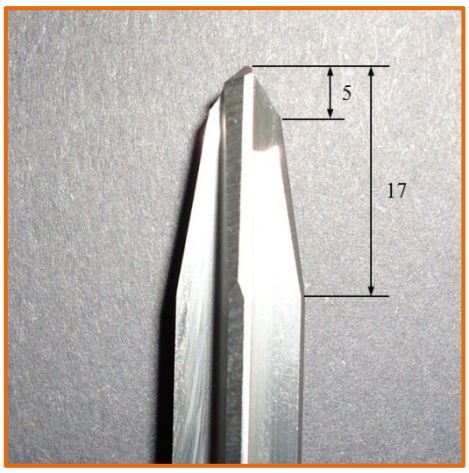


**Figure 4.12** Geometry of the 9 mm straight flute drill used in the experiments

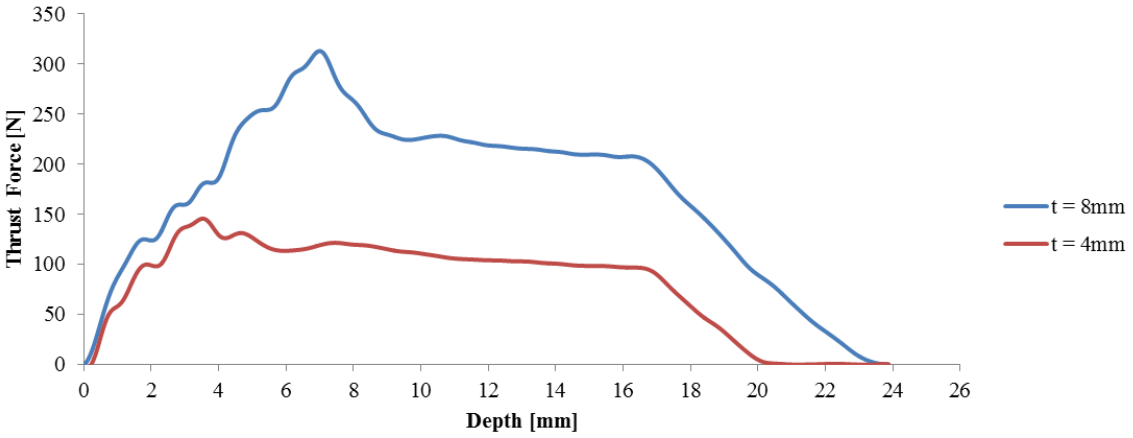


**Figure 4.13** Comparison between thrust force when drilling 4mm and 8mm thickness workpiece using the 9 mm straight flute drill (Tests S13 and S14)

Figure 4.14 and Figure 4.15 correspond to the variation of the measured thrust force when increasing the feed rate. At this case it is found that the thrust force increases with increased feed, as expected. In all surveyed studies concerning drilling of CFRP, the effect of the feed rate on the thrust force is noteworthy, and this is the most influent cutting parameter. Once again, as expected, it is observed that the lowest values of thrust force using straight flute drill geometry are obtained for the 9 mm diameter, when drilling a 4 mm specimen.

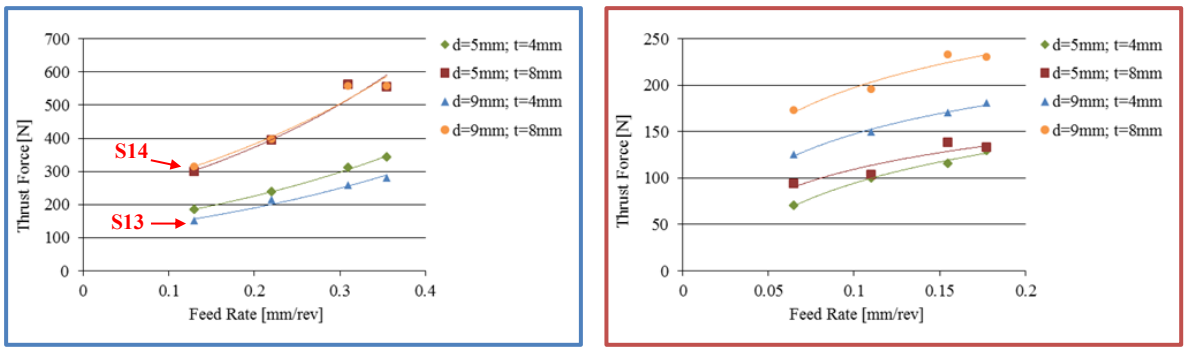


**a)** **b)**

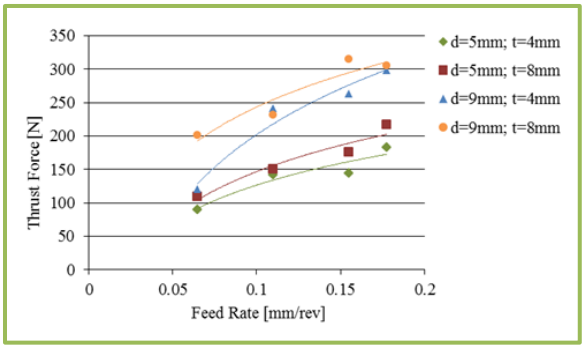


**c)**

**Figure 4.14** Variation trend of thrust force with feed rate ($S$ = 8 000 rpm): **a)** Straight flute drill; **b)** W-shape drill; **c)** Twist drill

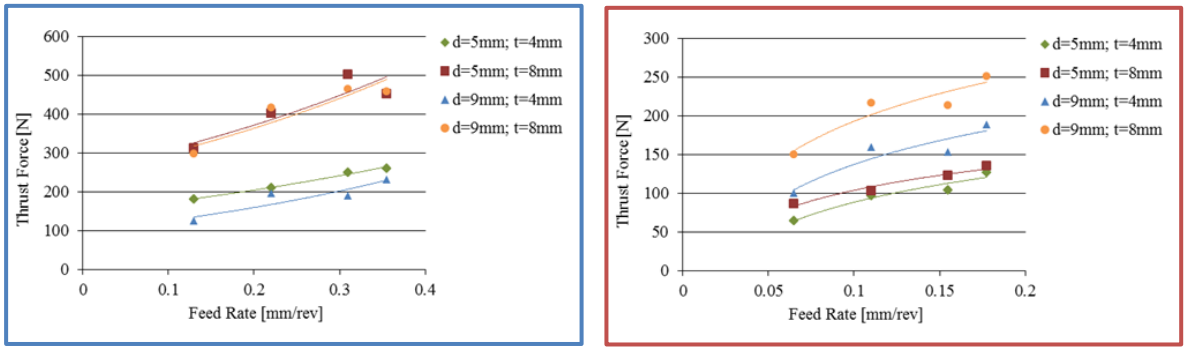


**a)** **b)**

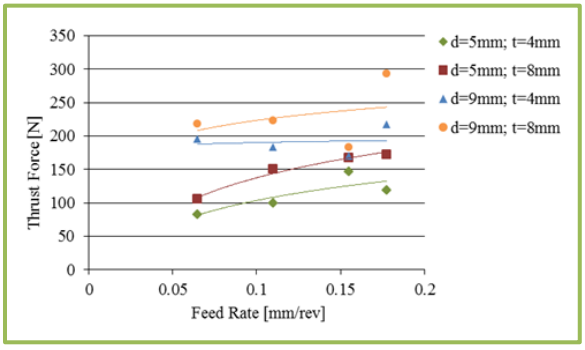


**c)**

**Figure 4.15** Variation trend of thrust force with feed rate ($S$ = 16 000 rpm): **a)** Straight flute drill; **b)** W-shape drill; **c)** Twist drill

The normalized measure of the variation between the experimental values and the predicted values is obtained calculating the relative error (RE) given by:

$$RE = \frac{F_{exp} - F_{pred}}{F_{exp}} \tag{4.1}$$

The prediction accuracy of model is obtained by the mean absolute percentage error (MAPE). The MAPE measures the average relative discrepancy, which is equivalent to the percentage prediction accuracy of model for any data set [73], and is given by:

$$\Delta = \frac{100}{n} \sum_{i=1}^{n} \left| \frac{F_{exp,i} - F_{pred,i}}{F_{exp,i}} \right| \tag{4.2}$$

Where $F_{exp,i}$ and $F_{pred,i}$ are, respectively, the experimental value and the predicted value of thrust force corresponding to data set *i* and *n* is the number of data sets.

The relative error for the three models corresponding to the tool geometries is presented in Appendix D (Table D.4). The average model performance error, calculated from (4.2), is found to be 9.95% for the straight flute drill model, 8.97% for the W-shape drill model and 8.78% for the twist drill model. The experimental values, when compared to the predicted values from the developed models presented similar maximum variation and the correspondent value was within 16.7% (twist drill) to 23.1% (straight flute drill) for validation data. The maximum variation for each model is highlighted in Table D.4.

Figures 4.16, 4.17 and 4.18 represent graphically the comparison of experimental and predicted values for, respectively, straight flute drill, W-shape drill and twist drill empirical models. The variation between values is also shown, according to the calculated values of relative error.

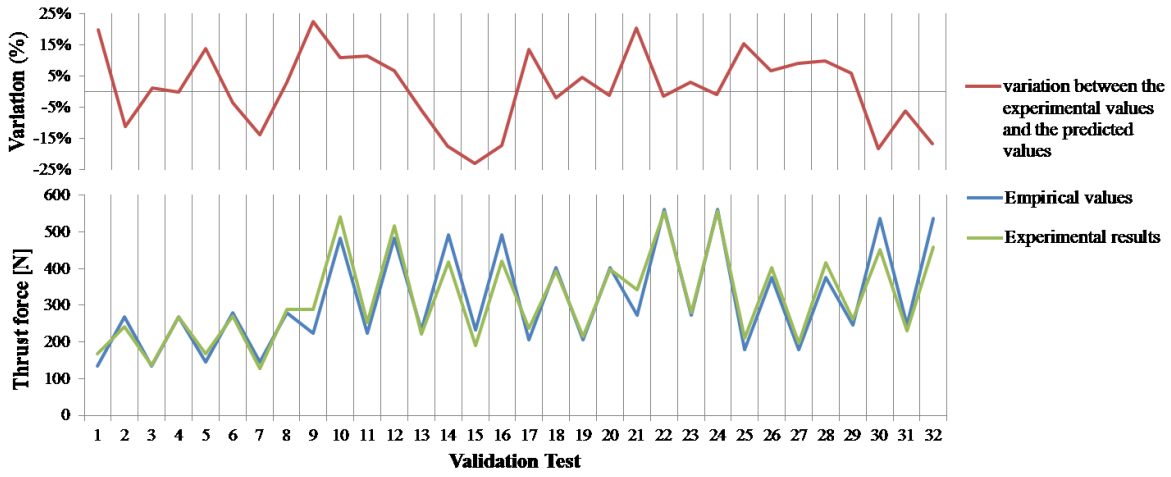


**Figure 4.16** Variation and comparison of experimental and predicted values from the empirical model for the straight flute drill geometry

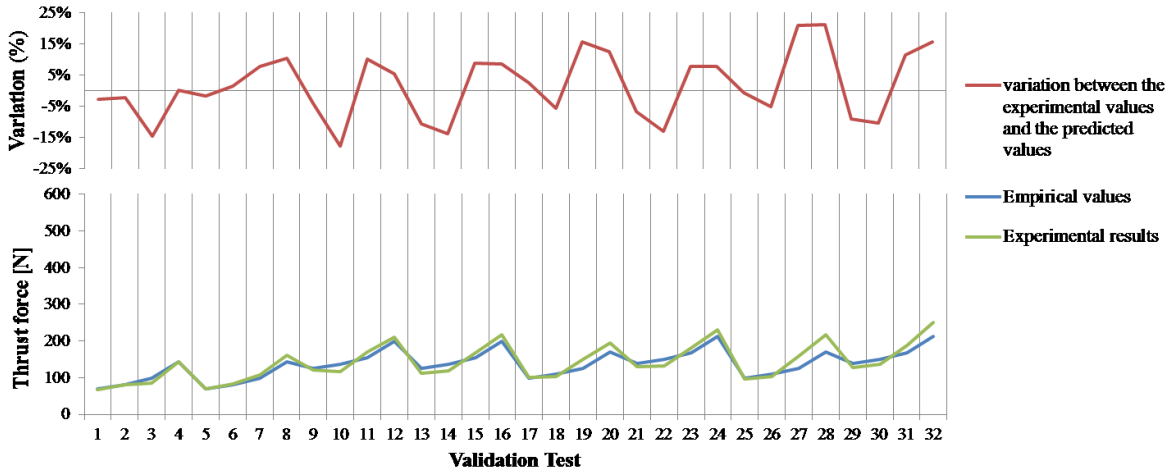


**Figure 4.17** Variation and comparison of experimental and predicted values from the empirical model for the W-shape drill geometry

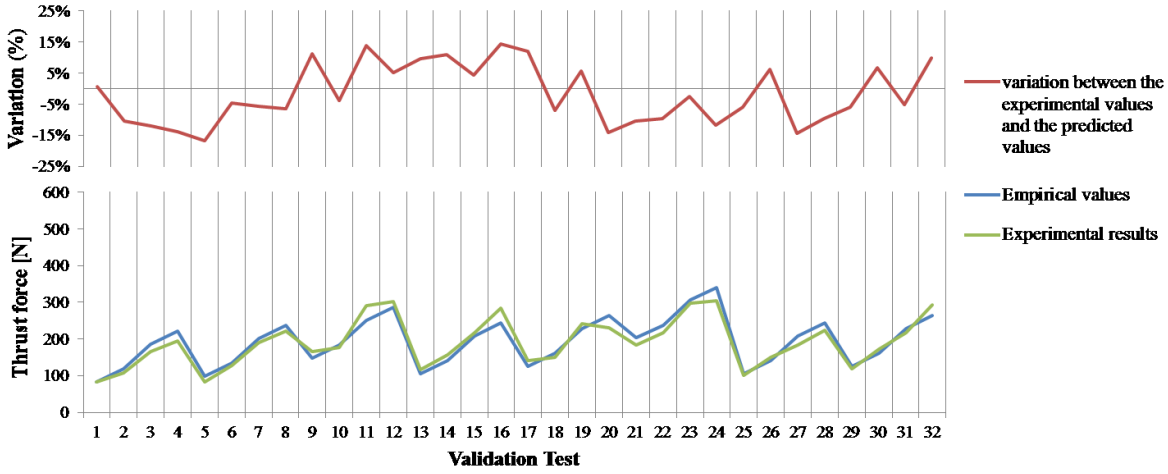


**Figure 4.18** Variation and comparison of experimental and predicted values from the empirical model for the twist drill geometry

By observing the graphs it can be seen that the behaviour of the empirical model is embodied by the values obtained in the experimental validation. However, the difference between experimental and predicted values is substantial, showing that the adequacy of the models is not completely fulfilled. However, the values of $\bar{R}^2$ found indicate goodness on fit. Therefore, the models represent the response of the process, but it is necessary to deepen their study in order to find a reason for this variation.

As one of the goals proposed for this work was the investigation of high productivity drilling, it is important to ascertain the influence of the power consumed by the process on the response.

Considering all the DOE runs, the values were represented on a scatter plot, and added their trend lines (Figure 4.19), showing that the thrust force tends to increase with increasing required power (*N*), the same happening with material removal rate (*MRR*). However, when observed by a physical point of view, this usual logarithmic representation of the variation trend does not seem to make much sense, since the dispersion of the results is very wide.

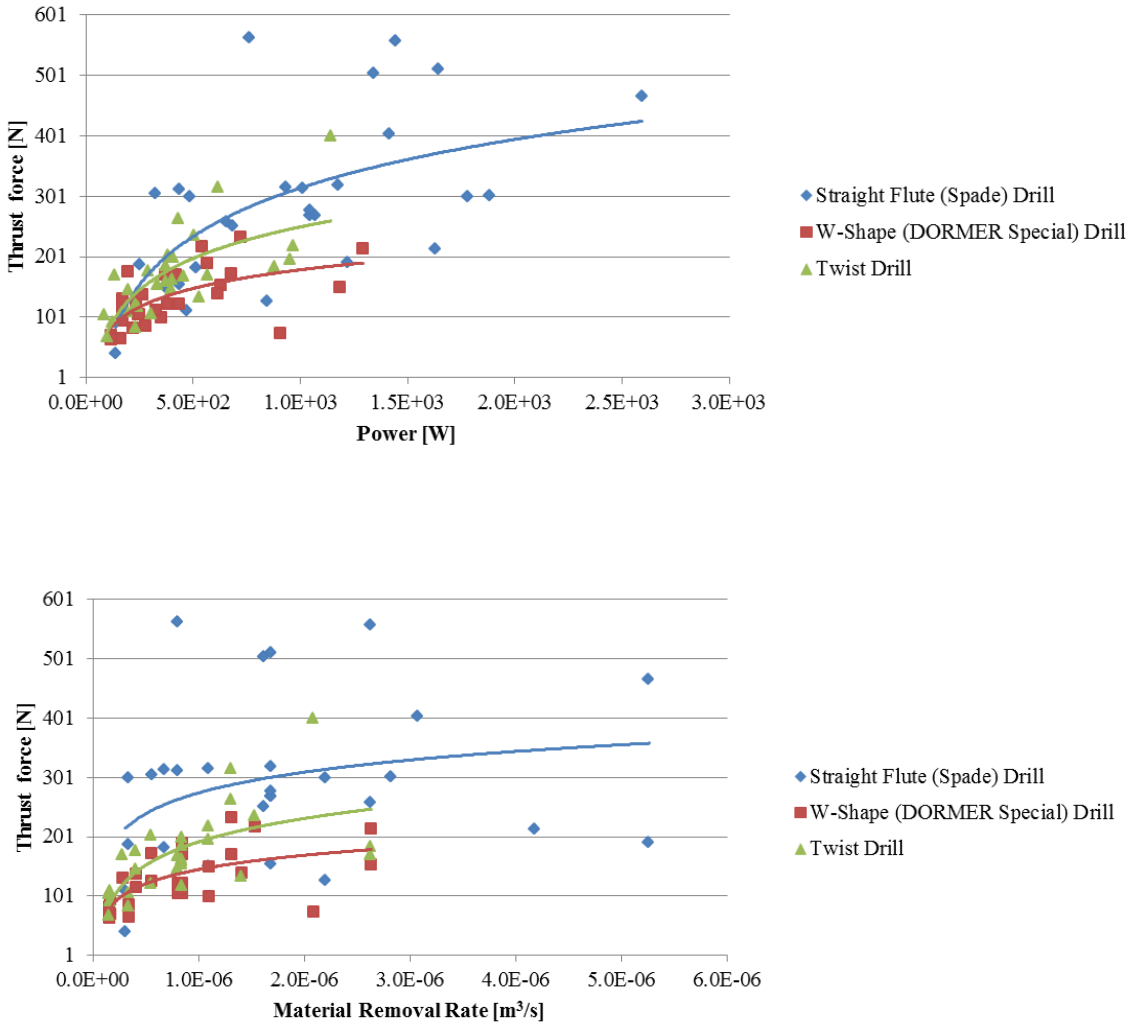


**Figure 4.19** Variation trends of thrust force with the consumed power (*N*) and the material removal rate (*MRR*)

## 4.3 Experimental Results for Torque

Similarly, a study for predict the torque response was made. The data collected was also processed using *MATLAB* software as the filtered signal was employed to represent the typical curves obtained with the different tool geometries. Figure 4.20 shows examples of the measured torque for the three geometries under analysis when drilling a specimen test with the following inputs: $S$ = 16 000 rpm, $f_z$ = 0.0325 mm/tooth, $d$ = 5 mm and $t$ = 8 mm.

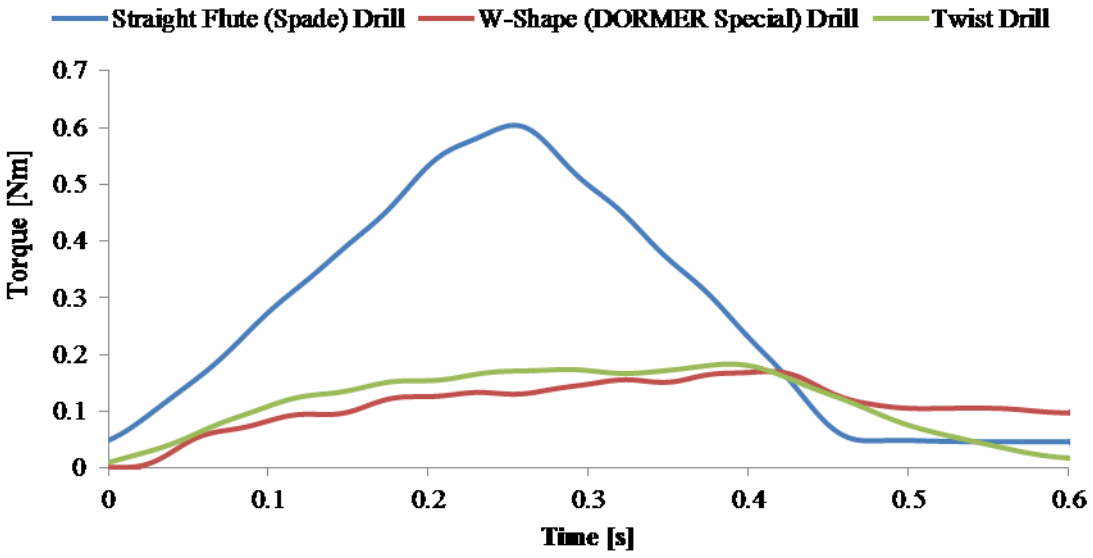


**Figure 4.20** Measured torque during drilling for the three different geometries

According to the literature [143], the key process points of the idealized response of torque during drilling, as shown in Figure 4.21 are:

**Table 4.5** Key process points of the idealized response of torque during drilling [143]

| | |
|---|---|
| A-B: | The cutting lips begin to engage in primary cutting. There is no sharp rise, indicating that the torque acting on chisel edge is relatively small. |
| B-C: | Full engagement of the drill – cutting torque acting on the chisel edge and cutting lips and increasing residual torque caused by the contact force between the flutes and the wall of the hole drilled. |
| C-D: | The drill emerges out of the workpiece. As the chisel edge and cutting lips exit, the torque decreases sharply. |
| D-E: | There is still a contact between the flutes and the wall of the hole drilled, therefore the torque has a constant residual value. |

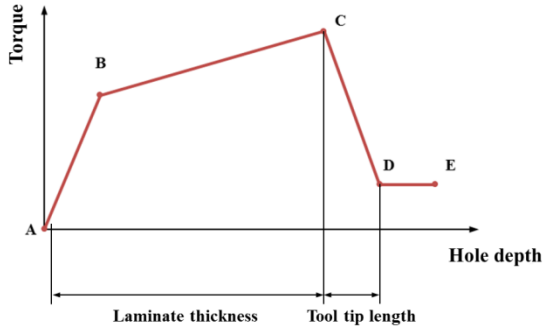


**Figure 4.21** Idealized torque response during drilling using carbide tipped twist drill [143]

In the same way as for the thrust force, Fernandes and Cook [58] and Lazar and Xirouchakis [85] divide the drilling process using carbide straight flute drills, when measuring torque, into the same drilling stages, as follows:

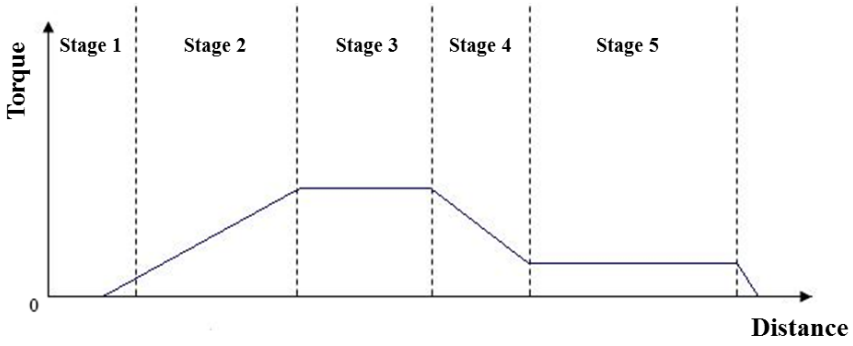


**Figure 4.22** Drilling stages for a straight flute drill when measuring torque [58]

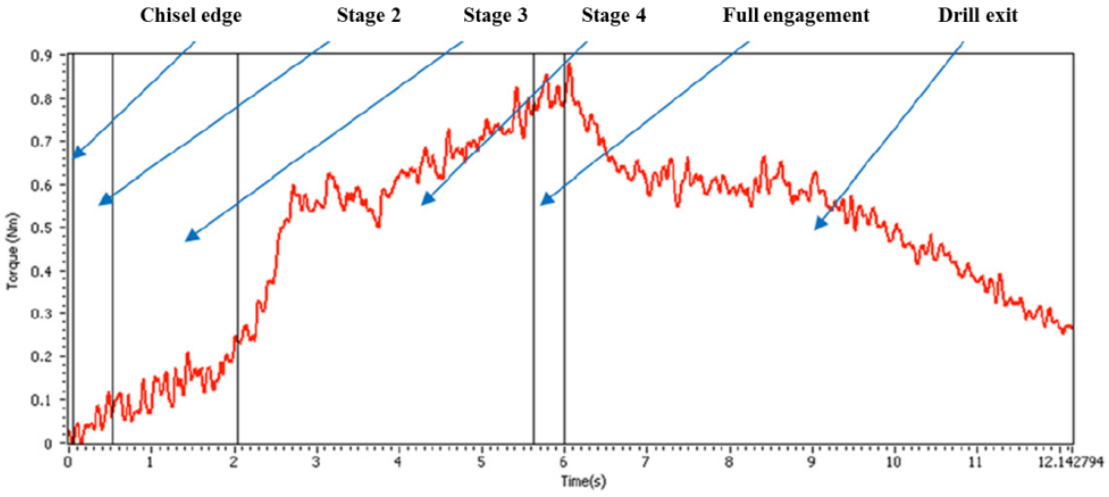


**Figure 4.23** Drilling stages for a straight flute drill [85]

The evolution trend for both geometries is once again consistent with the literature [58, 59, 85, 143].

The average values of the maximum torque measured when performing the tests conducted by the design of experiments are presented in Appendix C and the comparison made in Figure 4.24.

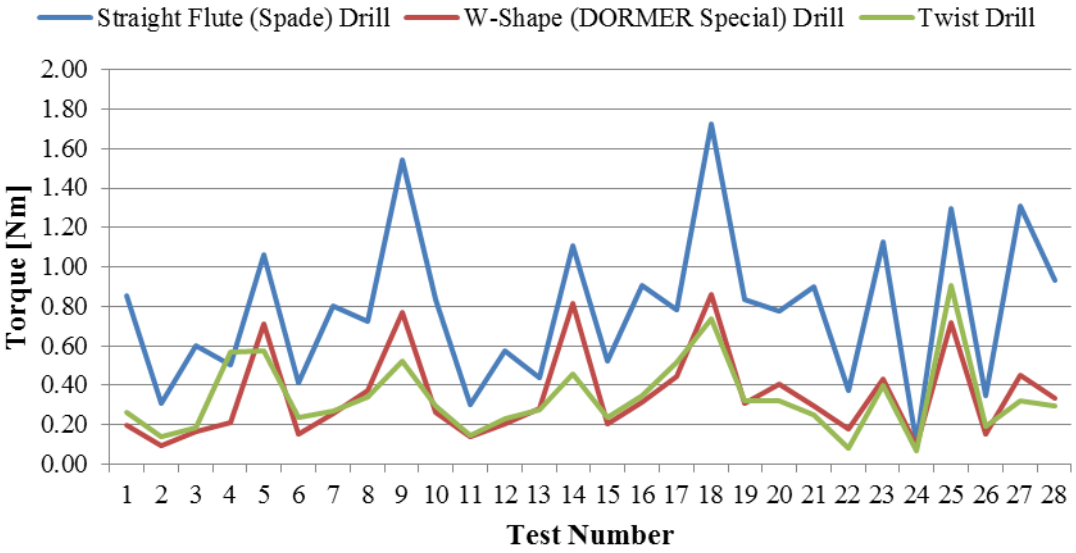


**Figure 4.24** Comparison of the torque for the different tool geometries

Concerning torque response, the higher values measured were obtained when drilling with the straight flute geometry. These results are consistent with the corresponding measured values for thrust force. Once again, the test performed with the 3 mm diameter straight flute drill (Test S24) is the one that presents the lower torque, and more like the values of the other geometries.

Response Surface Methodology was used to create the empirical model that describes this process and the adequacy of the model response was checked using the F-Test with a confidence interval of 95%. The application and results of this methodology are detailed in Appendix C.

The resulting empirical models, second-degree polynomials, to estimate each of the responses are presented below (Table 4.6).

Figure 4.25 represents the correspondent fitted response surfaces showing the interaction effect due to feed per tooth and spindle speed on torque for a drill diameter of 7 mm and a workpiece thickness of 6 mm (left) and to the most significant factors on torque (right).

**Table 4.6** Mathematical models to predict torque

| | |
|---|---|
| Straight Flute Drill ($\bar{R}^2 = 0.9722$) | $T = 0.840 + 0.168f_z - 0.026{f_z}^2 + 0.243d - 0.038d^2 + 0.261t - 0.031S \cdot f_z + 0.051f_z \cdot d + 0.046f_z \cdot t + 0.102d \cdot t$ |
| W-Shape Drill ($\bar{R}^2 = 0.9288$) | $T = 0.273 - 0.032S + 0.025S^2 + 0.053f_z + 0.174d + 0.039d^2 + 0.116t + 0.093d \cdot t$ |
| Twist Drill ($\bar{R}^2 = 0.8474$) | $T = 0.293 + 0.053f_z + 0.162d + 0.056d^2 + 0.047t - 0.051S \cdot f_z$ |

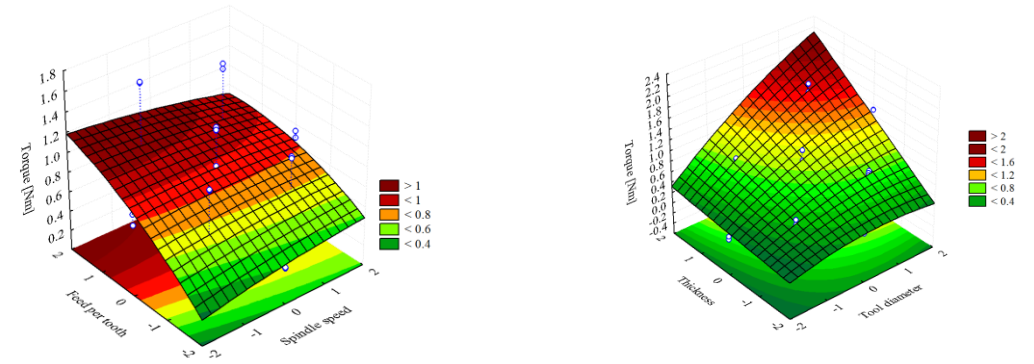


**a)**

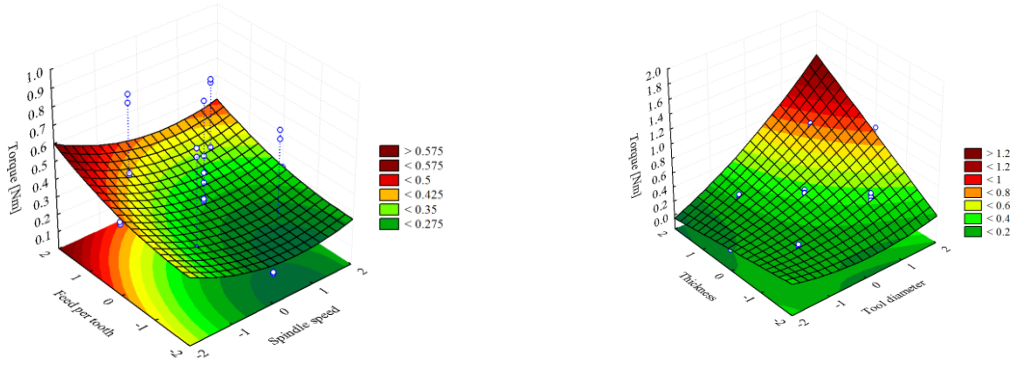


**b)**

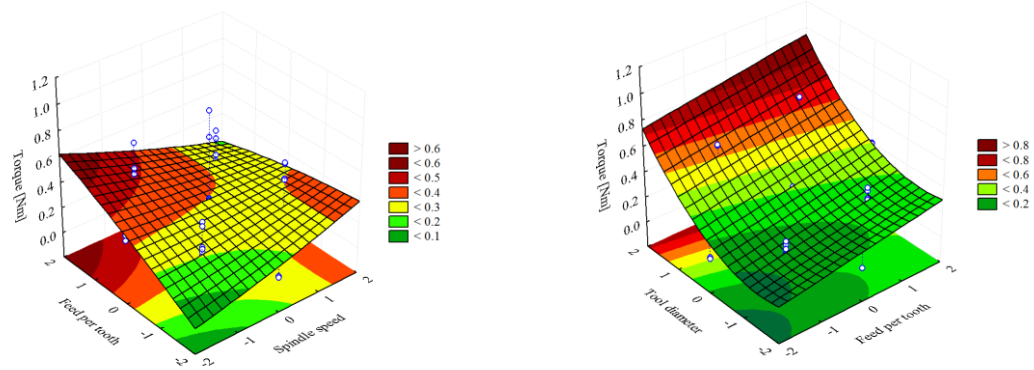


**c)**

**Figure 4.25** Fitted surface response. **Left:** $T$ = f($f$,$S$), $d$ = 7 mm; $t$ = 6 mm; **Right: a)** Straight flute drill: $T$ = f($d$,$t$), $S$ = 12 000 rpm; $f_z$ = 0.055 mm/tooth; **b)** W-shape drill: $T$ = f($d$,$t$), $S$ = 12 000 rpm; $f_z$ = 0.055 mm/tooth; **c)** Twist drill: $T$ = f($f_z$,$d$), $S$ = 12 000 rpm; $t$ = 6 mm

Likewise the models for the thrust force response, the effect of the input variables is not similar for the different tool geometries and, consequently, the significant terms of the regression analysis do not correspond to the same input variables for the three models. However it can be seen that for each model individually, the most significant variables match with those from the thrust force models, as expected. Figure 4.26 shows the different Pareto charts of standardized effects for the torque models resulting from the *Statistica* software analysis of a central composite (response surface) design.

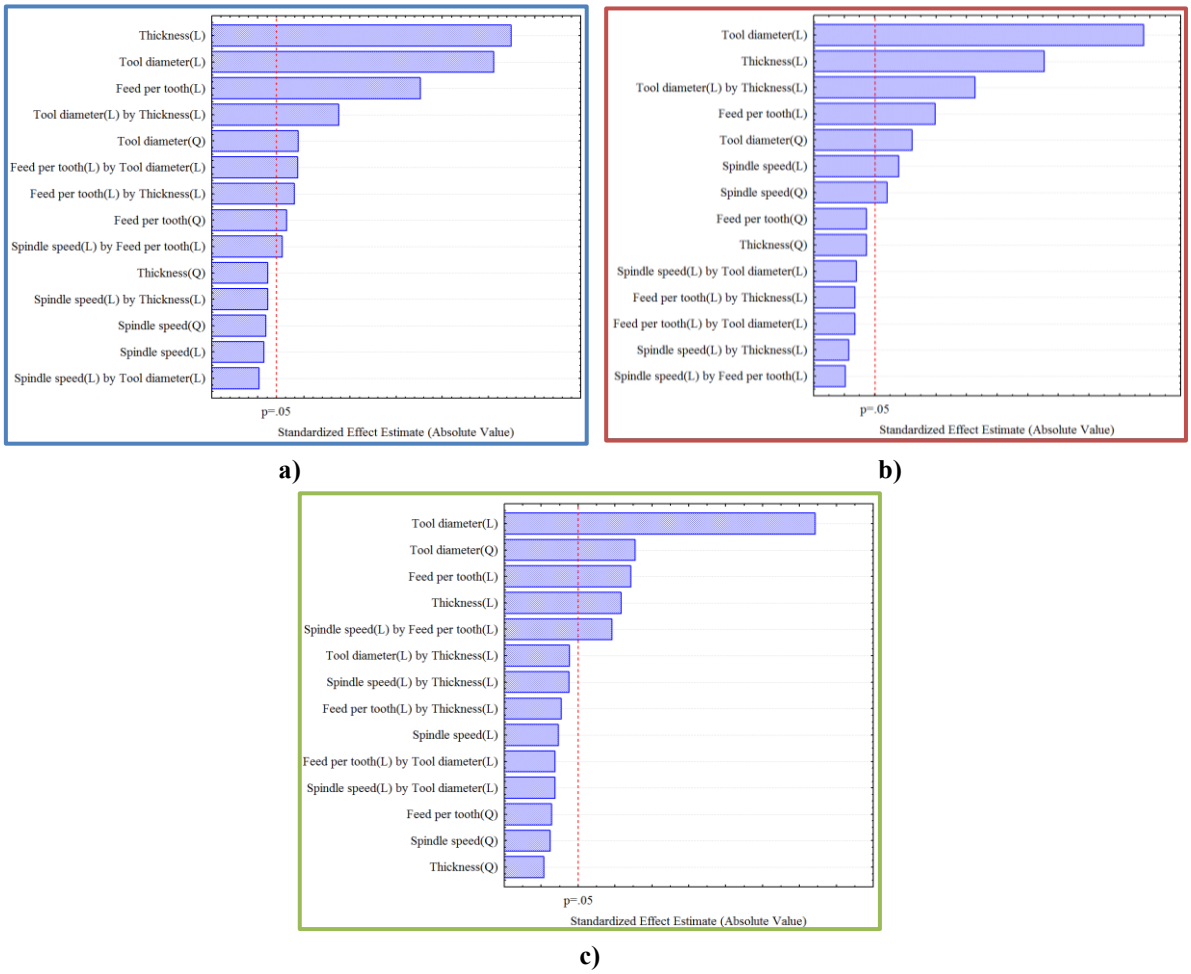


**Figure 4.26** Pareto chart of standardized effects for the response Torque: **a)** Straight flute drill; **b)** W-shape drill; **c)** Twist drill

In Appendix D (Table D.2) are shown the values obtained from the validation tests performed.

The trend analysis was also carried out, based on the complete results set, including DOE experiments and validation tests, although it is anticipated that there would be no great difference concerning the behaviour trend on the thrust force. The effect of spindle speed on the torque for the three tool geometries is shown in Figure 4.27 and Figure 4.28.

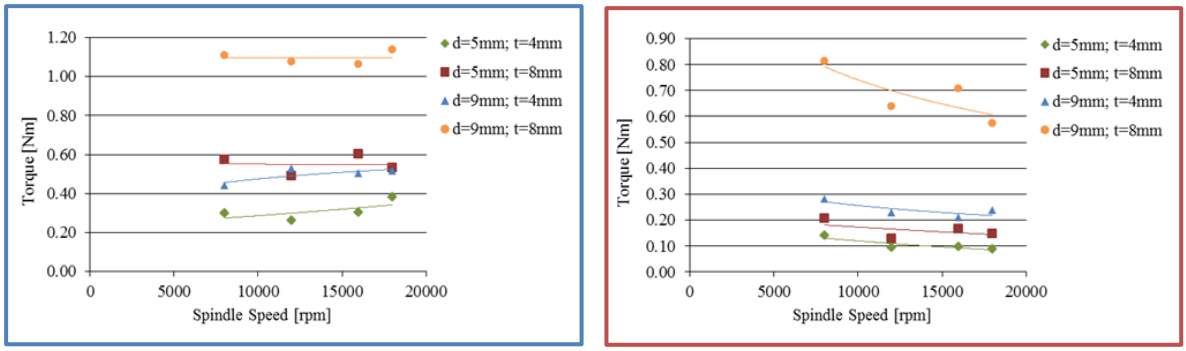


**a)** **b)**

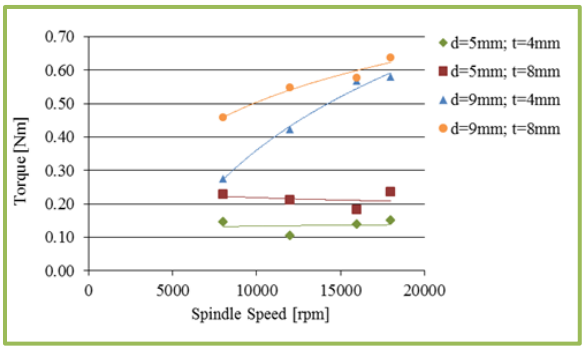


**c)**

**Figure 4.27** Variation trend of torque with spindle speed ($f_z$ = 0.0325 mm/tooth): **a)** Straight flute drill; **b)** W-shape drill; **c)** Twist drill

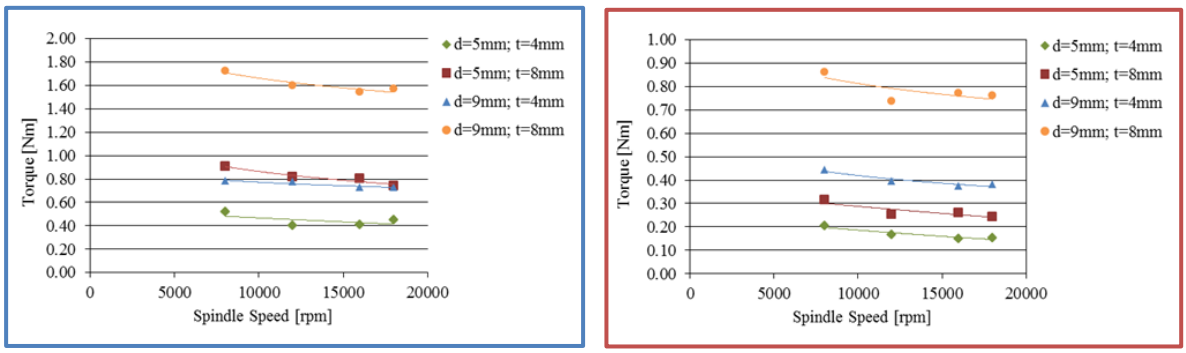


**a)** **b)**

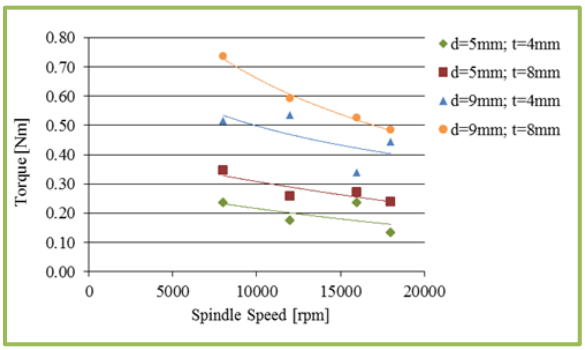


**c)**

**Figure 4.28** Variation trend of torque with spindle speed ($f_z$ = 0.0775 mm/tooth): **a)** Straight flute drill; **b)** W-shape drill; **c)** Twist drill

Similarly, Figure 4.29 and Figure 4.30 correspond to the variation of the measured torque when increasing the feed rate.

The variation trend of the torque response with feed rate and spindle speed is exactly like the one of thrust force. As can be verified the torque tends to decrease with increased spindle speed, and increase with increased feed. This response also increases with increased tool diameter and workpiece thickness, as expected.

The same unexpected trend observed in the analysis of the effect of spindle speed on thrust force is here reflected, attesting the correlation between these two responses. Likewise, the nonconformity of the graph corresponding to the effect of feed rate on the torque appears to be due to another case of process instability (Test T8), yielding a singular point that misrepresents the trend line. Therefore, this combination of parameters should be avoided. Apparently, drilling 9 mm holes with a twist drill in a 4 mm thickness composite laminate does not appear to be a good choice in this range of process parameters values, or without the existence of a pre-drilled hole.

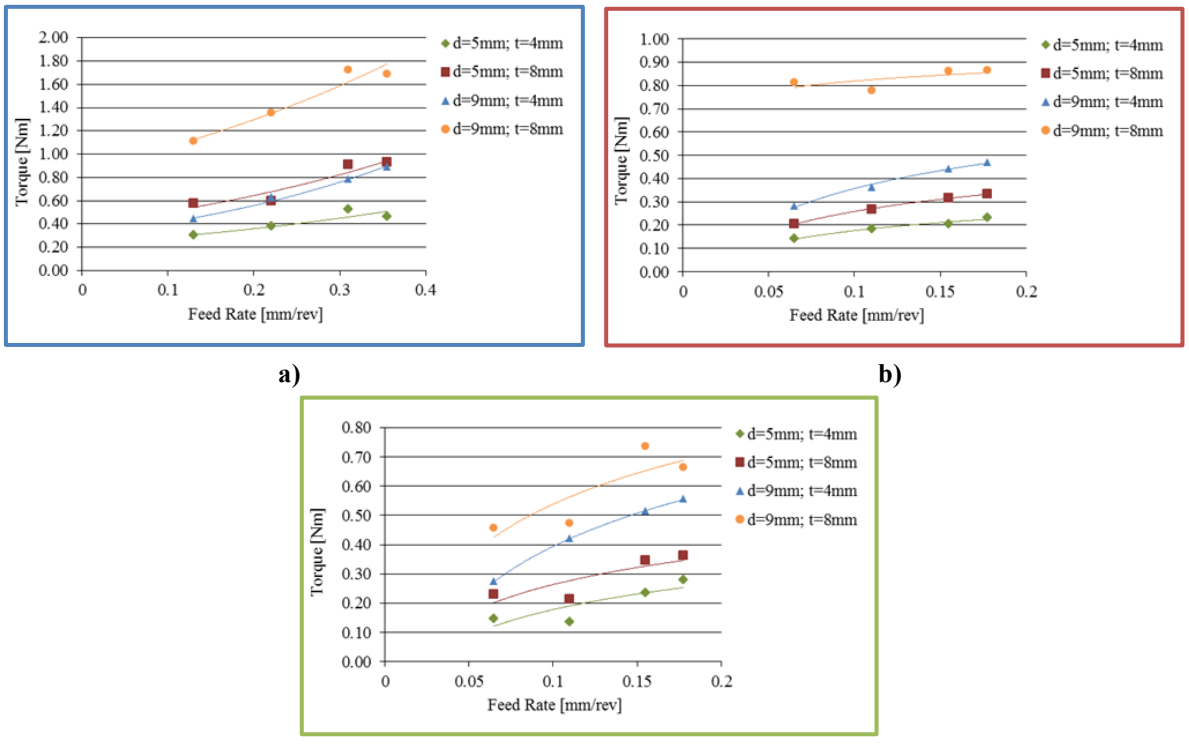


**Figure 4.29** Variation trend of torque with feed per tooth ($S$ = 8 000 rpm): **a)** Straight flute drill; **b)** W-shape drill; **c)** Twist drill

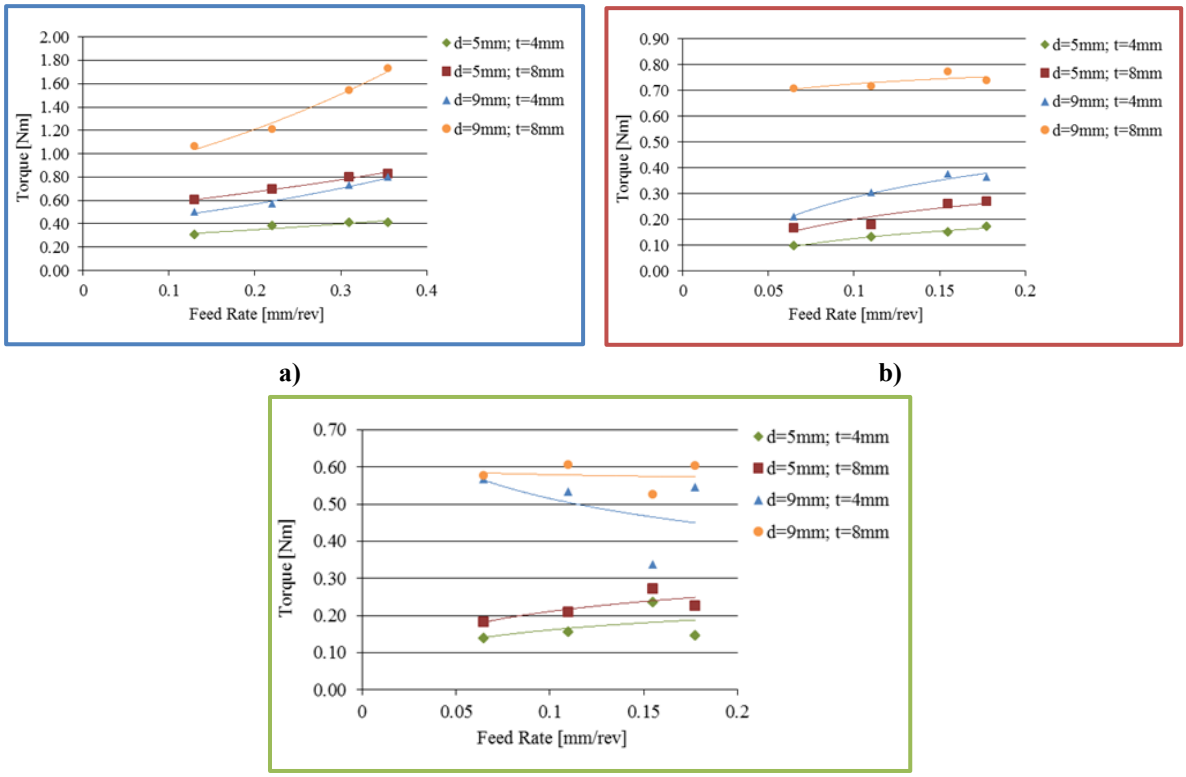


**Figure 4.30** Variation trend of torque with feed rate ($S$ = 16 000 rpm): **a)** Straight flute drill; **b)** W-shape drill; **c)** Twist drill

The relative error (RE) and the prediction accuracy of model were calculated using equations (4.1) and (4.2). The relative error for the three models corresponding to the tool geometries is presented in Appendix D (Table D.5). The average model performance error is found to be 7.16% for the straight flute drill model, 10.06% for the W-shape drill model and 9.04% for the twist drill model.

For the straight flute and twist drill geometries, the experimental values, when compared to the predicted values from the developed models presented similar maximum variation, namely 20.2% and 18.0%. The maximum variation for the torque model relative to the W-shape tool geometry is 34.0% which denotes failure to comply the adequacy of the model.

Figures 4.31, 4.32 and 4.33 represent graphically the comparison of experimental and predicted values for, respectively, straight flute drill, W-shape drill and twist drill empirical models. The variation between values is also shown, according to the calculated values of relative error. By observing the graphs it can be seen that the behaviour of the empirical model is also embodied by the values obtained in the experimental validation. The values of $\bar{R}^2$ found were 0.977 (straight flute drill), 0.938 (w-shape drill) and 0.847 (twist drill), which indicate goodness on fit.

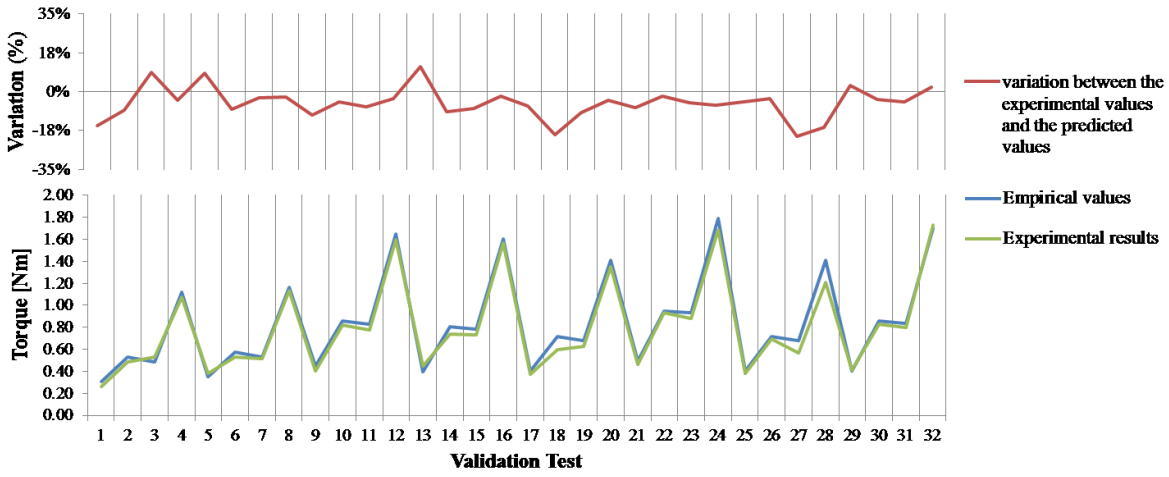


**Figure 4.31** Variation and comparison of experimental and predicted values from the empirical model of torque for the straight flute drill geometry

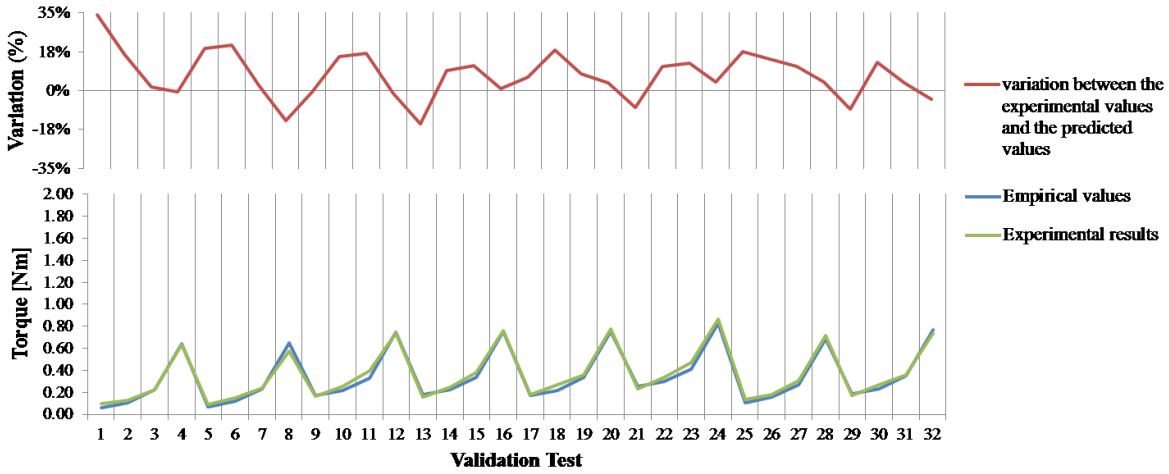


**Figure 4.32** Variation and comparison of experimental and predicted values from the empirical model of torque for the W-shape drill geometry

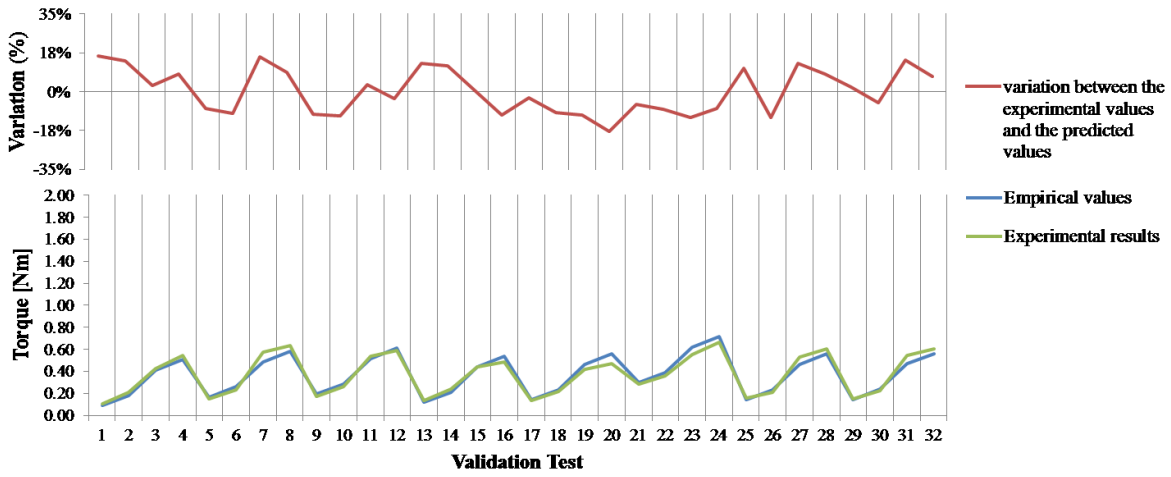


**Figure 4.33** Variation and comparison of experimental and predicted values from the empirical model of torque for the twist drill geometry

## 4.4 Experimental Results for Delamination Factor

The effect of input variables on delamination damage has been object of study by countless authors. According to those studies, delamination damage has been identified as one of the main problems during drilling. The quality of machined surfaces strongly depends on cutting parameters, mainly the feed rate. Drill geometry is also considered one of the most important factors affecting the performance of drilling.

The tearing of fibre bundles is a marker of the quality of the hole obtained. The anisotropy of the composite is at the origin of this defect, due to the configuration and the relative angle between the fibres and the cutting edge. When one intends to establish a prediction model of delamination factor, this must be taken into account, as well as the production of the laminate for the prior existence of damage in the material (e.g. voids) can itself serve as a means of accumulation of errors. The local properties of the material influence the damage due to the heterogeneous nature of carbon fibre reinforced plastics. Consequently, erroneous results can be obtained when measuring the extent of damage, and it is difficult to eliminate this source of error when establishing models. The characterization of damage, via the fibre tearing is usually qualitative or quantified by visual inspection. Therefore it requires extensive knowledge of the process from those who performs it.

The quantification of delamination is usually given by equation (1.1):

$$F_d = \frac{D_{max}}{D}$$

where $D_{max}$ is the maximum diameter of the damage zone and $D$ is the hole diameter.

When drilling carbon fibre reinforced plastics delamination presents an irregular form, then an adjusted delamination factor, as proposed by Davim et al. [60], is used (equation 1.2):

$$F_{da} = F_d + \frac{A_d}{A_{max} - A_0}\left({F_d}^2 - F_d\right)$$

where Fd represents the size of the crack contribution (delamination factor) and the second part the damage area contribution.

Several empirical models of delamination factor appear in the literature, but almost the totality consider the workpiece thickness and tool diameter constant, using as input variables cutting speed and feed rate [43, 44, 57] or spindle speed and feed rate [107]. Tsao and Hocheng [37] considered as input variables spindle speed and feed rate, and also the tool diameter. Khashaba et al. [112] added the effect of tool pre-wear to their study, and Gaitonde et al. [73] the effect of point angle. Since the only tool geometry common to all papers is the twist drill, the correspondent models will be presented in order to attempt to establish a comparison. The empirical models obtained by using linear regression analysis are shown below (Table 4.7).

**Table 4.7** Empirical models of delamination factor found in literature

| Reference | Drilling factors | Empirical model |
|---|---|---|
| Davim and Reis [44] | CFRP<br>*S:* 1 910-3 138 rpm<br>*f:* 0.05-0.2 mm/rev<br>*t* = 3 mm<br>*d* = 5 mm | $F_d = 0.923 + 3.463 \times 10^{-3}V + 1.559f$ |
| Davim and Reis [43] | CFRP<br>*S:* 1 019-2 037 rpm<br>*f:* 0.04-0.15 mm/rev<br>*t* = 4 mm<br>*d* = 5 mm | $F_d = 1.010 + 1.16 \times 10^{-4}V + 0.097f$ |
| Tsao and Hocheng [37] | CFRP<br>*S:* 800-1 200 rpm<br>*f:* 0.01-0.03 mm/rev<br>*t* = 5 mm<br>*d*: 6-10 mm | $F_d = 1.961 - 10.955f - 1.81 \times 10^{-4}S - 1.77 \times 10^{-2}d$ |
| Sardinas et al. [57] | CFRP<br>*S:* 1 910-3 138 rpm<br>*f:* 0.05-0.2 mm/rev<br>*t* = 4 mm<br>*d* = 5 mm | $F_d = 0.9104f^{0.01402}V^{0.04123}$ |
| Palanikumar et al. [107] | GFRP<br>*S:* 4 000-40 000 rpm<br>*f:* 1 000-9 000 mm/min<br>*t* = 2.5 mm<br>*d* = 5 mm | $F_d = 1.251 - 3.183 \times 10^{-5}S + 7.922 \times 10^{-5}f + 8.192 \times 10^{-10}S^2 - 1.759 \times 10^{-10}f^2 - 1.935 \times 10^{-9}S \cdot f$ |
| Gaitonde et al. [73] | CFRP<br>*S:* 3 820-38 197 rpm<br>*f:* 1 000-6 000 mm/min<br>*t* = 2.5 mm<br>*d* = 5 mm<br>*θ:* 85-130° | $F_d = -0.81044 - 1.889 \times 10^{-3}V - 0.10996f + 0.03454\theta + 1.1 \times 10^{-5}V \cdot f - 0.9 \times 10^{-5}V \cdot \theta + 0.0017f \cdot \theta + 0.3 \times 10^{-5}V^2 + 0.00553f^2 - 1.15 \times 10^{-4}\theta^2$ |
| Khashaba et al. [112] | GFRP<br>*S:* 255-2 015 rpm<br>*f:* 0.056-0.45 mm/rev<br>*t* = 8.3 mm<br>*d* = 8 mm<br>*W:*0-34 g ×$10^{-4}$ | $F_d = 1.482 + 1.44 \times 10^{-3}V + 3.143f + 0.0193W$ |

*V* – Cutting speed [m/min]

The presented models show that the spindle speed and the feed rate are important factors when estimating the delamination factor. However, in [44] it was verified that the feed rate did not present statistical or physical significance of contribution to the model. A similar observation is reported in [37], where only the feed rate shows statistical and physical significance, and the factors spindle speed and drill diameter did not present significance. For the models obtained in [107] and [73] it was performed the goodness of fit for the regression without considering the individual significance contribution of the factors. Therefore, all the variables and interactions appear in the model.

The response surface methodology (RSM) was applied to create the empirical model of delamination factor as shown in Appendix C. The resulting empirical models, second-degree polynomials including only the significant coefficients, to estimate the delamination factor are presented below (Table 4.8).

**Table 4.8** Mathematical models to predict delamination factor

| | |
|---|---|
| Straight Flute Drill ($\bar{R}^2 = 0.4714$) | $F_d = 1.213 - 0.034S^2 - 0.036{f_z}^2 - 0.045d + 0.024d^2 - 0.029t$ |
| W-Shape Drill ($\bar{R}^2 = 0.8038$) | $F_d = 1.157 - 0.124d + 0.046d^2 - 0.067t + 0.076t^2 - 0.036f_z \cdot d$ |
| Twist Drill ($\bar{R}^2 = 0.4321$) | $F_d = 1.227 - 0.061d + 0.058d^2 + 0.056t^2 - 0.056S \cdot f_z + 0.045S \cdot d$ |

Analysing the obtained models, a first observation shows that they differ considerably from the proposed by the authors referred previously. Comparing the twist drill model the factors spindle speed and feed rate doesn't show statistical and physical significance, and only their interaction is significant. Tool diameter is clearly the most significant term (linear and square effect) in all models obtained.

Figure 4.34 shows the different Pareto charts of standardized effects for the delamination factor models resulting from the *Statistica* software analysis of a central composite (response surface) design.

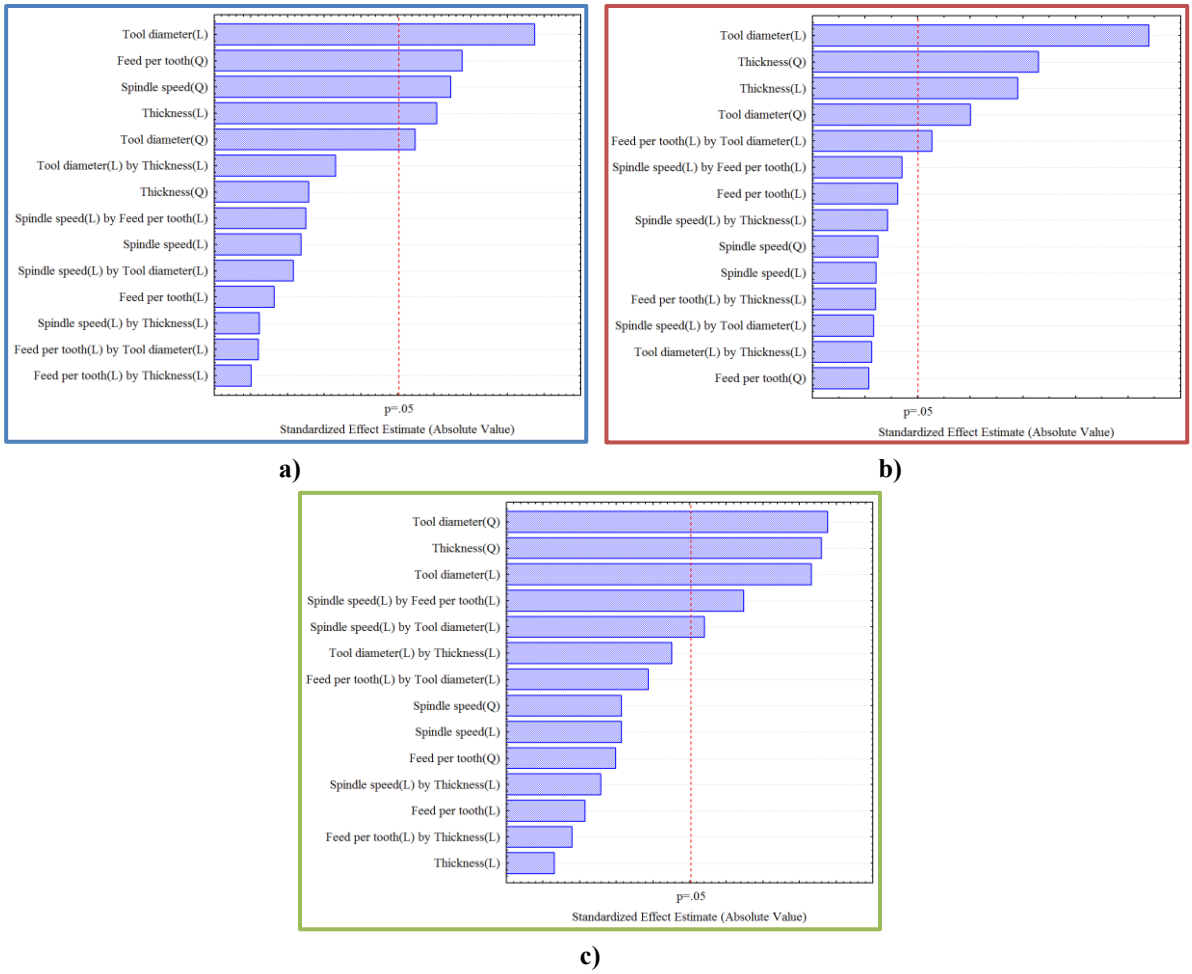


**Figure 4.34** Pareto chart of standardized effects for the response Delamination factor: **a)** Straight flute drill; **b)** W-shape drill; **c)** Twist drill

Figure 4.35 represents the correspondent fitted response surfaces showing the interaction effect, using all variables, due to feed per tooth and spindle speed on delamination factor for a drill diameter of 7 mm and a workpiece thickness of 6 mm (left). The fitted response surfaces of the models including only the significant terms and due to the most significant factors on delamination factor are represented on the right.

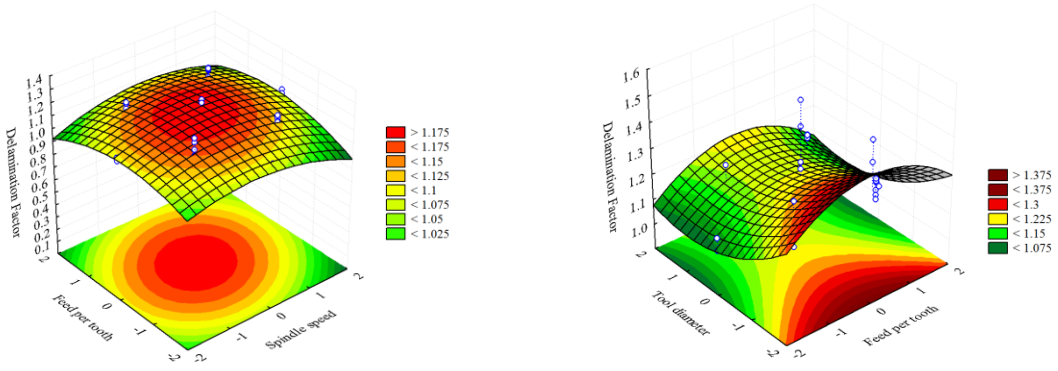


**a)**

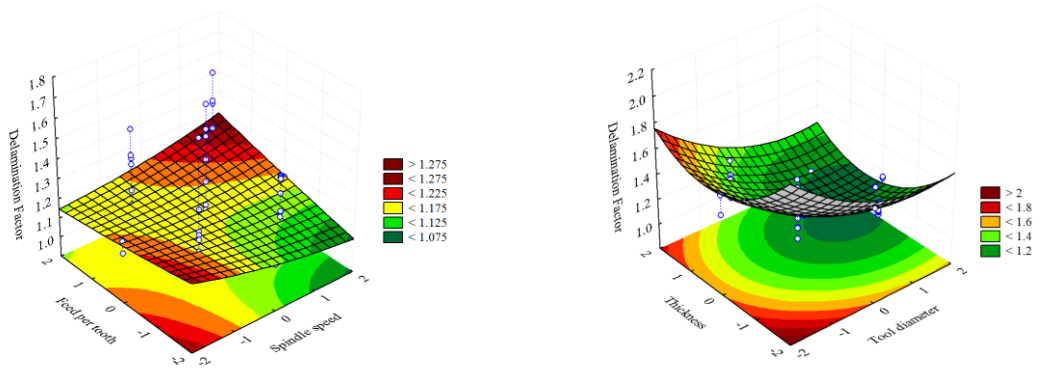


**b)**

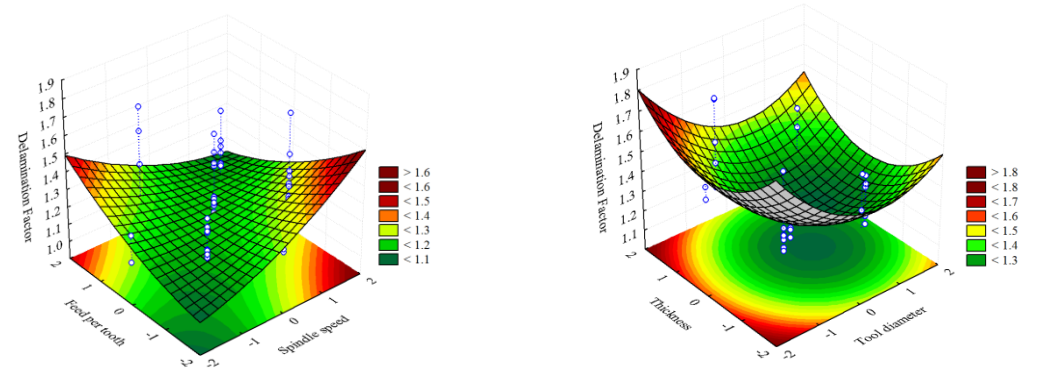


**c)**

**Figure 4.35** Fitted surface response. **Left:** $F_d$ = f($f$,$S$), $d$ = 7 mm; $t$ = 6 mm; **Right: a)** Straight flute drill: $F_d$ = f($f_z$,$d$), $S$ = 12 000 rpm; $t$ = 6 mm; **b)** W-shape drill and **c)** Twist drill: $F_d$ = f($d$,$t$), $S$ = 12 000 rpm; $f_z$ = 0.055 mm/tooth

Even though the spindle speed and feed rate do not influence significantly the delamination factor, from Figure 4.35 (left) it can be observed that, when using straight flute or twist drills, high spindle speed together with high feed rate tend to produce lower delamination, similar when using lower values for both variables, which is a good indicator that it is possible to use high productivity drilling. The W-shape geometry presents better behaviour using lower feed rate and higher spindle speed, which is in accordance with the supplier's recommendations.

From the fitted response surfaces represented on the right, showing the most significant input variables for each model, it can be observed the importance of the square effects of the variables.

If it concerns the W-shape tool geometry, one can observe that the empirical model does not include the factor spindle speed and only take account of the interaction between the feed rate and the tool diameter. Although it appears that cutting parameters have no meaning when using this tool, the fact is that when we think about the physical process, this does not seem absolutely correct. Thus, it is important to show the results of preliminary tests conducted for this tool geometry. As it was referred earlier, the preliminary tests allowed establishing the values of variables and the region of interest. Consequently, RSM was performed to evaluate the effects of the cutting parameters, when drilling a 4 mm specimen with a 5 mm drill. Understandably, the models obtained showed significance on the effect of the main factors.

In the particular case of W-shape geometry, the empirical model to predict delamination factor was given by:

$$F_d = 1.150569 + 0.224068S^2 \qquad \bar{R}^2 = 0.70169$$

And the correspondent fitted surface representation:

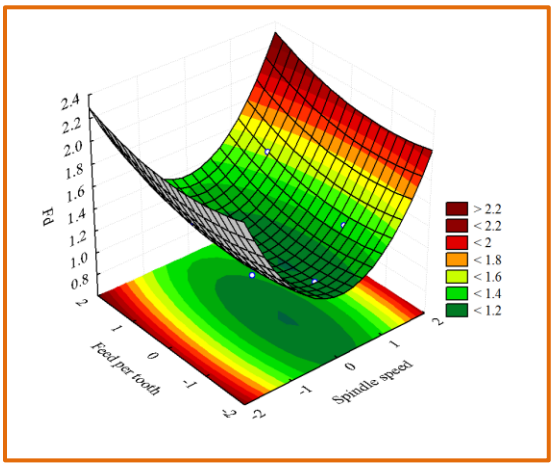


**Figure 4.36** Fitted surface response for preliminary test using W-shape drill: $F_d$ = f($S$,$f_z$), $t$ = 4 mm; $d$ = 5 mm

These circumstances may indicate that the effect of cutting parameters is being muffled when adding the variables tool diameter and workpiece thickness. In fact, statistically, the difference between the effects is so high that the cutting parameters loose significance relatively to the other two factors. Physically, is a known fact that the cutting parameters always affect the

drilling process, thus a more accurate methodology should be chosen when studying such phenomena. One solution could be the use of dynamic Taguchi methodology, dividing the study by blocking the input variables tool diameter and thickness. This will permit to inquire the behaviour of all the factors without disguises its effects.

The comparison of the delamination factor obtained for the three different geometries presented in Figure 4.37 shows that, on average, higher values were measured for the W-shape drill, but very similar with the twist drill. It is important to note that the tests conducted using higher values of spindle speed (Test 21) and higher values of feed per tooth (Test 23) present lower values of delamination factor which may indicate the possibility of using high productivity drilling without significant damage, or even reducing it.

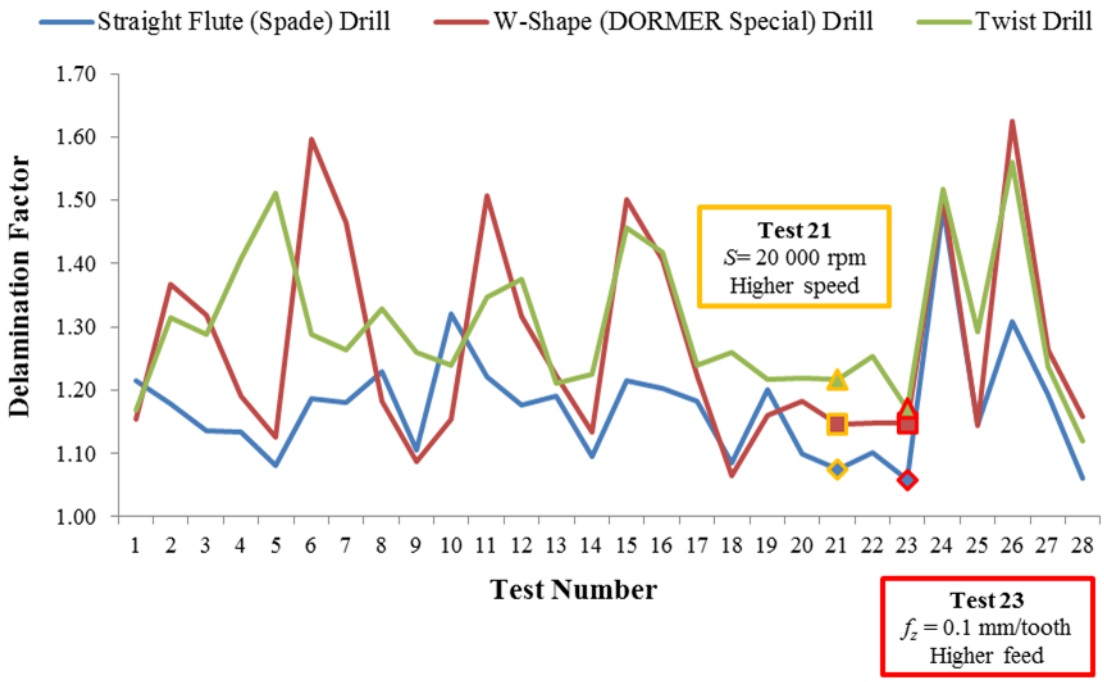


**Figure 4.37** Comparison of the delamination factor depending on the type of tool geometry

The radiographic analysis together with the image processing methodology was carried out to measure the delamination factor and the adjusted delamination factor. Figure 4.38 shows the radiographic images obtained from the holes with the better and worst values of delamination factor for each tool. The same holes were analysed using SEM images in order to understand the mechanisms and causes of damage.

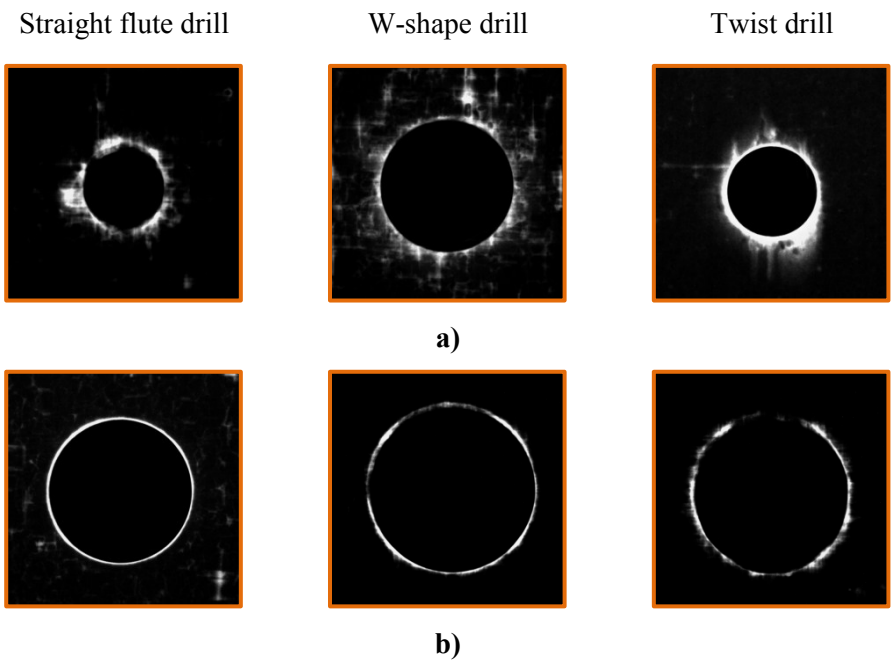


**Figure 4.38** Radiographic images illustrating: **a)** the highest values (SF24, W26 and T24) and **b)** the lower values (SF28, W18 and T28) of delamination factor for each geometry

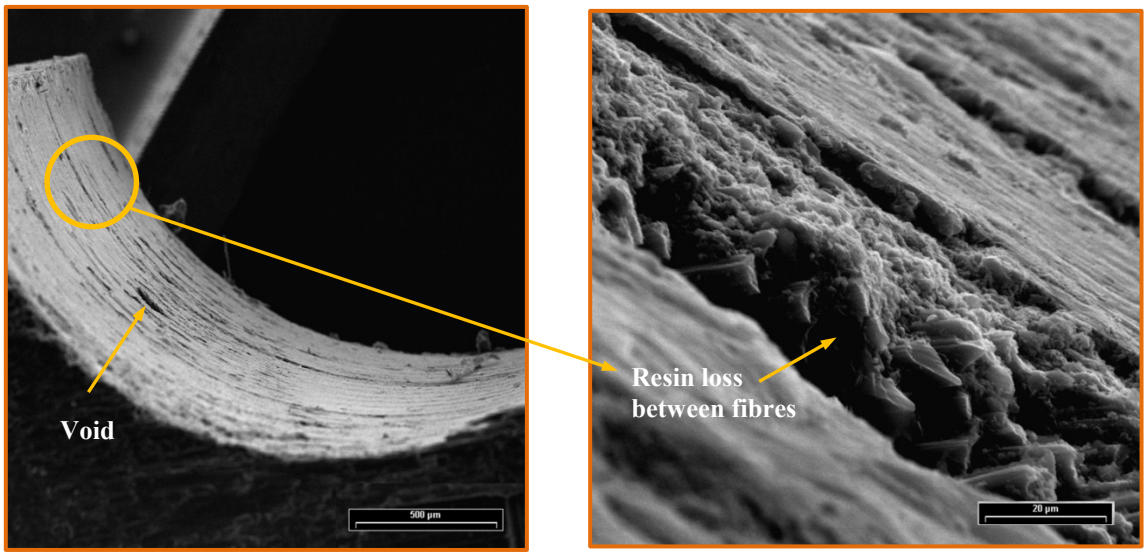


**Figure 4.39** SEM image showing different internal hole damage forms (Test SF24: $F_d = 1.529$)

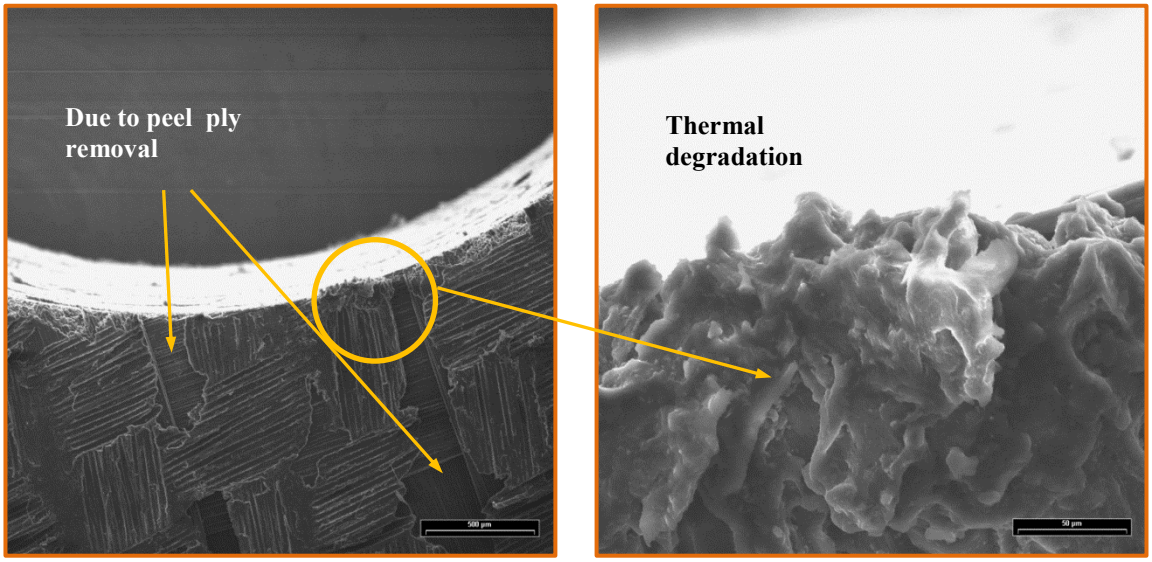


**Figure 4.40** SEM image showing damage observed during removal of peel ply and thermal degradation (Test SF28: $F_d$ = 1.064)

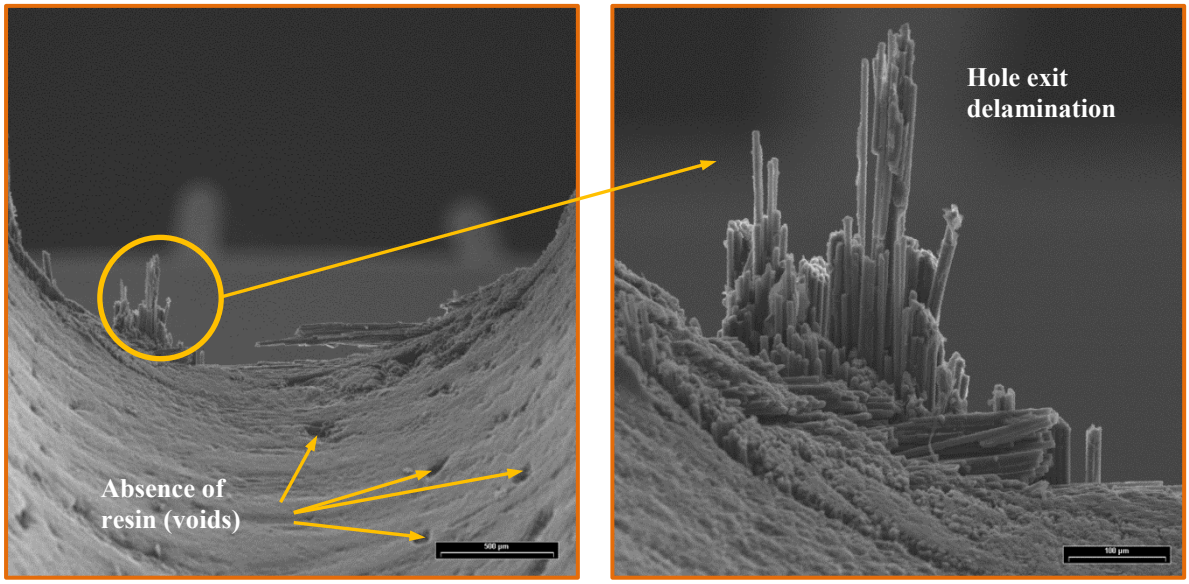


**Figure 4.41** SEM image showing hole exit delamination (Test T24: $F_d$ = 1.547)

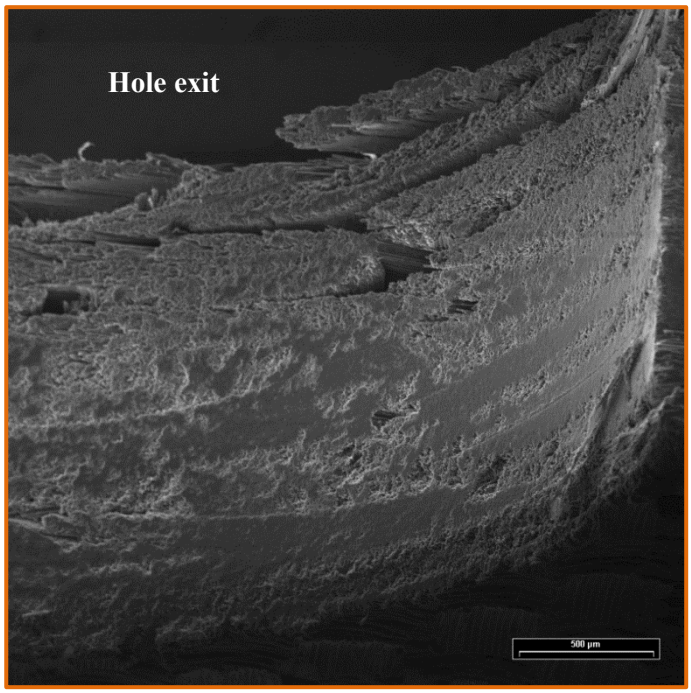


**Figure 4.42** SEM image showing severe hole exit delamination (Test W26: $F_d$ = 1.704)

The results of the validation tests are presented in Appendix D (Table D.3). Due to the different characteristics of the models, for better understanding, the variation between the empirical and experimental results will be described for each model individually.

In order to understand the influence of the cutting parameters in the high speed drilling process, the trends of variation of the response with these input factors were analysed.

Figure 4.43 and Figure 4.44 show the delamination factor in function of the spindle speed for the three tool geometries, namely, straight flute drill, W-shape drill and twist drill. Likewise, Figure 4.45 and Figure 4.46 show the delamination factor in function of the feed rate.

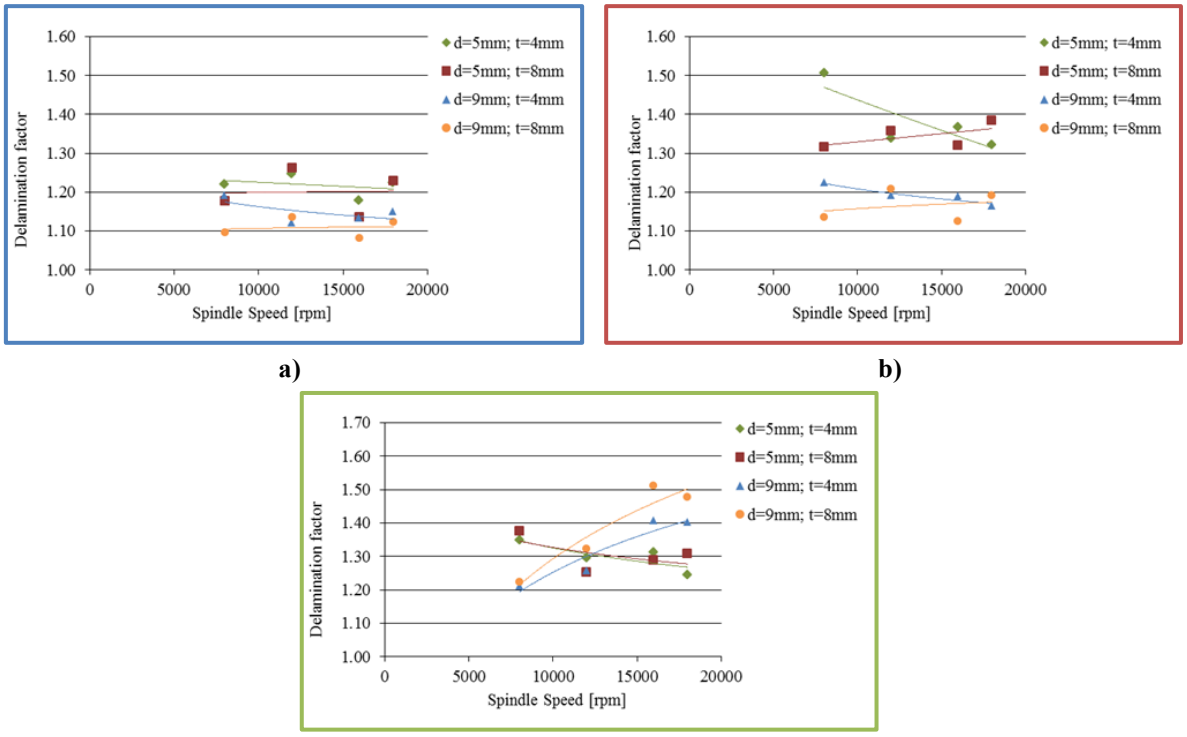


**Figure 4.43** Variation trend of delamination factor with spindle speed ($f_z$ = 0.0325 mm/tooth): **a)** Straight flute drill; **b)** W-shape drill; **c)** Twist drill

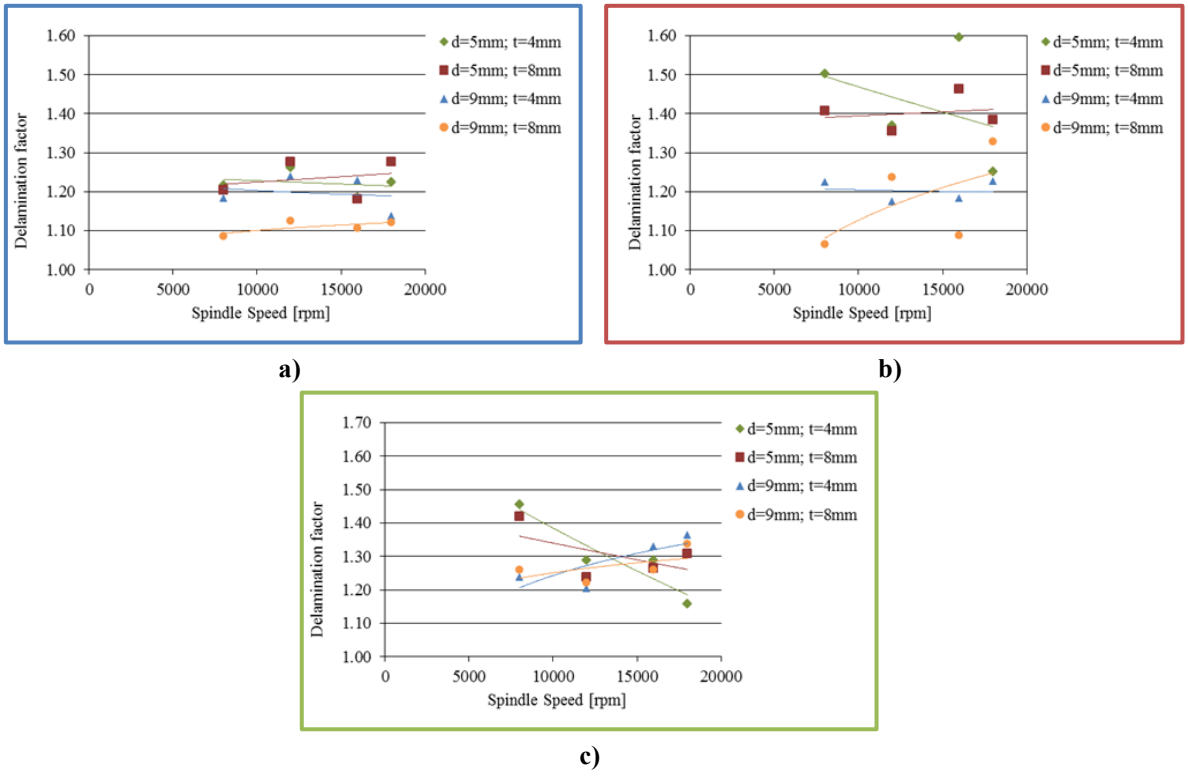


**Figure 4.44** Variation trend of delamination factor with spindle speed ($f_z$ = 0.0775 mm/tooth): **a)** Straight flute drill; **b)** W-shape drill; **c)** Twist drill

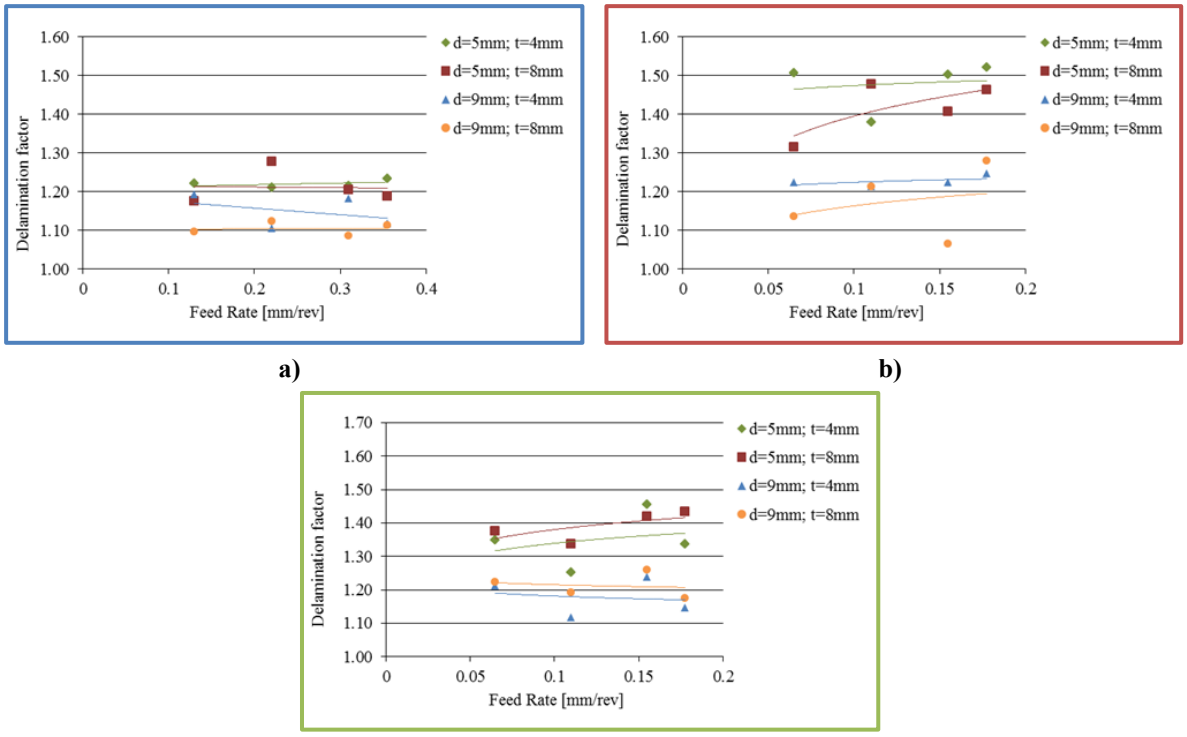


**Figure 4.45** Variation trend of delamination factor with feed rate ($S$ = 8 000 rpm): **a)** Straight flute drill; **b)** W-shape drill; **c)** Twist drill

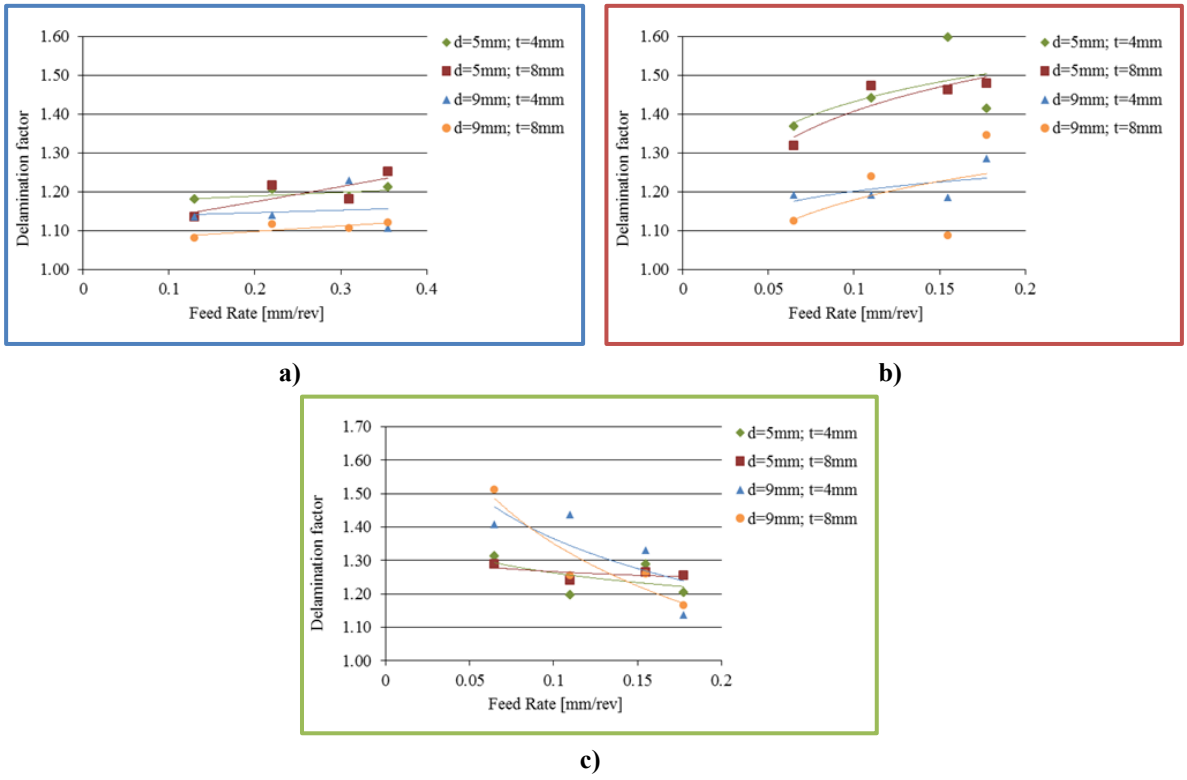


**Figure 4.46** Variation trend of delamination factor with feed rate ($S$ = 16 000 rpm): **a)** Straight flute drill; **b)** W-shape drill; **c)** Twist drill

In respect to the straight flute drill model, it can be seen that both the spindle speed and the feed rate does not have significant influence on the response. The delamination factor slightly decreases for lower workpiece thickness when spindle speed increases and increases for higher workpiece thickness. The same faintly trend occurs when increasing feed rate. For this tool geometry, $F_d$ tends to decrease with increasing tool diameter and workpiece thickness.

Nevertheless, it shows that the delamination factor is higher when producing smaller holes in thinner parts. This was also expected, and it was verified even with simple visual inspection of the produced holes.

The results analysis shows that $F_d$ tends to increase with increased spindle speed when drilling 8mm specimens, and decreases when using 4 mm thickness. When increasing feed speed the delamination factor increases in all cases.

Finally, as regards to the analysis of results for the twist drill it can be observed that the delamination factor increases with speed spindle increase when using higher diameter, and decreases using lower diameter. It is noteworthy that, considering the tool diameter and thickness effect, there is a range of spindle speed values where the trend diverges. Effectively, $F_d$ presents lower values for larger diameter at 8 000 rpm, but for speed higher than 12 000 rpm, the lower values of $F_d$ are obtained with smaller diameter.

It can be also noticed that for lower spindle speed (8 000 rpm) delamination factor decreases with feed rate when drilling with 5 mm twist drill, and increases when using 9 mm drill, increasing in all cases with the workpiece thickness. For higher spindle speed (16 000 rpm), the delamination factor decreases with increasing feed rate. This decrease is more significant for the larger tool diameter.

The relative error for the three models is presented in Appendix D (Table D.6). The average model performance error, calculated from (4.2), is found to be 3.89% for the straight flute drill model, 7.97% for the W-shape drill model and 11.32% for the twist drill model.

The experimental values, when compared to the predicted values from the developed models presented maximum relative errors with value within 10.7% (straight flute drill) to 37.2% (twist drill) for validation data. The maximum relative error for each model is highlighted.

Figures 4.47, 4.48 and 4.49 represent graphically the comparison of experimental and predicted values for, respectively, straight flute drill, W-shape drill and twist drill empirical models. The variation between values is also shown, according to the calculated values of relative error.

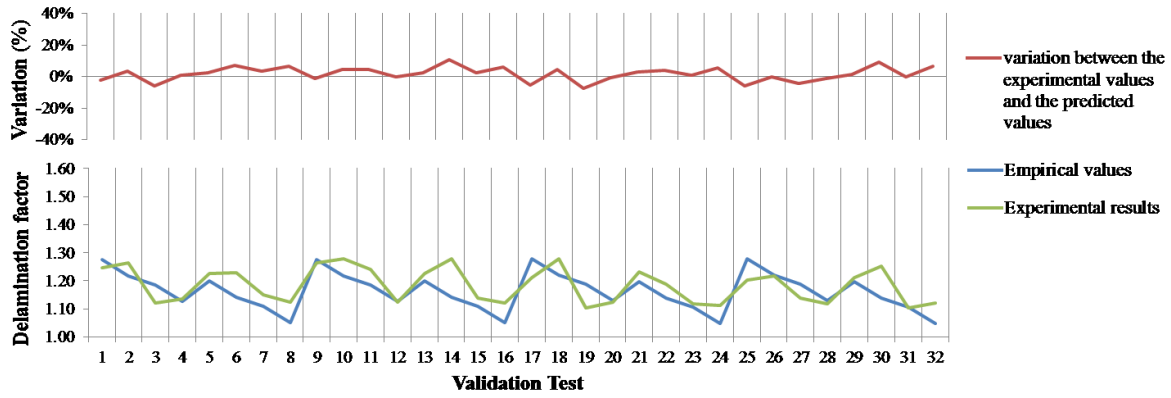


**Figure 4.47** Variation and comparison of experimental and predicted values from the empirical model for the straight flute drill geometry

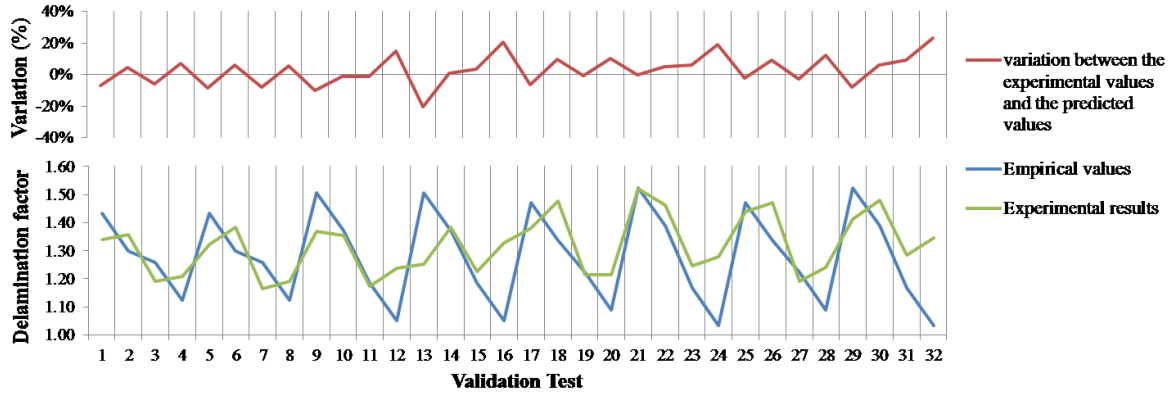


**Figure 4.48** Variation and comparison of experimental and predicted values from the empirical model for the W-shape drill geometry

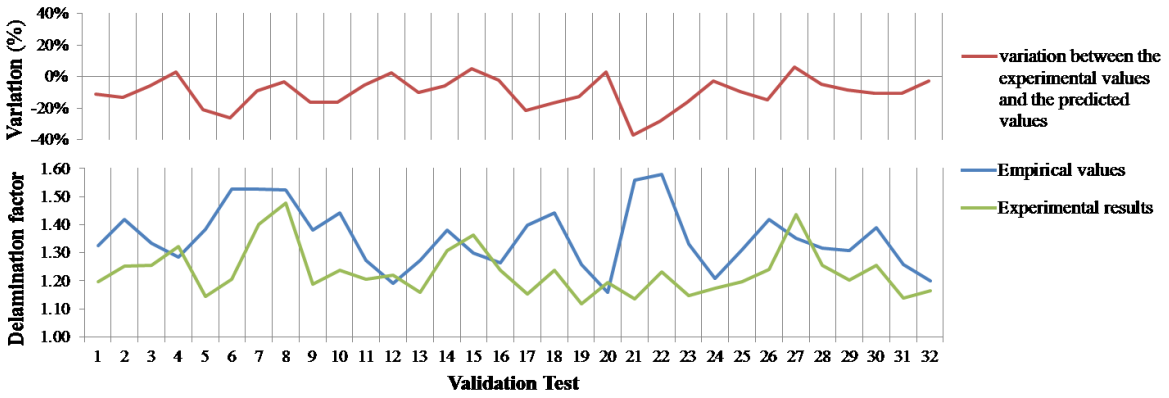


**Figure 4.49** Variation and comparison of experimental and predicted values from the empirical model for the twist drill geometry

The observation of the graphs denotes that the suitability of the models is not fully confirmed. However, the tendency of empirical models approaches the one of experimental values, where the greatest differences belong to the model of the twist drill. Effectively, the values of adjusted R-squared for these models are much lower than the obtained for the thrust force and torque prediction models, with exception of the W-shape drill tool geometry ($\bar{R}^2$=0.822). The value of $\bar{R}^2$ for the twist drill is 0.432, and shows that there is a lack of fit.

Interestingly, the maximum relative error of the models shows that the variation between experimental and empirical results is low, and the measured and calculated values are comparable.

The same analysis was carried out for obtaining prediction models of adjusted delamination factor. All the results obtained were consistent with the ones of the delamination factor, as expected.

Table 4.9 shows the maximum and the minimum variation between the measured results of the adjusted delamination factor ($F_{da}$) and the conventional delamination factor ($F_d$) for each tool geometry. Figures 4.50 and 4.51 illustrate the minimum and maximum variation between these values denoting as the delaminated area can be important in addition to the maximum diameter of delamination. Nevertheless, when the pretension is to study delamination in order to quantify and minimize the damage, $F_d$ demonstrates to be a sufficient parameter, since the adjusted delamination factor presents exactly the same behaviour of trend when comparing it to the input variables.

**Table 4.9** Maximum and minimum values of variation between $F_{da}$ and $F_d$

| | Maximum variation [%] | Minimum variation [%] |
|---|---|---|
| **Straight flute drill** | 16.3 | 3.6 |
| **W-shape drill** | 25.5 | 6.5 |
| **Twist drill** | 19.2 | 0.6 |

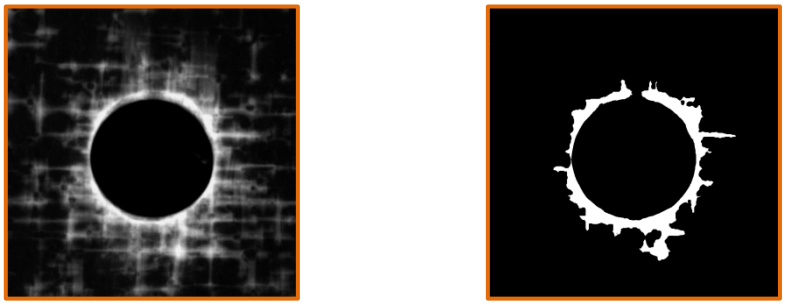

**a)** **b)**

**Figure 4.50 a)** Radiography and **b)** processed image of the hole performed in the test with maximum variation between $F_{da}$ and $F_d$ ($F_d$ = 1.384; $F_{da}$ = 1.859)

**a)** **b)**

**Figure 4.51 a)** Radiography and **b)** processed image of the hole performed in the test with minimum variation between $F_{da}$ and $F_d$ ($F_d$ = 1.204; $F_{da}$ = 1.210)

Since no relevant difference appeared in the data analysis relative to whether the behaviour of the models and the relations with the input parameters, merely the empirical models obtained will be presented (Table 4.10).

**Table 4.10** Mathematical models to predict adjusted delamination factor

| | |
|---|---|
| Straight Flute Drill ($\bar{R}^2 = 0.5141$) | $F_{da} = 1.267 - 0.036S^2 - 0.037{f_z}^2 - 0.061d + 0.033d^2$ |
| W-Shape Drill ($\bar{R}^2 = 0.8187$) | $F_{da} = 1.226 - 0.160d + 0.067d^2 - 0.062t + 0.081t^2 - 0.046f_z \cdot d$ |
| Twist Drill ($\bar{R}^2 = 0.4321$) | $F_{da} = 1.298 - 0.059d + 0.078d^2 + 0.086t^2 - 0.070S \cdot f_z + 0.067S \cdot d$ |

The most surprising results were observed when comparing the experimental values of the thrust force with the corresponding delamination factors measured. As shown in figures 4.52, 4.53 and 4.54, the mentioned relation between thrust force and delamination factor is not clear. Actually, from the results obtained for the w-shape geometry, higher values of thrust force correspond to lower values of delamination. The points having the major material removal rate are highlighted in the graphs, showing once again that combining high spindle speed with high feed rate does not imply having higher delamination. Thus, high productivity drilling can be used with no increase of damage.

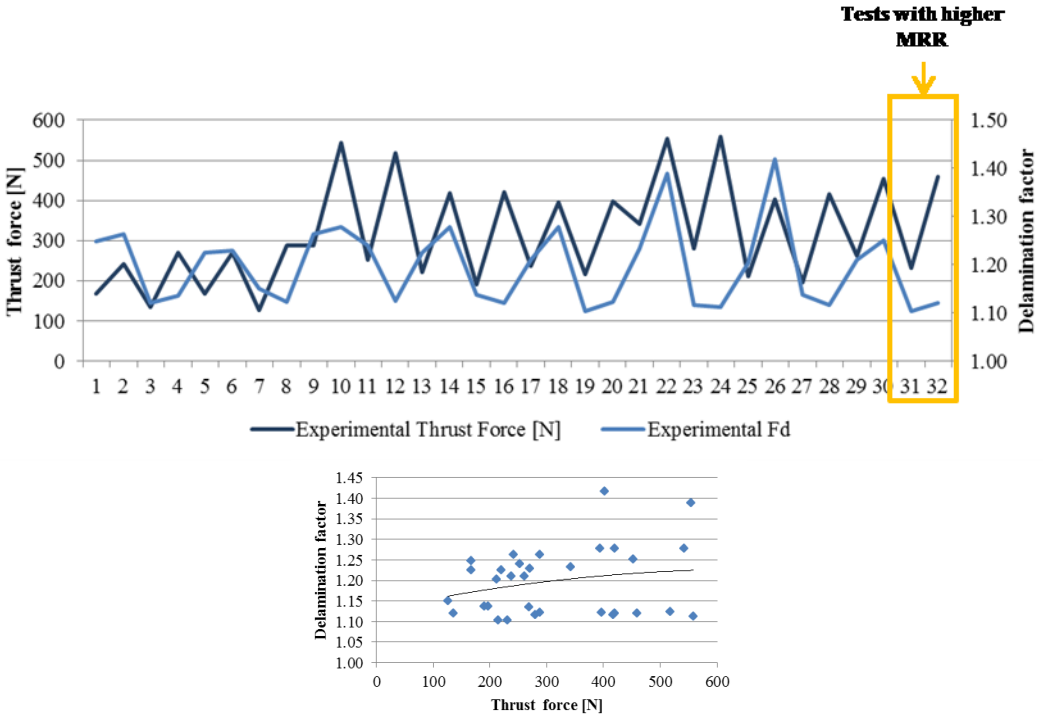


**Figure 4.52** Comparison between thrust force values and correspondent delamination factor for the straight flute drill and respective evolution trend

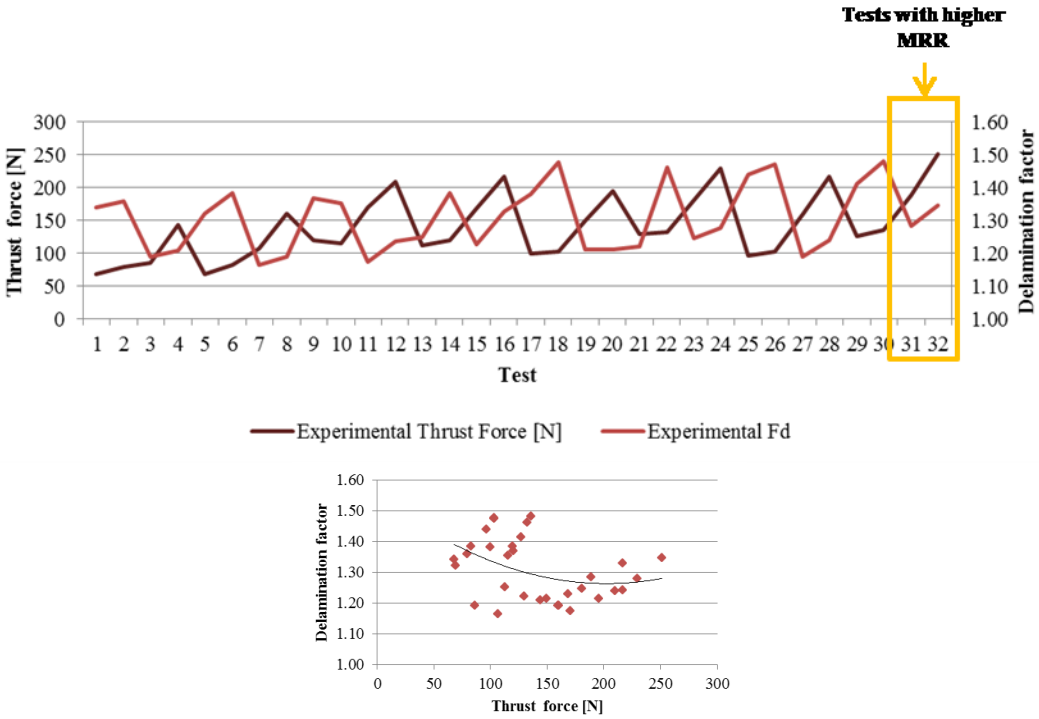


**Figure 4.53** Comparison between thrust force values and correspondent delamination factor for the w-shape drill and respective evolution trend

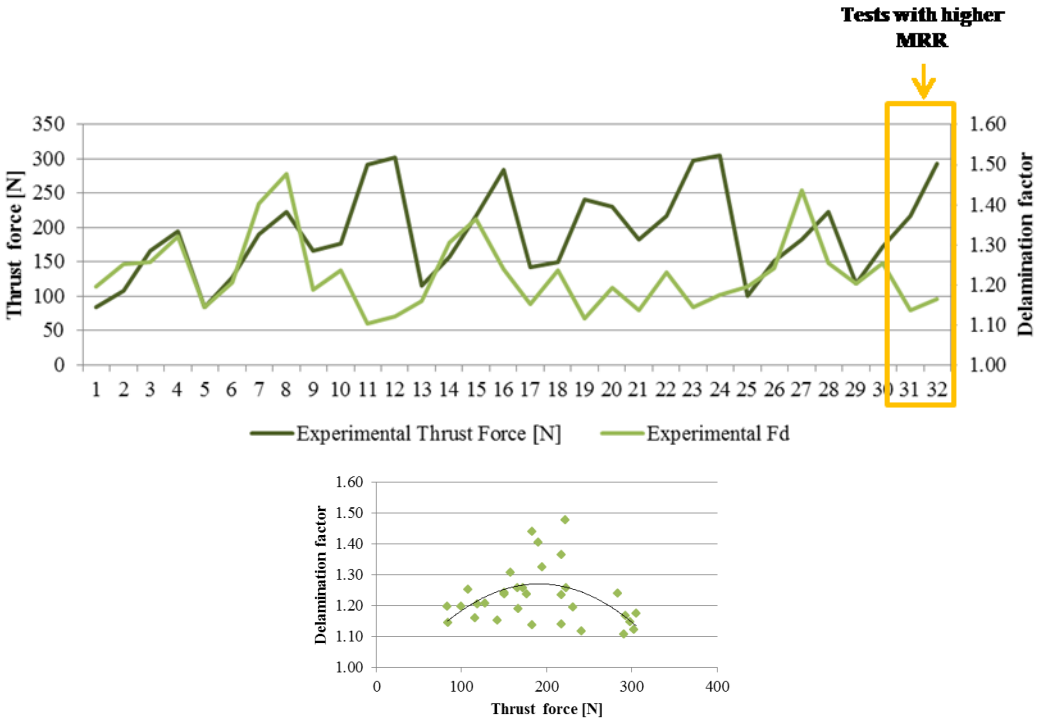


**Figure 4.54** Comparison between thrust force values and correspondent delamination factor for the twist drill and respective evolution trend

## 4.5 New Clamping Method Proposed

In addition to the characterization of delamination damage in the high speed drilling process, the other main focus of this study was to establish a new method to minimize delamination.

After performed the systematic study of the mechanisms of the high speed drilling process on carbon fibre reinforced plastic using various tool geometries, for this study the geometry chosen is the most problematic in terms of obtaining good quality holes, the twist drill. This is also the most commonly used geometry and whose tools have a lower price when compared to the other two.

On the other hand, being w-shape new concept geometry, expressly studied for drilling composite materials it could make sense to accomplish this same study. However, it was found during the characterization study that, as recommended by the supplier, this geometry has an improved performance when using lower advances. Therefore, and as the main focus of this work is the high-efficiency/high-productivity drilling process and the ability to minimize the damage under these conditions (high speed, high feed, high MMR), the use of this geometry is out of question.

Thus, the new method for fixing the workpiece will be developed and tested on the basis of experimental results obtained for the twist drill.

The concept here presented is based in the principles of blanking, more specifically in fine blanking. The main difference is that, instead of using a blanking punch as a tool, the process takes place with a twist drill.

The new clamping mechanism for high speed drilling of CFRP is then composed of a bottom plate, which is fixed to the machining equipment, and an upper plate connected to the bottom plate through bolted connection and guided by guide pins. The workpiece to drill is placed between the two plates, with pressure being exerted by tightening of the screws. Thus, the downward holding force is applied to the top of the workpiece.

The tool passes through a hole, both having the same diameter, previously drilled in these two plates, serving as a bushing. The clearance between tool and plate is maintained as small as possible, such as for fine blanking. This way it is intended to avoid edge bending and fracturing.

Figure 4.55 represents the clamping system proposed.

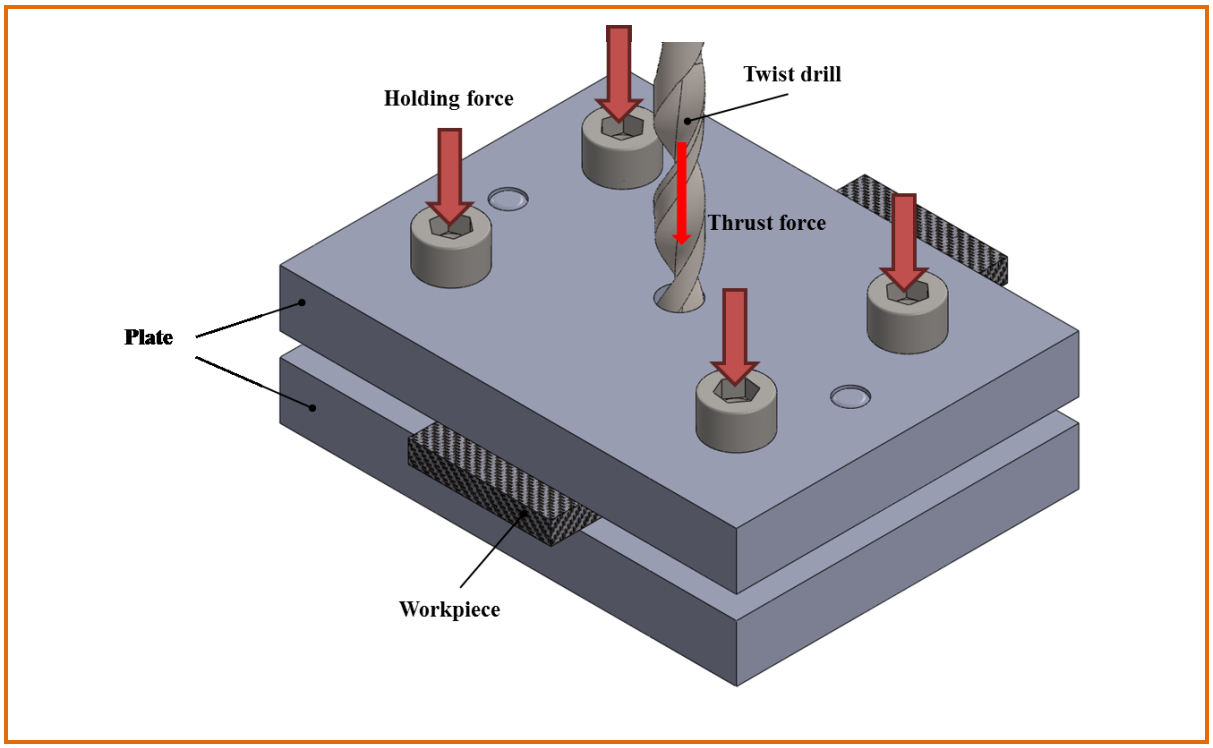


**Figure 4.55** Proposed clamping system

In terms of experiments, the clamping force was calculated based on the bolted joints theory [157], by the expression:

$$T = \frac{F_i d_m}{2}\left(\frac{1 + \pi\mu d_m \sec\alpha}{\pi d_m - \mu l \sec\alpha}\right) + \frac{F_i \mu_c d_c}{2}$$

Since four M6 screws were used and considering equal friction coefficients ($\mu = \mu_c = 0.2$), it has been found that applying a torque on each bolt of 10Nm, will produce a total force applied by those four screws around 25 kN. All tests were executed with the workpiece being compressed with such magnitude force.

A new set of experiments, taking the same parameters of the validation tests made previously, was conducted. The holes produced were radiographed and the images processed using the methodology followed to all other experiments.

The measured values for the delamination factor, adjusted delamination factor and the relative error calculated between these values and the ones obtained in the previous set of experiments are presented in Table 4.11. Figure 4.56 illustrate the comparison between conventional clamping and the new proposed system.

**Table 4.11** Calculated delamination factors using the proposed clamping system and variation from values obtained with conventional clamping

| Test | $F_d$ Conventional clamping | $F_d$ New clamping system | RE [%] | $F_{da}$ Conventional clamping | $F_{da}$ New clamping system | RE [%] |
|---|---|---|---|---|---|---|
| **01** | 1.20 | 1.10 | -8.71% | 1.31 | 1.19 | -9.90% |
| **02** | 1.25 | 1.12 | -11.53% | 1.42 | 1.24 | -14.75% |
| **03** | 1.26 | 1.04 | -20.99% | 1.36 | 1.10 | -24.43% |
| **04** | 1.32 | 1.11 | -18.86% | 1.57 | 1.24 | -27.21% |
| **05** | 1.14 | 1.13 | -1.62% | 1.23 | 1.21 | -1.89% |
| **06** | 1.21 | 1.15 | -4.77% | 1.33 | 1.28 | -4.39% |
| **07** | 1.40 | 1.06 | -31.92% | 1.59 | 1.10 | -44.62% |
| **08** | 1.48 | 1.17 | -25.74% | 1.83 | 1.28 | -42.65% |
| **09** | 1.19 | 1.13 | -5.56% | 1.32 | 1.24 | -6.75% |
| **10** | 1.24 | 1.12 | -10.56% | 1.37 | 1.27 | -7.78% |
| **11** | 1.10 | 1.02 | -8.06% | 1.11 | 1.07 | -3.65% |
| **12** | 1.12 | 1.12 | -0.38% | 1.20 | 1.14 | -4.79% |
| **13** | 1.16 | 1.10 | -5.70% | 1.23 | 1.18 | -4.44% |
| **14** | 1.31 | 1.14 | -14.18% | 1.48 | 1.29 | -15.13% |
| **15** | 1.36 | 1.04 | -31.38% | 1.53 | 1.07 | -42.48% |
| **16** | 1.24 | 1.10 | -12.96% | 1.40 | 1.22 | -14.05% |
| **17** | 1.15 | 1.12 | -2.97% | 1.22 | 1.14 | -7.33% |
| **18** | 1.24 | 1.17 | -6.00% | 1.41 | 1.14 | -23.00% |
| **19** | 1.12 | 1.02 | -9.02% | 1.16 | 1.08 | -7.30% |
| **20** | 1.19 | 1.13 | -5.46% | 1.31 | 1.19 | -9.55% |
| **21** | 1.14 | 1.10 | -3.68% | 1.21 | 1.18 | -2.60% |
| **22** | 1.23 | 1.11 | -10.60% | 1.40 | 1.30 | -7.53% |
| **23** | 1.15 | 1.08 | -6.07% | 1.22 | 1.05 | -16.23% |
| **24** | 1.17 | 1.06 | -10.88% | 1.29 | 1.17 | -10.74% |
| **25** | 1.20 | 1.10 | -8.32% | 1.30 | 1.19 | -9.32% |
| **26** | 1.24 | 1.11 | -12.02% | 1.41 | 1.30 | -8.92% |
| **27** | 1.44 | 1.08 | -33.13% | 1.64 | 1.05 | -56.07% |
| **28** | 1.25 | 1.10 | -14.03% | 1.40 | 1.21 | -15.26% |
| **29** | 1.20 | 1.13 | -6.90% | 1.29 | 1.14 | -12.57% |
| **30** | 1.25 | 1.17 | -7.57% | 1.44 | 1.25 | -15.44% |
| **31** | 1.14 | 1.08 | -5.34% | 1.17 | 1.05 | -11.38% |
| **32** | 1.17 | 1.06 | -9.88% | 1.30 | 1.14 | -13.89% |

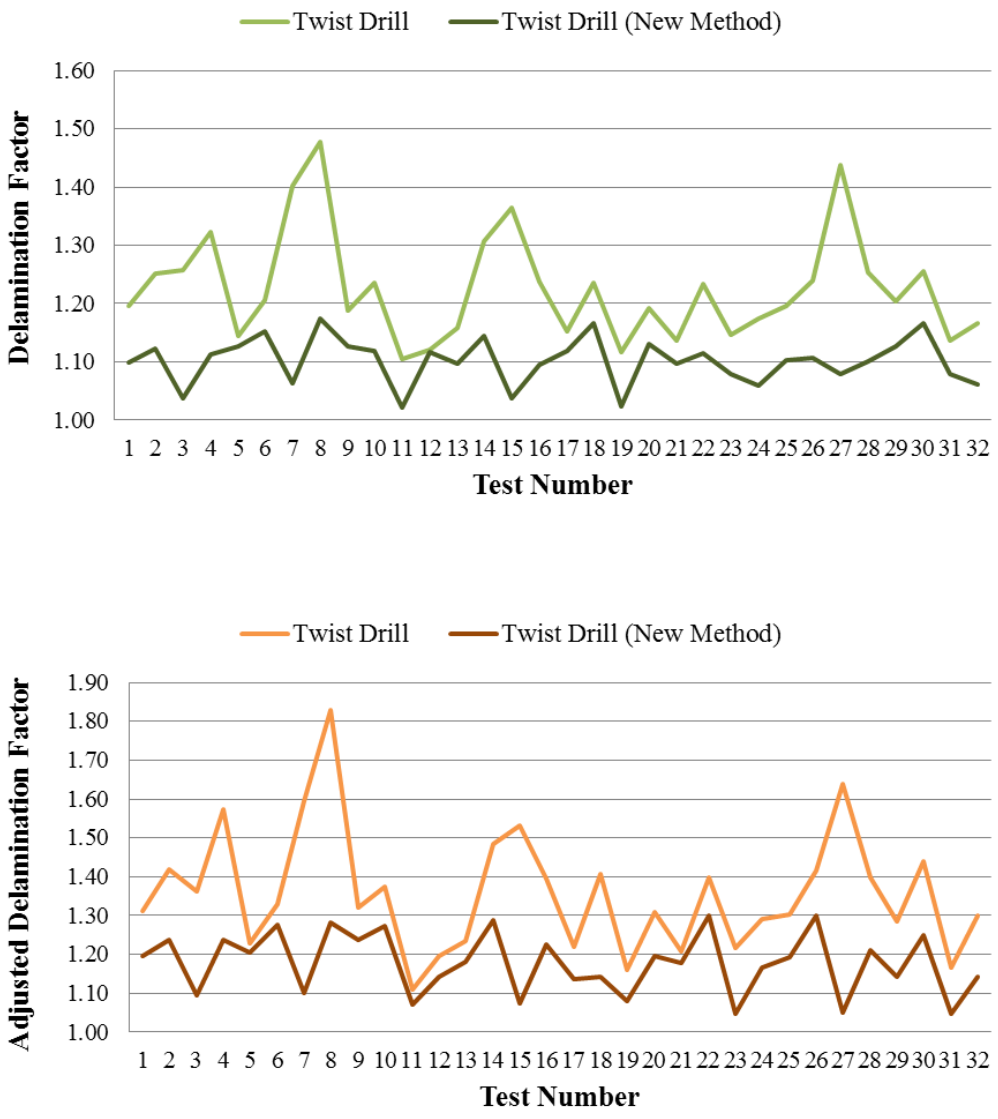


**Figure 4.56** $F_d$ and $F_{da}$ comparison between for the tests performed with the conventional and the proposed clamping system

The analysis of the results shows the excellent improvement in terms of damage minimization. Observing Figure 4.56 is remarkable the difference between values of delamination obtained with exactly the same process variables. Using the proposed clamping device, the reduction in delamination factor may up come to 33%. The maximum reduction in adjusted delamination factor was found to be 56%.

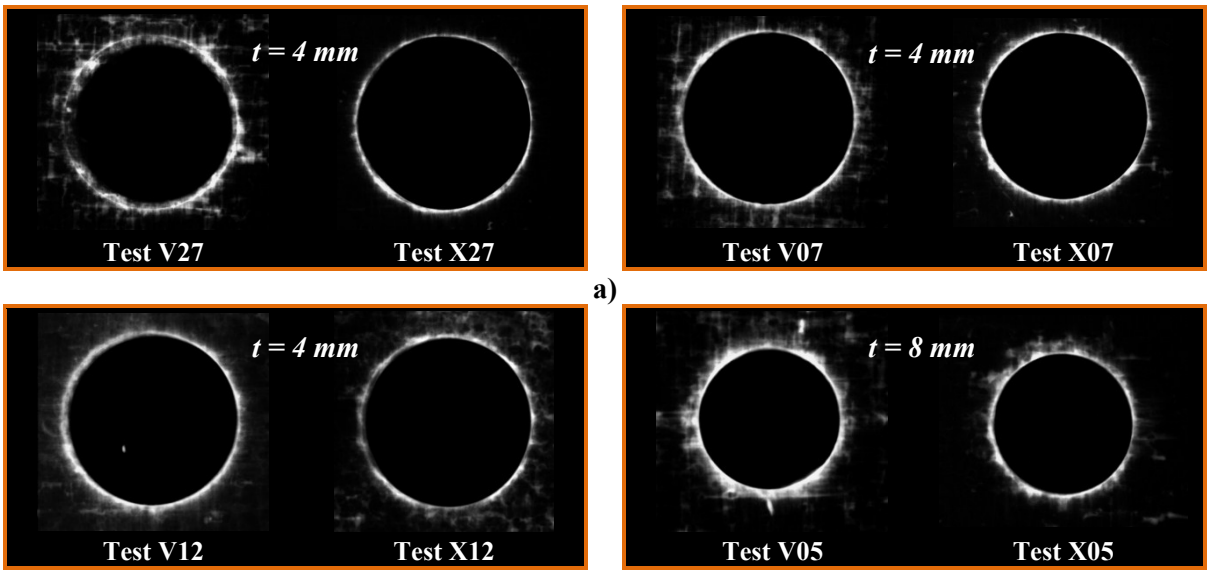


**Figure 4.57** Radiographic images of the tests: **a)** with higher and **b)** with lower variation when comparing the conventional and the proposed clamping system

## 4.6 Concluding Remarks

Based on the findings observed from analysis of experimental and empirical results the following remarks can be made:

- The curves obtained on the measurements of thrust force and torque follow the drilling evolution found in literature.
- Regarding the tool geometry, using the same input variables, the straight flute drill presents higher values of average thrust force and torque. Nevertheless, this tool geometry is the one that presents lower values of delamination factor.
- In general, higher torque and thrust force values were measured when using larger diameter. Additionally, with the same tool diameter, the torque and the thrust force tend to increase with increasing material thickness. When using straight flute and w-shape drills, the delamination factor increases using smaller diameter and workpiece thickness. However, when using the twist drill, the delamination is higher for smaller diameters at spindle speeds of 8 000 and 12 000 rpm. Considering higher spindle speeds, delamination increases for greater diameters. It must be noted that when drilling with higher spindle speed together with higher feed rate, the delamination value is bigger for larger tool diameter and thickness.
- For all tool geometries studied, average thrust force and torque tend to increase when increasing feed rate. This is also the demeanour of delamination factor for the straight flute

and w-shape drills. For the twist drill tool geometry, delamination factor decreases when increasing feed rate, except for smaller diameter at 8 000 rpm where the trend is to increase.

- Both average thrust force and torque decrease with increasing spindle speed. Delamination tends to increase with increased spindle speed for higher thickness and decrease for lower thickness. For the twist drill, delamination increases with spindle speed for larger diameters and decreases for small diameters.
- Concerning the statistical study, the input variables that most influence the thrust force and torque responses are the workpiece thickness, the tool diameter and the feed per tooth. The spindle speed is, in all cases, the factor which least affects the response. The tool diameter and workpiece thickness are the most significant factors with regard to the delamination factor and adjusted delamination factor responses.
- The developed models can be effectively used for predicting thrust force and torque in drilling CFRP composites. However, the models developed for predicting delamination factor showed lack of fit and must be further studied.
- The validation tests showed that the relative error associated with the responses is, in general, good.
- As one of the goals proposed for this work was the investigation of high productivity drilling, it was important to ascertain the influence of the power consumed by the process on the several responses. The following trends were observed: the torque and the thrust force increase with the required power increase, and the delamination tends to decrease with the increased power. The same trend exists for the effect of material removal rate.
- There were several good indicators that it can be possible to obtain good results, better or at least similar to those used in conventional drilling, with higher removal rates and smaller production times.
- With the proposed clamping system is possible to reduce delamination up to 50%, using the same input parameters.

# 5

# Conclusions and Future Work

## 5.1 Conclusions and contributions

The study in this thesis had as main objective to characterize the delamination damage in high-speed drilling CFRP composite materials and appraise the possibility of minimize the occurrence of this type of defect. To fulfil this objective, the relationship between the drilling conditions (input variables or factors) and the damage resulting from drilling process, the thrust force and the torque (output variables or responses) was established.

In a first stage, a literature review was held on the behaviour of drilling composite materials. There are numerous studies about the conventional drilling of various types of composite materials, but there are very few on high speed drilling, most of all concerning about tool wear. Nevertheless, this study led to the selection of the key parameters when drilling CFRP. The choice of tools, their condition (new, used) and their cutting geometries, the definition of the range for the operational parameters, and the typical workpiece thickness was based on this review.

The use of experimental design permitted to minimize the number of necessary experiments for characterizing the responses. Together with the response surface methodology allowed to generate sufficient information for describing empirical prediction models. Since different correlation of variables areas have been established leading to similar response values, it is possible to establish some compromises between input variables in order to enhance the efficiency of the process.

In what concerns the experimental results, in the previous chapter the conclusions regarding the effects of the input variables on the responses were exhaustively treated, being referred to in this chapter only the main conclusions and the original contributions as follows:

- ⇨ The selected range of process parameters is in the field of high productivity drilling. However, the delamination factor values obtained experimentally are not substantially different from those found in the literature. According to several authors, when using conventional drilling, it is recommendable to use lower feed rate values in order to reduce delamination. In this work, low values of delamination were obtained even when using high feed rate, which can denote some alterations in the process mechanisms.
- ⇨ In this domain of application, the delamination factor increases with increased diameter and thickness when using higher speed and higher feed rate. Consequently, the delamination tends to increase with increasing material removal rate.
- ⇨ When high speed drilling, mainly with higher spindle speed and higher feed values, the push-out delamination at exit is the primal mechanism of delamination. The peel-up delamination at entrance, generally, is not representative within this range of parameters.
- ⇨ The brittle nature of carbon fibres and the existence of previous damage (e.g. voids) contribute to the occurrence of delamination when drilling carbon fibre reinforced materials. The laminate heterogeneous nature makes the damage sensitive to the local properties of the material.
- ⇨ Analysis by digital radiography demonstrated to be a good option for measuring the delamination damage. However, the visualization of internal defects can only be accomplished with the use of a contrast medium.
- ⇨ The methodology approach to analyse and calculate the delamination factor was adequate for this work. As other methods for visual inspection, has the disadvantage of being largely dependent on the intuition of the observer, especially when the material has already prior defects. These drawbacks are being studied and a new methodology is being developed, based on digital image analysis, so that the previously existing damages can be digitally subtracted.
- ⇨ Both average thrust force and torque decrease with increasing spindle speed and tend to increase when increasing feed rate. This is also the behaviour of delamination factor, but only for the straight flute and w-shape tool geometries.

- ⇨ For twist drill geometry, delamination increases with feed rate increasing but only at lower spindle speed. Generally, delamination decreases when increasing feed rate for this tool geometry. Therefore, the crossed effect between thrust force and delamination should be targeted for further investigation since this differs from the classical premises. However, may indicate that it is indeed possible to drill holes with high productivity, with minimization of damage.
- ⇨ With the same cutting conditions, straight flute drill is the geometry that presents lower delamination factor values, and higher average thrust force and torque results.
- ⇨ The response surface methodology was adequate for the construction of empirical models to predict thrust force and torque in high speed drilling of composite materials.
- ⇨ The prediction model for delamination factor showed some weaknesses as the RSM provides results only from the mathematical and statistical standpoint. It was observed the need to thoroughly understand the mechanisms governing the process for estimating the inconsistencies that occur in models and establish a relation with the process physical phenomena. In this case, statistically, the main effect of tool diameter and workpiece thickness is so significant that drowns out the effect of cutting parameters.
- ⇨ The new clamping system proposed, based on the fine blanking process, showed good results when high speed drilling carbon fibre reinforced plastics. The reduction of damage was achieved and the improvements in terms of damage minimization were remarkable.

Finally, it may be stated that the proposed objectives for the present work were achieved. When conducting the systematic study that led to empirical models proposed, questions concerning the correlation between the output responses and the process variables were raised that can contribute to a better understanding of the phenomena involved in high speed drilling of CFRP. Thus, it can be seen that a further step was taken towards the characterization of damage in high productivity drilling process.

Moreover, with the use of the developed clamping device it was proven the possibility to minimize the occurrence of damage. With the proposed method for fixing the workpiece, when using the same cutting conditions, significant reductions on the damaged area around the hole were achieved.

The main contributions resulting from this work are:

- ⇨ The study of the correlation and interactions between input variables of the drilling process never considered in the literature for high speed drilling of composite materials.
- ⇨ The new empirical model developed for predicting the delamination in high speed drilling of carbon fibre reinforced plastics, considering as factors the tool diameter and the workpiece thickness.
- ⇨ The performance comparison between the conventional twist drill and the specific tools developed for composite materials and the finding that it is possible, with the proper selection of the cutting conditions, to minimize delamination using this type of geometry, without accrued charges for much higher costs of the other tools.
- ⇨ The achievement of reduced delamination by means of a new developed clamping system.

## 5.2 Suggestions for Future Work

Throughout the investigation presented in this work some aspects have been identified that could improve the quality of results. Observed this, the issues that surely will be treated in future work are listed below.

- ⇨ The radiographic data acquisition and methodology for analysis and measurement of the delamination factor based on the digital images needs a close attention. This ascertainment of the methodology has already started, by means of a research being carried out by an MSc student using the experiments specimens and tests performed in this work. The main objective is to automatize as much as possible the process of evaluation of damage, decreasing the factor-dependent sensitivity and drilling process knowledge of the operator.
- ⇨ The empirical models should be improved. Once it has been verified the tendency for the input variables relating to tool diameter and part thickness to overwhelm the cutting parameters variables, a new approach should be followed in order to distinguish their effects. One hypothesis to test is the dynamic Taguchi methodology, which considers these variables separately, although considering all in the same model.

- ⇨ As the considered drills had different number of cutting lips, the factor relative to feed chosen was the feed per tooth. It was interesting to compare the performance of the straight flute drill with the other geometries using the same feed rate as input factor.
- ⇨ This work could also be complemented by studying other tool geometries, as seen in the literature.
- ⇨ Temperature exerts a high effect when drilling composite materials, namely by softening the matrix. The temperature variation during the process should be taken into account in the future.
- ⇨ Since such good results were obtained using the new fixing system, a more systematic approach should be taken to their development. In this work a constant force of 25 kN was used. Other values of force must be tested to ascertain the force value at which no significant change occurs, and thus estimate the force applied to minimize delamination.
- ⇨ From this study and some of the above presuppositions, a new portable tool system can be developed to respond to the real problems that aroused the motivation for carrying out this work.

# References


[1] I. Singh, N. Bhatnagar, and P. Viswanath, "Drilling of uni-directional glass fiber reinforced plastics: Experimental and finite element study," *Materials & Design*, vol. 29, no. 2, pp. 546–553, 2008.

[2] N. S. Mohan, S. M. Kulkarni, and A. Ramachandra, "Delamination analysis in drilling process of glass fiber reinforced plastic (GFRP) composite materials," *Journal of Materials Processing Technology*, vol. 186, no. 1–3, pp. 265–271, 2007.

[3] R. Teti, "Machining of composite materials," *Cirp Annals-Manufacturing Technology*, vol. 51, no. 2, pp. 611–634, 2002.

[4] S. Arul, L. Vijayaraghavan, and S. K. Malhotra, "Online monitoring of acoustic emission for quality control in drilling of polymeric composites," *Journal of Materials Processing Technology*, vol. 185, no. 1–3, pp. 184–190, 2007.

[5] A. M. Abrao, J. C. C. Rubio, P. E. Faria, and J. P. Davim, "The effect of cutting tool geometry on thrust force and delamination when drilling glass fibre reinforced plastic composite," *Materials & Design*, vol. 29, no. 2, pp. 508–513, 2008.

[6] P. P. Camanho and F. L. Matthews, "A progressive damage model for mechanically fastened joints in composite laminates," *Journal of Composite Materials*, vol. 33, no. 24, pp. 2248–2280, 1999.

[7] P. P. Camanho and F. L. Matthews, "Delamination onset prediction in mechanically fastened joints in composite laminates," *Journal of Composite Materials*, vol. 33, no. 10, pp. 906–927, 1999.

[8] S. L. Donaldson and D. B. Miracle, *ASM Handbook Composites Volume 21*, 10th ed. ASM International, 2001.

[9] ACMA, "Composites Industry Overview," *American Composites Manufacturers Association*. [Online]. Available: http://www.acmanet.org/professionals/index.cfm. [Accessed: 27-Aug-2012].

[10] T. Johnson, "History of Composites," *About.com Composites / Plastics*. [Online]. Available: http://composite.about.com/od/aboutcompositesplastics/a/HistoryofComposites.htm. [Accessed: 22-Aug-2012].

[11] M. F. S. . Moura, A. B. Morais, and A. G. Magalhães, *Materiais Compósitos - Materiais, Fabrico e Comportamento Mecânico*, 2ª Edição. Publindústria, 2005.

[12] D. Gay, *Matériaux Composites*, 4e ed. Paris: HERMES SCIENCE PUBLICATIONS, 1997.

[13] Visiongain, "'Composites market to be worth $62.6bn in 2012' says visiongain report global composite trends 2012," *Free Press Release*. [Online]. Available: http://www.free-press-release.com/news-composites-market-to-be-worth-62-6bn-in-2012-says-visiongain-report-1342099172.html. [Accessed: 22-Aug-2012].

[14] V. McConnell, "The making of carbon fiber," *High-Performance Composites*, Jan-2009.

[15] S. Black, "Carbon fiber market: Gathering momentum," *High-Performance Composites*, vol. 20, no. 2, pp. 42–45, 2012.

[16] S. Mazumdar, "Growth opportunities: Materials innovation will drive composites usage to new heights," *High-Performance Composites*, vol. 20, no. 3, pp. 6–7, 2012.

[17] M. Kamiura, “Toray’s Strategy for Carbon Fiber Composite Materials,” Toray Industries Inc., 11-Apr-2008.

[18] Freedonia Group Inc, “High Performance Composites,” *Market Research.com*, Jun-2012. [Online]. Available: http://www.marketresearch.com/Freedonia-Group-Inc-v1247/High-Performance-Composites-7040209/. [Accessed: 22-Aug-2012].

[19] F. Smith, “UK Composites Supply Chain Study,” Institute of Materials, 02-Mar-2011.

[20] Committee on High-Performance Structural Fibers for Advanced Polymer Matrix Composites, National Research Council, *High-Performance Structural Fibers for Advanced Polymer Matrix Composites*. Washington, D.C.: The National Academies Press, 2005.

[21] J.-M. Berthelot, *Composite Materials: Mechanical Behavior and Structural Analysis*. Springer, 1999.

[22] Hexcel Corp., “Prepreg Technology.” Hexcel Technology Manuals, Mar-2005.

[23] S. Jain and D. Yang, “Effects of Feedrate and Chisel Edge on Delamination in Composites Drilling,” *Journal of Engineering for Industry-Transactions of the Asme*, vol. 115, no. 4, pp. 398–405, 1993.

[24] R. Stone and K. Krishnamurthy, “A neural network thrust force controller to minimize delamination during drilling of graphite-epoxy laminates,” *International Journal of Machine Tools & Manufacture*, vol. 36, no. 9, pp. 985–1003, 1996.

[25] S. Lin and I. Chen, “Drilling carbon fiber-reinforced composite material at high speed,” *Wear*, vol. 194, no. 1–2, pp. 156–162, 1996.

[26] W.-C. Chen, “Some experimental investigations in the drilling of carbon fiber-reinforced plastic (CFRP) composite laminates,” *International Journal of Machine Tools & Manufacture*, vol. 37, no. 8, pp. 1097–1108, 1997.

[27] E. Persson, I. Eriksson, and L. Zackrisson, “Effects of hole machining defects on strength and fatigue life of composite laminates,” *Composites Part A: Applied Science and Manufacturing*, vol. 28, no. 2, pp. 141–151, 1997.

[28] R. Piquet, B. Ferret, F. Lachaud, and P. Swider, “Experimental analysis of drilling damage in thin carbon/epoxy plate using special drills,” *Composites Part A: Applied Science and Manufacturing*, vol. 31, no. 10, pp. 1107–1115, 2000.

[29] L. Zhang, L. Wang, X. Liu, H. Zhao, X. Wang, and H. Luo, “Mechanical model for predicting thrust and torque in vibration drilling fibre-reinforced composite materials,” *International Journal of Machine Tools & Manufacture*, vol. 41, no. 5, pp. 641–657, 2001.

[30] L. Zhang, L. Wang, and X. Wang, “Study on vibration drilling of fiber reinforced plastics with hybrid variation parameters method,” *Composites Part A: Applied Science and Manufacturing*, vol. 34, no. 3, pp. 237–244, 2003.

[31] F. Lachaud, R. Piquet, F. Collombet, and L. Surcin, “Drilling of composite structures,” *Composite Structures*, vol. 52, no. 3–4, pp. 511–516, 2001.

[32] E. Enemuoh, A. El-Gizawy, and A. Okafor, “An approach for development of damage-free drilling of carbon fiber reinforced thermosets,” *Int. J. Mach. Tools Manuf.*, vol. 41, no. 12, pp. 1795–1814, 2001.

[33] E. Enemuoh and A. El-Gizawy, “Optimal neural network model for characterization of process-induced damage in drilling carbon fiber reinforced epoxy composites,” *Machining Science and Technology*, vol. 7, no. 3, pp. 389–400, 2003.

[34] C. Murphy, G. Byrne, and M. Gilchrist, "The performance of coated tungsten carbide drills when machining carbon fibre-reinforced epoxy composite materials," *Proceedings of the Institution of Mechanical Engineers Part B-Journal of Engineering Manufacture*, vol. 216, no. 2, pp. 143–152, 2002.

[35] M. Won and C. Dharan, "Chisel edge and pilot hole effects in drilling composite laminates," *Journal of Manufacturing Science and Engineering-Transactions of the Asme*, vol. 124, no. 2, pp. 242–247, 2002.

[36] C. Tsao and H. Hocheng, "The effect of chisel length and associated pilot hole on delamination when drilling composite materials," *International Journal of Machine Tools & Manufacture*, vol. 43, no. 11, pp. 1087–1092, 2003.

[37] C. Tsao and H. Hocheng, "Taguchi analysis of delamination associated with various drill bits in drilling of composite material," *International Journal of Machine Tools & Manufacture*, vol. 44, no. 10, pp. 1085–1090, 2004.

[38] C. Tsao and H. Hocheng, "Effects of exit back-up on delamination in drilling composite materials using a saw drill and a core drill," *International Journal of Machine Tools & Manufacture*, vol. 45, no. 11, pp. 1261–1270, 2005.

[39] C. Tsao and H. Hocheng, "Effect of tool wear on delamination in drilling composite materials," *International Journal of Mechanical Sciences*, vol. 49, no. 8, pp. 983–988, 2007.

[40] C. C. Tsao and H. Hocheng, "Parametric study on thrust force of core drill," *Journal of Materials Processing Technology*, vol. 192, pp. 37–40, 2007.

[41] C. C. Tsao and H. Hocheng, "Evaluation of thrust force and surface roughness in drilling composite material using Taguchi analysis and neural network," *Journal of Materials Processing Technology*, vol. 203, no. 1–3, pp. 342–348, 2008.

[42] C. C. Tsao and H. Hocheng, "Effects of peripheral drilling moment on delamination using special drill bits," *Journal of Materials Processing Technology*, vol. 201, no. 1–3, pp. 471–476, 2008.

[43] J. Davim and P. Reis, "Study of delamination in drilling carbon fiber reinforced plastics (CFRP) using design experiments," *Composite Structures*, vol. 59, no. 4, pp. 481–487, 2003.

[44] J. Davim and P. Reis, "Drilling carbon fiber reinforced plastics manufactured by autoclave - experimental and statistical study," *Materials & Design*, vol. 24, no. 5, pp. 315–324, 2003.

[45] X. Wang, L. Wang, and J. Tao, "Investigation on thrust in vibration drilling of fiber-reinforced plastics," *Journal of Materials Processing Technology*, vol. 148, no. 2, pp. 239–244, 2004.

[46] L. M. P. Durão, J. M. R. S. Tavares, A. Torres Marques, A. G. Magalhães, and M. Figueiredo, "Estudo da Furação de Laminados Carbono/Epóxido com Diferentes Brocas," in *Livro de Comunicações das 4as Jornadas Politécnicas de Engenharia Mecânica, Automóvel, Organização e Gestão Industrial, Energia e Ambiente*, Instituto Superior de Engenharia do Porto, 2004, pp. 801–809.

[47] L. M. P. Durão, J. M. R. S. Tavares, A. T. Marques, M. Freitas, and A. G. Magalhães, "Caracterização de Danos de Maquinagem em Placas Compósitas," in *Actas do CMCE2004 - Congresso de Métodos Computacionais em Engenharia*, Lisboa, 2004.

[48] L. M. Durão, A. Torres Marques, A. G. Magalhaes, and A. M. Baptista, "Maquinagem de Compósitos de Matriz Polimérica," *Revista Iberoamericana de Ingeniería Mecánica*, vol. 10, no. 2, pp. 59–67, 2006.

[49] L. M. Durão, "Machining of Hybrid Composites," PhD Thesis, Faculdade de Engenharia da Universidade do Porto, Porto, 2005.

[50] L. M. P. Durao, M. F. S. F. de Moura, and A. T. Marques, "Numerical simulation of the drilling process on carbon/epoxy composite laminates," *Composites Part A: Applied Science and Manufacturing*, vol. 37, no. 9, pp. 1325–1333, 2006.

[51] L. M. P. Durão, J. M. R. S. Tavares, A. Torres Marques, A. Gonçalves Magalhães, and M. Freitas, "Estudo da Influência da Pré-Furação no Dano em Laminados Carbono/Epóxido," *Mecânica Experimental*, vol. 15, pp. 73–81, 2008.

[52] L. Durao, M. Demoura, and A. Marques, "Numerical prediction of delamination onset in carbon/epoxy composites drilling," *Engineering Fracture Mechanics*, vol. 75, no. 9, pp. 2767–2778, 2008.

[53] L. M. P. Durão, D. J. S. Gonçalves, J. M. R. S. Tavares, V. H. C. de Albuquerque, A. Aguiar Vieira, and A. Torres Marques, "Drilling tool geometry evaluation for reinforced composite laminates," *Composite Structures*, vol. 92, no. 7, pp. 1545–1550, 2010.

[54] L. M. P. Durão, D. J. S. Gonçalves, J. M. R. S. Tavares, V. H. C. Albuquerque, A. T. Marques, and A. P. M. Baptista, "Drilling of Carbon Fibre Reinforced Laminates – A Comparative Analysis of Five Different Drills on Thrust Force, Roughness and Delamination," *Materials Science Forum*, vol. 636–637, pp. 206–213, 2010.

[55] H. Hocheng and C. C. Tsao, "Effects of special drill bits on drilling-induced delamination of composite materials," *International Journal of Machine Tools & Manufacture*, vol. 46, no. 12–13, pp. 1403–1416, 2006.

[56] Z. Hamdoun, L. Guillaumat, and J. Lataillade, "Influence of the drilling quality on the fatigue compression behaviour of carbon epoxy laminates," *International Journal of Fatigue*, vol. 28, no. 1, pp. 1–8, 2006.

[57] R. Q. Sardinas, P. Reis, and J. P. Davim, "Multi-objective optimization of cutting parameters for drilling laminate composite materials by using genetic algorithms," *Composites Science and Technology*, vol. 66, no. 15, pp. 3083–3088, 2006.

[58] M. Fernandes and C. Cook, "Drilling of carbon composites using a one shot drill bit. Part I: Five stage representation of drilling and factors affecting maximum force and torque," *International Journal of Machine Tools & Manufacture*, vol. 46, no. 1, pp. 70–75, 2006.

[59] M. Fernandes and C. Cook, "Drilling of carbon composites using a one shot drill bit. Part II: empirical modeling of maximum thrust force," *International Journal of Machine Tools & Manufacture*, vol. 46, no. 1, pp. 76–79, 2006.

[60] J. P. Davim, J. C. Rubio, and A. M. Abrao, "A novel approach based on digital image analysis to evaluate the delamination factor after drilling composite laminates," *Composites Science and Technology*, vol. 67, no. 9, pp. 1939–1945, 2007.

[61] C. C. Tsao, "Taguchi analysis of drilling quality associated with core drill in drilling of composite material," *The International Journal of Advanced Manufacturing Technology*, vol. 32, no. 9–10, pp. 877–884, 2007.

[62] C. C. Tsao, "Effect of deviation on delamination by saw drill," *International Journal of Machine Tools & Manufacture*, vol. 47, no. 7–8, pp. 1132–1138, 2007.

[63] C. C. Tsao, "Effect of pilot hole on thrust force by saw drill," *International Journal of Machine Tools & Manufacture*, vol. 47, no. 14, pp. 2172–2176, 2007.

[64] C. C. Tsao, "Experimental study of drilling composite materials with step-core drill," *Materials & Design*, vol. 29, no. 9, pp. 1740–1744, 2008.

[65] C. Tsao, "Investigation into the effects of drilling parameters on delamination by various step-core drills," *Journal of Materials Processing Technology*, vol. 206, no. 1–3, pp. 405–411, 2008.

[66] C. C. Tsao, "Prediction of thrust force of step drill in drilling composite material by Taguchi method and radial basis function network," *The International Journal of Advanced Manufacturing Technology*, vol. 36, no. 1–2, pp. 11–18, 2008.

[67] C. C. Tsao, "Comparison between response surface methodology and radial basis function network for core-center drill in drilling composite materials," *The International Journal of Advanced Manufacturing Technology*, vol. 37, no. 11–12, pp. 1061–1068, 2008.

[68] C. C. Tsao, "Thrust force and delamination of core-saw drill during drilling of carbon fiber reinforced plastics (CFRP)," *The International Journal of Advanced Manufacturing Technology*, vol. 37, no. 1–2, pp. 23–28, 2008.

[69] R. Zitoune and F. Collombet, "Numerical prediction of the thrust force responsible of delamination during the drilling of the long-fibre composite structures," *Composites Part A: Applied Science and Manufacturing*, vol. 38, no. 3, pp. 858–866, 2007.

[70] J. Campos Rubio, A. Abrao, P. Faria, A. Correia, and J. Davim, "Effects of high speed in the drilling of glass fibre reinforced plastic: Evaluation of the delamination factor," *International Journal of Machine Tools & Manufacture*, vol. 48, no. 6, pp. 715–720, 2008.

[71] J. C. Campos Rubio, A. M. Abrão, P. Eustáquio Faria, A. E. Correia, and J. P. Davim, "Delamination in High Speed Drilling of Carbon Fiber Reinforced Plastic (CFRP)," *Journal of Composite Materials*, vol. 42, no. 15, pp. 1523 –1532, 2008.

[72] S. Karnik, V. Gaitonde, J. Rubio, A. Correia, A. Abrao, and J. Davim, "Delamination analysis in high speed drilling of carbon fiber reinforced plastics (CFRP) using artificial neural network model," *Materials & Design*, vol. 29, no. 9, pp. 1768–1776, 2008.

[73] V. Gaitonde, S. Karnik, J. Rubio, A. Correia, A. Abrao, and J. Davim, "Analysis of parametric influence on delamination in high-speed drilling of carbon fiber reinforced plastic composites," *Journal of Materials Processing Technology*, vol. 203, no. 1–3, pp. 431–438, 2008.

[74] A. Faraz, D. Biermann, and K. Weinert, "Cutting edge rounding: An innovative tool wear criterion in drilling CFRP composite laminates," *International Journal of Machine Tools & Manufacture*, vol. 49, no. 15, pp. 1185–1196, 2009.

[75] A. T. Marques, L. M. Durão, A. G. Magalhães, J. F. Silva, and J. M. R. S. Tavares, "Delamination analysis of carbon fibre reinforced laminates: Evaluation of a special step drill," *Composites Science and Technology*, vol. 69, no. 14, pp. 2376–2382, 2009.

[76] S. Rawat and H. Attia, "Characterization of the dry high speed drilling process of woven composites using Machinability Maps approach," *Cirp Annals-Manufacturing Technology*, vol. 58, no. 1, pp. 105–108, 2009.

[77] S. Rawat and H. Attia, "Wear mechanisms and tool life management of WC–Co drills during dry high speed drilling of woven carbon fibre composites," *Wear*, vol. 267, no. 5–8, pp. 1022–1030, 2009.

[78] I. S. Shyha, D. K. Aspinwall, S. L. Soo, and S. Bradley, "Drill geometry and operating effects when cutting small diameter holes in CFRP," *International Journal of Machine Tools & Manufacture*, vol. 49, no. 12–13, pp. 1008–1014, 2009.

[79] I. Shyha, S. L. Soo, D. Aspinwall, and S. Bradley, "Effect of laminate configuration and feed rate on cutting performance when drilling holes in carbon fibre reinforced plastic composites," *Journal of Materials Processing Technology*, vol. 210, no. 8, pp. 1023–1034, 2010.

[80] D. Iliescu, D. Gehin, M. E. Gutierrez, and F. Girot, "Modeling and tool wear in drilling of CFRP," *International Journal of Machine Tools & Manufacture*, vol. 50, no. 2, pp. 204–213, 2010.

[81] P. Curnick, “An investigation into the drilling of fibre-reinforced polymer composites using the optical microscopy inspection method,” *Insight - Non-Destructive Testing and Condition Monitoring*, vol. 53, no. 5, pp. 248–252, 2011.

[82] A. Krishnamoorthy, S. Rajendra Boopathy, and K. Palanikumar, “Delamination Prediction in Drilling of CFRP Composites Using Artificial Neural Network,” *Journal of Engineering Science and Technology*, vol. 6, no. 2, pp. 191–203, 2011.

[83] P. Rahme, Y. Landon, F. Lachaud, R. Piquet, and P. Lagarrigue, “Analytical models of composite material drilling,” *International Journal of Advanced Manufacturing Technology*, vol. 52, no. 5–8, pp. 609–617, 2011.

[84] C. C. Tsao and Y. C. Chiu, “Evaluation of drilling parameters on thrust force in drilling carbon fiber reinforced plastic (CFRP) composite laminates using compound core-special drills,” *International Journal of Machine Tools & Manufacture*, vol. 51, pp. 740–744, 2011.

[85] M.-B. Lazar and P. Xirouchakis, “Experimental analysis of drilling fiber reinforced composites,” *International Journal of Machine Tools & Manufacture*, vol. 51, no. 12, pp. 937–946, 2011.

[86] J. Sedlacek and M. Slany, “Analysis of delamination in drilling of composite materials,” *Modern Machinery (MM) Science Journal*, pp. 194–197, 2010.

[87] V. Krishnaraj, A. Prabukarthi, A. Ramanathan, N. Elanghovan, M. Senthil Kumar, R. Zitoune, and J. P. Davim, “Optimization of machining parameters at high speed drilling of carbon fiber reinforced plastic (CFRP) laminates,” *Composites Part B: Engineering*, vol. 43, no. 4, pp. 1791–1799, 2012.

[88] H. Inoue, E. Aoyama, T. Hirogaki, K. Ogawa, H. Matushita, Y. Kitahara, and T. Katayama, “Influence of tool wear on internal damage in small diameter drilling in GFRP,” *Composite Structures*, vol. 39, no. 1–2, pp. 55–62, 1997.

[89] J. Mathew, N. Ramakrishnan, and N. K. Naik, “Trepanning on unidirectional composites: delamination studies,” *Composites Part A: Applied Science and Manufacturing*, vol. 30, no. 8, pp. 951–959, 1999.

[90] S.-C. Lin and J.-M. Shen, “Drilling Unidirectional Glass Fiber-Reinforced Composite Materials at High Speed,” *Journal of Composite Materials*, vol. 33, no. 9, pp. 827 –851, 1999.

[91] I. Singh, D. Nayak, R. Saxena, and N. Bathnagar, “Drilling Induced Damage in FRP Composite Laminates,” *The Institution of Engineers (India) Journal - Metallurgical and Materials Engineering*, vol. 85, pp. 37–40, 2004.

[92] J. Ramkumar, S. Aravindan, S. Malhotra, and R. Krishnamurthy, “An enhancement of the machining performance of GFRP by oscillatory assisted drilling,” *International Journal of Advanced Manufacturing Technology*, vol. 23, no. 3–4, pp. 240–244, 2004.

[93] J. Ramkumar, S. Malhotra, and R. Krishnamurthy, “Effect of workpiece vibration on drilling of GFRP laminates,” *Journal of Materials Processing Technology*, vol. 152, no. 3, pp. 329–332, 2004.

[94] J. Ramkumar, S. Malhotra, and R. Krishnamurthy, “Effect of microwave treatment on WC inserts for drilling of GFRP composites,” *Machining Science and Technology*, vol. 9, no. 2, pp. 263–269, 2005.

[95] U. Khashaba, “Delamination in drilling GFR-thermoset composites,” *Composite Structures*, vol. 63, no. 3–4, pp. 313–327, 2004.

[96] E. Capello, “Workpiece damping and its effect on delamination damage in drilling thin composite laminates,” *Journal of Materials Processing Technology*, vol. 148, no. 2, pp. 186–195, 2004.

[97] I. El-Sonbaty, U. Khashaba, and T. Machaly, "Factors affecting the machinability of GFR/epoxy composites," *Composite Structures*, vol. 63, no. 3–4, pp. 329–338, 2004.

[98] N. Bhatnagar, I. Singh, and D. Nayak, "Damage Investigation in Drilling of Glass Fiber Reinforced Plastic Composite Laminates," *Materials and Manufacturing Processes*, vol. 19, no. 6, pp. 995–1007, 2004.

[99] A. Langella, L. Nele, and A. Maio, "A torque and thrust prediction model for drilling of composite materials," *Composites Part A: Applied Science and Manufacturing*, vol. 36, no. 1, pp. 83–93, 2005.

[100] V. Krishnaraj, S. Vijayarangan, and G. Suresh, "An investigation on high speed drilling of glass fibre reinforced plastic (GFRP)," *Indian Journal of Engineering and Materials Sciences*, vol. 12, no. 3, pp. 189–195, 2005.

[101] I. Singh and N. Bhatnagar, "Drilling-induced damage in uni-directional glass fiber reinforced plastic (UD-GFRP) composite laminates," *The International Journal of Advanced Manufacturing Technology*, vol. 27, no. 9–10, pp. 877–882, 2005.

[102] S. Arul, D. Raj, L. Vijayaraghavan, S. Malhotra, and R. Krishnamurthy, "Modeling and optimization of process parameters for defect toleranced drilling of GFRP composites," *Materials and Manufacturing Processes*, vol. 21, no. 4, pp. 357–365, 2006.

[103] S. Arul, L. Vijayaraghavan, S. Malhotra, and R. Krishnamurthy, "Influence of tool material on dynamics of drilling of GFRP composites," *International Journal of Advanced Manufacturing Technology*, vol. 29, no. 7–8, pp. 655–662, 2006.

[104] S. Arul, L. Vijayaraghavan, S. Malhotra, and R. Krishnamurthy, "The effect of vibratory drilling on hole quality in polymeric composites," *International Journal of Machine Tools & Manufacture*, vol. 46, no. 3–4, pp. 252–259, 2006.

[105] K. Palanikumar and J. Paulo Davim, "Mathematical model to predict tool wear on the machining of glass fibre reinforced plastic composites," *Materials & Design*, vol. 28, no. 7, pp. 2008–2014, 2007.

[106] P. E. Faria, R. F. Campos, A. M. Abrao, G. C. D. Godoy, and J. P. Davim, "Thrust Force and Wear Assessment When Drilling Glass Fiber-Reinforced Polymeric Composite," *Journal of Composite Materials*, vol. 42, no. 14, pp. 1401–1414, 2008.

[107] K. Palanikumar, J. Campos Rubio, A. M. Abrao, A. Esteves Correia, and J. P. Davim, "Influence of Drill Point Angle in High Speed Drilling of Glass Fiber Reinforced Plastics," *Journal of Composite Materials*, vol. 42, no. 24, pp. 2585–2597, 2008.

[108] B. Srinivasa Rao, R. Rudramoorthy, S. Srinivas, and B. Nageswara Rao, "Effect of drilling induced damage on notched tensile and pin bearing strengths of woven GFR-epoxy composites," *Materials Science and Engineering: A*, vol. 472, no. 1–2, pp. 347–352, 2008.

[109] M. K. A. M. Ariffin, M. I. M. Ali, S. M. Sapuan, and N. Ismail, "An optimise drilling process for an aircraft composite structure using design of experiments," *Scientific Research and Essays*, vol. 4, no. 10, pp. 1109–1116, 2009.

[110] B. Latha and V. S. Senthilkumar, "Analysis of Thrust Force in Drilling Glass Fiber-Reinforced Plastic Composites Using Fuzzy Logic," *Materials and Manufacturing Processes*, vol. 24, no. 4, pp. 509–516, 2009.

[111] U. A. Khashaba, I. A. El-Sonbaty, A. I. Selmy, and A. A. Megahed, "Machinability analysis in drilling woven GFR/epoxy composites: Part I – Effect of machining parameters," *Composites Part A: Applied Science and Manufacturing*, vol. 41, no. 3, pp. 391–400, 2010.

[112] U. A. Khashaba, I. A. El-Sonbaty, A. I. Selmy, and A. A. Megahed, "Machinability analysis in drilling woven GFR/epoxy composites: Part II – Effect of drill wear," *Composites Part A: Applied Science and Manufacturing*, vol. 41, no. 9, pp. 1130–1137, 2010.

[113] E. Kilickap, "Determination of optimum parameters on delamination in drilling of GFRP composites by Taguchi method," *Indian Journal of Engineering and Materials Science*, vol. 17, no. 4, pp. 265–274, 2010.

[114] E. Kilickap, "Optimization of cutting parameters on delamination based on Taguchi method during drilling of GFRP composite," *Expert Systems with Applications*, vol. 37, no. 8, pp. 6116–6122, 2010.

[115] R. Mishra, J. Malik, and I. Singh, "Prediction of drilling-induced damage in unidirectional glass-fibre-reinforced plastic laminates using an artificial neural network," *Proceedings of the Institution of Mechanical Engineers, Part B: Journal of Engineering Manufacture*, vol. 224, no. 5, pp. 733–738, 2010.

[116] R. Mishra, J. Malik, I. Singh, and J. P. Davim, "Neural network approach for estimating the residual tensile strength after drilling in uni-directional glass fiber reinforced plastic laminates," *Materials & Design*, vol. 31, no. 6, pp. 2790–2795, 2010.

[117] G. Baskaran, S. Gowri, and R. Krishnamurthy, "Study on vital static properties of fine blanking of GFRP composites with that of conventional drilling," *The International Journal of Advanced Manufacturing Technology*, vol. 50, no. 5–8, pp. 659–666, 2010.

[118] K. Palanikumar, "Experimental investigation and optimisation in drilling of GFRP composites," *Measurement*, vol. 44, no. 10, pp. 2138–2148, 2011.

[119] K. Palanikumar, "Modeling and Analysis of Delamination Factor and Surface Roughness in Drilling GFRP Composites," *Materials and Manufacturing Processes*, vol. 25, no. 10, pp. 1059–1067, 2010.

[120] B. Latha, V. S. Senthilkumar, and K. Palanikumar, "Influence of drill geometry on thrust force in drilling GFRP composites," *Journal of Reinforced Plastics and Composites*, vol. 30, no. 6, pp. 463–472, 2011.

[121] J. Sudha, S. Sampathkumar, and R. K. Kumar, "Condition monitoring of delamination during drilling of GFRP composites using the acoustic emission technique - a neural network model," *Insight*, vol. 53, no. 8, pp. 445–449, 2011.

[122] G. Caprino and V. Tagliaferri, "Damage development in drilling glass fibre reinforced plastics," *International Journal of Machine Tools & Manufacture*, vol. 35, no. 6, pp. 817–829, 1995.

[123] G. Dini, "On-Line Prediction of Delamination in Drilling of GFRP by Using a Neural Network Approach," *Machining Science and Technology*, vol. 7, no. 3, pp. 295–314, 2003.

[124] U. Khashaba, M. Seif, and M. Elhamid, "Drilling analysis of chopped composites," *Composites Part A: Applied Science and Manufacturing*, vol. 38, no. 1, pp. 61–70, 2007.

[125] J. Davim, P. Reis, and C. Antonio, "Drilling fiber reinforced plastics (FRPs) manufactured by hand lay-up: influence of matrix (Viapal VUP 9731 and ATLAC 382-05)," *Journal of Materials Processing Technology*, vol. 155, pp. 1828–1833, 2004.

[126] J. Davim, P. Reis, and C. Antonio, "Experimental study of drilling glass fiber reinforced plastics (GFRP) manufactured by hand lay-up," *Composites Science and Technology*, vol. 64, no. 2, pp. 289–297, 2004.

[127] N. Mohan, A. Ramachandra, and S. Kulkarni, "Influence of process parameters on cutting force and torque during drilling of glass-fiber polyester reinforced composites," *Composite Structures*, vol. 71, no. 3–4, pp. 407–413, 2005.

[128] R. Varatharajan, S. Malhotra, L. Vijayaraghavan, and R. Krishnamurthy, "Mechanical and machining characteristics of GF/PP and GF/Polyester composites," *Materials Science and Engineering: B*, vol. 132, no. 1–2, pp. 134–137, 2006.

[129] J. P. Davim and F. Mata, "New machinability study of glass fibre reinforced plastics using polycrystalline diamond and cemented carbide (K15) tools," *Materials & Design*, vol. 28, no. 3, pp. 1050–1054, 2007.

[130] J. Sedláček and A. Humár, "Analysis of fracture mechanisms and surface quality in drilling of composite materials," *Strength of Materials*, vol. 40, no. 1, pp. 40–43, 2008.

[131] B. Işık and E. Ekici, "Experimental investigations of damage analysis in drilling of woven glass fiber-reinforced plastic composites," *The International Journal of Advanced Manufacturing Technology*, vol. 49, no. 9–12, pp. 861–869, 2009.

[132] S. Jayabal and U. Natarajan, "Influence of cutting parameters on thrust force and torque in drilling of E-glass/polyestercomposites," *Indian Journal of Engineering and Materials Science*, vol. 17, no. 6, pp. 463–470, 2010.

[133] S. Jayabal and U. Natarajan, "Regression & neuro fuzzy models for prediction of thrust force and torque in drilling of glass fiber reinforced composites," *Journal of Scientific & Industrial Research*, vol. 69, no. 10, pp. 741–745, 2010.

[134] V. Schulze, C. Becke, K. Weidenmann, and S. Dietrich, "Machining strategies for hole making in composites with minimal workpiece damage by directing the process forces inwards," *Journal of Materials Processing Technology*, vol. 211, no. 3, pp. 329–338, 2011.

[135] A. Velayudham, R. Krishnamurthy, and T. Soundarapandian, "Evaluation of drilling characteristics of high volume fraction fibre glass reinforced polymeric composite," *International Journal of Machine Tools & Manufacture*, vol. 45, no. 4–5, pp. 399–406, 2005.

[136] A. Velayudham and R. Krishnamurthy, "Effect of point geometry and their influence on thrust and delamination in drilling of polymeric composites," *Journal of Materials Processing Technology*, vol. 185, no. 1–3, pp. 204–209, 2007.

[137] D. Bhattacharyya and D. P. W. Horrigan, "A study of hole drilling in Kevlar composites," *Composites Science and Technology*, vol. 58, no. 2, pp. 267–283, 1998.

[138] A. N. Shuaib, F. A. Al-Sulaiman, and F. Hamid, "Machinability of Kevlar49 Composite Laminates While Using Standard TiN Coated HSS Drills," *Machining Science and Technology*, vol. 8, no. 3, pp. 449–467, 2004.

[139] M. Rahman, S. Ramakrishna, J. R. . Prakash, and D. C. . Tan, "Machinability study of carbon fiber reinforced composite," *Journal of Materials Processing Technology*, vol. 89–90, no. 0, pp. 292–297, 1999.

[140] X. M. Wang and L. C. Zhang, "An experimental investigation into the orthogonal cutting of unidirectional fibre reinforced plastics," *International Journal of Machine Tools & Manufacture*, vol. 43, no. 10, pp. 1015–1022, 2003.

[141] W. H. Kao, "Tribological properties and high speed drilling application of MoS2–Cr coatings," *Wear*, vol. 258, no. 5–6, pp. 812–825, 2005.

[142] C. Tsao and H. Hocheng, "Computerized tomography and C-Scan for measuring delamination in the drilling of composite materials using various drills," *International Journal of Machine Tools & Manufacture*, vol. 45, no. 11, pp. 1282–1287, 2005.

[143] C. K. Dharan and M. Won, "Machining parameters for an intelligent machining system for composite laminates," *International Journal of Machine Tools & Manufacture*, vol. 40, no. 3, pp. 415–426, 2000.

[144] J. Campos Rubio, T. H. Panzera, A. M. Abrao, P. E. Faria, and J. Paulo Davim, "Effects of high speed in the drilling of glass whisker-reinforced polyamide composites (PA66 GF30): statistical analysis of the roughness parameters," *Journal of Composite Materials*, vol. 45, no. 13, pp. 1395–1402, 2010.

[145] H. Hocheng and C. K. . Dharan, "Delamination During Drilling in Composite Laminates," *Journal of Engineering for Industry-Transactions of the Asme*, vol. 112, no. 3, pp. 236–239, 1990.

[146] S.-L. Gao and J.-K. Kim, "Scanning acoustic microscopy as a tool for quantitative characterisation of damage in CFRPs," *Composites Science and Technology*, vol. 59, pp. 345–354, 1999.

[147] H. Hocheng and C. Tsao, "Comprehensive analysis of delamination in drilling of composite materials with various drill bits," *Journal of Materials Processing Technology*, vol. 140, no. 1–3, pp. 335–339, 2003.

[148] H. Hocheng and C. C. Tsao, "The path towards delamination-free drilling of composite materials," *Journal of Materials Processing Technology*, vol. 167, no. 2–3, pp. 251–264, 2005.

[149] D. Liu, Y. Tang, and W. L. Cong, "A review of mechanical drilling for composite laminates," *Composite Structures*, vol. 94, no. 4, pp. 1265–1279, 2012.

[150] D. C. Montgomery, *Design and Analysis of Experiments*, 6th ed. Wiley, 2004.

[151] G. E. P. Box and N. R. Draper, *Empirical Model-Building and Response Surfaces*, 1st ed. Wiley, 1987.

[152] R. H. Myers and D. C. Montgomery, *Response Surface Methodology: Process and Product Optimization Using Designed Experiments*, 2nd ed. Wiley, 2002.

[153] J. A. Cornell, *How to Apply Response Surface Methodology*, Revised. Amer Society for Quality, 1990.

[154] E. D. Castillo, *Process Optimization: A Statistical Approach*. Springer London, Limited, 2007.

[155] "NIST/SEMATECH e-Handbook of Statistical Methods," 2011. [Online]. Available: http://www.itl.nist.gov/div898/handbook/.

[156] U.S. Department of Defense, *Military Handbook - MIL-HDBK-17-1F: Composite Materials Handbook*, vol. Volume 1 - Polymer Matrix Composites Guidelines for Characterization of Structural Materials. 2002.

[157] J. Shigley and C. Mischke, *Mechanical Engineering Design*, Fifth ed. McGraw-Hill, 1989.

[158] M. Jouaneh, *Fundamentals of Mechatronics, Si Edition*. Cengage Learning, 2012.

# Appendix A

## Development of a Torque Sensor

The torque sensor was specially developed for this work. This is a strain gage based sensor that is used, in conjunction with the data acquisition (DAQ) system, for static torque measurement.

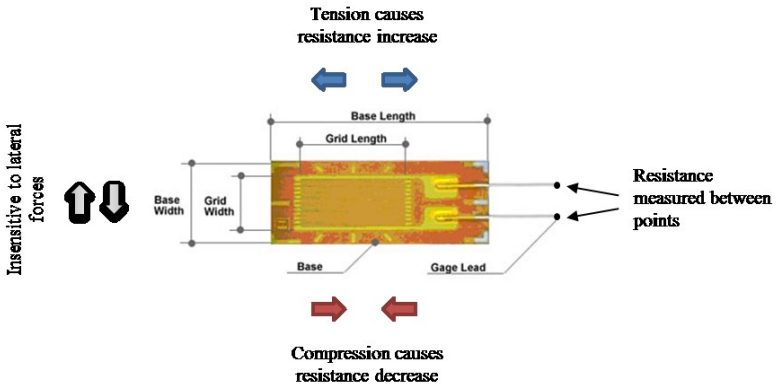


**Figure A.1** Strain gage characteristics (Adapted from FREDMA and Sensorland)

The strain gages are configured into a Wheatstone bridge circuit, as primary sensing element. The sensing element gets the elastic deformation under the action of the external torque being applied. In this particular case, the application for torque sensor is to determine the amount of power the rotating device consumes under the conditions determined by the drilling parameters, thus measuring the material removal rate, and verify the influence of increasing power in each of the responses. It measures the torque that is transferred by the tool to the restraining elements.

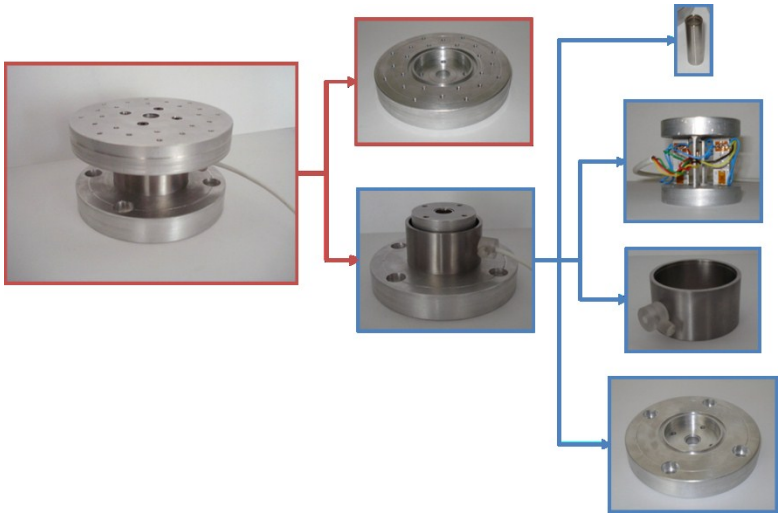

**Figure A.2** Components of the torque sensor developed and manufactured

This is a reaction torque sensor, hence is a rigid structure with no moving parts, attached in a fixed position. Strain gages are bonded on stationary support member. The output voltage produced by a resistance change in strain gages that are mounted to the torque sensor structure signal varies proportionally to the applied torsional force. It was also intended that the mechanical design and gauge placement minimizes transverse effects.

The most usual structures for torque sensors are solid or hollow circular shaft, solid or hollow square shaft and solid or hollow cruciform, as shown in Figure A.3.

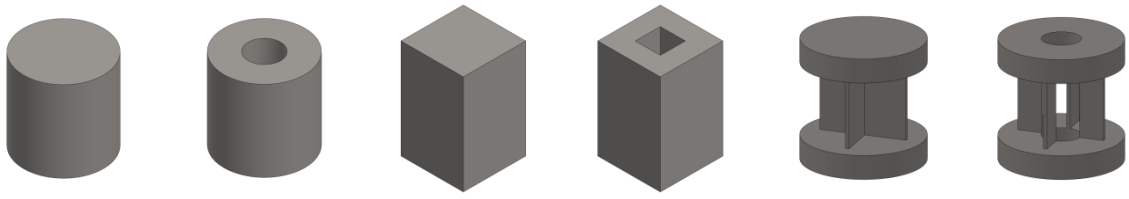

**a)** **b)** **c)** **d)** **e)** **f)**

**Figure A.3** Different structure for torque sensor: **a)** Solid circular shaft; **b)** Hollow circular shaft; **c)** Solid square shaft; **d)** Hollow square shaft; **e)** Solid cruciform; **f)** Hollow cruciform

The choice of ideal configuration for this work came upon the hollow cruciform structure as it is typically used for low-torque measured applications [158].

Once determined the shape of the sensor, the 3D model was built using *SolidWorks* software, and FEA analysis was performed, after the choice of material (AISI 316 stainless steel), and application of suitable boundary conditions, to optimize the sensor dimensions and to determine the placement and size of the strain gages.

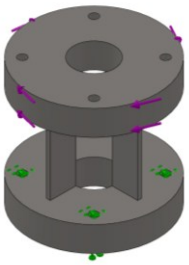

**Figure A.4** Constraints definition for FEA analysis

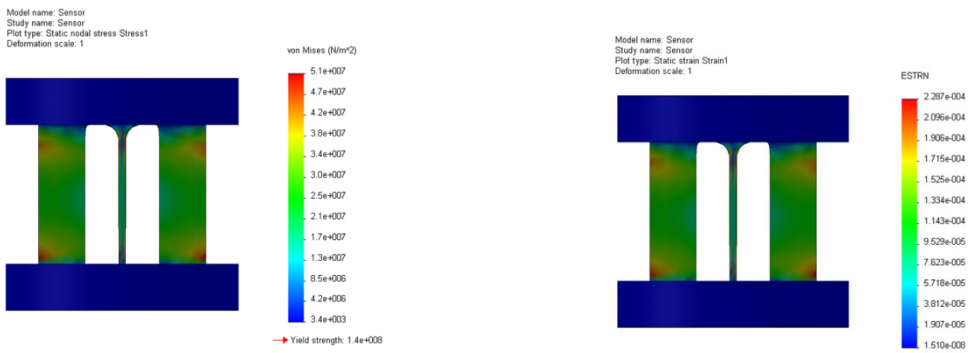


**a)** **b)**

**Figure A.5 a)** Stress distributions in torque sensor**; b)** Strain distributions in torque sensor

As mentioned earlier, the strain gages are bonded in a Wheatstone bridge configuration, illustrated below (Figure A.6). The placement defined is shown in Figure A.7.

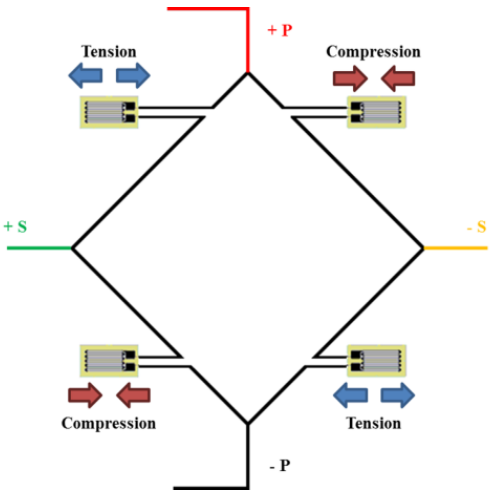


**Figure A.6** Wheatstone full-bridge circuit (Adapted from Sensorland)

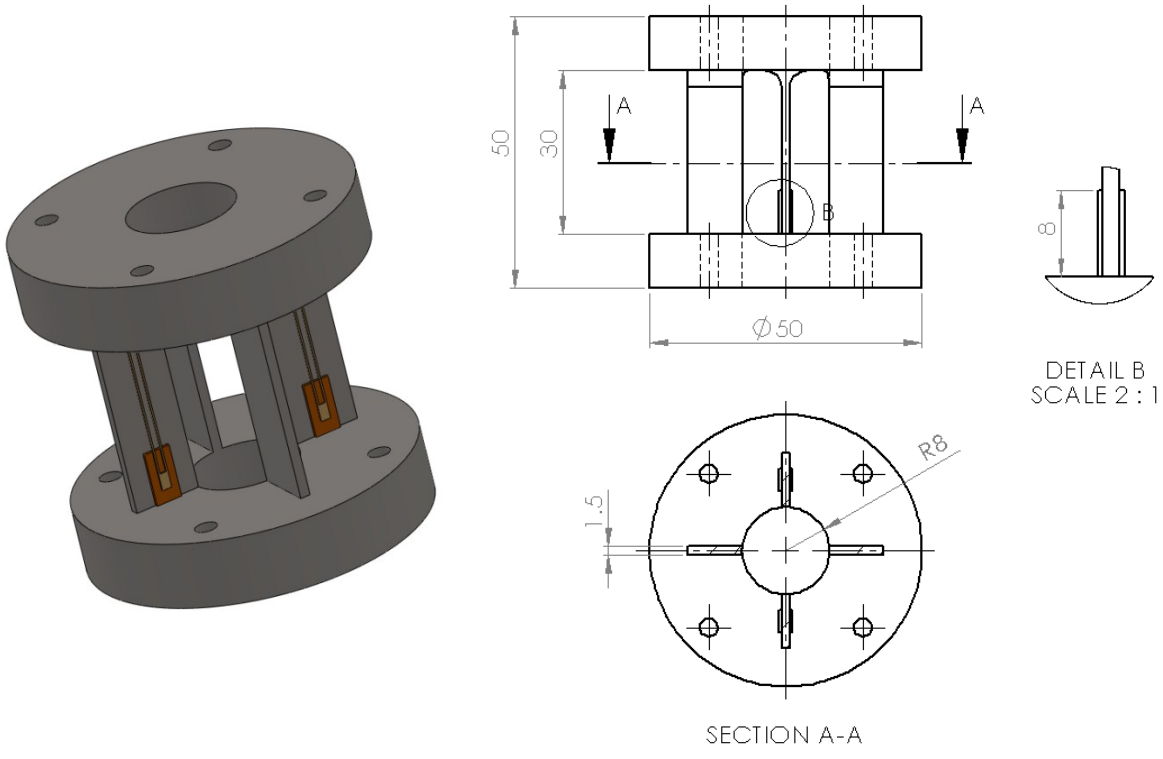


**a)** **b)**

**Figure A.7 a)** Torque sensor model and **b)** Torque sensor characteristics with strain gages placement defined

# Appendix B

## *LabVIEW* Block Diagram Program

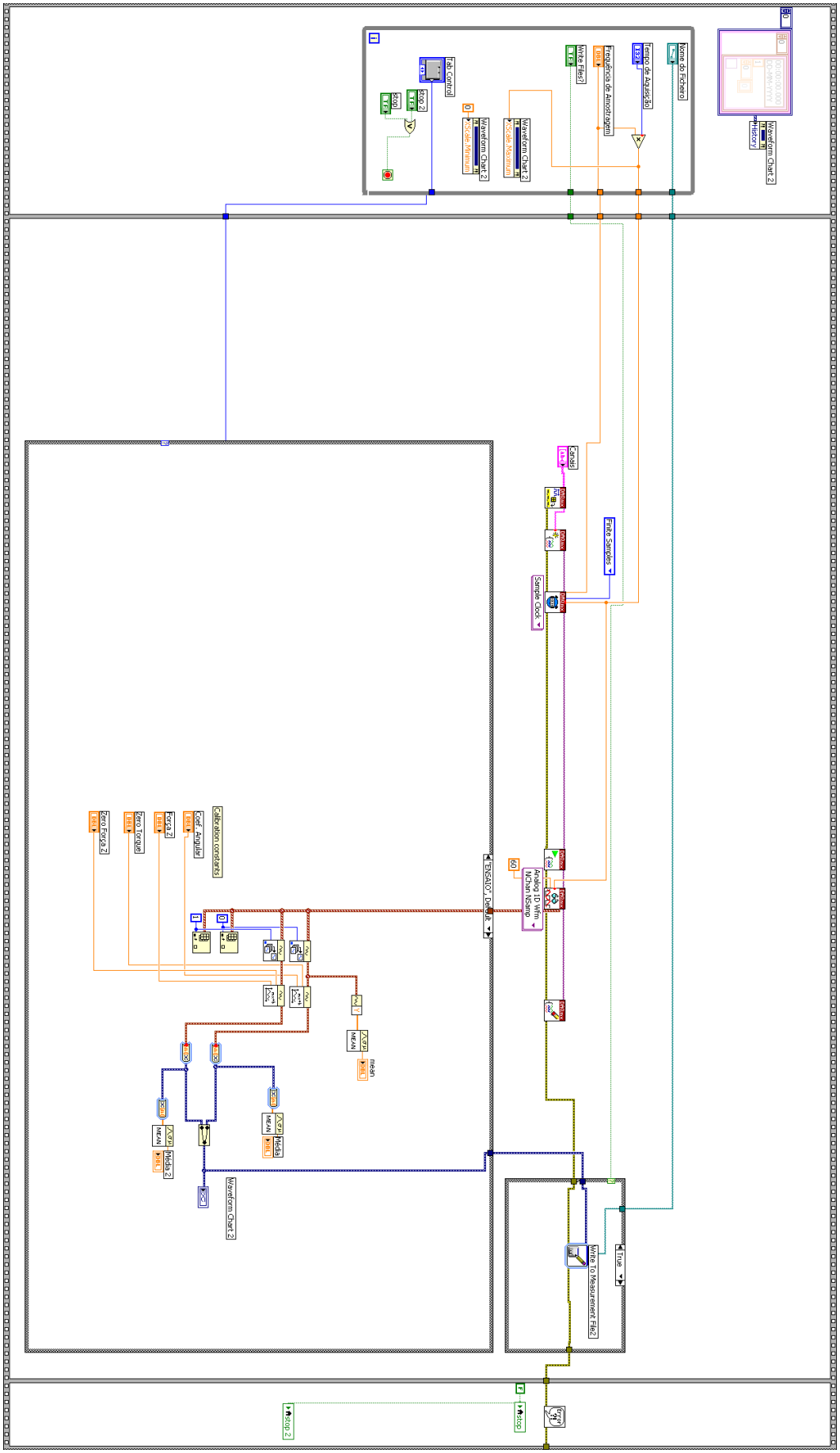
Path Control
stop 2
Waveform Chart 2
Escala Máximum
Escala Mínimo
Waveform Chart 2
Mínimo Files?
Frequência de Amostragem
Tempo de Aquisição
Nome do Ficheiro
Waveform Chart 2
History
Canais
Finite Samples
Sample Clock
"ENSAIO" Default
60
Analog 1D Wfm NChan NSamp
Zero Força 2
Zero Torque
Força 2
Coef. Angular
Calibration constants
MEAN
Média
Média 2
Waveform Chart 2
Write To Measurement File2
True
stop 2
stop

# Appendix C

## Response Surface Models

## C.1 W-Shape special Drill (DORMER)

**Table C.1** DOE results using W-Shape Drill

| Test | Spindle Speed [rpm] | Feed Rate [mm/rev] | Tool Diameter [mm] | Thickness [mm] | Torque [Nm] | Force [N] | $F_d$ | $F_{da}$ |
|---|---|---|---|---|---|---|---|---|
| **W01** | 12 000 | 0.11 | 7 | 6 | 0.19 | 105.63 | 1.155 | 1.220 |
| **W02** | 16 000 | 0.065 | 5 | 4 | 0.10 | 64.31 | 1.367 | 1.458 |
| **W03** | 16 000 | 0.065 | 5 | 8 | 0.17 | 86.09 | 1.319 | 1.416 |
| **W04** | 16 000 | 0.065 | 9 | 4 | 0.21 | 100.12 | 1.190 | 1.236 |
| **W05** | 16 000 | 0.065 | 9 | 8 | 0.71 | 150.45 | 1.125 | 1.191 |
| **W06** | 16 000 | 0.155 | 5 | 4 | 0.15 | 104.23 | 1.596 | 1.744 |
| **W07** | 16 000 | 0.155 | 5 | 8 | 0.26 | 122.97 | 1.464 | 1.609 |
| **W08** | 16 000 | 0.155 | 9 | 4 | 0.37 | 152.90 | 1.183 | 1.243 |
| **W09** | 16 000 | 0.155 | 9 | 8 | 0.77 | 213.66 | 1.087 | 1.135 |
| **W10** | 12 000 | 0.11 | 7 | 6 | 0.26 | 112.61 | 1.154 | 1.216 |
| **W11** | 8 000 | 0.065 | 5 | 4 | 0.14 | 70.32 | 1.507 | 1.626 |
| **W12** | 8 000 | 0.065 | 5 | 8 | 0.21 | 94.21 | 1.316 | 1.448 |
| **W13** | 8 000 | 0.065 | 9 | 4 | 0.28 | 125.38 | 1.224 | 1.282 |
| **W14** | 8 000 | 0.065 | 9 | 8 | 0.81 | 173.17 | 1.135 | 1.206 |
| **W15** | 8 000 | 0.155 | 5 | 4 | 0.20 | 115.77 | 1.502 | 1.619 |
| **W16** | 8 000 | 0.155 | 5 | 8 | 0.31 | 137.71 | 1.406 | 1.540 |
| **W17** | 8 000 | 0.155 | 9 | 4 | 0.44 | 170.37 | 1.224 | 1.271 |
| **W18** | 8 000 | 0.155 | 9 | 8 | 0.86 | 232.40 | 1.064 | 1.097 |
| **W19** | 12 000 | 0.11 | 7 | 6 | 0.31 | 122.19 | 1.161 | 1.223 |
| **W20** | 4 000 | 0.11 | 7 | 6 | 0.41 | 131.19 | 1.182 | 1.246 |
| **W21** | 20 000 | 0.11 | 7 | 6 | 0.29 | 139.37 | 1.146 | 1.187 |
| **W22** | 12 000 | 0.02 | 7 | 6 | 0.17 | 82.80 | 1.148 | 1.211 |
| **W23** | 12 000 | 0.2 | 7 | 6 | 0.43 | 218.28 | 1.149 | 1.209 |
| **W24** | 12 000 | 0.11 | 3 | 6 | 0.10 | 62.65 | 1.508 | 1.737 |
| **W25** | 12 000 | 0.11 | 11 | 6 | 0.72 | 73.34 | 1.143 | 1.214 |
| **W26** | 12 000 | 0.11 | 7 | 2 | 0.15 | 175.24 | 1.625 | 1.697 |
| **W27** | 12 000 | 0.11 | 7 | 10 | 0.45 | 190.18 | 1.264 | 1.369 |
| **W28** | 12 000 | 0.11 | 7 | 6 | 0.33 | 170.38 | 1.159 | 1.222 |

In order to create the empirical model that describes this process, the Response Surface Methodology was used after the design of experiments defined previously on Chapter 3. The adequacy of the model response was checked using the F-Test with a confidence interval of 95%. The histogram of residuals and scatter plots of residual values vs. predicted and observed values were done to verify the existence of other factors which influence the responses and the consistency of the model.

The resulting empirical models, second-degree polynomials, to estimate each of the responses are presented below (Table C.2).

**Table C.2** Empirical Models (W-Shape drill)

| Response | Empirical Model |
|---|---|
| **Torque** | $T = 0.273 - 0.032S + 0.025S^2 + 0.053f_z + 0.174d + 0.039d^2 + 0.116t + 0.093d \cdot t$ |
| **Thrust Force** | $F = 127.703 + 27.371f_z + 22.676d - 15.260d^2 + 14.048t + 13.418t^2 + 8.411d \cdot t$ |
| **Delamination Factor** | $F_d = 1.157 - 0.124d + 0.046d^2 - 0.067t + 0.076t^2 - 0.036f_z \cdot d$ |
| **Adjusted Delamination Factor** | $F_{da} = 1.220 - 0.160d + 0.068d^2 - 0.062t + 0.082t^2 - 0.046f_z \cdot d$ |

## C.1.1 Torque Model (W-Shape Drill)

**Table C.3** Analysis of variance table to test adequacy for the torque model (W-Shape drill)

| ANOVA; Var.: Torque; $R^2$=0.94473; $\overline{R}^2$:0.92585<br>4 factors. 1 Blocks. 56 Runs | | | | | |
|---|---|---|---|---|---|
| | **SS** | **df** | **MS** | **F** | **p** |
| ***S*** | **0.047988** | **1** | **0.047988** | **12.6587** | **0.000961** |
| ***S²*** | **0.030076** | **1** | **0.030076** | **7.9336** | **0.007430** |
| ***f*** | **0.134631** | **1** | **0.134631** | **35.5142** | **0.000000** |
| *f²* | 0.008136 | 1 | 0.008136 | 2.1461 | 0.150558 |
| ***d*** | **1.453304** | **1** | **1.453304** | **383.3672** | **0.000000** |
| ***d²*** | **0.074450** | **1** | **0.074450** | **19.6392** | **0.000068** |
| ***t*** | **0.649722** | **1** | **0.649722** | **171.3902** | **0.000000** |
| *t²* | 0.007942 | 1 | 0.007942 | 2.0949 | 0.155394 |
| *S × f* | 0.000018 | 1 | 0.000018 | 0.0049 | 0.944717 |
| *S × d* | 0.002400 | 1 | 0.002400 | 0.6330 | 0.430851 |
| *S × t* | 0.000316 | 1 | 0.000316 | 0.0833 | 0.774380 |
| *f × d* | 0.001902 | 1 | 0.001902 | 0.5017 | 0.482761 |
| *f × t* | 0.001945 | 1 | 0.001945 | 0.5132 | 0.477836 |
| ***d × t*** | **0.278127** | **1** | **0.278127** | **73.3673** | **0.000000** |
| *Error* | 0.155427 | 41 | 0.003791 | | |
| *Total SS* | 2.812037 | 55 | | | |

**Table C.4** Regression Coefficients tested by t (Torque model; W-Shape drill)

| Regression Coefficients; Var.:Torque | | | |
|---|---|---|---|
| | **Regression Coefficients** | **Std.Err.** | **t(41)** |
| ***Mean/Interc.*** | **0.273425** | **0.021768** | **12.56066** |
| ***S*** | **-0.031619** | **0.008887** | **-3.55791** |
| ***S²*** | **0.025031** | **0.008887** | **2.81667** |
| ***f*** | **0.052960** | **0.008887** | **5.95938** |
| *f²* | 0.013019 | 0.008887 | 1.46496 |
| ***d*** | **0.174003** | **0.008887** | **19.57976** |
| ***d²*** | **0.039383** | **0.008887** | **4.43162** |
| ***t*** | **0.116344** | **0.008887** | **13.09161** |
| *t²* | 0.012863 | 0.008887 | 1.44738 |
| *S × f* | -0.000759 | 0.010884 | -0.06977 |
| *S × d* | -0.008659 | 0.010884 | -0.79559 |
| *S × t* | -0.003141 | 0.010884 | -0.28855 |
| *f × d* | 0.007709 | 0.010884 | 0.70831 |
| *f × t* | -0.007797 | 0.010884 | -0.71635 |
| ***d × t*** | **0.093228** | **0.010884** | **8.56547** |

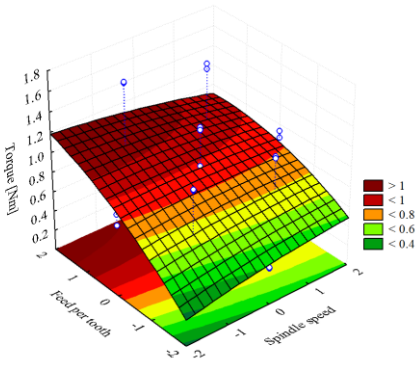


*T= f (S,f); d and t constants at level 0*

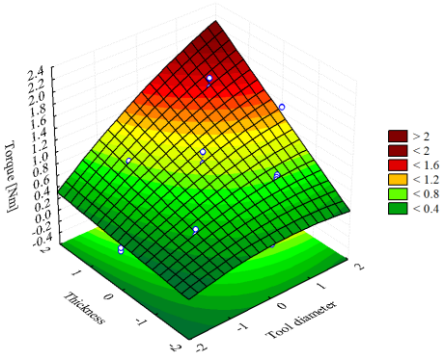


*T= f (t,d); S and f constants at level 0*

**Figure C.1** Fitted response surface: Torque model; W-Shape drill

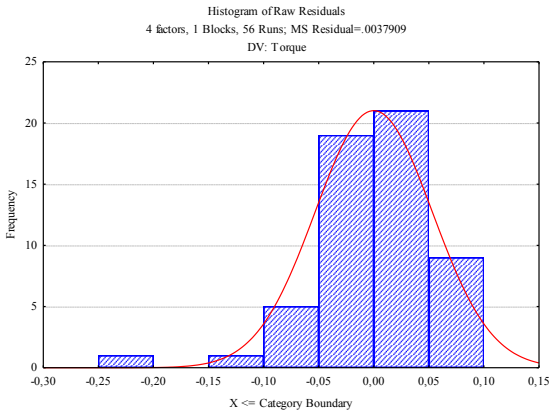


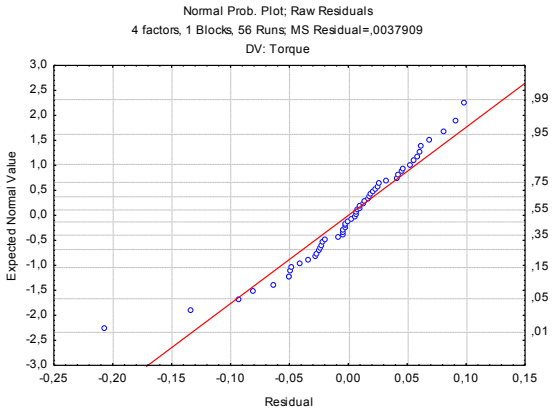


**a)**

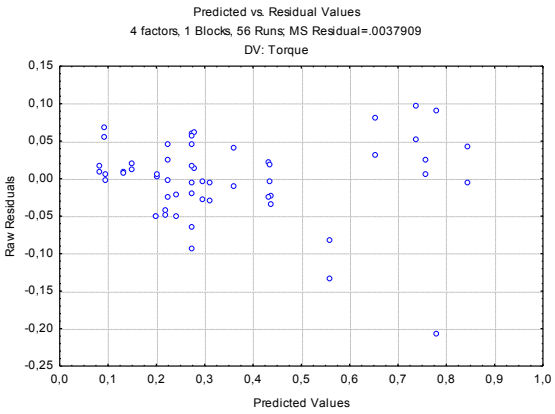


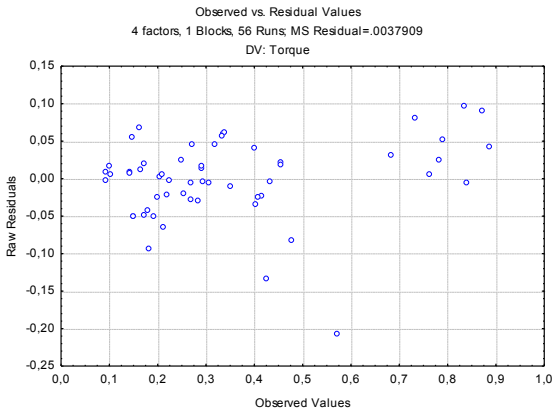


**b)**

**Figure C.2 a)** Residuals normality testing; **b)** Plots of residuals versus corresponding predicted and observed values (Torque model; W-Shape drill)

## C.1.2 Thrust Force Model (W-Shape Drill)

**Table C.5** Analysis of variance table to test adequacy for the Thrust force model (W-Shape drill)

| ANOVA; Var.: Thrust force; $R^2$=0.83491; $\bar{R}^2$: 0.77853<br>4 factors. 1 Blocks. 56 Runs | | | | | |
|---|---|---|---|---|---|
| | **SS** | **df** | **MS** | **F** | **p** |
| *S* | 976.1 | 1 | 976.08 | 1.98010 | 0.166915 |
| $S^2$ | 116.8 | 1 | 116.80 | 0.23695 | 0.629013 |
| ***f*** | **35 961.0** | **1** | **35 961.02** | **72.95175** | **0.000000** |
| $f^2$ | 1 386.9 | 1 | 1 386.87 | 2.81344 | 0.101087 |
| ***d*** | **24 681.3** | **1** | **24 681.27** | **50.06926** | **0.000000** |
| $d^2$ | **11 177.9** | **1** | **11 177.94** | **22.67595** | **0.000024** |
| ***t*** | **9 472.5** | **1** | **9 472.48** | **19.21620** | **0.000079** |
| $t^2$ | **8 641.5** | **1** | **8 641.55** | **17.53054** | **0.000146** |
| *S* × *f* | 0.0 | 1 | 0.02 | 0.00004 | 0.995120 |
| *S* × *d* | 239.6 | 1 | 239.61 | 0.48609 | 0.489612 |
| *S* × *t* | 2.0 | 1 | 2.05 | 0.00416 | 0.948899 |
| *f* × *d* | 370.8 | 1 | 370.80 | 0.75223 | 0.390820 |
| *f* × *t* | 48.5 | 1 | 48.51 | 0.09840 | 0.755348 |
| ***d* × *t*** | **2 264.1** | **1** | **2 264.05** | **4.59294** | **0.038087** |
| *Error* | 20 210.6 | 41 | 492.94 | | |
| *Total SS* | 122 420.3 | 55 | | | |

**Table C.6** Regression Coefficients tested by t (Thrust force model; W-Shape drill)

| Regression Coefficients; Var.:Thrust force | | | |
|---|---|---|---|
| | **Regression Coefficients** | **Std.Err.** | **t(41)** |
| ***Mean/Interc.*** | **127.7029** | **7.849701** | **16.26851** |
| *S* | -4.5094 | 3.204627 | -1.40716 |
| $S^2$ | 1.5599 | 3.204627 | 0.48677 |
| ***f*** | **27.3713** | **3.204627** | **8.54118** |
| $f^2$ | 5.3752 | 3.204627 | 1.67733 |
| ***d*** | **22.6758** | **3.204627** | **7.07596** |
| $d^2$ | **-15.2602** | **3.204627** | **-4.76193** |
| ***t*** | **14.0479** | **3.204627** | **4.38363** |
| $t^2$ | **13.4176** | **3.204627** | **4.18695** |
| *S* × *f* | -0.0241 | 3.924851 | -0.00615 |
| *S* × *d* | -2.7364 | 3.924851 | -0.69720 |
| *S* × *t* | -0.2531 | 3.924851 | -0.06448 |
| *f* × *d* | 3.4041 | 3.924851 | 0.86731 |
| *f* × *t* | 1.2312 | 3.924851 | 0.31369 |
| ***d* × *t*** | **8.4114** | **3.924851** | **2.14311** |

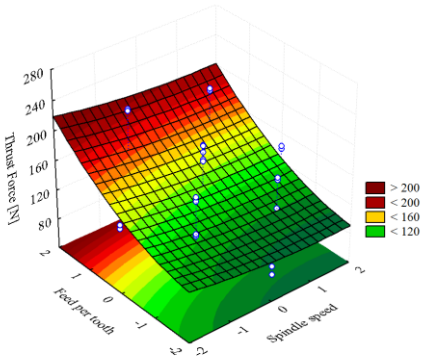


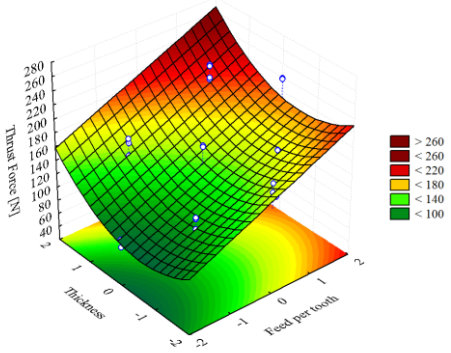


*F= f (S,f); d and t constants at level 0* *F= f (t,f); S and d constants at level 0*

**Figure C.3** Fitted response surface: Thrust force model; W-Shape drill

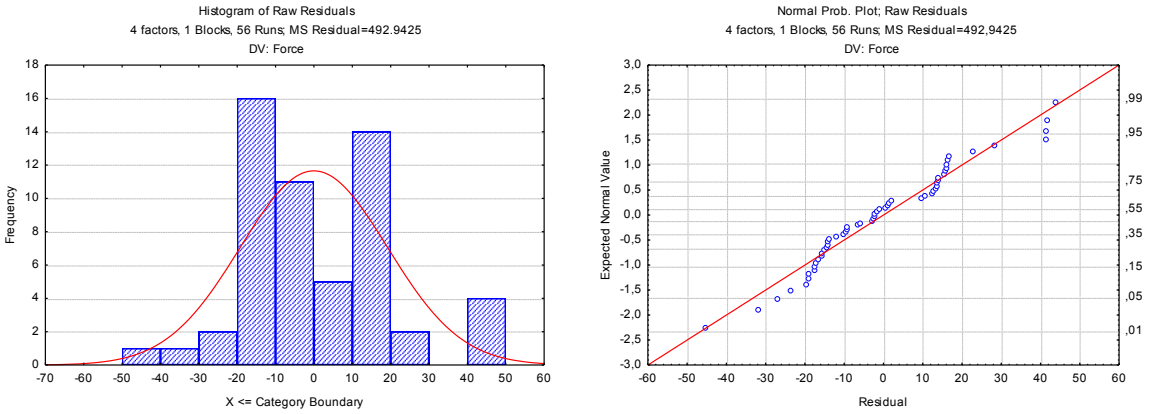


**a)**

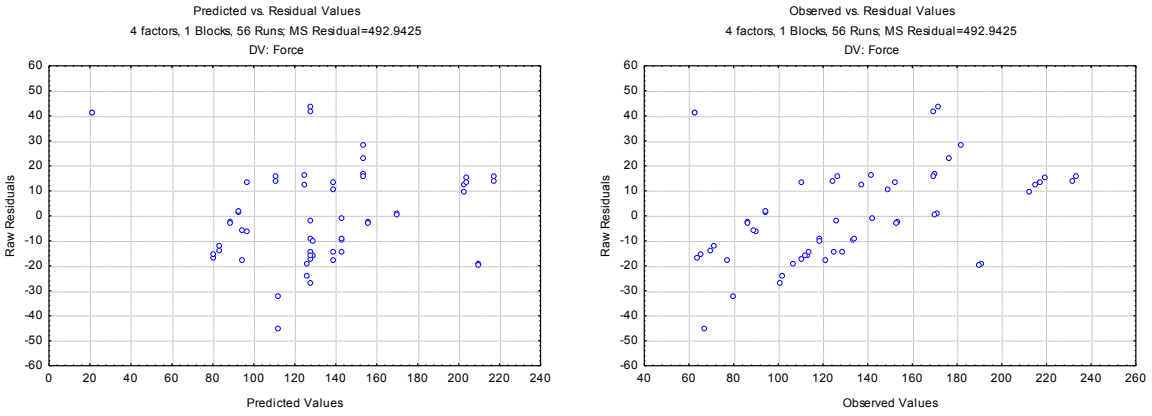


**b)**

**Figure C.4 a)** Residuals normality testing; **b)** Plots of residuals versus corresponding predicted and observed values (Thrust force model; W-Shape drill)

## C.1.3 Delamination Factor Model (W-Shape Drill)

**Table C.7** Analysis of variance table to test adequacy for the Delamination factor model (W-Shape drill)

| ANOVA; Var.: Delamination factor; $R^2$=0.84113; $\bar{R}^2$: 0.78688<br>4 factors. 1 Blocks. 56 Runs | | | | | |
|---|---|---|---|---|---|
| | **SS** | **df** | **MS** | **F** | **p** |
| *S* | 0.001136 | 1 | 0.001136 | 0.1795 | 0.673998 |
| $S^2$ | 0.001542 | 1 | 0.001542 | 0.2436 | 0.624241 |
| *f* | 0.009857 | 1 | 0.009857 | 1.5573 | 0.219146 |
| $f^2$ | 0.000134 | 1 | 0.000134 | 0.0211 | 0.885225 |
| ***d*** | **0.736443** | **1** | **0.736443** | **116.3439** | **0.000000** |
| $d^2$ | **0.101762** | **1** | **0.101762** | **16.0764** | **0.000251** |
| ***t*** | **0.213392** | **1** | **0.213392** | **33.7118** | **0.000001** |
| $t^2$ | **0.275480** | **1** | **0.275480** | **43.5206** | **0.000000** |
| *S* × *f* | 0.012452 | 1 | 0.012452 | 1.9672 | 0.168272 |
| *S* × *d* | 0.000690 | 1 | 0.000690 | 0.1090 | 0.742985 |
| *S* × *t* | 0.004756 | 1 | 0.004756 | 0.7514 | 0.391073 |
| ***f* × *d*** | **0.041149** | **1** | **0.041149** | **6.5008** | **0.014618** |
| *f* × *t* | 0.001008 | 1 | 0.001008 | 0.1592 | 0.691995 |
| *d* × *t* | 0.000396 | 1 | 0.000396 | 0.0625 | 0.803805 |
| *Error* | 0.259525 | 41 | 0.006330 | | |
| *Total SS* | 1.633557 | 55 | | | |

**Table C.8** Regression Coefficients tested by t (Delamination factor model; W-Shape drill)

| Regression Coefficients; Var.:Delamination Factor | | | |
|---|---|---|---|
| | **Regression Coefficients** | **Std.Err.** | **t(41)** |
| ***Mean/Interc.*** | **1.157232** | **0.028129** | **41.1403** |
| *S* | -0.004866 | 0.011484 | -0.4237 |
| $S^2$ | 0.005668 | 0.011484 | 0.4936 |
| *f* | 0.014330 | 0.011484 | 1.2479 |
| $f^2$ | 0.001668 | 0.011484 | 0.1452 |
| ***d*** | **-0.123865** | **0.011484** | **-10.7863** |
| $d^2$ | **0.046044** | **0.011484** | **4.0095** |
| ***t*** | **-0.066676** | **0.011484** | **-5.8062** |
| $t^2$ | **0.075757** | **0.011484** | **6.5970** |
| *S* × *f* | 0.019726 | 0.014064 | 1.4026 |
| *S* × *d* | -0.004643 | 0.014064 | -0.3301 |
| *S* × *t* | 0.012192 | 0.014064 | 0.8668 |
| ***f* × *d*** | **-0.035860** | **0.014064** | **-2.5497** |
| *f* × *t* | -0.005611 | 0.014064 | -0.3990 |
| *d* × *t* | 0.003517 | 0.014064 | 0.2500 |

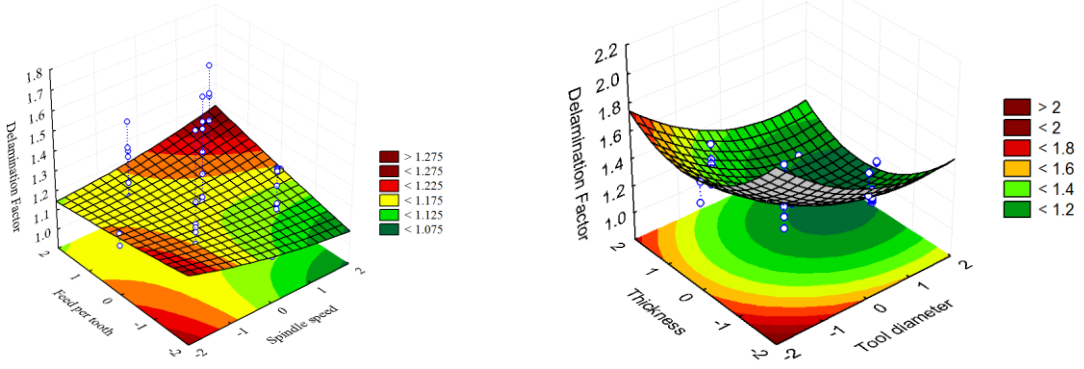


$F_d = f(S,f)$; *d and t constants at level 0* $F_d = f(t,d)$; *S and f constants at level 0*

**Figure C.5** Fitted response surface: Delamination factor model; W-Shape drill

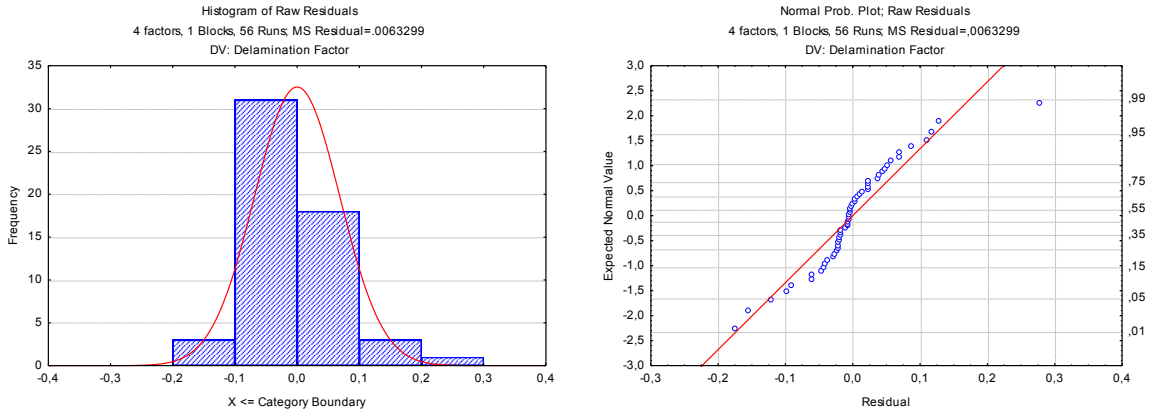


**a)**

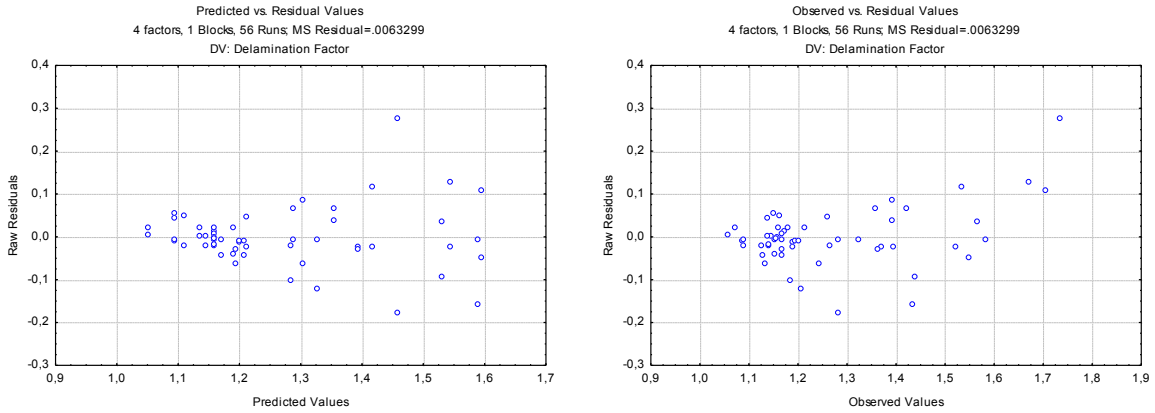


**b)**

**Figure C.6 a)** Residuals normality testing; **b)** Plots of residuals versus corresponding predicted and observed values (Delamination factor model; W-Shape drill)

## C.1.4 Adjusted Delamination Factor Model (W-Shape Drill)

**Table C.9** Analysis of variance table to test adequacy for the adjusted delamination factor model (W-Shape drill)

| ANOVA; Var.: Adjusted delamination factor; $R^2$=0. 85609; $\bar{R}^2$: 0. 80694<br>4 factors. 1 Blocks. 56 Runs | | | | | |
|---|---|---|---|---|---|
| | **SS** | **df** | **MS** | **F** | **p** |
| *S* | 0.002555 | 1 | 0.002555 | 0.3050 | 0.583753 |
| $S^2$ | 0.000449 | 1 | 0.000449 | 0.0536 | 0.818036 |
| *f* | 0.012837 | 1 | 0.012837 | 1.5323 | 0.222814 |
| $f^2$ | 0.000097 | 1 | 0.000097 | 0.0115 | 0.914945 |
| ***d*** | **1.232001** | **1** | **1.232001** | **147.0596** | **0.000000** |
| $d^2$ | **0.220748** | **1** | **0.220748** | **26.3499** | **0.000007** |
| ***t*** | **0.185903** | **1** | **0.185903** | **22.1906** | **0.000028** |
| $t^2$ | **0.323796** | **1** | **0.323796** | **38.6504** | **0.000000** |
| *S* × *f* | 0.026886 | 1 | 0.026886 | 3.2093 | 0.080605 |
| *S* × *d* | 0.000269 | 1 | 0.000269 | 0.0321 | 0.858711 |
| *S* × *t* | 0.003838 | 1 | 0.003838 | 0.4581 | 0.502315 |
| ***f* × *d*** | **0.067064** | **1** | **0.067064** | **8.0052** | **0.007188** |
| *f* × *t* | 0.002997 | 1 | 0.002997 | 0.3577 | 0.553069 |
| *d* × *t* | 0.000118 | 1 | 0.000118 | 0.0141 | 0.906081 |
| *Error* | 0.343480 | 41 | 0.008378 | | |
| *Total SS* | 2.386699 | 55 | | | |

**Table C.10** Regression Coefficients tested by t (Adjusted delamination factor model; W-Shape drill)

| Regression Coefficients; Var.: Adjusted delamination factor | | | |
|---|---|---|---|
| | **Regression Coefficients** | **Std.Err.** | **t(41)** |
| ***Mean/Interc.*** | **1.220253** | **0.032360** | **37.7082** |
| *S* | -0.007296 | 0.013211 | -0.5523 |
| $S^2$ | 0.003059 | 0.013211 | 0.2316 |
| *f* | 0.016353 | 0.013211 | 1.2378 |
| $f^2$ | 0.001420 | 0.013211 | 0.1075 |
| ***d*** | **-0.160208** | **0.013211** | **-12.1268** |
| $d^2$ | **0.067815** | **0.013211** | **5.1332** |
| ***t*** | **-0.062233** | **0.013211** | **-4.7107** |
| $t^2$ | **0.082132** | **0.013211** | **6.2169** |
| *S* × *f* | 0.028986 | 0.016180 | 1.7914 |
| *S* × *d* | -0.002898 | 0.016180 | -0.1791 |
| *S* × *t* | 0.010951 | 0.016180 | 0.6768 |
| ***f* × *d*** | **-0.045780** | **0.016180** | **-2.8294** |
| *f* × *t* | -0.009677 | 0.016180 | -0.5981 |
| *d* × *t* | 0.001921 | 0.016180 | 0.1187 |

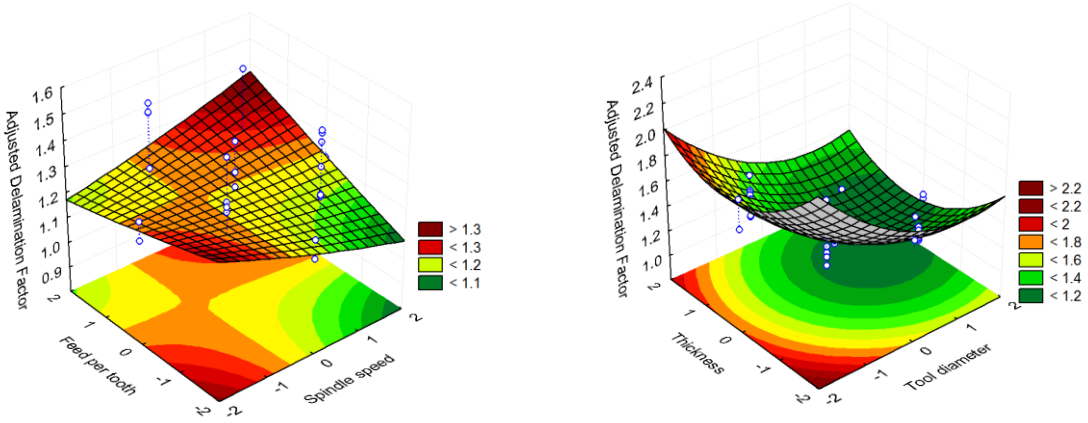


$F_{da}$= *f (S,f); d and t constants at level 0* $F_{da}$= *f (t,d); S and f constants at level 0*

**Figure C.7** Fitted response surface: Adjusted delamination factor model; W-Shape drill

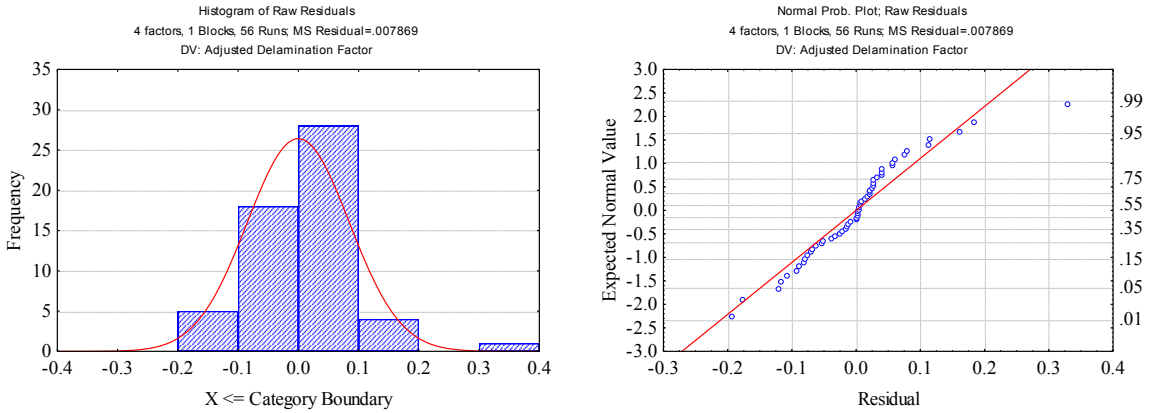


**a)**

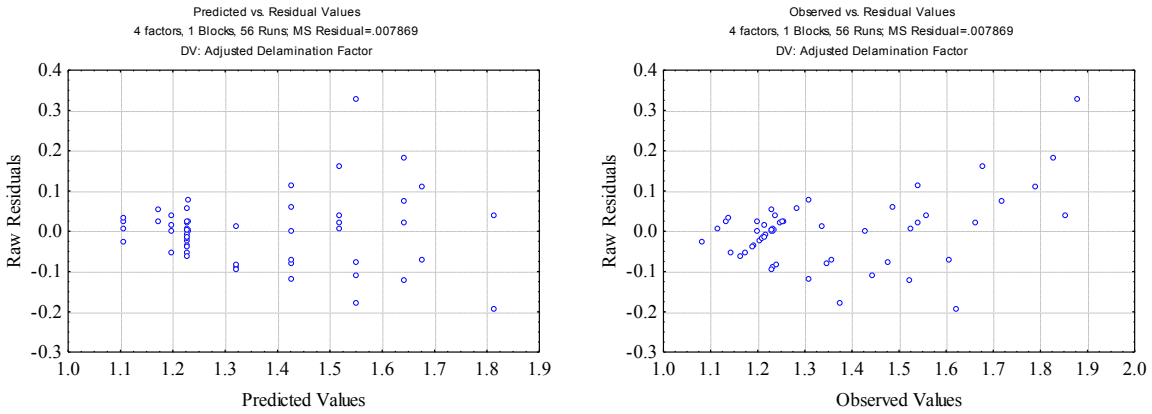


**b)**

**Figure C.8 a)** Residuals normality testing; **b)** Plots of residuals versus corresponding predicted and observed values (Adjusted delamination factor model; W-Shape drill)

## C.2 Straight Flute Drill

**Table C.11** DOE results using Straight flute drill

| Test | Spindle Speed [rpm] | Feed Rate [mm/rev] | Tool Diameter [mm] | Thickness [mm] | Torque [Nm] | Force [N] | $F_d$ | $F_{da}$ |
|---|---|---|---|---|---|---|---|---|
| **SF01** | 12 000 | 0.11 | 7 | 6 | 0.85 | 267.90 | 1.215 | 1.278 |
| **SF02** | 16 000 | 0.065 | 5 | 4 | 0.31 | 181.88 | 1.178 | 1.247 |
| **SF03** | 16 000 | 0.065 | 5 | 8 | 0.60 | 312.40 | 1.135 | 1.205 |
| **SF04** | 16 000 | 0.065 | 9 | 4 | 0.50 | 125.59 | 1.134 | 1.171 |
| **SF05** | 16 000 | 0.065 | 9 | 8 | 1.06 | 298.46 | 1.081 | 1.130 |
| **SF06** | 16 000 | 0.155 | 5 | 4 | 0.41 | 250.53 | 1.186 | 1.240 |
| **SF07** | 16 000 | 0.155 | 5 | 8 | 0.80 | 502.51 | 1.181 | 1.258 |
| **SF08** | 16 000 | 0.155 | 9 | 4 | 0.73 | 190.61 | 1.228 | 1.259 |
| **SF09** | 16 000 | 0.155 | 9 | 8 | 1.55 | 464.88 | 1.106 | 1.158 |
| **SF10** | 12 000 | 0.11 | 7 | 6 | 0.83 | 268.19 | 1.321 | 1.384 |
| **SF11** | 8 000 | 0.065 | 5 | 4 | 0.30 | 185.65 | 1.221 | 1.287 |
| **SF12** | 8 000 | 0.065 | 5 | 8 | 0.58 | 298.34 | 1.176 | 1.254 |
| **SF13** | 8 000 | 0.065 | 9 | 4 | 0.44 | 150.18 | 1.191 | 1.232 |
| **SF14** | 8 000 | 0.065 | 9 | 8 | 1.11 | 313.65 | 1.096 | 1.157 |
| **SF15** | 8 000 | 0.155 | 5 | 4 | 0.52 | 311.26 | 1.216 | 1.284 |
| **SF16** | 8 000 | 0.155 | 5 | 8 | 0.91 | 562.27 | 1.204 | 1.282 |
| **SF17** | 8 000 | 0.155 | 9 | 4 | 0.78 | 257.16 | 1.182 | 1.221 |
| **SF18** | 8 000 | 0.155 | 9 | 8 | 1.72 | 556.72 | 1.085 | 1.132 |
| **SF19** | 12 000 | 0.11 | 7 | 6 | 0.83 | 276.77 | 1.201 | 1.268 |
| **SF20** | 4 000 | 0.11 | 7 | 6 | 0.77 | 304.39 | 1.100 | 1.160 |
| **SF21** | 20 000 | 0.11 | 7 | 6 | 0.90 | 299.74 | 1.075 | 1.116 |
| **SF22** | 12 000 | 0.02 | 7 | 6 | 0.37 | 109.47 | 1.102 | 1.174 |
| **SF23** | 12 000 | 0.2 | 7 | 6 | 1.13 | 403.38 | 1.058 | 1.086 |
| **SF24** | 12 000 | 0.11 | 3 | 6 | 0.11 | 39.27 | 1.488 | 1.626 |
| **SF25** | 12 000 | 0.11 | 11 | 6 | 1.30 | 212.34 | 1.147 | 1.196 |
| **SF26** | 12 000 | 0.11 | 7 | 2 | 0.35 | 154.25 | 1.308 | 1.327 |
| **SF27** | 12 000 | 0.11 | 7 | 10 | 1.31 | 509.34 | 1.192 | 1.279 |
| **SF28** | 12 000 | 0.11 | 7 | 6 | 0.94 | 318.01 | 1.061 | 1.090 |

**Table C.12 -** Empirical Models (Straight flute drill)

| Response | Empirical Model |
|---|---|
| **Torque** | $T = 0.840 + 0.168f_z - 0.026{f_z}^2 + 0.243d - 0.038d^2 + 0.261t - 0.031S \cdot f_z + 0.051f_z \cdot d + 0.046f_z \cdot t + 0.102d \cdot t$ |
| **Thrust Force** | $F = 286.883 - 13.236S + 13.495S^2 + 75.733f_z - 30.571d^2 + 98.606t + 20.926t^2 + 31.080f_z \cdot t$ |
| **Delamination Factor** | $F_d = 1.213 - 0.034S^2 - 0.036{f_z}^2 - 0.045d + 0.024d^2 - 0.029t$ |
| **Adjusted Delamination Factor** | $F_{da} = 1.267 - 0.035S^2 - 0.037{f_z}^2 - 0.061d + 0.033d^2$ |

## C.2.1 Torque Model (Straight Flute Drill)

**Table C.13** Analysis of variance table to test adequacy for the torque model (Straight flute drill)

| ANOVA; Var.: Torque; $R^2$=0. 97847; $\bar{R}^2$:0. 97112<br>4 factors. 1 Blocks. 56 Runs | | | | | |
|---|---|---|---|---|---|
| | **SS** | **df** | **MS** | **F** | **p** |
| *S* | 0.002018 | 1 | 0.002018 | 0.4647 | 0.499291 |
| $S^2$ | 0.003140 | 1 | 0.003140 | 0.7232 | 0.400029 |
| ***f*** | **1.351931** | **1** | **1.351931** | **311.3461** | **0.000000** |
| $f^2$ | **0.042808** | **1** | **0.042808** | **9.8585** | **0.003131** |
| ***d*** | **2.840090** | **1** | **2.840090** | **654.0650** | **0.000000** |
| $d^2$ | **0.082822** | **1** | **0.082822** | **19.0736** | **0.000083** |
| ***t*** | **3.270434** | **1** | **3.270434** | **753.1723** | **0.000000** |
| $t^2$ | 0.005255 | 1 | 0.005255 | 1.2103 | 0.277693 |
| ***S* × *f*** | **0.030901** | **1** | **0.030901** | **7.1164** | **0.010887** |
| *S* × *d* | 0.000093 | 1 | 0.000093 | 0.0215 | 0.884265 |
| *S* × *t* | 0.005202 | 1 | 0.005202 | 1.1980 | 0.280109 |
| ***f* × *d*** | **0.081749** | **1** | **0.081749** | **18.8267** | **0.000091** |
| ***f* × *t*** | **0.068265** | **1** | **0.068265** | **15.7213** | **0.000287** |
| ***d* × *t*** | **0.335421** | **1** | **0.335421** | **77.2467** | **0.000000** |
| *Error* | 0.178031 | 41 | 0.004342 | | |
| *Total SS* | 8.268854 | 55 | | | |

**Table C.14** Regression Coefficients tested by t (Torque model; Straight flute drill)

| Regression Coefficients; Var.:Torque | | | |
|---|---|---|---|
| | | | |
| **Mean/Interc.** | **0.862437** | **0.023298** | **37.01835** |
| *S* | -0.006483 | 0.009511 | -0.68165 |
| $S^2$ | -0.008089 | 0.009511 | -0.85042 |
| ***f*** | **0.167825** | **0.009511** | **17.64500** |
| $f^2$ | **-0.029864** | **0.009511** | **-3.13983** |
| ***d*** | **0.243246** | **0.009511** | **25.57470** |
| $d^2$ | **-0.041539** | **0.009511** | **-4.36733** |
| ***t*** | **0.261025** | **0.009511** | **27.44398** |
| $t^2$ | -0.010464 | 0.009511 | -1.10013 |
| ***S* × *f*** | **-0.031075** | **0.011649** | **-2.66766** |
| *S* × *d* | -0.001706 | 0.011649 | -0.14647 |
| *S* × *t* | -0.012750 | 0.011649 | -1.09453 |
| ***f* × *d*** | **0.050544** | **0.011649** | **4.33897** |
| ***f* × *t*** | **0.046187** | **0.011649** | **3.96501** |
| ***d* × *t*** | **0.102381** | **0.011649** | **8.78901** |

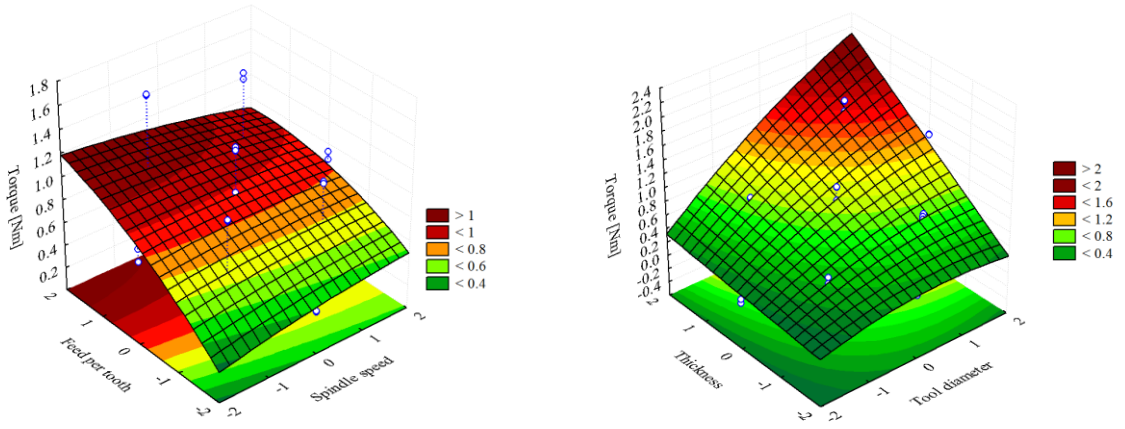


*T= f (S,f); d and t constants at level 0* *T= f (t,d); S and f constants at level 0*

**Figure C.9** Fitted response surface: Torque model; Straight flute drill

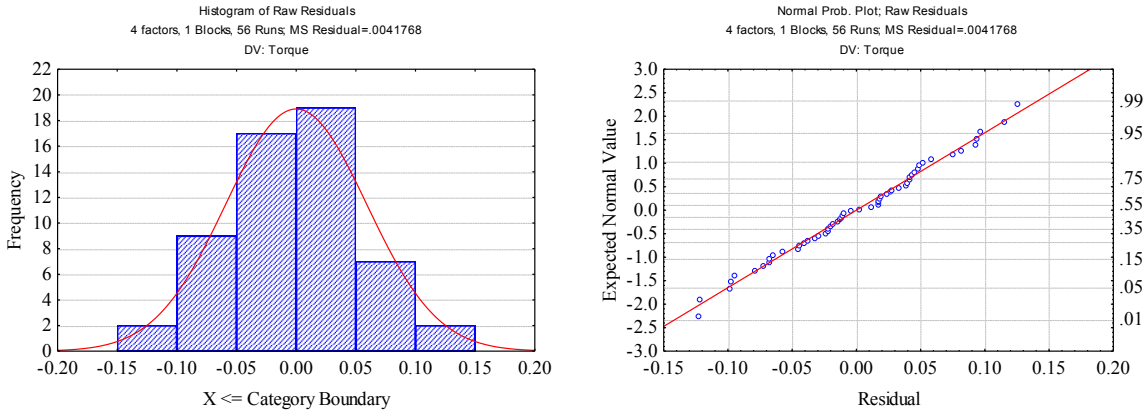


**a)**

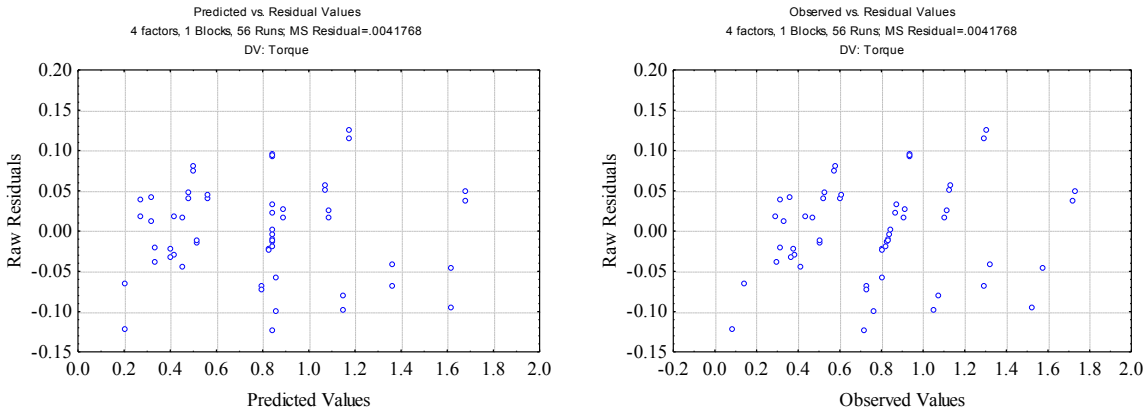


**b)**

**Figure C.10 a)** Residuals normality testing; **b)** Plots of residuals versus corresponding predicted and observed values (Torque model; Straight flute drill)

## C.2.2 Thrust Force Model (Straight Flute Drill)

**Table C.15** Analysis of variance table to test adequacy for the Thrust force model (Straight flute drill)

| ANOVA; Var.: Thrust force; $R^2$=0.91572; $\bar{R}^2$: 0. 88695<br>4 factors. 1 Blocks. 56 Runs | | | | | |
|---|---|---|---|---|---|
| | **SS** | **df** | **MS** | **F** | **p** |
| ***S*** | **8 409.8** | **1** | **8 409.8** | **4.1882** | **0.047153** |
| ***S*²** | **9 664.6** | **1** | **9 664.6** | **4.8132** | **0.033968** |
| ***f*** | **275 306.6** | **1** | **275 306.6** | **137.1088** | **0.000000** |
| *f*² | 370.6 | 1 | 370.6 | 0.1846 | 0.669735 |
| *d* | 808.9 | 1 | 808.9 | 0.4029 | 0.529140 |
| ***d*²** | **42 844.2** | **1** | **42 844.2** | **21.3374** | **0.000038** |
| ***t*** | **466 711.0** | **1** | **466 711.0** | **232.4324** | **0.000000** |
| ***t*²** | **22 436.9** | **1** | **22 436.9** | **11.1741** | **0.001779** |
| *S* × *f* | 7 773.8 | 1 | 7 773.8 | 3.8715 | 0.055901 |
| *S* × *d* | 967.4 | 1 | 967.4 | 0.4818 | 0.491530 |
| *S* × *t* | 1.1 | 1 | 1.1 | 0.0005 | 0.981635 |
| *f* × *d* | 558.1 | 1 | 558.1 | 0.2780 | 0.600886 |
| ***f* × *t*** | **30 911.2** | **1** | **30 911.2** | **15.3945** | **0.000326** |
| *d* × *t* | 3 360.8 | 1 | 3 360.8 | 1.6737 | 0.202998 |
| *Error* | 82 325.6 | 41 | 2 007.9 | | |
| *Total SS* | 976 862.2 | 55 | | | |

**Table C.16** Regression Coefficients tested by t (Thrust force model; Straight flute drill)

| Regression Coefficients; Var.:Thrust force | | | |
|---|---|---|---|
| | **Regression Coefficients** | **Std.Err.** | **t(41)** |
| ***Mean/Interc.*** | **282.7154** | **15.84275** | **17.84509** |
| ***S*** | **-13.2364** | **6.46778** | **-2.04652** |
| ***S*²** | **14.1896** | **6.46778** | **2.19389** |
| ***f*** | **75.7334** | **6.46778** | **11.70935** |
| *f*² | 2.7786 | 6.46778 | 0.42960 |
| *d* | 4.1052 | 6.46778 | 0.63472 |
| ***d*²** | **-29.8762** | **6.46778** | **-4.61924** |
| ***t*** | **98.6060** | **6.46778** | **15.24573** |
| ***t*²** | **21.6203** | **6.46778** | **3.34277** |
| *S* × *f* | -15.5863 | 7.92138 | -1.96763 |
| *S* × *d* | -5.4983 | 7.92138 | -0.69411 |
| *S* × *t* | 0.1835 | 7.92138 | 0.02316 |
| *f* × *d* | -4.1763 | 7.92138 | -0.52721 |
| ***f* × *t*** | **31.0802** | **7.92138** | **3.92358** |
| *d* × *t* | 10.2482 | 7.92138 | 1.29373 |

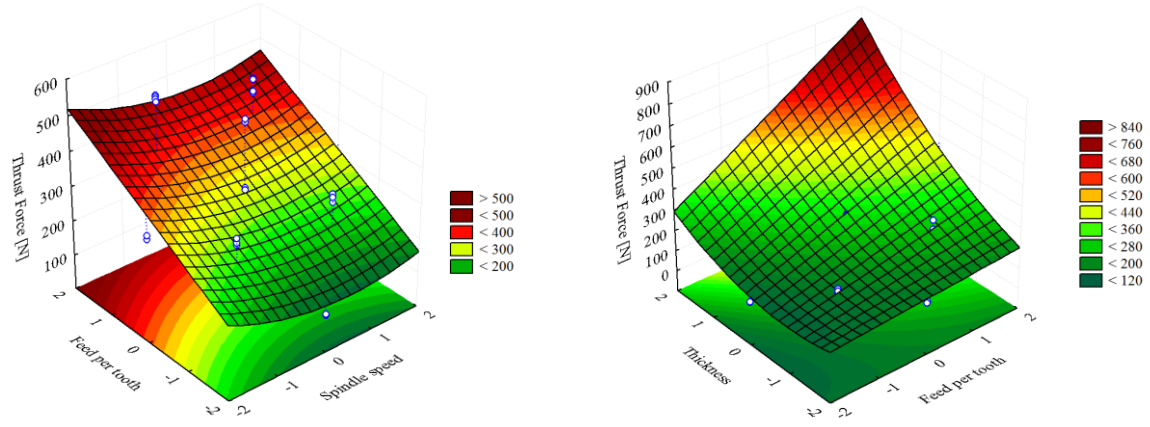


*F= f (S,f); d and t constants at level 0* *F= f (f,t); S and d constants at level 0*

**Figure C.11** Fitted response surface: Thrust force model; Straight flute drill

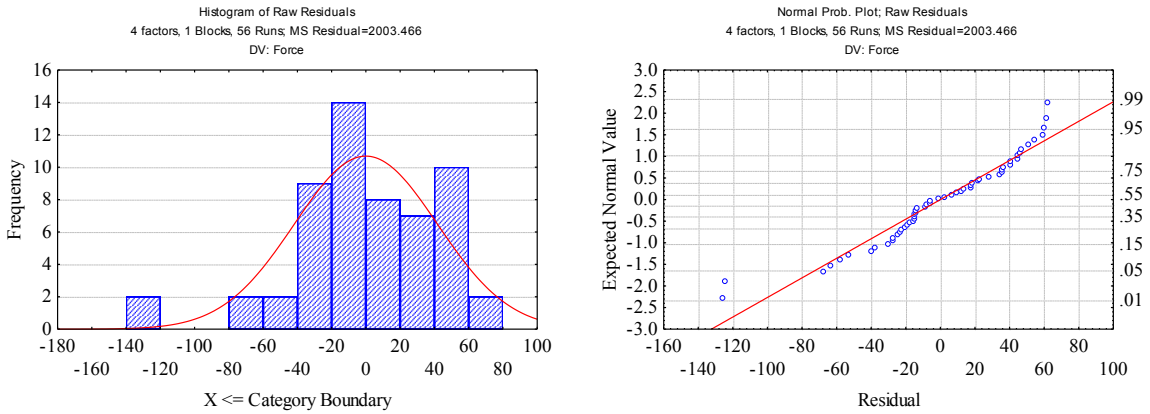


**a)**

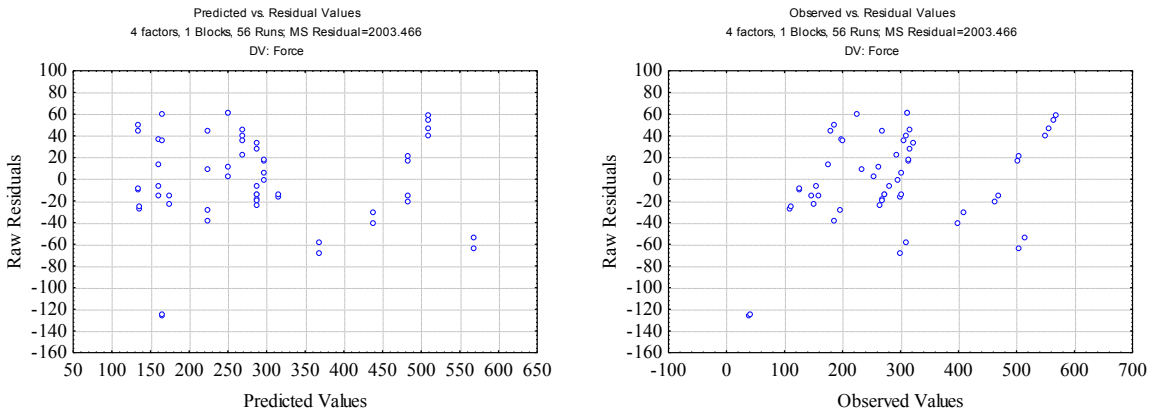


**b)**

**Figure C.12 a)** Residuals normality testing; **b)** Plots of residuals versus corresponding predicted and observed values (Thrust force model; Straight flute drill)

## C.2.3 Delamination Factor Model (Straight Flute Drill)

**Table C.17** Analysis of variance table to test adequacy for the Delamination factor model (Straight flute drill)

| ANOVA; Var.: Delamination factor; $R^2$=0.55678; $\overline{R}^2$: 0.40543<br>4 factors. 1 Blocks. 56 Runs | | | | | |
|---|---|---|---|---|---|
| | **SS** | **df** | **MS** | **F** | **p** |
| *S* | 0.003015 | 1 | 0.003015 | 0.46833 | 0.497608 |
| ***S²*** | **0.047830** | **1** | **0.047830** | **7.42877** | **0.009397** |
| *f* | 0.000649 | 1 | 0.000649 | 0.10085 | 0.752424 |
| ***f²*** | **0.053595** | **1** | **0.053595** | **8.32414** | **0.006211** |
| ***d*** | **0.096391** | **1** | **0.096391** | **14.97097** | **0.000383** |
| ***d²*** | **0.032368** | **1** | **0.032368** | **5.02733** | **0.030422** |
| ***t*** | **0.041430** | **1** | **0.041430** | **6.43469** | **0.015094** |
| $t^2$ | 0.003993 | 1 | 0.003993 | 0.62018 | 0.435511 |
| *S* × *f* | 0.003625 | 1 | 0.003625 | 0.56306 | 0.457315 |
| *S* × *d* | 0.002162 | 1 | 0.002162 | 0.33583 | 0.565415 |
| *S* × *t* | 0.000085 | 1 | 0.000085 | 0.01320 | 0.909083 |
| *f* × *d* | 0.000068 | 1 | 0.000068 | 0.01054 | 0.918730 |
| *f* × *t* | 0.000000 | 1 | 0.000000 | 0.00001 | 0.997709 |
| *d* × *t* | 0.008641 | 1 | 0.008641 | 1.34208 | 0.253370 |
| *Error* | 0.263979 | 41 | 0.006439 | | |
| *Total SS* | 0.595591 | 55 | | | |

**Table C.18** Regression Coefficients tested by t (Delamination factor model; Straight flute drill)

| Regression Coefficients; Var.:Delamination Factor | | | |
|---|---|---|---|
| | **Regression Coefficients** | **Std.Err.** | **t(41)** |
| ***Mean/Interc.*** | **1.199429** | **0.028369** | **42.27922** |
| *S* | -0.007926 | 0.011582 | -0.68434 |
| ***S²*** | **-0.031567** | **0.011582** | **-2.72558** |
| *f* | 0.003678 | 0.011582 | 0.31757 |
| ***f²*** | **-0.033415** | **0.011582** | **-2.88516** |
| ***d*** | **-0.044812** | **0.011582** | **-3.86923** |
| ***d²*** | **0.025968** | **0.011582** | **2.24217** |
| ***t*** | **-0.029379** | **0.011582** | **-2.53667** |
| $t^2$ | 0.009121 | 0.011582 | 0.78751 |
| *S* × *f* | 0.010644 | 0.014185 | 0.75037 |
| *S* × *d* | 0.008220 | 0.014185 | 0.57951 |
| *S* × *t* | 0.001630 | 0.014185 | 0.11490 |
| *f* × *d* | 0.001456 | 0.014185 | 0.10266 |
| *f* × *t* | 0.000041 | 0.014185 | 0.00289 |
| *d* × *t* | -0.016433 | 0.014185 | -1.15848 |

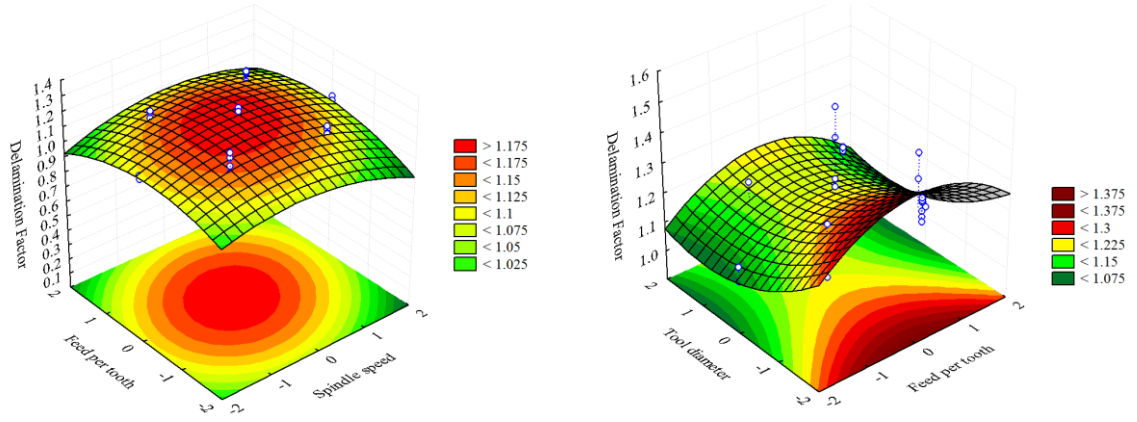


$F_d = f(S,f)$; *d and t constants at level 0* $F_d = f(t,d)$; *S and f constants at level 0*

**Figure C.13** Fitted response surface: Delamination factor model; Straight flute drill

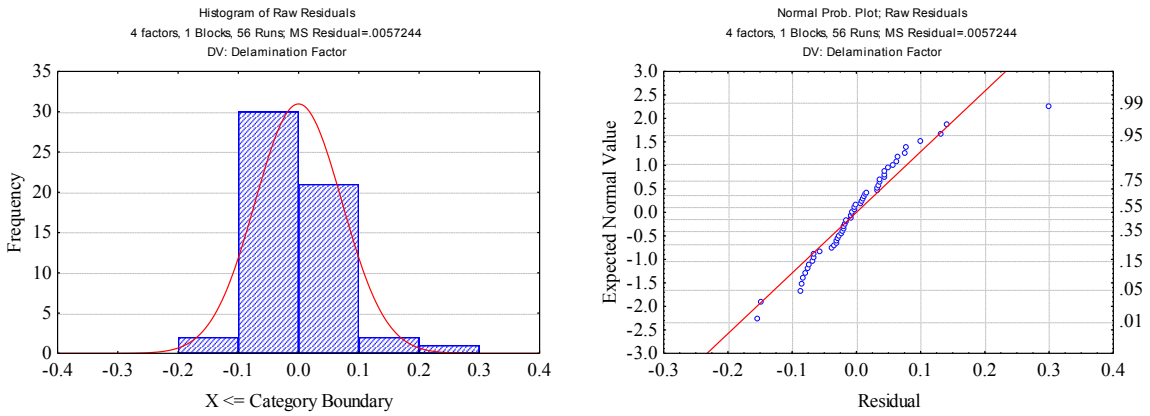


**a)**

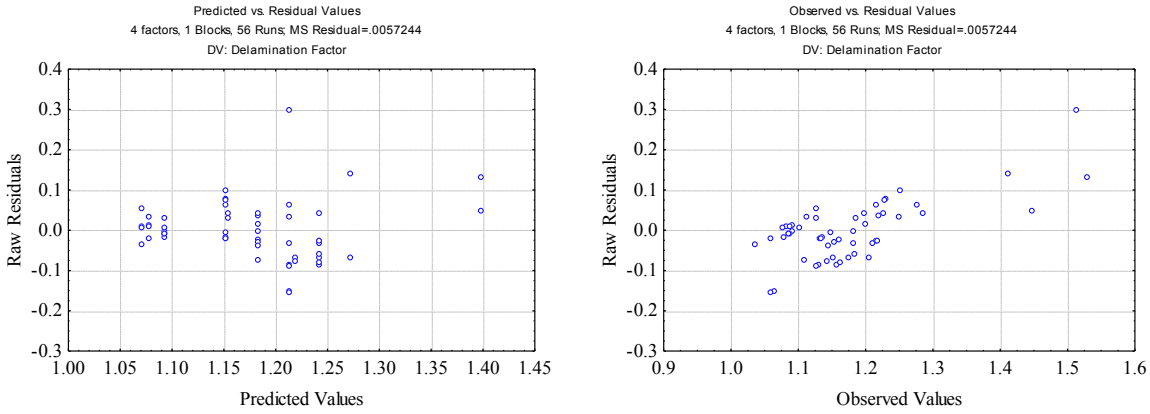


**b)**

**Figure C.14 a)** Residuals normality testing; **b)** Plots of residuals versus corresponding predicted and observed values (Delamination factor model; Straight flute drill)

## C.2.4 Adjusted Delamination Factor Model (Straight Flute Drill)

**Table C.19** Analysis of variance table to test adequacy for the adjusted delamination factor model (Straight flute drill)

| ANOVA; Var.: Adjusted delamination factor; $R^2$=0.56573; $\overline{R}^2$: 0.41744<br>4 factors. 1 Blocks. 56 Runs | | | | | |
|---|---|---|---|---|---|
| | **SS** | **df** | **MS** | **F** | **p** |
| *S* | 0.005918 | 1 | 0.005918 | 0.71656 | 0.402188 |
| ***S²*** | **0.053997** | **1** | **0.053997** | **6.53817** | **0.014356** |
| *f* | 0.000052 | 1 | 0.000052 | 0.00636 | 0.936840 |
| ***f²*** | **0.060467** | **1** | **0.060467** | **7.32162** | **0.009882** |
| ***d*** | **0.176752** | **1** | **0.176752** | **21.40180** | **0.000037** |
| ***d²*** | **0.057769** | **1** | **0.057769** | **6.99492** | **0.011534** |
| *t* | 0.017840 | 1 | 0.017840 | 2.16010 | 0.149268 |
| $t^2$ | 0.002833 | 1 | 0.002833 | 0.34307 | 0.561273 |
| *S* × *f* | 0.003690 | 1 | 0.003690 | 0.44674 | 0.507631 |
| *S* × *d* | 0.002199 | 1 | 0.002199 | 0.26624 | 0.608639 |
| *S* × *t* | 0.000129 | 1 | 0.000129 | 0.01565 | 0.901044 |
| *f* × *d* | 0.000012 | 1 | 0.000012 | 0.00149 | 0.969352 |
| *f* × *t* | 0.000033 | 1 | 0.000033 | 0.00399 | 0.949967 |
| *d* × *t* | 0.007557 | 1 | 0.007557 | 0.91504 | 0.344387 |
| *Error* | 0.338609 | 41 | 0.008259 | | |
| *Total SS* | 0.779717 | 55 | | | |

**Table C.20** Regression Coefficients tested by t (Adjusted delamination factor model; Straight flute drill)

| Regression Coefficients; Var.: Adjusted delamination factor | | | |
|---|---|---|---|
| | **Regression Coefficients** | **Std.Err.** | **t(41)** |
| ***Mean/Interc.*** | **1.255012** | **0.032130** | **39.06030** |
| *S* | -0.011104 | 0.013117 | -0.84650 |
| ***S²*** | **-0.033540** | **0.013117** | **-2.55698** |
| *f* | -0.001046 | 0.013117 | -0.07973 |
| ***f²*** | **-0.035493** | **0.013117** | **-2.70585** |
| ***d*** | **-0.060682** | **0.013117** | **-4.62621** |
| ***d²*** | **0.034692** | **0.013117** | **2.64479** |
| *t* | -0.019279 | 0.013117 | -1.46973 |
| $t^2$ | 0.007683 | 0.013117 | 0.58572 |
| *S* × *f* | 0.010738 | 0.016065 | 0.66839 |
| *S* × *d* | 0.008289 | 0.016065 | 0.51598 |
| *S* × *t* | 0.002010 | 0.016065 | 0.12512 |
| *f* × *d* | 0.000621 | 0.016065 | 0.03866 |
| *f* × *t* | 0.001014 | 0.016065 | 0.06313 |
| *d* × *t* | -0.015367 | 0.016065 | -0.95658 |

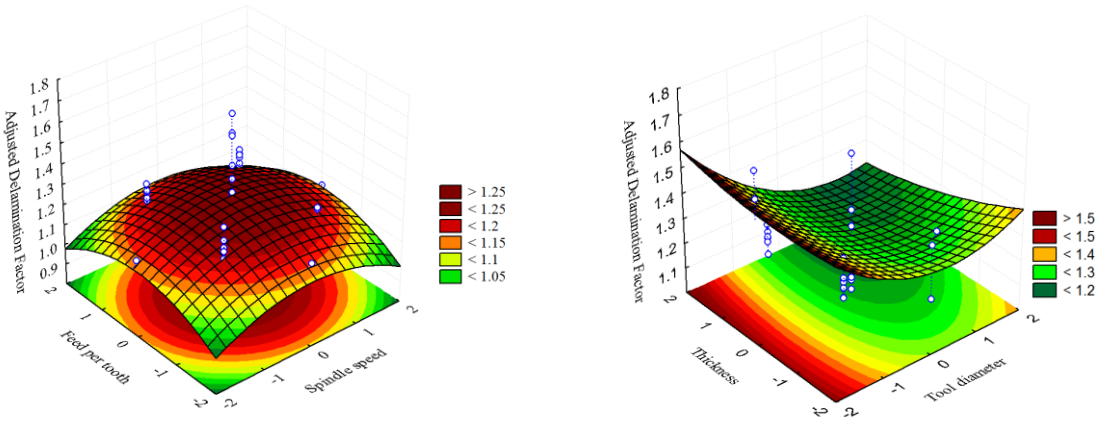


$F_{da} = f(S,f)$; *d and t constants at level 0* $F_{da} = f(t,d)$; *S and f constants at level 0*

**Figure C.15** Fitted response surface: Adjusted delamination factor model; Straight flute drill

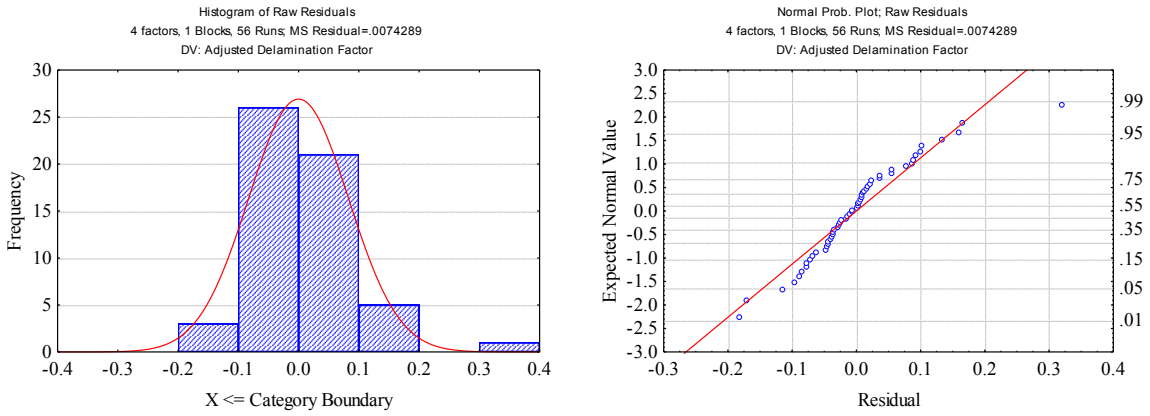


**a)**

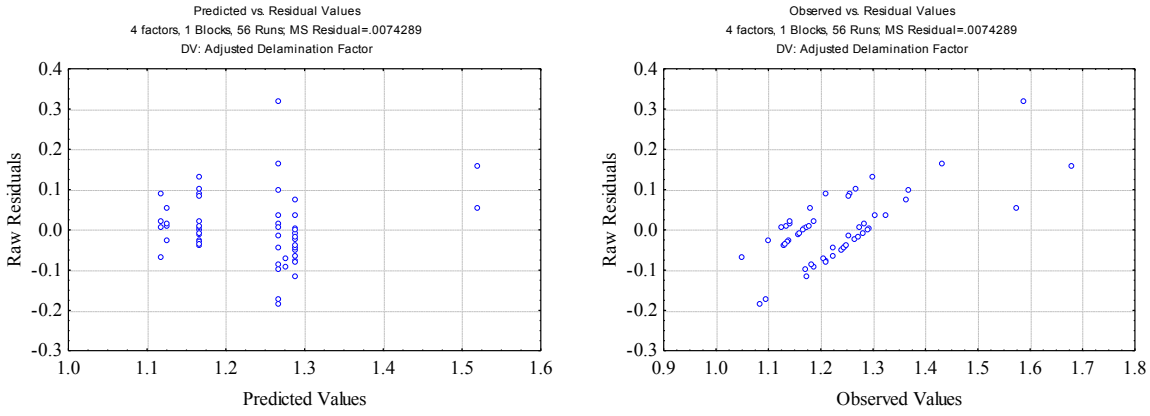


**b)**

**Figure C.16 a)** Residuals normality testing; **b)** Plots of residuals versus corresponding predicted and observed values (Adjusted delamination factor model; Straight flute drill)

## C.3 Twist Drill

**Table C.21** DOE results using Twist drill

| Test | Spindle Speed [rpm] | Feed Rate [mm/rev] | Tool Diameter [mm] | Thickness [mm] | Torque [Nm] | Force [N] | $F_d$ | $F_{da}$ |
|---|---|---|---|---|---|---|---|---|
| **T01** | 12 000 | 0.11 | 7 | 6 | 0.26 | 154.20 | 1.169 | 1.224 |
| **T02** | 16 000 | 0.065 | 5 | 4 | 0.14 | 82.67 | 1.314 | 1.411 |
| **T03** | 16 000 | 0.065 | 5 | 8 | 0.18 | 105.00 | 1.288 | 1.416 |
| **T04** | 16 000 | 0.065 | 9 | 4 | 0.57 | 194.58 | 1.407 | 1.573 |
| **T05** | 16 000 | 0.065 | 9 | 8 | 0.58 | 217.49 | 1.511 | 1.813 |
| **T06** | 16 000 | 0.155 | 5 | 4 | 0.24 | 146.80 | 1.289 | 1.393 |
| **T07** | 16 000 | 0.155 | 5 | 8 | 0.27 | 166.98 | 1.264 | 1.609 |
| **T08** | 16 000 | 0.155 | 9 | 4 | 0.34 | 169.46 | 1.329 | 1.472 |
| **T09** | 16 000 | 0.155 | 9 | 8 | 0.53 | 182.85 | 1.260 | 1.402 |
| **T10** | 12 000 | 0.11 | 7 | 6 | 0.30 | 157.82 | 1.239 | 1.295 |
| **T11** | 8 000 | 0.065 | 5 | 4 | 0.15 | 90.40 | 1.348 | 1.450 |
| **T12** | 8 000 | 0.065 | 5 | 8 | 0.23 | 109.22 | 1.376 | 1.487 |
| **T13** | 8 000 | 0.065 | 9 | 4 | 0.27 | 119.77 | 1.211 | 1.288 |
| **T14** | 8 000 | 0.065 | 9 | 8 | 0.46 | 201.26 | 1.224 | 1.348 |
| **T15** | 8 000 | 0.155 | 5 | 4 | 0.24 | 144.11 | 1.456 | 1.579 |
| **T16** | 8 000 | 0.155 | 5 | 8 | 0.35 | 175.34 | 1.418 | 1.772 |
| **T17** | 8 000 | 0.155 | 9 | 4 | 0.51 | 263.23 | 1.239 | 1.310 |
| **T18** | 8 000 | 0.155 | 9 | 8 | 0.74 | 314.96 | 1.260 | 1.391 |
| **T19** | 12 000 | 0.11 | 7 | 6 | 0.32 | 162.73 | 1.217 | 1.277 |
| **T20** | 4 000 | 0.11 | 7 | 6 | 0.32 | 169.46 | 1.218 | 1.271 |
| **T21** | 20 000 | 0.11 | 7 | 6 | 0.25 | 132.07 | 1.217 | 1.296 |
| **T22** | 12 000 | 0.02 | 7 | 6 | 0.08 | 66.80 | 1.254 | 1.319 |
| **T23** | 12 000 | 0.2 | 7 | 6 | 0.40 | 234.38 | 1.171 | 1.228 |
| **T24** | 12 000 | 0.11 | 3 | 6 | 0.07 | 102.52 | 1.517 | 1.678 |
| **T25** | 12 000 | 0.11 | 11 | 6 | 0.91 | 399.27 | 1.292 | 1.382 |
| **T26** | 12 000 | 0.11 | 7 | 2 | 0.19 | 117.10 | 1.560 | 1.810 |
| **T27** | 12 000 | 0.11 | 7 | 10 | 0.32 | 199.22 | 1.238 | 1.321 |
| **T28** | 12 000 | 0.11 | 7 | 6 | 0.29 | 184.80 | 1.120 | 1.159 |

**Table C.22** Empirical Models (Twist drill)

| Response | Empirical Model |
|---|---|
| **Torque** | $T = 0.293 + 0.053f_z + 0.162d + 0.056d^2 + 0.047t - 0.051S \cdot f_z$ |
| **Thrust Force** | $F = 164.888 - 9.468S + 32.437f_z + 51.524d + 19.862d^2 + 17.764t - 19.415S \cdot f_z$ |
| **Delamination Factor** | $F_d = 1.227 - 0.061d + 0.058d^2 + 0.056t^2 - 0.056S \cdot f_z + 0.045S \cdot d$ |
| **Adjusted Delamination Factor** | $F_{da} = 1.298 - 0.059d + 0.078d^2 + 0.086t^2 - 0.070S \cdot f_z + 0.067S \cdot d$ |

## C.3.1 Torque Model (Twist Drill)

**Table C.23** Analysis of variance table to test adequacy for the torque model (Twist drill)

| ANOVA; Var.: Torque; $R^2$=0.88528; $\overline{R}^2$:0.84611<br>4 factors. 1 Blocks. 56 Runs | | | | | |
|---|---|---|---|---|---|
| | **SS** | **df** | **MS** | **F** | **p** |
| *S* | 0.004961 | 1 | 0.004961 | 0.8706 | 0.356263 |
| $S^2$ | 0.001338 | 1 | 0.001338 | 0.2348 | 0.630548 |
| ***f*** | **0.134006** | **1** | **0.134006** | **23.5140** | **0.000018** |
| $f^2$ | 0.001820 | 1 | 0.001820 | 0.3193 | 0.575098 |
| ***d*** | **1.257057** | **1** | **1.257057** | **220.5745** | **0.000000** |
| $d^2$ | **0.148113** | **1** | **0.148113** | **25.9892** | **0.000008** |
| ***t*** | **0.107239** | **1** | **0.107239** | **18.8171** | **0.000091** |
| $t^2$ | 0.000134 | 1 | 0.000134 | 0.0235 | 0.878958 |
| ***S × f*** | **0.084153** | **1** | **0.084153** | **14.7662** | **0.000415** |
| *S × d* | 0.003168 | 1 | 0.003168 | 0.5559 | 0.460170 |
| *S × t* | 0.012800 | 1 | 0.012800 | 2.2460 | 0.141621 |
| *f × d* | 0.003188 | 1 | 0.003188 | 0.5594 | 0.458772 |
| *f × t* | 0.006827 | 1 | 0.006827 | 1.1979 | 0.280126 |
| *d × t* | 0.013613 | 1 | 0.013613 | 2.3886 | 0.129910 |
| *Error* | 0.233659 | 41 | 0.005699 | | |
| *Total SS* | 2.036859 | 55 | | | |

**Table C.24** Regression Coefficients tested by t (Torque model; Twist drill)

| Regression Coefficients; Var.:Torque | | | |
|---|---|---|---|
| | **Regression Coefficients** | **Std.Err.** | **t(41)** |
| ***Mean/Interc.*** | **0.293400** | **0.026690** | **10.99272** |
| *S* | -0.010167 | 0.010896 | -0.93304 |
| $S^2$ | 0.005280 | 0.010896 | 0.48459 |
| ***f*** | **0.052837** | **0.010896** | **4.84912** |
| $f^2$ | -0.006157 | 0.010896 | -0.56508 |
| ***d*** | **0.161829** | **0.010896** | **14.85175** |
| $d^2$ | **0.055549** | **0.010896** | **5.09796** |
| ***t*** | **0.047267** | **0.010896** | **4.33786** |
| $t^2$ | -0.001670 | 0.010896 | -0.15324 |
| ***S × f*** | **-0.051281** | **0.013345** | **-3.84268** |
| *S × d* | 0.009950 | 0.013345 | 0.74559 |
| *S × t* | -0.020000 | 0.013345 | -1.49867 |
| *f × d* | -0.009981 | 0.013345 | -0.74793 |
| *f × t* | 0.014606 | 0.013345 | 1.09450 |
| *d × t* | 0.020625 | 0.013345 | 1.54550 |

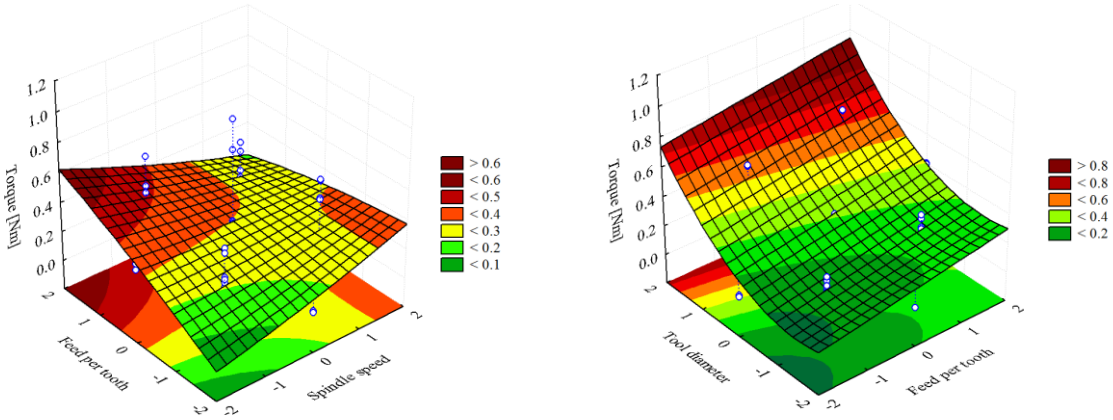


*T= f (S,f); d and t constants at level 0* *T= f (t,f); S and d constants at level 0*

**Figure C.17** Fitted response surface: Torque model; Twist drill

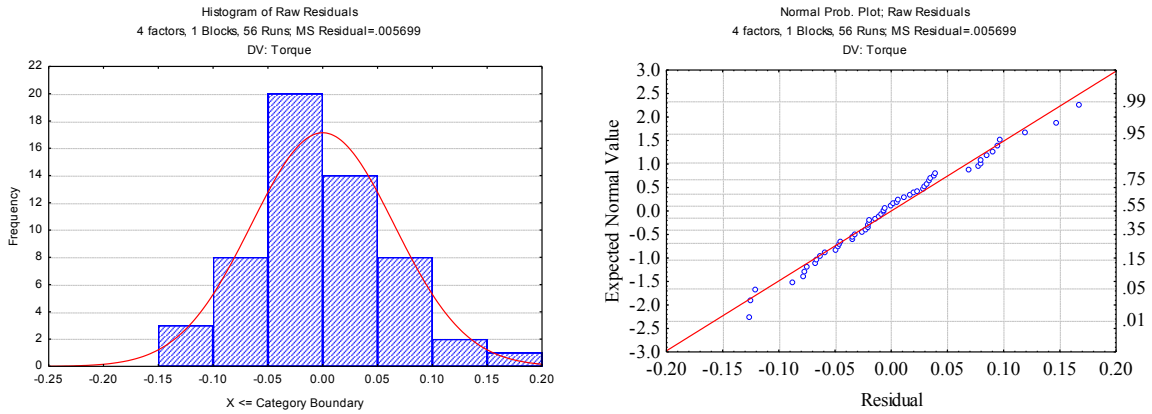


**a)**

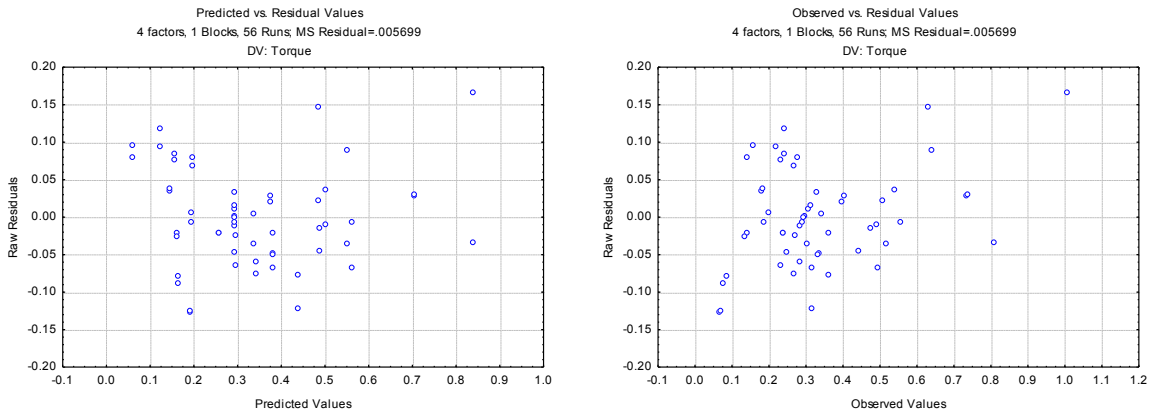


**b)**

**Figure C.18 a)** Residuals normality testing; **b)** Plots of residuals versus corresponding predicted and observed values (Torque model; Twist drill)

## C.3.2 Thrust Force Model (Twist Drill)

**Table C.25** Analysis of variance table to test adequacy for the Thrust force model (Twist drill)

| ANOVA; Var.: Thrust force; $R^2$=0.83491; $\bar{R}^2$: 0.77853<br>4 factors. 1 Blocks. 56 Runs | | | | | |
|---|---|---|---|---|---|
| | **SS** | **df** | **MS** | **F** | **p** |
| ***S*** | **4 303.2** | **1** | **4 303.2** | **4.3844** | **0.042495** |
| $S^2$ | 1 283.4 | 1 | 1 283.4 | 1.3076 | 0.259460 |
| ***f*** | **50 503.6** | **1** | **50 503.6** | **51.4569** | **0.000000** |
| $f^2$ | 1 306.1 | 1 | 1 306.1 | 1.3307 | 0.255356 |
| ***d*** | **127 426.7** | **1** | **127 426.7** | **129.8321** | **0.000000** |
| $d^2$ | **18 935.1** | **1** | **18 935.1** | **19.2925** | **0.000077** |
| ***t*** | **15 146.2** | **1** | **15 146.2** | **15.4322** | **0.000321** |
| $t^2$ | 529.8 | 1 | 529.8 | 0.5398 | 0.466690 |
| ***S*** × ***f*** | **12 062.3** | **1** | **12 062.3** | **12.2900** | **0.001118** |
| *S* × *d* | 1 717.0 | 1 | 1 717.0 | 1.7494 | 0.193281 |
| *S* × *t* | 1 364.5 | 1 | 1 364.5 | 1.3902 | 0.245166 |
| *f* × *d* | 294.5 | 1 | 294.5 | 0.3001 | 0.586811 |
| *f* × *t* | 105.1 | 1 | 105.1 | 0.1071 | 0.745185 |
| *d* × *t* | 740.5 | 1 | 740.5 | 0.7545 | 0.390109 |
| *Error* | 40 240.4 | 41 | 981.5 | | |
| *Total SS* | 282 963.6 | 55 | | | |

**Table C.26** Regression Coefficients tested by t (Thrust force model; Twist drill)

| Regression Coefficients; Var.:Thrust force | | | |
|---|---|---|---|
| | **Regression Coefficients** | **Std.Err.** | **t(41)** |
| ***Mean/Interc.*** | **164.8878** | **11.07629** | **14.88656** |
| ***S*** | **-9.4683** | **4.52187** | **-2.09389** |
| $S^2$ | -5.1708 | 4.52187 | -1.14351 |
| ***f*** | **32.4370** | **4.52187** | **7.17335** |
| $f^2$ | -5.2163 | 4.52187 | -1.15357 |
| ***d*** | **51.5240** | **4.52187** | **11.39439** |
| $d^2$ | **19.8615** | **4.52187** | **4.39232** |
| ***t*** | **17.7636** | **4.52187** | **3.92838** |
| $t^2$ | -3.3223 | 4.52187 | -0.73472 |
| ***S*** × ***f*** | **-19.4151** | **5.53814** | **-3.50571** |
| *S* × *d* | -7.3250 | 5.53814 | -1.32265 |
| *S* × *t* | -6.5299 | 5.53814 | -1.17907 |
| *f* × *d* | -3.0337 | 5.53814 | -0.54778 |
| *f* × *t* | -1.8121 | 5.53814 | -0.32720 |
| *d* × *t* | 4.8106 | 5.53814 | 0.86862 |

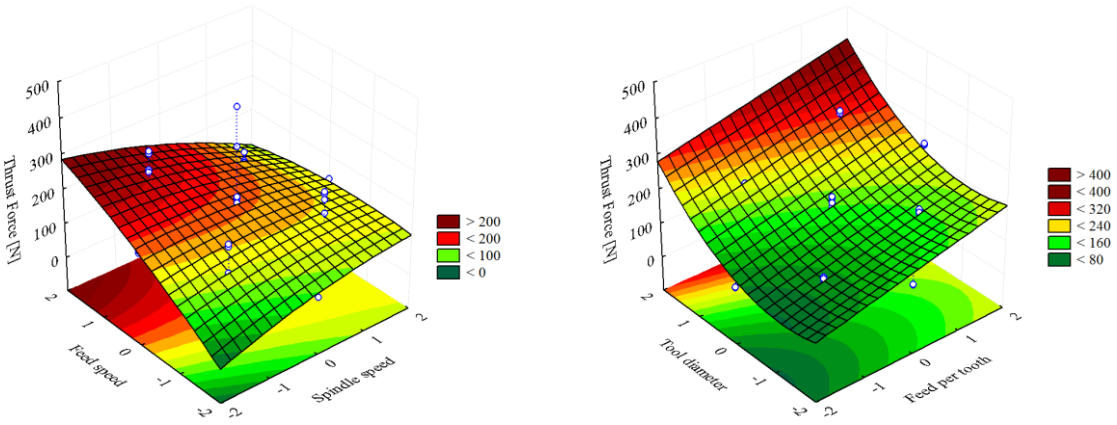


*F= f (S,f); d and t constants at level 0* *F= f (f,d); S and t constants at level 0*

**Figure C.19** Fitted response surface: Thrust force model; Twist drill

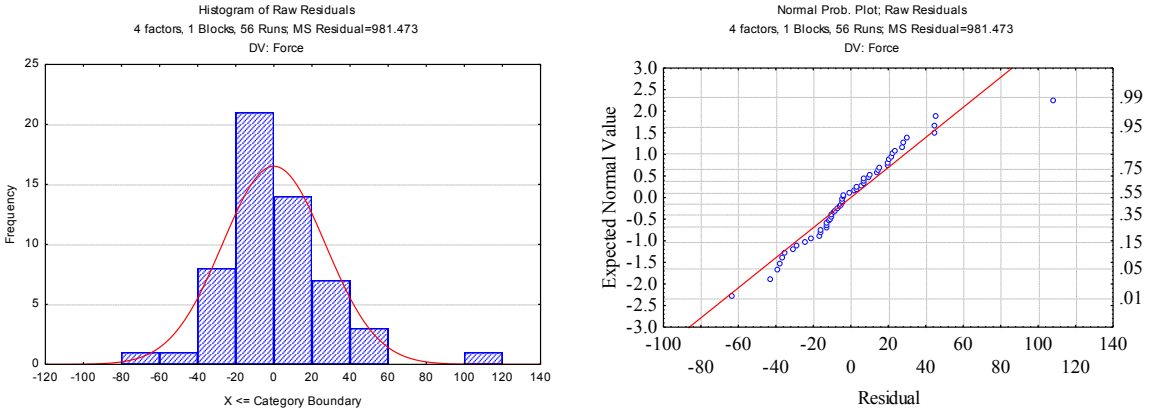


**a)**

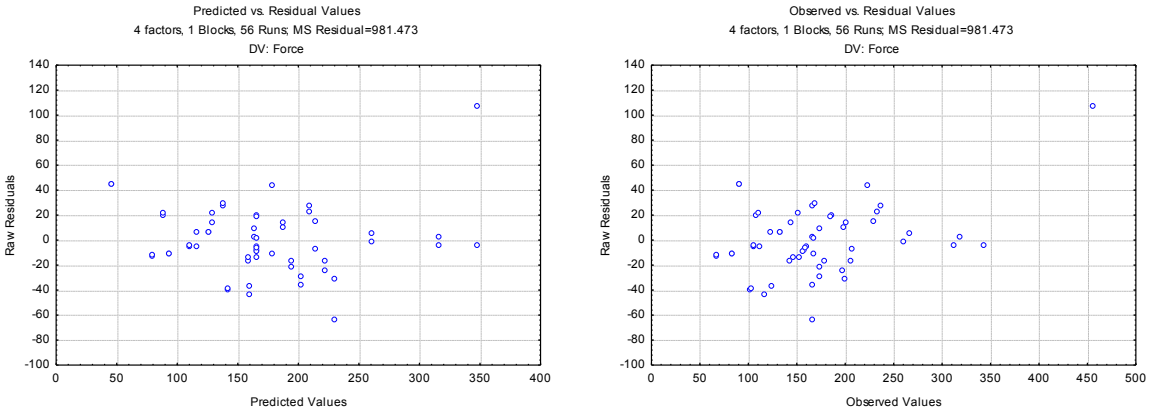


**b)**

**Figure C.20 a)** Residuals normality testing; **b)** Plots of residuals versus corresponding predicted and observed values (Thrust force model; Twist drill)

## C.3.3 Delamination Factor Model (Twist Drill)

**Table C.27** Analysis of variance table to test adequacy for the Delamination factor model (Twist drill)

| ANOVA; Var.: Delamination factor; $R^2$=0.58315; $\overline{R}^2$: 0.44081<br>4 factors. 1 Blocks. 56 Runs | | | | | |
|---|---|---|---|---|---|
| | **SS** | **df** | **MS** | **F** | **p** |
| *S* | 0.015225 | 1 | 0.015225 | 1.15059 | 0.289698 |
| $S^2$ | 0.015230 | 1 | 0.015230 | 1.15096 | 0.289623 |
| *f* | 0.004403 | 1 | 0.004403 | 0.33277 | 0.567187 |
| $f^2$ | 0.013082 | 1 | 0.013082 | 0.98866 | 0.325902 |
| ***d*** | **0.177345** | **1** | **0.177345** | **13.40248** | **0.000711** |
| $d^2$ | **0.199898** | **1** | **0.199898** | **15.10690** | **0.000364** |
| *t* | 0.000320 | 1 | 0.000320 | 0.02415 | 0.877266 |
| $t^2$ | **0.191269** | **1** | **0.191269** | **14.45475** | **0.000469** |
| ***S* × *f*** | **0.099505** | **1** | **0.099505** | **7.51988** | **0.009004** |
| ***S* × *d*** | **0.064303** | **1** | **0.064303** | **4.85956** | **0.033163** |
| *S* × *t* | 0.008301 | 1 | 0.008301 | 0.62734 | 0.432891 |
| *f* × *d* | 0.027286 | 1 | 0.027286 | 2.06206 | 0.158592 |
| *f* × *t* | 0.002086 | 1 | 0.002086 | 0.15766 | 0.693378 |
| *d* × *t* | 0.040754 | 1 | 0.040754 | 3.07986 | 0.086738 |
| *Error* | 0.542523 | 41 | 0.013232 | | |
| *Total SS* | 1.301471 | 55 | | | |

**Table C.28** Regression Coefficients tested by t (Delamination factor model; Twist drill)

| Regression Coefficients; Var.:Delamination Factor | | | |
|---|---|---|---|
| | **Regression Coefficients** | **Std.Err.** | **t(41)** |
| ***Mean/Interc.*** | **1.186286** | **0.040670** | **29.16871** |
| *S* | 0.017810 | 0.016603 | 1.07266 |
| $S^2$ | 0.017813 | 0.016603 | 1.07283 |
| *f* | -0.009578 | 0.016603 | -0.57686 |
| $f^2$ | 0.016509 | 0.016603 | 0.99431 |
| ***d*** | **-0.060784** | **0.016603** | **-3.66094** |
| $d^2$ | **0.064533** | **0.016603** | **3.88676** |
| *t* | 0.002580 | 0.016603 | 0.15540 |
| $t^2$ | **0.063125** | **0.016603** | **3.80194** |
| ***S* × *f*** | **-0.055763** | **0.020335** | **-2.74224** |
| ***S* × *d*** | **0.044827** | **0.020335** | **2.20444** |
| *S* × *t* | 0.016106 | 0.020335 | 0.79205 |
| *f* × *d* | -0.029201 | 0.020335 | -1.43599 |
| *f* × *t* | -0.008074 | 0.020335 | -0.39707 |
| *d* × *t* | -0.035687 | 0.020335 | -1.75495 |

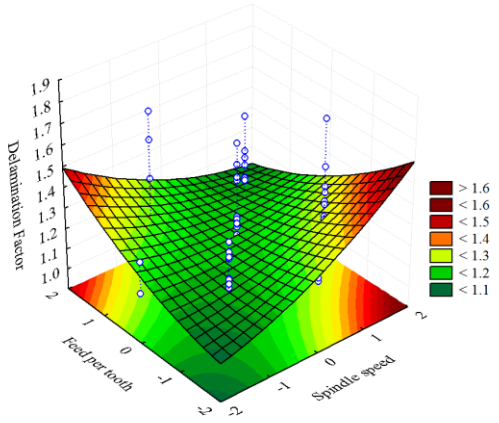


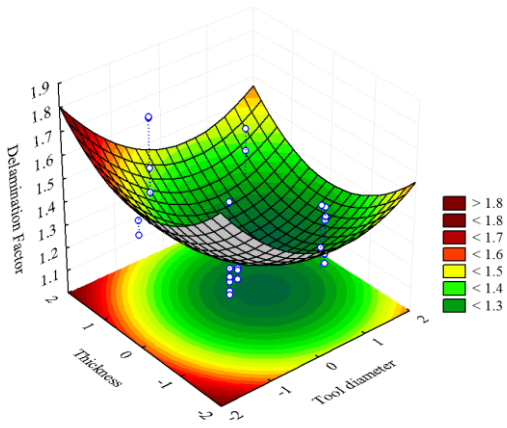


$F_d = f(S,f)$; *d and t constants at level 0* $F_d = f(t,d)$; *S and f constants at level 0*

**Figure C.21** Fitted response surface: Delamination factor model; Twist drill

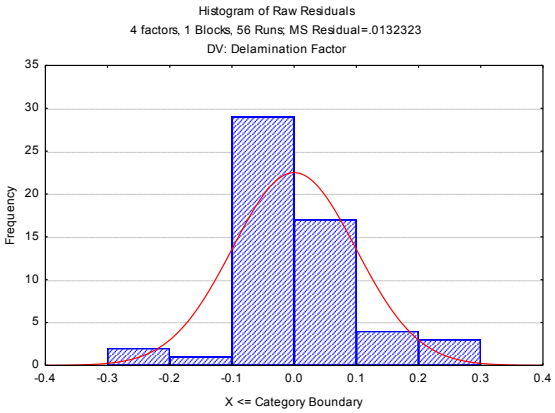


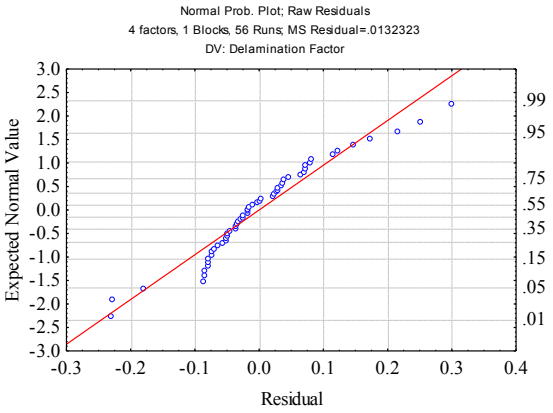


**a)**

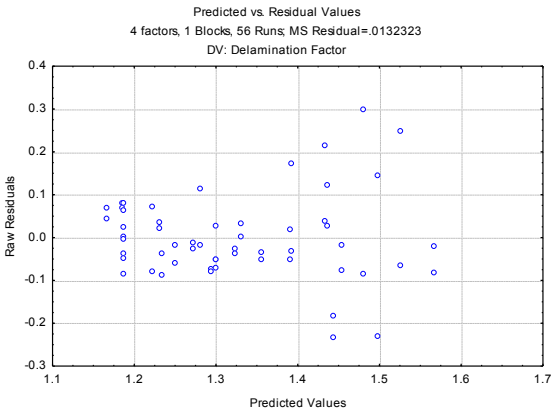


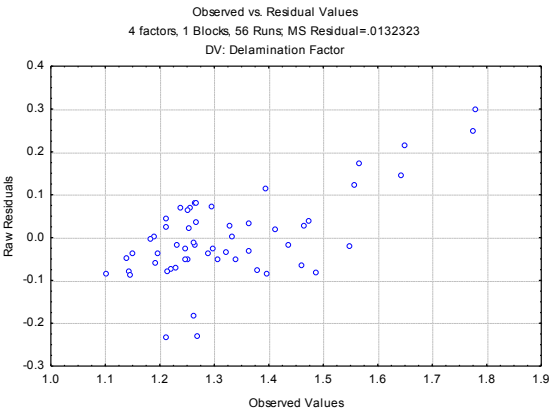


**b)**

**Figure C.22 a)** Residuals normality testing; **b)** Plots of residuals versus corresponding predicted and observed values (Delamination factor model; Twist drill)

## C.3.4 Adjusted Delamination Factor Model (Twist Drill)

**Table C.29** Analysis of variance table to test adequacy for the adjusted delamination factor model (Twist drill)

| ANOVA; Var.: Adjusted delamination factor; $R^2$=0. 58413; $\bar{R}^2$: 0. 44213<br>4 factors. 1 Blocks. 56 Runs | | | | | |
|---|---|---|---|---|---|
| | **SS** | **df** | **MS** | **F** | **p** |
| *S* | 0.056958 | 1 | 0.056958 | 2.49396 | 0.121969 |
| $S^2$ | 0.032217 | 1 | 0.032217 | 1.41064 | 0.241785 |
| *f* | 0.010228 | 1 | 0.010228 | 0.44786 | 0.507105 |
| $f^2$ | 0.026522 | 1 | 0.026522 | 1.16127 | 0.287503 |
| ***d*** | **0.169046** | **1** | **0.169046** | **7.40179** | **0.009517** |
| $d^2$ | **0.368037** | **1** | **0.368037** | **16.11480** | **0.000248** |
| *t* | 0.000749 | 1 | 0.000749 | 0.03278 | 0.857225 |
| $t^2$ | **0.445595** | **1** | **0.445595** | **19.51073** | **0.000071** |
| ***S* × *f*** | **0.158107** | **1** | **0.158107** | **6.92286** | **0.011936** |
| ***S* × *d*** | **0.143576** | **1** | **0.143576** | **6.28660** | **0.016221** |
| *S* × *t* | 0.013725 | 1 | 0.013725 | 0.60097 | 0.442657 |
| *f* × *d* | 0.065390 | 1 | 0.065390 | 2.86315 | 0.098218 |
| *f* × *t* | 0.006778 | 1 | 0.006778 | 0.29677 | 0.588865 |
| *d* × *t* | 0.025289 | 1 | 0.025289 | 1.10730 | 0.298832 |
| *Error* | 0.936377 | 41 | 0.022838 | | |
| *Total SS* | 2.251636 | 55 | | | |

**Table C.30** Regression Coefficients tested by t (Adjusted delamination factor model; Twist drill)

| Regression Coefficients; Var.: Adjusted delamination factor | | | |
|---|---|---|---|
| | **Regression Coefficients** | **Std.Err.** | **t(41)** |
| ***Mean/Interc.*** | **1.238737** | **0.053430** | **23.18411** |
| *S* | 0.034447 | 0.021813 | 1.57923 |
| $S^2$ | 0.025907 | 0.021813 | 1.18770 |
| *f* | -0.014598 | 0.021813 | -0.66922 |
| $f^2$ | 0.023506 | 0.021813 | 1.07762 |
| ***d*** | **-0.059345** | **0.021813** | **-2.72062** |
| $d^2$ | **0.087564** | **0.021813** | **4.01432** |
| *t* | 0.003949 | 0.021813 | 0.18104 |
| $t^2$ | **0.096350** | **0.021813** | **4.41710** |
| ***S* × *f*** | **-0.070291** | **0.026715** | **-2.63113** |
| ***S* × *d*** | **0.066983** | **0.026715** | **2.50731** |
| *S* × *t* | 0.020710 | 0.026715 | 0.77522 |
| *f* × *d* | -0.045204 | 0.026715 | -1.69208 |
| *f* × *t* | -0.014554 | 0.026715 | -0.54477 |
| *d* × *t* | -0.028112 | 0.026715 | -1.05228 |

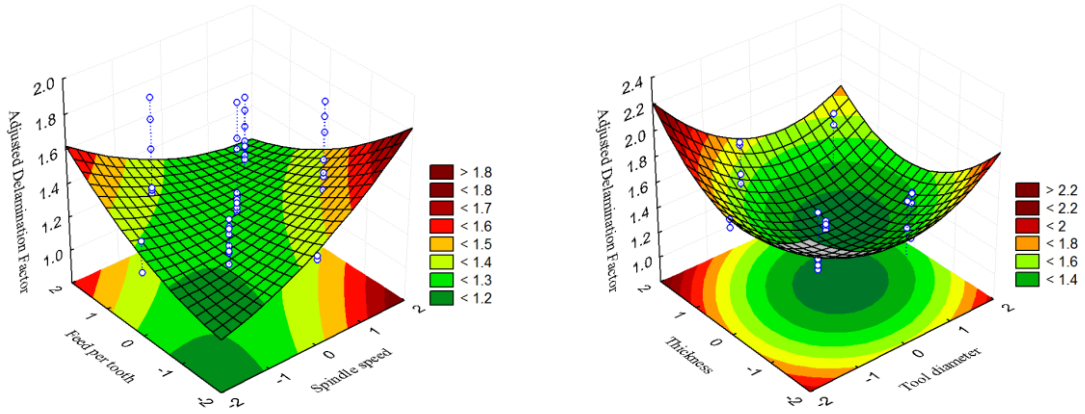


$F_{da} = f(S,f)$; *d and t constants at level 0* $F_{da} = f(t,d)$; *S and f constants at level 0*

**Figure C.23** Fitted response surface: Adjusted delamination factor model; Twist drill

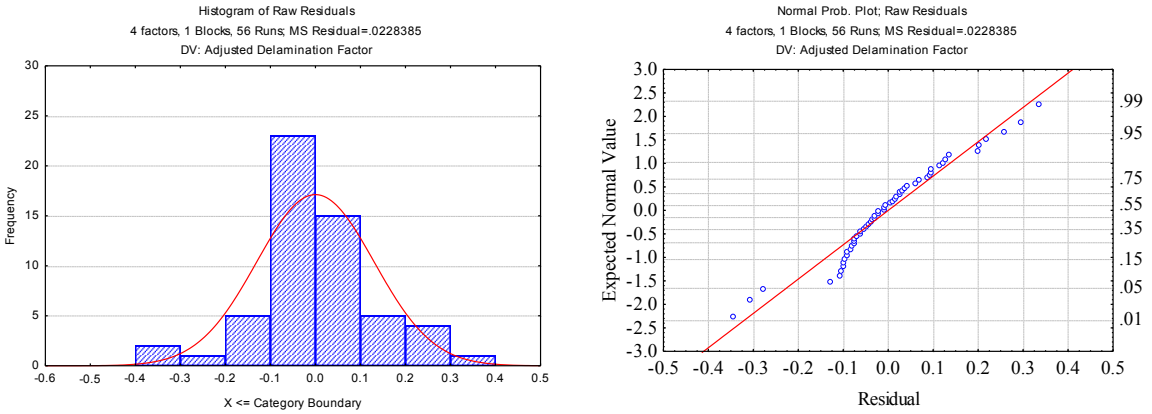


**a)**

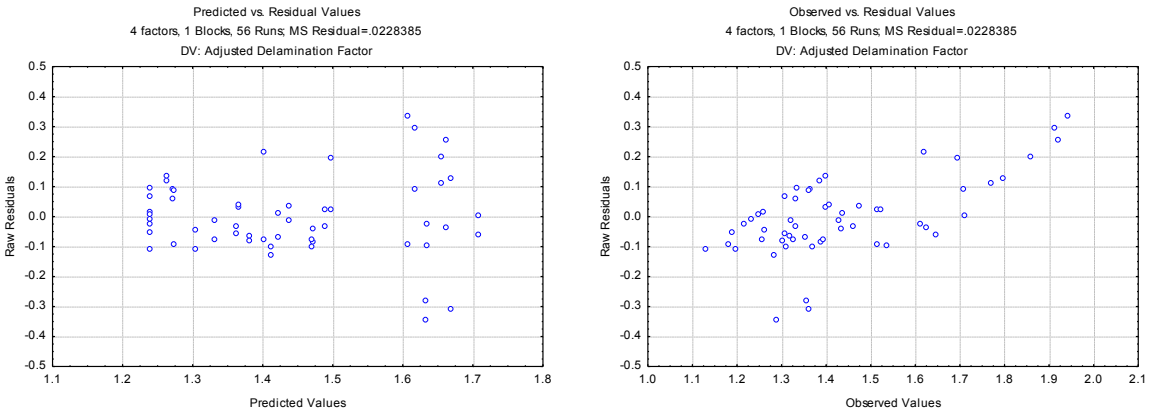


**b)**

**Figure C.24 a)** Residuals normality testing; **b)** Plots of residuals versus corresponding predicted and observed values (Adjusted delamination factor model; Twist drill)

# Appendix D

## Results from the Validation Tests

**Table D.1** Validation tests results for Thrust force

| Test | $S$ [rpm] | $f_z$ [mm/tooth] | $d$ [mm] | $t$ [mm] | Thrust Force [N] | | |
|---|---|---|---|---|---|---|---|
| | | | | | Straight flute drill | W-shape drill | Twist drill |
| **V01** | 12 000 | 0.0325 | 5 | 4 | 167 | 68 | 84 |
| **V02** | 12 000 | 0.0325 | 5 | 8 | 242 | 80 | 107 |
| **V03** | 12 000 | 0.0325 | 9 | 4 | 136 | 86 | 166 |
| **V04** | 12 000 | 0.0325 | 9 | 8 | 269 | 144 | 195 |
| **V05** | 18 000 | 0.0325 | 5 | 4 | 168 | 69 | 84 |
| **V06** | 18 000 | 0.0325 | 5 | 8 | 270 | 83 | 128 |
| **V07** | 18 000 | 0.0325 | 9 | 4 | 127 | 107 | 190 |
| **V08** | 18 000 | 0.0325 | 9 | 8 | 289 | 160 | 222 |
| **V09** | 12 000 | 0.0775 | 5 | 4 | 288 | 120 | 167 |
| **V10** | 12 000 | 0.0775 | 5 | 8 | 543 | 115 | 177 |
| **V11** | 12 000 | 0.0775 | 9 | 4 | 252 | 171 | 291 |
| **V12** | 12 000 | 0.0775 | 9 | 8 | 517 | 210 | 302 |
| **V13** | 18 000 | 0.0775 | 5 | 4 | 220 | 113 | 116 |
| **V14** | 18 000 | 0.0775 | 5 | 8 | 419 | 120 | 157 |
| **V15** | 18 000 | 0.0775 | 9 | 4 | 190 | 168 | 217 |
| **V16** | 18 000 | 0.0775 | 9 | 8 | 420 | 217 | 284 |
| **V17** | 8 000 | 0.055 | 5 | 4 | 238 | 100 | 142 |
| **V18** | 8 000 | 0.055 | 5 | 8 | 395 | 103 | 150 |
| **V19** | 8 000 | 0.055 | 9 | 4 | 215 | 149 | 241 |
| **V20** | 8 000 | 0.055 | 9 | 8 | 398 | 195 | 231 |
| **V21** | 8 000 | 0.08875 | 5 | 4 | 343 | 130 | 183 |
| **V22** | 8 000 | 0.08875 | 5 | 8 | 554 | 133 | 217 |
| **V23** | 8 000 | 0.08875 | 9 | 4 | 280 | 181 | 298 |
| **V24** | 8 000 | 0.08875 | 9 | 8 | 558 | 230 | 305 |
| **V25** | 16 000 | 0.055 | 5 | 4 | 211 | 97 | 100 |
| **V26** | 16 000 | 0.055 | 5 | 8 | 403 | 103 | 151 |
| **V27** | 16 000 | 0.055 | 9 | 4 | 196 | 160 | 183 |
| **V28** | 16 000 | 0.055 | 9 | 8 | 417 | 217 | 223 |
| **V29** | 16 000 | 0.08875 | 5 | 4 | 261 | 127 | 118 |
| **V30** | 16 000 | 0.08875 | 5 | 8 | 453 | 136 | 172 |
| **V31** | 16 000 | 0.08875 | 9 | 4 | 231 | 189 | 217 |
| **V32** | 16 000 | 0.08875 | 9 | 8 | 459 | 251 | 293 |

**Table D.2** Validation tests results for Torque

| Test | $S$ [rpm] | $f_z$ [mm/tooth] | $d$ [mm] | $t$ [mm] | Torque [Nm] | | |
|---|---|---|---|---|---|---|---|
| | | | | | Straight flute drill | W-shape drill | Twist drill |
| **V01** | 12 000 | 0.0325 | 5 | 4 | 0.26 | 0.09 | 0.10 |
| **V02** | 12 000 | 0.0325 | 5 | 8 | 0.49 | 0.13 | 0.21 |
| **V03** | 12 000 | 0.0325 | 9 | 4 | 0.53 | 0.23 | 0.42 |
| **V04** | 12 000 | 0.0325 | 9 | 8 | 1.08 | 0.64 | 0.55 |
| **V05** | 18 000 | 0.0325 | 5 | 4 | 0.38 | 0.09 | 0.15 |
| **V06** | 18 000 | 0.0325 | 5 | 8 | 0.53 | 0.15 | 0.23 |
| **V07** | 18 000 | 0.0325 | 9 | 4 | 0.52 | 0.24 | 0.58 |
| **V08** | 18 000 | 0.0325 | 9 | 8 | 1.14 | 0.57 | 0.64 |
| **V09** | 12 000 | 0.0775 | 5 | 4 | 0.40 | 0.17 | 0.18 |
| **V10** | 12 000 | 0.0775 | 5 | 8 | 0.82 | 0.25 | 0.26 |
| **V11** | 12 000 | 0.0775 | 9 | 4 | 0.78 | 0.40 | 0.53 |
| **V12** | 12 000 | 0.0775 | 9 | 8 | 1.60 | 0.74 | 0.59 |
| **V13** | 18 000 | 0.0775 | 5 | 4 | 0.45 | 0.15 | 0.13 |
| **V14** | 18 000 | 0.0775 | 5 | 8 | 0.74 | 0.24 | 0.24 |
| **V15** | 18 000 | 0.0775 | 9 | 4 | 0.73 | 0.38 | 0.44 |
| **V16** | 18 000 | 0.0775 | 9 | 8 | 1.57 | 0.76 | 0.48 |
| **V17** | 8 000 | 0.055 | 5 | 4 | 0.37 | 0.18 | 0.14 |
| **V18** | 8 000 | 0.055 | 5 | 8 | 0.60 | 0.27 | 0.21 |
| **V19** | 8 000 | 0.055 | 9 | 4 | 0.62 | 0.36 | 0.42 |
| **V20** | 8 000 | 0.055 | 9 | 8 | 1.35 | 0.78 | 0.47 |
| **V21** | 8 000 | 0.08875 | 5 | 4 | 0.46 | 0.23 | 0.28 |
| **V22** | 8 000 | 0.08875 | 5 | 8 | 0.93 | 0.33 | 0.36 |
| **V23** | 8 000 | 0.08875 | 9 | 4 | 0.88 | 0.47 | 0.56 |
| **V24** | 8 000 | 0.08875 | 9 | 8 | 1.69 | 0.86 | 0.66 |
| **V25** | 16 000 | 0.055 | 5 | 4 | 0.38 | 0.13 | 0.16 |
| **V26** | 16 000 | 0.055 | 5 | 8 | 0.70 | 0.18 | 0.21 |
| **V27** | 16 000 | 0.055 | 9 | 4 | 0.57 | 0.30 | 0.53 |
| **V28** | 16 000 | 0.055 | 9 | 8 | 1.21 | 0.71 | 0.63 |
| **V29** | 16 000 | 0.08875 | 5 | 4 | 0.41 | 0.17 | 0.15 |
| **V30** | 16 000 | 0.08875 | 5 | 8 | 0.83 | 0.27 | 0.23 |
| **V31** | 16 000 | 0.08875 | 9 | 4 | 0.80 | 0.36 | 0.40 |
| **V32** | 16 000 | 0.08875 | 9 | 8 | 1.73 | 0.74 | 0.54 |

**Table D.3** Validation tests results for Delamination factor

| Test | $S$ [rpm] | $f_z$ [mm/tooth] | $d$ [mm] | $t$ [mm] | Delamination factor | | |
|---|---|---|---|---|---|---|---|
| | | | | | Straight flute drill | W-shape drill | Twist drill |
| **V01** | 12 000 | 0.0325 | 5 | 4 | 1.248 | 1.340 | 1.296 |
| **V02** | 12 000 | 0.0325 | 5 | 8 | 1.263 | 1.358 | 1.251 |
| **V03** | 12 000 | 0.0325 | 9 | 4 | 1.121 | 1.190 | 1.256 |
| **V04** | 12 000 | 0.0325 | 9 | 8 | 1.135 | 1.209 | 1.322 |
| **V05** | 18 000 | 0.0325 | 5 | 4 | 1.225 | 1.321 | 1.244 |
| **V06** | 18 000 | 0.0325 | 5 | 8 | 1.229 | 1.384 | 1.307 |
| **V07** | 18 000 | 0.0325 | 9 | 4 | 1.149 | 1.164 | 1.402 |
| **V08** | 18 000 | 0.0325 | 9 | 8 | 1.123 | 1.190 | 1.476 |
| **V09** | 12 000 | 0.0775 | 5 | 4 | 1.263 | 1.369 | 1.288 |
| **V10** | 12 000 | 0.0775 | 5 | 8 | 1.277 | 1.354 | 1.237 |
| **V11** | 12 000 | 0.0775 | 9 | 4 | 1.240 | 1.174 | 1.204 |
| **V12** | 12 000 | 0.0775 | 9 | 8 | 1.125 | 1.238 | 1.221 |
| **V13** | 18 000 | 0.0775 | 5 | 4 | 1.225 | 1.251 | 1.159 |
| **V14** | 18 000 | 0.0775 | 5 | 8 | 1.277 | 1.384 | 1.307 |
| **V15** | 18 000 | 0.0775 | 9 | 4 | 1.137 | 1.227 | 1.364 |
| **V16** | 18 000 | 0.0775 | 9 | 8 | 1.121 | 1.328 | 1.338 |
| **V17** | 8 000 | 0.055 | 5 | 4 | 1.211 | 1.380 | 1.252 |
| **V18** | 8 000 | 0.055 | 5 | 8 | 1.277 | 1.477 | 1.337 |
| **V19** | 8 000 | 0.055 | 9 | 4 | 1.104 | 1.213 | 1.117 |
| **V20** | 8 000 | 0.055 | 9 | 8 | 1.123 | 1.213 | 1.193 |
| **V21** | 8 000 | 0.08875 | 5 | 4 | 1.233 | 1.521 | 1.337 |
| **V22** | 8 000 | 0.08875 | 5 | 8 | 1.189 | 1.462 | 1.433 |
| **V23** | 8 000 | 0.08875 | 9 | 4 | 1.117 | 1.245 | 1.146 |
| **V24** | 8 000 | 0.08875 | 9 | 8 | 1.112 | 1.279 | 1.174 |
| **V25** | 16 000 | 0.055 | 5 | 4 | 1.203 | 1.439 | 1.196 |
| **V26** | 16 000 | 0.055 | 5 | 8 | 1.218 | 1.473 | 1.240 |
| **V27** | 16 000 | 0.055 | 9 | 4 | 1.137 | 1.190 | 1.437 |
| **V28** | 16 000 | 0.055 | 9 | 8 | 1.117 | 1.240 | 1.254 |
| **V29** | 16 000 | 0.08875 | 5 | 4 | 1.211 | 1.414 | 1.203 |
| **V30** | 16 000 | 0.08875 | 5 | 8 | 1.251 | 1.480 | 1.255 |
| **V31** | 16 000 | 0.08875 | 9 | 4 | 1.104 | 1.283 | 1.137 |
| **V32** | 16 000 | 0.08875 | 9 | 8 | 1.121 | 1.346 | 1.166 |

**Table D.4** Variation between the experimental values and the calculated values from the empirical models (Thrust force)

| Test | $S$ [rpm] | $f_z$ [mm/tooth] | $d$ [mm] | $t$ [mm] | RE [%] | | |
|---|---|---|---|---|---|---|---|
| | | | | | Straight flute drill | W-shape drill | Twist drill |
| **V01** | 12 000 | 0.0325 | 5 | 4 | 19.9% | -2.9% | 0.7% |
| **V02** | 12 000 | 0.0325 | 5 | 8 | -11.3% | -2.3% | -10.3% |
| **V03** | 12 000 | 0.0325 | 9 | 4 | 1.1% | -14.6% | -12.1% |
| **V04** | 12 000 | 0.0325 | 9 | 8 | -0.1% | 0.2% | -13.8% |
| **V05** | 18 000 | 0.0325 | 5 | 4 | 13.9% | -1.7% | **-16.7%** |
| **V06** | 18 000 | 0.0325 | 5 | 8 | -3.5% | 1.5% | -4.6% |
| **V07** | 18 000 | 0.0325 | 9 | 4 | -13.8% | 7.7% | -5.8% |
| **V08** | 18 000 | 0.0325 | 9 | 8 | 3.1% | 10.5% | -6.4% |
| **V09** | 12 000 | 0.0775 | 5 | 4 | 22.5% | -4.1% | 11.2% |
| **V10** | 12 000 | 0.0775 | 5 | 8 | 11.1% | -17.9% | -3.8% |
| **V11** | 12 000 | 0.0775 | 9 | 4 | 11.5% | 10.2% | 13.8% |
| **V12** | 12 000 | 0.0775 | 9 | 8 | 6.7% | 5.5% | 5.3% |
| **V13** | 18 000 | 0.0775 | 5 | 4 | -6.0% | -10.7% | 9.7% |
| **V14** | 18 000 | 0.0775 | 5 | 8 | -17.6% | -13.8% | 10.9% |
| **V15** | 18 000 | 0.0775 | 9 | 4 | **-23.1%** | 8.9% | 4.4% |
| **V16** | 18 000 | 0.0775 | 9 | 8 | -17.4% | 8.4% | 14.3% |
| **V17** | 8 000 | 0.055 | 5 | 4 | 13.6% | 2.5% | 12.1% |
| **V18** | 8 000 | 0.055 | 5 | 8 | -2.0% | -5.6% | -6.9% |
| **V19** | 8 000 | 0.055 | 9 | 4 | 4.6% | 15.6% | 5.5% |
| **V20** | 8 000 | 0.055 | 9 | 8 | -1.3% | 12.5% | -14.1% |
| **V21** | 8 000 | 0.08875 | 5 | 4 | 20.5% | -6.9% | -10.5% |
| **V22** | 8 000 | 0.08875 | 5 | 8 | -1.5% | -13.1% | -9.6% |
| **V23** | 8 000 | 0.08875 | 9 | 4 | 2.9% | 7.7% | -2.6% |
| **V24** | 8 000 | 0.08875 | 9 | 8 | -0.9% | 7.8% | -11.8% |
| **V25** | 16 000 | 0.055 | 5 | 4 | 15.4% | -0.8% | -6.0% |
| **V26** | 16 000 | 0.055 | 5 | 8 | 6.6% | -5.2% | 6.2% |
| **V27** | 16 000 | 0.055 | 9 | 4 | 8.9% | 21.0% | -14.4% |
| **V28** | 16 000 | 0.055 | 9 | 8 | 9.8% | **21.1%** | -9.7% |
| **V29** | 16 000 | 0.08875 | 5 | 4 | 6.0% | -9.2% | -6.0% |
| **V30** | 16 000 | 0.08875 | 5 | 8 | -18.4% | -10.4% | 6.6% |
| **V31** | 16 000 | 0.08875 | 9 | 4 | -6.3% | 11.4% | -5.2% |
| **V32** | 16 000 | 0.08875 | 9 | 8 | -16.8% | 15.7% | 9.8% |

**Table D.5** Variation between the experimental values and the calculated values from the empirical models (Torque)

| Test | S [rpm] | $f_z$ [mm/tooth] | d [mm] | t [mm] | RE [%] | | |
|---|---|---|---|---|---|---|---|
| | | | | | Straight flute drill | W-shape drill | Twist drill |
| **V01** | 12 000 | 0.0325 | 5 | 4 | -15.4% | **34.0%** | 16.1% |
| **V02** | 12 000 | 0.0325 | 5 | 8 | -8.3% | 16.4% | 13.9% |
| **V03** | 12 000 | 0.0325 | 9 | 4 | 8.6% | 1.6% | 2.6% |
| **V04** | 12 000 | 0.0325 | 9 | 8 | -3.8% | -0.7% | 7.9% |
| **V05** | 18 000 | 0.0325 | 5 | 4 | 8.2% | 18.8% | -7.8% |
| **V06** | 18 000 | 0.0325 | 5 | 8 | -8.2% | 20.6% | -9.7% |
| **V07** | 18 000 | 0.0325 | 9 | 4 | -2.7% | 2.3% | 15.6% |
| **V08** | 18 000 | 0.0325 | 9 | 8 | -2.4% | -13.5% | 8.8% |
| **V09** | 12 000 | 0.0775 | 5 | 4 | -10.5% | -0.6% | -10.0% |
| **V10** | 12 000 | 0.0775 | 5 | 8 | -4.6% | 15.2% | -10.9% |
| **V11** | 12 000 | 0.0775 | 9 | 4 | -6.8% | 16.7% | 3.1% |
| **V12** | 12 000 | 0.0775 | 9 | 8 | -3.0% | -1.3% | -3.2% |
| **V13** | 18 000 | 0.0775 | 5 | 4 | 11.4% | -15.0% | 12.9% |
| **V14** | 18 000 | 0.0775 | 5 | 8 | -9.2% | 9.0% | 11.5% |
| **V15** | 18 000 | 0.0775 | 9 | 4 | -7.5% | 11.4% | 0.5% |
| **V16** | 18 000 | 0.0775 | 9 | 8 | -2.1% | 0.7% | -10.4% |
| **V17** | 8 000 | 0.055 | 5 | 4 | -6.7% | 5.9% | -2.6% |
| **V18** | 8 000 | 0.055 | 5 | 8 | -19.6% | 18.1% | -9.3% |
| **V19** | 8 000 | 0.055 | 9 | 4 | -9.3% | 7.7% | -10.6% |
| **V20** | 8 000 | 0.055 | 9 | 8 | -4.0% | 3.3% | **-18.0%** |
| **V21** | 8 000 | 0.08875 | 5 | 4 | -7.1% | -7.8% | -5.7% |
| **V22** | 8 000 | 0.08875 | 5 | 8 | -2.0% | 11.0% | -7.8% |
| **V23** | 8 000 | 0.08875 | 9 | 4 | -5.2% | 12.2% | -11.5% |
| **V24** | 8 000 | 0.08875 | 9 | 8 | -6.3% | 3.7% | -7.5% |
| **V25** | 16 000 | 0.055 | 5 | 4 | -4.6% | 17.6% | 10.4% |
| **V26** | 16 000 | 0.055 | 5 | 8 | -3.0% | 14.1% | -11.8% |
| **V27** | 16 000 | 0.055 | 9 | 4 | **-20.2%** | 11.0% | 12.8% |
| **V28** | 16 000 | 0.055 | 9 | 8 | -16.2% | 3.7% | 7.9% |
| **V29** | 16 000 | 0.08875 | 5 | 4 | 2.6% | -8.2% | 2.1% |
| **V30** | 16 000 | 0.08875 | 5 | 8 | -3.4% | 12.7% | -5.2% |
| **V31** | 16 000 | 0.08875 | 9 | 4 | -4.6% | 3.3% | 14.3% |
| **V32** | 16 000 | 0.08875 | 9 | 8 | 1.8% | -4.0% | 6.8% |

**Table D.6** Variation between the experimental values and the calculated values from the empirical models (Delamination factor)

| Test | $S$ [rpm] | $f_z$ [mm/tooth] | $d$ [mm] | $t$ [mm] | RE [%] | | |
|---|---|---|---|---|---|---|---|
| | | | | | Straight flute drill | W-shape drill | Twist drill |
| **V01** | 12 000 | 0.0325 | 5 | 4 | -2.2% | -7.0% | -10.8% |
| **V02** | 12 000 | 0.0325 | 5 | 8 | 3.6% | 4.3% | -13.3% |
| **V03** | 12 000 | 0.0325 | 9 | 4 | -5.7% | -5.7% | -6.1% |
| **V04** | 12 000 | 0.0325 | 9 | 8 | 0.7% | 7.0% | 2.9% |
| **V05** | 18 000 | 0.0325 | 5 | 4 | 2.2% | -8.5% | -21.0% |
| **V06** | 18 000 | 0.0325 | 5 | 8 | 7.2% | 6.1% | -26.4% |
| **V07** | 18 000 | 0.0325 | 9 | 4 | 3.6% | -8.1% | -8.9% |
| **V08** | 18 000 | 0.0325 | 9 | 8 | 6.4% | 5.6% | -3.3% |
| **V09** | 12 000 | 0.0775 | 5 | 4 | -1.0% | -10.0% | -16.2% |
| **V10** | 12 000 | 0.0775 | 5 | 8 | 4.7% | -1.3% | -16.5% |
| **V11** | 12 000 | 0.0775 | 9 | 4 | 4.4% | -1.0% | -5.6% |
| **V12** | 12 000 | 0.0775 | 9 | 8 | -0.2% | 15.0% | 2.5% |
| **V13** | 18 000 | 0.0775 | 5 | 4 | 2.2% | -20.4% | -9.8% |
| **V14** | 18 000 | 0.0775 | 5 | 8 | **10.7%** | 0.9% | -5.7% |
| **V15** | 18 000 | 0.0775 | 9 | 4 | 2.5% | 3.4% | 4.8% |
| **V16** | 18 000 | 0.0775 | 9 | 8 | 6.3% | 20.8% | -2.1% |
| **V17** | 8 000 | 0.055 | 5 | 4 | -5.5% | -6.5% | -21.3% |
| **V18** | 8 000 | 0.055 | 5 | 8 | 4.6% | 9.5% | -16.6% |
| **V19** | 8 000 | 0.055 | 9 | 4 | -7.5% | -0.8% | -12.6% |
| **V20** | 8 000 | 0.055 | 9 | 8 | -0.6% | 10.3% | 2.8% |
| **V21** | 8 000 | 0.08875 | 5 | 4 | 3.0% | -0.2% | **-37.2%** |
| **V22** | 8 000 | 0.08875 | 5 | 8 | 4.3% | 4.9% | -28.2% |
| **V23** | 8 000 | 0.08875 | 9 | 4 | 0.9% | 6.2% | -16.3% |
| **V24** | 8 000 | 0.08875 | 9 | 8 | 5.8% | 19.1% | -3.0% |
| **V25** | 16 000 | 0.055 | 5 | 4 | -6.1% | -2.1% | -9.7% |
| **V26** | 16 000 | 0.055 | 5 | 8 | -0.1% | 9.3% | -14.5% |
| **V27** | 16 000 | 0.055 | 9 | 4 | -4.4% | -2.7% | 6.0% |
| **V28** | 16 000 | 0.055 | 9 | 8 | -1.1% | 12.2% | -5.0% |
| **V29** | 16 000 | 0.08875 | 5 | 4 | 1.2% | -7.8% | -8.5% |
| **V30** | 16 000 | 0.08875 | 5 | 8 | 9.1% | 6.1% | -10.8% |
| **V31** | 16 000 | 0.08875 | 9 | 4 | -0.1% | 8.9% | -10.6% |
| **V32** | 16 000 | 0.08875 | 9 | 8 | 6.5% | **23.2%** | -2.9% |